AD-A144 696 STEERABILITY ANALYSIS OF MULTIAXLE WHEELED EEHICLES REPORT 1 DEVELOPMENT O.. (U) ARMY ENGINEER WATERWAYS EXPERIMENT STATION VICKSBURG MS GEOTE..

1/2

UNCLASSIFIED G Y BALADI ET AL. JAN 84 WES/TR/GL-84-1 F/G 8/13 NL

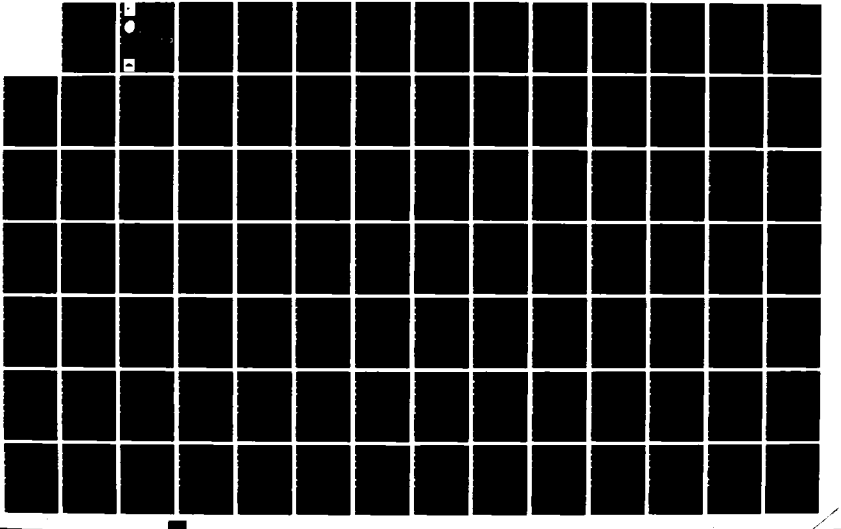

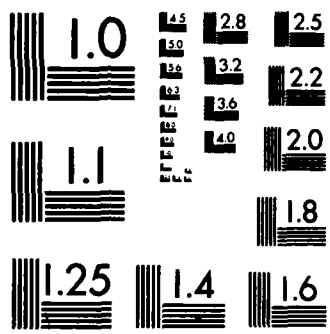

MICROCOPY RESOLUTION TEST CHART
NATIONAL BUREAU OF STANDARDS-1963-A

US Army Corps of Engineers

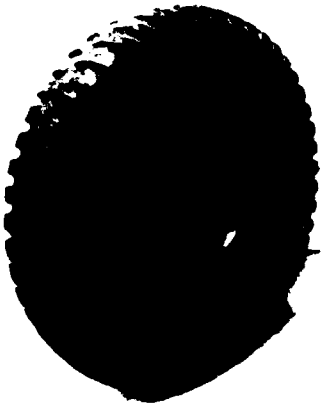

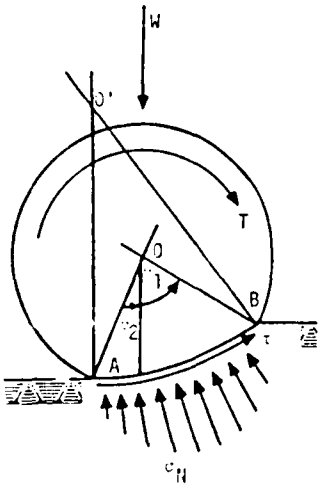

GEOTECHNICAL LABORATORY

TECHNICAL REPORT GL-84-1

12

STEERABILITY ANALYSIS OF MULTIAXLE WHEELED VEHICLES

Report 1

DEVELOPMENT OF A SOIL-WHEEL INTERACTION MODEL

by

George Y. Baladi, Behzad Rohani, Donald E. Barnes

Structures Laboratory

DEPARTMENT OF THE ARMY
Waterways Experiment Station, Corps of Engineers
PO Box 631
Vicksburg, Mississippi 39180

January 1984
Report 1 of a Series

Approved For Public Release: Distribution Unlimited

Prepared for DEPARTMENT OF THE ARMY
US Army Corps of Engineers
Washington, DC 20314

Under Project 4A161102AT22
Task CO, Work Unit 004

Monitored by Geotechnical Laboratory
US Army Engineer Waterways Experiment Station
PO Box 631, Vicksburg, Mississippi 39180

Destroy this report when no longer needed. Do not return it to the originator.

The findings in this report are not to be construed as an official Department of the Army position unless so designated by other authorized documents.

The contents of this report are not to be used for advertising, publication, or promotional purposes. Citation of trade names does not constitute an official endorsement or approval of the use of such commercial products.

Unclassified

SECURITY CLASSIFICATION OF THIS PAGE (When Data Entered)

REPORT DOCUMENTATION PAGE		READ INSTRUCTIONS BEFORE COMPLETING FORM
1. REPORT NUMBER Technical Report GL-84-1	2. GOVT ACCESSION NO.	3. RECIPIENT'S CATALOG NUMBER
4. TITLE (and Subtitle) STEERABILITY ANALYSIS OF MULTIAXLE WHEELED VEHICLES; REPORT 1: DEVELOPMENT OF A SOIL-WHEEL INTERACTION MODEL		5. TYPE OF REPORT & PERIOD COVERED Report 1 of a series 6. PERFORMING ORG. REPORT NUMBER
7. AUTHOR(s) George Y. Baladi Behzad Rohani Donald E. Barnes		8. CONTRACT OR GRANT NUMBER(s)
9. PERFORMING ORGANIZATION NAME AND ADDRESS US Army Engineer Waterways Experiment Station Structures Laboratory PO Box 631, Vicksburg, Mississippi 39180		10. PROGRAM ELEMENT, PROJECT, TASK AREA & WORK UNIT NUMBERS Project 4A161102AT22 Task CO, Work Unit 004
11. CONTROLLING OFFICE NAME AND ADDRESS DEPARTMENT OF THE ARMY US Army Corps of Engineers Washington, DC 20314		12. REPORT DATE January 1984 13. NUMBER OF PAGES 133
14. MONITORING AGENCY NAME & ADDRESS(if different from Controlling Office) US Army Engineer Waterways Experiment Station Geotechnical Laboratory PO Box 631, Vicksburg, Mississippi 39180		15. SECURITY CLASS. (of this report) Unclassified 15a. DECLASSIFICATION/DOWNGRADING SCHEDULE

16. DISTRIBUTION STATEMENT (of this Report)

Approved for public release; distribution unlimited.

17. DISTRIBUTION STATEMENT (of the abstract entered in Block 20, if different from Report)

18. SUPPLEMENTARY NOTES

Available from National Technical Information Service, 5285 Port Royal Road, Springfield, Virginia 22161.

19. KEY WORDS (Continue on reverse side if necessary and identify by block number)

Flexible tire	Soil model
Mobility	Soil-wheel interaction
Numerical analyses	Spherical cavity expansion
Sinkage	Tire model

20. ABSTRACT (Continue on reverse side if necessary and identify by block number)

This report describes the development of a mathematical model for calculating the motion resistance, sinkage, drawbar pull, torque, and side force for a flexible wheel traversing a yielding (or deformable) surface. To facilitate computations, the deformed boundary of the wheel is assumed to be an arc of a larger circular wheel. The entire soil-wheel interaction process is treated as two springs in series, one describing the flexibility of the tire

(Continued)

DD FORM 1 JAN 73 1473 EDITION OF 1 NOV 65 IS OBSOLETE

Unclassified

SECURITY CLASSIFICATION OF THIS PAGE (When Data Entered)

20. ABSTRACT (Continued).

and one describing the elastic-plastic deformation of the soil. Mathematical expressions are derived for the two spring constants in terms of the load deflection characteristics of the tire, the undeflected configuration of the wheel, and the mechanical properties of the soil (both shearing response and compressibility characteristics).

The system of equations describing the performance of the wheel is solved numerically via a computer program called TIRE. An extensive series of parametric calculations is conducted with TIRE to demonstrate the application of the methodology and to study the performance of flexible wheels on different types of soil under various kinematic conditions. A partial validation of the proposed interaction model is established by comparing the results of laboratory tests for clay, sand, and mixed soils with corresponding model predictions.

PREFACE

This investigation was conducted for the Office, Chief of Engineers, U. S. Army, by personnel of the U. S. Army Engineer Waterways Experiment Station (WES) as a part of Project 4A161102AT22, Task CO, Work Unit 004, "Wheel, Track, and Soil Dynamics Influence on Mobility."

The prediction methodology, the numerical analyses, and the design of the mathematical model discussed herein originated with Drs. George Y. Baladi and Behzad Rohani and Mr. Donald E. Barnes of the Geomechanics Division (GD), Structures Laboratory, during the period October 1982-October 1983 under the general direction of Mr. C. J. Nuttall, Jr., Chief, Mobility Systems Division (MSD), Geotechnical Laboratory (GL), and Dr. W. F. Marcuson III, Chief, GL.

COL Tilford C. Creel, CE, was Commander and Director of the WES during the investigation. Mr. Fred R. Brown was Technical Director.

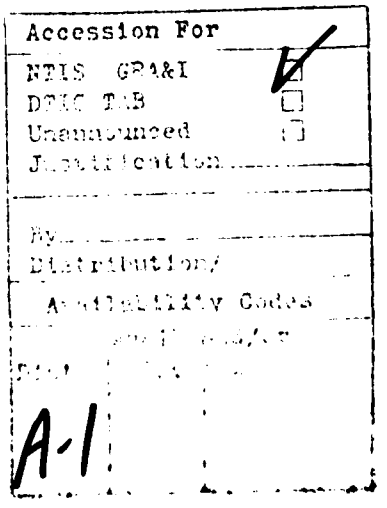

CONTENTS

CONVERSION FACTORS, NON-SI TO SI (METRIC) UNITS OF MEASUREMENT

Non-SI units of measurement used in this report can be converted to SI (metric) units as follows:

Multiply	By	To Obtain
feet	0.3048	metres
inches	25.4	millimetres
pounds (force) per square inch	6.894757	kilopascals
pounds (mass)	0.4535924	kilograms
pounds (mass) per cubic foot	16.01846	kilograms per cubic metre

STEERABILITY ANALYSIS OF MULTIAXLE WHEELED VEHICLES

DEVELOPMENT OF A SOIL-WHEEL INTERACTION MODEL

PART I: INTRODUCTION

Background and Objective

1. The determination of the response of a single flexible wheel traversing a yielding (or deformable) surface is essential for the analysis of the steering performance of wheeled vehicles. Specifically, the sinkage, motion resistance, drawbar pull, torque, and side forces acting on a powered flexible wheel moving on a yielding soil must be accurately determined. Due to the overwhelming complexity of this problem, previous research in this area has been directed, by and large, toward extensive experimentation and the development of empirical equations relating the various parameters of the problem (Turnage 1972). Unfortunately, these equations are not generic and apply only within the range of the experimental data on which they are based. On the other hand, most of the analytical investigations conducted in this area are based on the assumption of a rigid wheel (Wong and Reece 1967). That is, the effect of the flexibility (elasticity) of the tire on the kinematics of the wheel is neglected. Even in the case of the rigid wheel, there is no general equation that can predict accurately the sinkage as a function of applied load, configuration of the wheel, and the engineering properties of soil (Hvorslev 1970). In a recent article, Fujimoto (1977) introduced the flexibility of the tire in his analysis of the performance of elastic wheels on cohesive soils. He introduced an empirical relation between the central angle of the wheel, the internal pressure of the tire, and the radial stress acting on the periphery of the tire. The radial stress was assumed to be constant over the periphery of the tire where interfaced with the soil. Fujimoto concluded that the determination of the radial stress is the most difficult problem in the analysis of soil-wheel interaction and recommended a relationship between the mobility cone index and the radial stress.

2. The objective of the present investigation is to develop a rational soil-wheel interaction model that is free from excessive empiricism and is general enough to treat a wide range of problems. The core of the model is a

method for predicting the sinkage as a function of applied load, deflection of the tire, slip, undeformed geometry of the wheel, and the fundamental engineering properties of the soil (cohesion, angle of internal friction, density, compressibility, etc.). Accordingly, the model can be used to predict sinkage in sand, clay, or soils exhibiting both cohesive and frictional properties. The equilibrium conditions and the sinkage of the wheel are then combined to calculate motion resistance, drawbar pull, torque, etc.

3. This report is the first in a series of three on steerability analysis of multiaxle wheeled vehicles. In the second report, the soil-wheel interaction model will be coupled with the dynamic equilibrium equations of multiaxle wheeled vehicles for analysis of steering performance of such vehicles. The third report will contain an evaluation of the theories developed in the first and second reports.

Scope

4. The mathematical development of the soil-wheel interaction model is presented in Part II. Detailed parametric studies of the kinematics of a single wheel traversing different types of terrains are documented in Part III. Correlations of model predictions with experimental data for a variety of wheels are discussed in Part IV. A summary and recommendations are presented in Part V. The report contains three appendixes: Appendix A discusses a rheological soil model describing the engineering properties of soil, Appendix B summarizes the basic equations for internal pressure necessary to maintain a slow expansion of a spherical cavity in an elastic-plastic medium, and Appendix C presents a notation. The equations from Appendixes A and B are used in Part II of the main text for the development of the soil-wheel interaction model.

PART II: DERIVATION OF THE SOIL-WHEEL INTERACTION MODEL

General Procedure

5. The most essential element of the soil-wheel interaction model is the procedure for determining the sinkage of a flexible wheel. The basic parameters that must be included in such a procedure are the applied load, the configuration and flexibility or elasticity of the tire, slip, and the fundamental engineering properties of the soil (such as shear strength and compressibility). The development of the soil-wheel interaction model is presented in detail in the subsequent sections and is based on the assumption that the entire interaction process can be simulated by two springs in series, with one spring defining the elasticity of the tire and the other describing the elastic-plastic deformation of the soil. The procedure by which each spring constant is determined is as follows:

a. From the static equilibrium and the load-deflection characteristics of the tire on a rigid surface, determine the spring constant k_t* for the tire.

b. Assume that the maximum normal stress acting on the periphery of a given wheel being embedded in soil is equal to the radial stress inside a slowly expanding spherical cavity in a compressible elastic-plastic medium characterized by the Mohr-Coulomb failure condition (Appendix B). Determine the elastic-plastic spring constant k_s for the soil by simulating the resistance of the soil to the embedment of the wheel by a series of radial springs. This spring constant defines the resistance of the soil to the embedment of the wheel in terms of the fundamental engineering properties of the soil and the configuration of the wheel.

6. The simulation of the resistance of the soil by an apparent spring constant leads to a nonuniform distribution of normal stresses at the soil-wheeled interface. The spring constants k_t and k_s are combined in order to determine the equivalent spring constant k_e describing the interaction of the soil-wheel system. Once k_e is determined, the deflection of a flexible wheel on a yielding soil can be calculated from the corresponding deflection on a rigid surface. Similarly, the sinkage of a flexible wheel in a yielding soil can be obtained from the corresponding sinkage of a rigid wheel.

---

* For convenience, symbols and unusual abbreviations are listed and defined in the Notation (Appendix C).

7. The load-deflection relation for a flexible wheel on a rigid surface can be determined experimentally. The sinkage of a rigid wheel in a yielding soil, however, is calculated from the balance of the applied load and the normal and shear stresses at the soil-wheel interface.

8. Finally, the motion resistance, drawbar pull, torque, efficiency, and side force for the flexible wheel traversing a yielding surface are calculated. These parameters can be readily determined by assuming that the deformed boundary of the tire is an arc of a larger circular wheel.

Derivation of a Spring Constant for a Flexible Tire

9. A typical load-deflection curve for a flexible tire on a rigid surface is shown in Figure 1 where Δ denotes the deflection of the tire at point A. In practice, Δ is usually expressed as a percentage of the unloaded section height of the tire (Figure 2). The radial deflection at a generic point B along the periphery of the tire at an angle α is specified by Δ_α (Figure 1). If the deformed section of the tire is characterized by a continuous spring with constant k_t, then the vertical differential force dF applied at point B can be expressed as

$$dF = k_t \Delta_\alpha \cos \alpha \, d\alpha \tag{1}$$

From Figure 1, Δ_α can be expressed in terms of Δ, α, and the undeflected radius of the wheel R

$$\Delta_\alpha = R - \frac{R - \Delta}{\cos \alpha} = \frac{R}{\cos \alpha}\left[\cos \alpha - \left(1 - \frac{\Delta}{R}\right)\right] \tag{2}$$

Substitution of Equation 2 into Equation 1 leads to

$$dF = Rk_t\left[\cos \alpha - \left(1 - \frac{\Delta}{R}\right)\right] d\alpha \tag{3}$$

Also, from Figure 1

$$\cos \frac{\theta_t}{2} = 1 - \frac{\Delta}{R} \tag{4}$$

In view of Equations 3 and 4 and static equilibrium, the applied load W can be expressed as

$$W = 2\int_0^{\theta_{t/2}} dF \simeq 2Rk_t \int_0^{\theta_{t/2}} \left(\cos\alpha - \cos\frac{\theta_t}{2}\right) d\alpha \tag{5}$$

Integration of Equation 5 leads to the following relation for the spring constant k_t:

$$k_t = \frac{W}{2R\left(\sin\frac{\theta_t}{2} - \frac{\theta_t}{2}\cos\frac{\theta_t}{2}\right)} \tag{6}$$

The spring constant k_t can also be expressed in terms of Δ by combining Equations 4 and 6.

$$k_t = \frac{W}{2\Delta\left[\sqrt{\frac{2R}{\Delta} - 1} - \left(\frac{R}{\Delta} - 1\right)\cos^{-1}\left(1 - \frac{\Delta}{R}\right)\right]} \tag{7}$$

Equation 7 is portrayed in the top of Figure 1.

Derivation of a Spring Constant for Soil

10. Let σ_c be the radial stress necessary to maintain a slow expansion of a spherical cavity in an elastic-plastic medium from radius R_o to R (Figure 3a). The radial stress σ_c is expressed in terms of the fundamental engineering properties of soil (Appendix B). The resistance of the soil to expansion of the spherical cavity can be simulated by a continuous spring characterized by the spring constant k_s. From Figure 3a, the spring constant k_s can be expressed as

$$k_s = \frac{\pi\left(R^2 - R_o^2\right)\sigma_c}{R - R_o} = \pi(R + R_o)\sigma_c \tag{8}$$

where $R - R_o$ corresponds to spring deflection.

11. Consider a wheel of radius R embedded in soil to a depth $R - R_o$ (Figure 3b). The normal stress at point A resisting the embedment of the wheel is assumed to be equal to the radial stress σ_c inside the expanding cavity. Similar to expansion of the spherical cavity (Figure 3a), the

resistance of soil to the embedment of the wheel can also be simulated by a continuous spring with constant k_s given by

$$k_s = \frac{RD}{R - R_o} \sigma_c \tag{9}$$

where D is the unloaded section width of the wheel (Figure 2). Combining Equations 8 and 9 we obtain

$$\frac{\pi(R + R_o)(R - R_o)}{RD} = 1 \tag{10}$$

where, from Figure 3b, we then obtain

$$R + R_o = R\left(1 + \cos \frac{\theta_s}{2}\right) \tag{11}$$

$$R - R_o = R\left(1 - \cos \frac{\theta_s}{2}\right) \tag{12}$$

Substituting Equations 11 and 12 into Equation 10 and solving for $\cos \theta_s/2$ and θ_s, we obtain

$$\cos \frac{\theta_s}{2} = \sqrt{1 - \frac{D}{\pi R}} \tag{13}$$

$$\theta_s = 2 \cos^{-1} \sqrt{1 - \frac{D}{\pi R}} \tag{14}$$

Substitution of Equations 11 and 13 into Equation 8 leads to the following expression for the spring constant k_s:

$$k_s = \pi R\left(1 + \sqrt{1 - \frac{D}{\pi R}}\right) \sigma_c \tag{15}$$

It is clear from Equation 15 that the apparent spring constant of the soil is a function of the engineering properties of soil through σ_c and the geometry of the tire.

Equivalent Spring Constant for the Soil-Tire System

12. The model of the soil-tire system in terms of two continuous springs in series characterized by the spring constants k_t and k_s is shown in Figure 4. If the radial deflection of the tire at a generic point is denoted by δ_t and the corresponding deflection of the soil is denoted by δ_s, then we can write

$$\delta_t k_t = \delta_s k_s = \delta k_e \tag{16}$$

where k_e is the equivalent spring constant of the soil-tire system and

$$\delta = \delta_t + \delta_s \tag{17}$$

Substitution of Equation 17 into Equation 16 gives the following expression for k_e:

$$k_e = \frac{k_t k_s}{k_s + k_t} \tag{18}$$

Normal Stress Distribution at the Soil-Tire Interface

13. Based on the concept of the spring analogy advanced in the previous sections, the distribution of normal stress at the soil-tire interface (σ_N) is nonuniform (Figure 5). According to Figure 5a, the vertical force dF applied at an angle α can be expressed as

$$dF = DR\ \sigma_N \cos\left(\alpha + \frac{\theta_s}{2}\right) d\alpha \tag{19a}$$

Also, according to Figure 5b, dF can be expressed in terms of soil deflection δ_s and soil spring constant k_s.

$$dF = k_s \delta_s = \frac{k_s R\left(\cos\alpha - \cos\frac{\theta_s}{2}\right) \cos\left(\alpha + \frac{\theta_s}{2}\right) d\alpha}{\cos\alpha}, \quad -\frac{\theta_s}{2} \le \alpha \le \frac{\theta_s}{2} \tag{19b}$$

Solving Equations 19a and 19b for σ_N, we obtain

$$\sigma_N = \frac{k_s\left(\cos\alpha - \cos\frac{\theta_s}{2}\right)}{D\cos\alpha} \tag{20}$$

Substitution of Equations 9 and 12 into Equation 20 leads to

$$\sigma_N = \frac{\left(\cos\alpha - \cos\frac{\theta_s}{2}\right)\sigma_c}{\left(1 - \cos\frac{\theta_s}{2}\right)\cos\alpha} \tag{21}$$

Note that at point A (Figure 5) where $\alpha = 0$, Equation 21 indicates that $\sigma_N = \sigma_c$, which is consistent with the assumption made in the previous sections. On the other hand, at the free surface where $\alpha = \pm\theta_s/2$ (Figure 5), Equation 21 indicates that $\sigma_N = 0$ at these points. From Equation 21 it follows that the vertical stress distribution at the soil-tire interface is

$$\sigma_V = \frac{\left(\cos\alpha - \cos\frac{\theta_s}{2}\right)\cos\left(\alpha + \frac{\theta_s}{2}\right)\sigma_c}{\left(1 - \cos\frac{\theta_s}{2}\right)\cos\alpha} \tag{22}$$

Similarly, the horizontal stress distribution is

$$\sigma_H = \frac{\left(\cos\alpha - \cos\frac{\theta_s}{2}\right)\sin\left(\alpha + \frac{\theta_s}{2}\right)\sigma_c}{\left(1 - \cos\frac{\theta_s}{2}\right)\cos\alpha} \tag{23}$$

Shear Stress Distribution Along the Soil-Tire Interface

14. Figure 6 shows the plan view of a tire with a turn angle η with respect to the direction of motion. If slip in the plane of the wheel is defined by the slip ratio* S, then slip in the direction of the motion can be expressed as

$$S_m = \frac{S}{\cos\eta} \tag{24}$$

---

* For this analysis, slip ratio S is an input quantity.

The components of shear stress parallel and perpendicular to the plane of the wheel, τ_p and τ_N, respectively, can be obtained from the soil model presented in Appendix A. In view of Equation 23, the components of shear stress become

$$\tau_p = \frac{G\left(C + \sigma_N \tan \phi\right)S}{\left|\frac{GS}{\cos \eta}\right| + C + \sigma_N \tan \phi} \tag{25}$$

$$\tau_N = \frac{G\left(C + \sigma_N \tan \phi\right)S \tan \eta}{\left|\frac{GS}{\cos \eta}\right| + C + \sigma_N \tan \phi} \tag{26}$$

where σ_N is given by Equation 21. In Equations 25 and 26, G, C, and ϕ correspond, respectively, to the shear modulus, apparent cohesion, and apparent angle of internal friction of the material for the unconsolidated-undrained condition.

Deflection and Sinkage of a Flexible Tire

15. If the deflection of a flexible tire on a rigid surface under a given load W is denoted by Δ (Figure 1), then the corresponding deflection on a yielding soil Δ_t (Figure 7b) can be determined from the application of Equations 16 and 18.

$$\Delta_t = \frac{k_s}{k_s + k_t} \Delta \tag{27}$$

Similarly, if Z_r is the sinkage of a rigid wheel under a given load W (Figure 7c), then the corresponding sinkage Z of a flexible wheel (Figure 7b) is

$$Z = \left(\frac{k_t}{k_s + k_t}\right) Z_r \tag{28}$$

The sinkage Z_r can be calculated from the balance of forces in the vertical direction (Figure 8a)

$$W = DR \int_{-\frac{\theta_1}{2}}^{\frac{\theta_1}{2}} \left[\sigma_N \cos\left(\alpha + \frac{\theta_1}{2}\right) + \tau \sin\left(\alpha + \frac{\theta_1}{2}\right)\right] d\alpha \tag{29}$$

where θ_1 is defined in Figure 7c and σ_N is given by (see Equation 21)

$$\sigma_N = \frac{\left(\cos\alpha - \cos\frac{\theta_1}{2}\right)\sigma_c}{\cos\alpha\left(1 - \cos\frac{\theta_1}{2}\right)} \quad , \; -\frac{\theta_1}{2} \leq \alpha \leq \frac{\theta_1}{2} \tag{30}$$

The shear stress τ in Equation 29 can be obtained from the soil model described in Appendix A and has the following form:

$$\tau = \frac{G(C + \sigma_N \tan\phi)S}{|GS| + C + \sigma_N \tan\phi} \tag{31}$$

where σ_N is given by Equation 30. The slip ratio S is equivalent to the shearing strain ε in Appendix A. Note that the rate effect term appearing in Equation A4 of Appendix A is eliminated from Equation 31 as well as throughout the following derivations. However, if the mechanical properties of the terrain of interest indicate that the material is sensitive to rate of deformation, then the rate effect term must be included in the soil-wheel interaction model. The solution of Equation 29 leads to an expression for θ_1. The actual sinkage Z_r can then be calculated from (Figure 7c)

$$Z_r = R(1 - \cos\theta_1) \tag{32}$$

Relationships Governing Single Wheel Performance

Geometry of the problem

16. The geometry and boundary conditions for a flexible wheel-soil system are shown schematically in Figure 8b. The contact surface between the wheel and the soil is assumed to be an arc of a circle with a radius equal to or larger than the undeflected radius of the wheel. (Only in the case of the

rigid wheel is the radius equal to the undeflected radius.) The center of this circle O' is located at the intersection of the vertical line through point A and the bisector of the angle AOB. According to Figure 7b, the relationship between the angle θ_1, the sinkage Z, and the deflection of the tire Δ_t is

$$\theta_1 = \cos^{-1}\left(1 - \frac{Z + \Delta_t}{R}\right) \tag{33}$$

Also, from the geometry of Figure 7b

$$\theta_2 = \cos^{-1}\left(1 - \frac{\Delta_t}{R}\right) \tag{34}$$

From the geometry of Figure 8b

$$R' = \frac{Z}{1 - \cos\left(\theta_1 - \theta_2\right)} \tag{35}$$

Using Equations 33 and 34 to eliminate Z from Equation 35, we obtain the following relation for R' in terms of R and the central angles θ_1 and θ_2:

$$R' = R\,\frac{\sin\dfrac{\theta_1 + \theta_2}{2}}{\sin\dfrac{\theta_1 - \theta_2}{2}} \tag{36}$$

Equations 33 through 36 completely define the shape of the contact surface between the soil and the tire.

Tire internal motion resistance

17. The internal motion resistance (IMR) of the tire is expressed in terms of the deflection of the tire on a rigid surface. Data from a number of experiments where IMR has been measured are portrayed in Figure 9 (Turnage 1976) which shows that IMR increases rapidly with deflection. The dashed curves in Figure 9 are approximate upper and lower bounds to the test data. The solid curve in Figure 9 may be viewed as the average response. For the purpose of this study the solid curve is fitted with the following mathematical

expression for calculations of internal motion resistance:

$$IMR = \left[4\left(\frac{\Delta}{h}\right)^2 + 0.2\left(\frac{\Delta}{h}\right)\right]\frac{W}{10} \tag{37}$$

Motion resistance, drawbar pull,
torque, efficiency, and side force

18. We can now proceed to develop appropriate equations for motion resistance (MR), drawbar pull (DBP), torque (T), and efficiency (E). From Figures 6 and 8b

$$MR = R'D \int_{-\frac{(\theta_1 - \theta_2)}{2}}^{\frac{(\theta_1 - \theta_2)}{2}} \sigma_N \sin\left(\alpha + \frac{\theta_1 - \theta_2}{2}\right) d\alpha + IMR + MF \cos\eta \tag{38}$$

$$DBP = R'D \int_{-\frac{(\theta_1 - \theta_2)}{2}}^{\frac{(\theta_1 - \theta_2)}{2}} \tau_p \cos\left(\alpha + \frac{\theta_1 - \theta_2}{2}\right) d\alpha - MR \tag{39}$$

$$T = R'D \int_{-\frac{(\theta_1 - \theta_2)}{2}}^{\frac{(\theta_1 - \theta_2)}{2}} \tau_p \left(R' - \frac{R \sin\theta_2}{\sin\frac{\theta_1 - \theta_2}{2}} \cos\alpha\right) d\alpha \tag{40}$$

$$E = \frac{DBP}{T}(1 - S)(R - \Delta_t) \tag{41}$$

where σ_N and τ_p are given by Equations 21 and 25, respectively, with θ replaced by $\theta_1 - \theta_2$ and $MF = R^2\left[\theta_1 - (\sin 2\theta_1)/2\right]\sigma_c \sin\eta$. Similarly, from Figures 6 and 8 the side force (SF) is

$$SF = R'D \int_{-\frac{(\theta_1 - \theta_2)}{2}}^{\frac{(\theta_1 - \theta_2)}{2}} \tau_N \, d\alpha + MR \tan \eta \qquad (42)$$

where τ_N is given by Equation 26. The above system of equations provides a complete solution to the performance of a flexible tire traversing a yielding soil. A computer program called TIRE has been developed by the authors, which numerically solves the above system of equations.

PART III: PARAMETRIC STUDIES OF THE PERFORMANCE OF A FLEXIBLE WHEEL ON A YIELDING SOIL

General

19. In this part, the performance of a flexible wheel on different types of soil is parametrically investigated using the model developed in Part II. In addition, the effects of the applied load, the unloaded section width, the deflection of the tire, and the slip on the performance of the wheel are analyzed. The parametric studies are divided into three general areas: (a) wheel performance for a zero turn angle, (b) wheel performance for a nonzero turn angle, and (c) effects of soil parameters on wheel performance. Under the first area the effects of soil type, slip ratio, tire deflection, wheel load, and tire width on sinkage, motion resistance, drawbar pull, torque, and efficiency are studied. Under the second area the effects of soil type, slip ratio, and tire deflection on motion resistance, drawbar pull, side force, and efficiency are investigated. Under the third area the effects of variation of soil parameters (such as cohesion, angle of friction, and shear modulus) on the performance of a wheel for zero turn angle are studied.

20. The generic tire used in all the calculations was tire No. 4 which is described in Table 1. The tire radius was 14.1 in.*, its width 8.28 in., and its carcass section height was 6.35 in. All calculations were conducted for an applied wheel load W_o of 1000 lb except for cases where the wheel load was a variable. As indicated in Appendixes A and B, the soil was characterized by nine independent parameters. Two of these parameters, C_d and Λ (the rate effect parameters), were set to zero for the parametric studies. In addition, the soil density γ was taken to be the same for all soils studied here and assumed to be 117.5 lb/ft^3. Three types of soils were chosen for the parametric analysis of wheel performance for both zero and nonzero turn angles: a soft clay, a medium dense sand, and a mixed soil having both cohesive and frictional strengths. The soil types and the associated material constants are given in Table 2. It should be pointed out that the numerical values of the material constants in Table 2 are not for any specific site but

---

* A table of factors for converting non-SI units of measurement to SI (metric) units is given on page 3.

are chosen as "typical" values for the type of soil being simulated. For reference purposes and possible future use, Table 2 also includes the values of the WES cone index (CI) for each material. The results of the parametric studies are presented in the following sections.

Wheel Performance for Zero Turn Angle

Sinkage

21. The results of the calculations for assessing the effect of soil type, slip ratio, tire deflection Δ/h, wheel load W/W_o, and tire width D/R on sinkage Z/R are presented in Figures 10-27. Figures 10, 12, and 14 indicate that for all soils sinkage increases with increasing slip ratio. The rate of increase in sinkage, however, is higher for lower tire deflection. Figures 11, 13, and 15 present relationships between sinkage and tire deflection for clay, sand, and mixed soil, respectively. As indicated in these figures, the sinkage decreases rapidly with increasing tire deflections from zero (rigid tire) up to approximately 40 percent deflection. Beyond 40 percent deflection, the rate of decrease in sinkage is very small. Relationships between sinkage and wheel load for each of the three soils are presented in Figures 16-21. As expected, the sinkage increases with increasing wheel load. At high wheel loads (i.e., $W/W_o > 0.8$), doubling the wheel load more than doubles the sinkage for all soils. Figures 22-27 present relationships between sinkage and tire width. These figures show that for all soils sinkage decreases rapidly as tire width increases from R/10 up to a tire width of about half the radius. For tire widths larger than half the radius, however, the decrease in sinkage is very small.

Motion resistance

22. The effects of soil type, slip ratio, tire deflection, wheel load, and tire width on motion resistance MR/W are portrayed in Figures 28-45. Figures 28, 30, and 32 indicate that motion resistance initially decreases with increasing slip ratio up to a slip ratio of approximately 4 percent and increases thereafter. This initial decrease in motion resistance has been observed experimentally and is attributed to the plowing action of the tire. The increase in motion resistance at higher slip ratios is due to an increase in sinkage (see Figures 10, 12, and 14). Relationships between motion resistance and tire deflection for each soil type studied are shown in Figures 29,

31, and 33. The motion resistance initially decreases with increasing tire deflection and reaches a minimum value at about 30 percent deflection. At tire deflections higher than 30 percent, the motion resistance increases again. The initial decrease in motion resistance can be attributed to the initial and rapid decrease in sinkage (Figures 11, 13, and 15). The increase in motion resistance at deflections larger than 40 percent is due to a rapid increase in the internal motion resistance of the tire (Figure 9). Figures 34-39 present relationships between the motion resistance and wheel load. As indicated in these figures, the motion resistance increases as the wheel load increases. This is the consequence of increase in the sinkage as the wheel load increases (Figures 16-21). Relationships between motion resistance and tire width are portrayed in Figures 40-45. These figures show that the motion resistance decreases as the width of the tire increases. This is expected because as the width of the tire increases, the sinkage decreases (Figures 22-27). It should be pointed out that in Figures 40-45 the internal motion resistance of the tire was assumed to be independent of the width of the tire. If the effect of width on the internal motion resistance of the tire were taken into consideration, the results in Figures 40-45 would have been different.

Drawbar pull

23. Figures 46-63 portray the effects of soil type, slip ratio, tire deflection, wheel load, and tire width on drawbar pull P/W. Figure 46 indicates that for clay soil the drawbar pull increases rapidly for slip ratios between zero and about 10 percent. For higher slip ratios, the increase in the drawbar pull is relatively small. For sand and mixed soil, on the other hand, the drawbar pull increases rapidly and reaches a peak value at about 20 percent slip ratio (Figures 48 and 50). The drawbar pull then drops for slip ratios in the range of about 20 to 50 percent. Beyond 50 percent slip ratio, the drawbar pull increases very slowly. This type of behavior also has been observed experimentally. Relationships between drawbar pull and tire deflection for each type of soil studied are presented in Figures 47, 49, and 51. As indicated in Figures 47 and 49, the drawbar pull initially increases with deflection up to a deflection of approximately 50 percent. Beyond this deflection, the drawbar pull decreases because of a rapid increase in the internal motion resistance of the tire (Figure 9). This trend is less evident in the case of mixed soil (Figure 51) because of shallow sinkage. Figures 52-57

present relationships between drawbar pull and wheel load. As expected, the drawbar pull decreases rapidly as the wheel load increases. This rapid decrease in the drawbar pull is due to an increase in sinkage (Figures 16-21), which ultimately leads to an increase in motion resistance of the tire (Figures 34-39). Relationships between drawbar pull and tire width are presented in Figures 58-63. As indicated in these figures, the drawbar pull increases as the tire width increases. Most of the increase in the drawbar pull takes place for tire widths less than 50 percent of the radius. For larger tire widths, the rate of increase in drawbar pull is relatively small. This behavior is also related to sinkage (Figures 22-27), where it is observed that most of the decrease in sinkage takes place for tire widths less than 50 percent of the radius.

Torque

24. The results of the calculations for assessing the effect of soil type, slip ratio, tire deflection, wheel load, and tire width on torque T/WR are presented in Figures 64-81. The trends in these figures are similar to those in Figures 46-63. In fact, if the wheel is rigid and the motion resistance is negligible, the results of Figures 64-81 can be obtained from the corresponding results of Figures 46-63 by multiplying the latter results by the radius of the wheel R.

Efficiency

25. Figures 82-99 portray the effects of soil type, slip ratio, tire deflection, wheel load, and tire width on efficiency E. Figures 82, 84, and 86 indicate that for all soils efficiency increases rapidly and reaches a peak value at a relatively small slip ratio and then decreases to zero at a slip ratio of 100 percent. Relationships between efficiency and tire deflection are shown in Figures 83, 85, and 87. It is observed from these figures that the tire reaches its maximum efficiency at a tire deflection between 30 and 40 percent. Figures 88-93 present relationships between efficiency and wheel load. As expected, efficiency decreases with increasing wheel load. Figures 94-99 portray relationships between efficiency and tire width. These figures indicate that efficiency increases as tire width increases. Most of the increase in efficiency takes place at tire widths less than 50 percent of the radius.

Wheel Performance for Nonzero Turn Angle

Motion resistance

26. The effects of turn angle on motion resistance for the three soils considered for the parameter study are presented in Figures 100-105. Motion resistance, as expected, increases with increasing turn angle for all soils.

Drawbar pull

27. Figures 106-111 show the effects of turn angle on drawbar pull. Drawbar pull decreases with increasing turn angle, as it should, and actually becomes negative for higher turn angles. The decrease in the drawbar pull is a direct result of the corresponding increase in motion resistance shown in Figures 100-105.

Side force

28. Figures 112-117 portray the relationships between side force SF/W and turn angle for the three soils considered in this study and they indicate that side force increases rapidly with the turn angle.

Efficiency

29. The effects of turn angle on efficiency are shown in Figures 118-123. These figures indicate that efficiency drops rapidly with increasing turn angle for all three soils considered in this study. The efficiency actually becomes negative at turn angles where the drawbar pull also becomes negative (Figures 106-111).

Effects of Soil Parameters on Wheel Performance

30. This section investigates the effects of the shear strength parameters C and ϕ and the shear modulus G on the performance of the wheel for zero turn angle. As indicated earlier, the calculations are for tire No. 4 of Table 1 and for an applied wheel load of 1000 lb. The calculations are figured for 20 percent slip and 35 percent deflection and are divided into two parts. The first part deals with clay soil ($\phi = 0$ material) where C and G are varied and the remaining material parameters K, I_s, and $\bar{\eta}$ are kept constant and correspond to the values given in Table 2 for soft clay. The second part deals with sand ($C = 0$ material) where ϕ and G are varied and parameters K, I_s, and $\bar{\eta}$ are kept constant, corresponding to the values given in Table 2 for medium dense sand.

Sinkage

31. Figures 124 and 125 demonstrate the effects of soil parameters C, ϕ, and G on sinkage. The calculations are conducted for three values of shear modulus, 20, 200, and 2000 psi, and a range of values for C and ϕ. The results of Figures 124 and 125 indicate that sinkage decreases with an increase in the strength parameters C, ϕ, and G. In the case of clay soil the decrease in sinkage with increasing cohesion is very pronounced for low values of cohesion (C approximately less than 6 psi). Beyond this value of C sinkage is not very sensitive to cohesion for this particular tire configuration and wheel load. In the case of sand, the decrease in sinkage with increasing angles of friction is gradual and steady. An important conclusion drawn from Figures 124 and 125 is that for a physically realistic range of values of shear modulus (200 to 2000 psi), an order of magnitude change in G has only a small effect on the calculated value of sinkage. The same trends have been observed for resistance of soil to cone penetration by Rohani and Baladi (1981). Therefore, reasonable uncertainties in the value of G do not greatly affect the calculated value of sinkage.

Motion resistance

32. The effects of soil parameters on the calculated value of motion resistance are depicted in Figures 126 and 127. The trends in these figures are similar to those observed for sinkage. Motion resistance decreases with increasing C and ϕ. This is a consequence of the corresponding decrease in sinkage.

Drawbar pull

33. Figures 128 and 129 show the effects of the soil parameters C, ϕ, and G on drawbar pull. The drawbar pull increases with increasing values of these parameters. But the rate of increase diminishes as the shear strength parameters increase. The trends in these figures are reflections of the previous figures (Figures 124 through 127).

Torque

34. Figures 130 and 131 demonstrate the effects of the soil parameters on torque. These figures show the increase in torque with increasing shear strength and exhibit the same trends as the drawbar pull (Figures 128 and 129).

PART IV: CORRELATION OF TEST DATA WITH MODEL PREDICTIONS

Background

35. The results of the parameter studies presented in Part III indicated that the model predictions are qualitatively in agreement with the observed performance of flexible wheels on a yielding soil. A detailed quantitative validation of the proposed model requires controlled laboratory tests and the measurement of the appropriate soil properties discussed in Appendixes A and B. A partial validation of the model, however, can be accomplished by using test data already documented in the literature. The deficiency in using existing data from the literature is the lack of information on the mechanical properties of the soil used in their experiment. Usually the soil is characterized in terms of simple indexes such as the mobility cone index (CI). These indexes must be translated to the appropriate soil properties required by the proposed model. This requires a separate analysis (divorced from the soil-wheel interaction model) to make such a translation. The numerical values of several material constants from an index such as the CI must be determined. This introduces uncertainties (or a bias) in the numerical values of the constants which, of course, will affect the degree of correlation between the model predictions and the test data. In spite of such uncertainties, a partial validation of the proposed soil-wheel interaction model is attempted in this part of the report.

Test Parameters

36. Test data for 14 different tires and two soil types (clay and sand) were selected from the literature for correlation with model predictions (Turnage 1972 and Durham 1976). The data reported by Turnage are for the zero turn angle; the data reported by Durham are for the nonzero turn angle. The characteristics of the test tires are given in Table 1. As indicated in the table, the test tires range from a bicycle tire (tire No. 6) to tires with $D/R > 1$ (tire Nos. 8-11). Both Turnage and Durham used the WES mobility CI to characterize the soil used in their experiments. Using a methodology developed by Rohani and Baladi (1981), the authors of the study reported herein estimated the appropriate soil properties required by the model from the CI

data. Correlations of the test data with the corresponding model predictions are presented in the subsequent sections. The correlations include a least-square fit and the calculation of the standard deviation $\bar{\sigma}$. The parameter $\bar{\sigma}$ signifies the deviation between the experimental data and the corresponding model predictions. It is a measure of the deviation of the data from the line of perfect correlation.

Correlation for Zero Turn Angle

Clay

37. Table 3 contains the pertinent information for the clay experiments as well as the corresponding model predictions. It contains 65 data points for 10 flexible tires (Table 1) at different deflections and wheel loads. The tests, however, were all conducted at 20 percent slip. Column 4 in Table 3 shows the measured CI for each test. Columns 5-8 present the corresponding soil properties required by the model. As indicated earlier, these properties were estimated from the CI data. In addition to the soil properties shown in Table 3, the model requires two more soil constants related to volume change characteristics of the material due to shearing strain (parameters $\bar{\eta}$ and I_s in Equation B10 of Appendix B). The numerical values of these constants were estimated based on typical triaxial test data available in the literature and were assumed to be the same for all tests. They are $\bar{\eta} = 3$ and $I_s = 0.075$.

38. The last six columns of Table 3 contain the test results and the corresponding model predictions for drawbar pull, torque, and sinkage in dimensionless forms. The calculated results are plotted against the corresponding measured data in Figures 132-134 for drawbar pull, torque, and sinkage, respectively. Comparisons between the least-square lines and the 45-deg lines indicate that the overall correlation of the model predictions with the test data is very reasonable in spite of the general scatter in the test data and the uncertainty in estimating several soil properties from a single CI. In particular, the sinkage (which is one of the most difficult parameters to predict) correlates well with the test results. It should be pointed out that the gross discrepancies between the predicted and measured sinkage results in Table 3 are for very shallow depths which, from a practical point of view, should be viewed as zero. The degree of correlation exhibited between the

test results and model predictions indicates that the physical basis of the proposed soil-wheel interaction model is sound.

Sand

39. The experimental results and the corresponding model predictions for sand are presented in Table 4 and consist of 100 data points. The data represent 10 flexible tires and 3 rigid wheels (Table 1), all tested at 20 percent slip. The measured CI and the estimated soil properties for each test are also presented in Table 4. The numerical values of the parameters $\bar{\eta}$ and I_s were estimated from available triaxial test data and were assumed to be the same for all tests. They are $\bar{\eta} = 3$ and $I_s = 0.01$.

40. The measured test results and the corresponding model predictions are plotted in Figures 135-137 for drawbar pull, torque, and sinkage, respectively. Again, similar to the clay data, the degree of correlation between the measured and calculated results is very reasonable, indicating that the physical basis of the model is sound for both cohesive soil and granular materials. Therefore, it may be concluded that the proposed model is capable of simulating the interaction between a flexible tire and a soil exhibiting both cohesive and frictional properties.

Correlation for Nonzero Turn Angle

Clay

41. Table 5 contains the results of 19 tests in clay at four different turn angles and the corresponding model predictions. These results are for one tire (tire No. 14 in Table 1) at different deflections, wheel loads, and slips. The measured data, consisting of drawbar pull, torque, and side force, are plotted against the corresponding calculated parameters in Figures 138-140, respectively. Considering the limited nature of the data, the degree of correlation shown in Figures 138-140 is similar to the previous results for the zero turn angle. This indicates that the model is capable of correctly treating the kinematics of the wheel for the nonzero turn angle. Additional data for different types of tires are needed to further investigate the effects of the turn angle on the performance of the wheel.

Sand

42. The test results and the corresponding model predictions for sand are given in Table 6 for four different turn angles. Table 6 contains the

results of 43 tests for one tire (tire No. 14 in Table 1) at different deflections, wheel loads, and slips. Figures 141-143 portray the correlation between the measured data and the corresponding calculated results for drawbar pull, torque, and side force, respectively. Again, the correlation between the measured data and the calculated results is very good. Therefore, the treatment of the nonzero turn angle in the model is physically sound for both clay and sand. This indicates that the model is capable of predicting the performance of a flexible wheel in a nonzero turn angle mode on soils exhibiting both cohesive and frictional strength components.

PART V: SUMMARY AND RECOMMENDATIONS

43. A mathematical model for calculating the motion resistance, sinkage, drawbar pull, torque, and side force of a flexible wheel traversing a yielding soil was developed and computerized for numerical application. The entire soil-wheel interaction process was treated as two springs in series, one describing the flexibility of the tire and the other describing the strength of the soil. Mathematical expressions were derived for the two spring constants in terms of load-deflection characteristics of the tire, the undeflected configuration of the wheel, and the mechanical properties of the soil. The spring constant for the soil was developed using considerations of geometry and spherical cavity expansion in an elastic-plastic medium. The motion resistance, drawbar pull, torque, efficiency, and side force for the flexible wheel were obtained from the equilibrium equations by assuming that the deformed boundary of the tire is an arc of a circle with a radius equal to or greater than the undeflected radius of the wheel.

44. An extensive series of parametric calculations was conducted to demonstrate the reasonableness of the trends predicted by the methodology and to study the performance of a flexible wheel on different types of soil under various kinematic conditions. From the results of this series of parameter studies, the following qualitative conclusions can be drawn:

a. The shear strength of soft soil strongly affects the performance of a flexible wheel.

b. The sinkage of a flexible wheel traversing a yielding surface increases with (1) increasing slip ratio, (2) decreasing tire deflections, (3) increasing tire load, and (4) decreasing tire width.

c. The motion resistance of a flexible wheel on soft soil generally increases with (1) increasing slip ratio, (2) increasing tire load, (3) decreasing tire width, and (4) increasing turn angle. In addition, the motion resistance initially decreases with increasing tire deflection and reaches a minimum value at about 30 percent deflection. Beyond 30 percent deflection the motion resistance increases as the tire deflection continues to increase.

d. The drawbar pull of a flexible wheel on soft soil decreases with (1) increasing tire load, (2) decreasing tire width, and (3) increasing turn angle. For cohesive material (clay), the drawbar pull increases as slip ratio increases. For either frictional material (sand) or mixed soil, however, the drawbar pull increases rapidly and reaches a peak at about 20 percent

slip ratio. For slip ratios between 20 and 50 percent the drawbar pull decreases. It then increases slowly beyond 50 percent slip ratio. The drawbar pull initially increases as the tire deflection increases and reaches a peak value at about 50 percent deflection. Beyond 50 percent deflection, the drawbar pull decreases.

e. The relationships between torque and soil type, slip ratio, tire deflection, wheel load, and tire width are very similar to the corresponding relationships for the drawbar pull.

f. The efficiency of a flexible tire on soft soil increases with (1) decreasing tire load, (2) increasing tire width, and (3) decreasing turn angle. A maximum efficiency could be obtained at relatively small slip ratios and a tire deflection between 30 and 40 percent.

45. Although a partial validation of the proposed interaction model was established by comparing the results of a large number of laboratory test data for both clay and sand with the corresponding model predictions, it is recommended that a detailed quantitative validation of the model be conducted to determine the accuracy and range of application of the proposed model.

REFERENCES

Baladi, G. Y., and Rohani, B. 1979. "A Terrain-Vehicle Interaction Model for Analysis of Steering Performance of Track-Laying Vehicles," Technical Report GS-79-6, U. S. Army Engineer Waterways Experiment Station, CE, Vicksburg, Miss.

Bernard, R. S., and Creighton, D. C. 1976. "Projectile Penetration in Earth Materials: Theory and Computer Analysis," Technical Report S-76-13, U. S. Army Engineer Waterways Experiment Station, CE, Vicksburg, Miss.

Durham, G. N. 1976. "Powered Wheels in the Turned Mode Operating on Yielding Soils," Technical Report M-76-9, U. S. Army Engineer Waterways Experiment Station, CE, Vicksburg, Miss.

Fujimoto, Y. 1977. "Performance of Elastic Wheels on Yielding Cohesive Soils," Journal of Terramechanics, Vol 14, No. 4.

Hvorslev, M. J. 1970. "The Basic Sinkage Equations and Bearing Capacity Theories," Technical Report M-70-1, U. S. Army Engineer Waterways Experiment Station, CE, Vicksburg, Miss.

Kondner, R. L. 1963. "Hyperbolic Stress-Strain Response: Cohesive Soils," Journal, Soil Mechanics and Foundation Division, American Society of Civil Engineers, Vol 89, No. SM1, pp 115-143.

Rohani, B. and Baladi, G. Y. 1981. "Correlation of Mobility Cone Index with Fundamental Engineering Properties of Soil," Miscellaneous Paper SL-81-4, U. S. Army Engineer Waterways Experiment Station, CE, Vicksburg, Miss.

Turnage, G. W. 1972. "Performance of Soils Under Tire Loads; Report 8, Application of Test Results to Tire Selection for Off-Road Vehicles," Technical Report 3-666, U. S. Army Engineer Waterways Experiment Station, CE, Vicksburg, Miss.

Turnage, G. W. 1976. "In-Soil Tractive Performance of Selected Radial and Bias-Ply Tires," 1976 Annual Meeting of the American Society of Agricultural Engineers, Paper 76-1520, Chicago, Ill.

Vesic, A. S. 1972. "Expansion of Cavities in Infinite Soil Mass," Journal, Soil Mechanics and Foundation Division, American Society of Civil Engineers, Vol 98, No. SM3, Proc Paper 8790.

Wong, J., and Reece, A. R. 1967. "Prediction of Rigid Wheel Performance Based on the Analysis of Soil-Wheel Stresses," Journal of Terramechanics, Vol 4, No. 1.

Table 1

Characteristics of Laboratory Test Tires

Tire No.	Tire Width D, in.	Tire Radius R, in.	Carcass Section Height h, in.
1	4.18	7.08	3.10
2	4.18	14.00	3.16
3	6.60	14.15	5.30
4	8.28	14.10	6.35
5	11.40	20.66	9.03
6	1.73	14.08	1.40
7	6.42	8.05	3.40
8	11.12	8.87	5.40
9	15.20	8.75	5.30
10	16.13	12.15	6.05
11	15.00	14.85	7.65
12A	12.00	13.95	Rigid
12B	6.00	13.90	Rigid
12C	3.00	13.95	Rigid
13	7.00	13.92	5.17
14	6.26	10.16	5.04

Table 2

Matrix of Material Types and Associated Constants

Material Simulated	Approximate Standard Cone Index CI (0 - 6 in. Depth)	Cohesion C psi	Angle of Friction ϕ, deg	Shear Modulus G psi	Bulk Modulus K psi	I_s*	$\bar{\eta}$*
Soft clay	30	2.5	0	200	400	3	0.075
Medium dense sand	30	0	30	75	150	3	0.01
Mixed soil	120	2.5	30	75	150	3	0.075

* The parameters I_s and $\bar{\eta}$ are related to the volume change characteristics of soil due to shearing strain.

Table 3

Comparison of Test Data with Model Predictions for Clay; 20 Percent Slip and Zero Turn Angle

				SOIL PROPERTIES				TEST RESULTS			MODEL PREDICTIONS		
TIRE NO	TIRE DEFLECTION PERCENT	WHEEL LOAD LB	MEASURED CONE INDEX	COHESION C PSI	ANGLE OF FRICTION ϕ, DEG	SHEAR MODULUS G, PSI	BULK MODULUS K, PSI	DRAWBAR PULL P/W	TORQUE T/WR	SINKAGE Z/R	DRAWBAR PULL P/W	TORQUE T/WR	SINKAGE Z/R
1	15	230	66	5.5	0.	150	300	0.457	0.508	0.047	0.431	0.462	0.038
1	15	341	66	5.5	0.	150	300	0.378	0.442	0.088	0.277	0.369	0.102
1	15	441	66	5.5	0.	150	300	0.263	0.377	0.144	0.179	0.332	0.188
1	25	220	62	5.0	0.	150	300	0.450	0.508	0.034	0.526	0.525	0.024
1	25	341	66	5.5	0.	150	300	0.405	0.452	0.056	0.360	0.402	0.063
1	25	448	65	5.4	0.	150	300	0.330	0.420	0.112	0.241	0.336	0.130
1	35	224	66	5.5	0.	150	300	0.893	0.817	0.001	0.618	0.591	0.013
1	35	337	66	5.5	0.	150	300	0.605	0.593	0.031	0.415	0.435	0.041
1	35	449	68	5.7	0.	150	300	0.479	0.521	0.071	0.300	0.359	0.081
1	15	230	46	4.5	0.	100	200	0.300	0.398	0.065	0.331	0.394	0.069
1	25	117	46	4.5	0.	100	200	1.034	0.942	0.014	0.742	0.704	0.006
1	15	94	26	2.0	0.	80	160	0.298	0.361	0.085	0.414	0.449	0.042
1	15	336	41	4.3	0.	100	200	0.155	0.333	0.155	0.175	0.327	0.186
1	25	330	42	4.4	0.	100	200	0.218	0.354	0.099	0.263	0.344	0.109
1	35	440	37	4.0	0.	100	200	0.050	0.270	0.131	0.155	0.284	0.183
1	25	51	26	2.0	0.	80	160	0.882	0.864	0.001	0.823	0.775	0.005
1	25	185	22	2.0	0.	75	150	0.141	0.385	0.151	0.221	0.322	0.136
1	25	195	21	2.0	0.	75	150	0.149	0.391	0.171	0.200	0.313	0.154
2	8	308	48	4.7	0.	150	300	0.399	0.473	0.051	0.328	0.396	0.038
2	15	221	48	4.7	0.	150	300	0.611	0.593	0.023	0.563	0.576	0.010
2	25	652	40	4.2	0.	100	200	0.276	0.381	0.114	0.167	0.305	0.137
2	15	196	20	1.9	0.	75	150	0.296	0.398	0.081	0.280	0.362	0.063
2	25	370	19	1.9	0.	75	150	0.111	0.361	0.159	0.126	0.282	0.165
2	35	222	19	1.9	0.	75	150	0.414	0.436	0.061	0.338	0.400	0.037
2	35	406	19	1.9	0.	75	150	0.219	0.378	0.129	0.119	0.271	0.146

(Continued)

Table 3 (Continued)

TIRE NO	TIRE DEFLECTION PERCENT	WHEEL LOAD LB	MEASURED CONE INDEX	SOIL PROPERTIES				TEST RESULTS			MODEL PREDICTIONS		
				COHESION C PSI	ANGLE OF FRICTION ϕ, DEG	SHEAR MODULUS G, PSI	BULK MODULUS K, PSI	DRAWBAR PULL P/W	TORQUE T/WR	SINKAGE Z/R	DRAWBAR PULL P/W	TORQUE T/WR	SINKAGE Z/R
2	15	448	46	4.5	0.	100	200	0.404	0.432	0.047	0.254	0.351	0.077
2	15	628	48	4.7	0.	150	300	0.304	0.377	0.079	0.188	0.330	0.132
2	25	640	47	4.7	0.	150	300	0.275	0.348	0.071	0.234	0.337	0.091
2	35	635	45	4.5	0.	100	200	0.294	0.335	0.056	0.222	0.326	0.081
2	8	301	22	2.0	0.	75	150	0.259	0.407	0.110	0.109	0.315	0.197
2	25	201	22	2.0	0.	75	150	0.458	0.461	0.044	0.353	0.405	0.038
3	25	676	22	2.0	0.	75	150	0.083	0.301	0.136	0.152	0.282	0.164
3	15	660	40	4.2	0.	100	200	0.327	0.416	0.081	0.327	0.389	0.061
3	15	423	20	1.9	0.	75	150	0.189	0.331	0.132	0.239	0.339	0.103
3	25	606	20	1.9	0.	75	150	0.058	0.294	0.171	0.177	0.292	0.142
3	35	439	20	1.9	0.	75	150	0.362	0.417	0.052	0.342	0.385	0.048
3	35	634	21	2.0	0.	75	150	0.215	0.310	0.085	0.212	0.302	0.101
3	35	834	21	2.0	0.	75	150	0.035	0.339	0.172	0.109	0.251	0.181
4	35	444	40	4.2	0.	100	200	0.928	0.897	0.001	0.762	0.702	0.004
4	25	1095	50	4.8	0.	100	200	0.217	0.304	0.062	0.367	0.401	0.054
4	15	643	30	2.0	0.	100	200	0.300	0.363	0.092	0.220	0.331	0.129
4	25	765	19	1.9	0.	75	150	0.195	0.367	0.114	0.196	0.298	0.139
4	25	1804	43	4.5	0.	100	200	0.001	0.250	0.186	0.146	0.285	0.200
4	35	449	32	2.3	0.	75	150	0.650	0.624	0.017	0.546	0.530	0.018
4	35	648	22	2.0	0.	75	150	0.344	0.398	0.049	0.321	0.363	0.061
4	35	862	23	2.0	0.	75	150	0.143	0.283	0.085	0.220	0.302	0.108
6	15	107	40	4.2	0.	100	200	0.439	0.440	0.033	0.315	0.375	0.028
6	15	214	40	4.2	0.	100	200	0.271	0.386	0.081	0.140	0.312	0.139
7	35	449	42	4.4	0.	100	200	0.341	0.412	0.020	0.397	0.431	0.051
7	15	214	40	4.2	0.	100	200	0.388	0.453	0.005	0.555	0.565	0.020

(Continued)

Table 3 (Concluded)

TIRE NO	TIRE DEFLECTION PERCENT	WHEEL LOAD LB	MEASURED CONE INDEX	SOIL PROPERTIES				TEST RESULTS			MODEL PREDICTIONS		
				COHESION C PSI	ANGLE OF FRICTION ϕ, DEG	SHEAR MODULUS G, PSI	BULK MODULUS K, PSI	DRAWBAR PULL P/W	TORQUE T/WR	SINKAGE Z/R	DRAWBAR PULL P/W	TORQUE T/WR	SINKAGE Z/R
8	15	440	21	2.0	0.	75	150	0.132	0.341	0.161	0.304	0.387	0.107
8	15	458	27	2.0	0.	85	170	0.279	0.455	0.098	0.296	0.384	0.113
8	35	459	46	4.5	0.	100	200	0.739	0.828	0.001	0.747	0.657	0.008
8	15	214	25	2.0	0.	75	150	0.500	0.607	0.018	0.645	0.632	0.018
8	15	572	23	2.0	0.	75	150	0.056	0.241	0.129	0.197	0.339	0.189
9	15	222	29	2.0	0.	100	200	0.586	0.642	0.014	0.808	0.777	0.010
9	15	222	27	2.0	0.	85	170	0.586	0.642	0.014	0.781	0.755	0.011
9	25	446	28	2.0	0.	100	200	0.498	0.587	0.018	0.567	0.555	0.035
11	8	226	28	2.0	0.	100	200	0.730	0.844	0.001	0.853	0.840	0.004
11	25	878	28	2.0	0.	100	200	0.440	0.552	0.027	0.465	0.477	0.042
11	15	445	29	2.0	0.	100	200	0.506	0.617	0.013	0.691	0.676	0.013
11	25	877	24	2.0	0.	75	150	0.324	0.438	0.022	0.432	0.451	0.048
11	25	1139	22	2.0	0.	75	150	0.176	0.337	0.075	0.314	0.373	0.089
13	1	213	22	2.0	0.	75	150	0.296	0.397	0.077	0.236	0.353	0.054
13	3	427	22	2.0	0.	75	150	0.096	0.323	0.144	0.116	0.330	0.182

Table 4

Comparison of Test Data with Model Predictions for Sand; 20 Percent Slip and Zero Turn Angle

				SOIL PROPERTIES				TEST RESULTS			MODEL PREDICTIONS		
TIRE NO	TIRE DEFLECTION PERCENT	WHEEL LOAD LB	MEASURED CONE INDEX	COHESION C PSI	ANGLE OF FRICTION ϕ, DEG	SHEAR MODULUS G, PSI	BULK MODULUS K, PSI	DRAWBAR PULL P/W	TORQUE T/WR	SINKAGE Z/R	DRAWBAR PULL P/W	TORQUE T/WR	SINKAGE Z/R
1	15	83	103	0.	41.0	145	290	0.217	0.368	0.093	0.358	0.393	0.072
1	15	98	95	0.	40.0	140	280	0.265	0.311	0.138	0.325	0.372	0.093
1	25	117	106	0.	41.0	150	300	0.427	0.391	0.129	0.419	0.447	0.075
1	15	113	59	0.	36.0	150	300	0.142	0.360	0.178	0.260	0.328	0.133
1	15	202	59	0.	36.0	150	300	0.025	0.378	0.225	0.191	0.305	0.246
1	25	231	62	0.	38.0	145	290	0.099	0.308	0.160	0.271	0.363	0.209
1	35	204	26	0.	25.0	50	100	-0.078	0.316	0.428	0.083	0.252	0.400
1	25	231	117	0.	41.0	200	400	0.229	0.323	0.083	0.346	0.418	0.167
1	35	106	112	0.	41.0	175	350	0.443	0.448	0.031	0.514	0.518	0.045
1	35	150	109	0.	41.0	175	350	0.367	0.373	0.044	0.466	0.490	0.075
1	35	219	117	0.	41.0	200	400	0.333	0.371	0.052	0.419	0.468	0.123
1	25	339	73	0.	39.0	175	350	0.088	0.260	0.209	0.237	0.359	0.294
2	15	416	73	0.	39.0	175	350	0.118	0.367	0.159	0.230	0.330	0.158
2	15	425	76	0.	39.0	200	400	0.134	0.363	0.119	0.238	0.337	0.156
2	35	246	19	0.	25.0	35	70	0.122	0.380	0.219	0.115	0.250	0.192
2	15	210	98	0.	40.0	165	330	0.257	0.380	0.063	0.314	0.371	0.074
2	15	420	97	0.	40.0	150	300	0.157	0.347	0.108	0.225	0.328	0.160
2	25	329	97	0.	40.0	150	300	0.313	0.370	0.057	0.330	0.403	0.098
2	35	424	98	0.	40.0	165	330	0.351	0.412	0.059	0.362	0.448	0.105
2	15	415	57	0.	36.0	150	300	0.077	0.382	0.186	0.185	0.298	0.184
2	15	402	33	0.	30.0	50	100	0.035	0.377	0.286	0.040	0.203	0.309
2	35	602	29	0.	30.0	40	80	-0.038	0.413	0.406	0.013	0.222	0.401
3	15	218	94	0.	40.0	140	280	0.431	0.455	0.031	0.372	0.387	0.031
3	35	238	98	0.	40.0	165	330	0.500	0.470	0.020	0.549	0.542	0.014
3	35	440	104	0.	41.0	150	300	0.484	0.478	0.024	0.470	0.484	0.034

(Continued)

Table 4 (Continued)

TIRE NO	TIRE DEFLECTION PERCENT	WHEEL LOAD LB	MEASURED CONE INDEX	SOIL PROPERTIES				TEST RESULTS			MODEL PREDICTIONS		
				COHESION C PSI	ANGLE OF FRICTION ϕ, DEG	SHEAR MODULUS G, PSI	BULK MODULUS K, PSI	DRAWBAR PULL P/W	TORQUE T/WR	SINKAGE Z/R	DRAWBAR PULL P/W	TORQUE T/WR	SINKAGE Z/R
3	15	443	63	0.	38.0	150	300	0.235	0.375	0.090	0.284	0.335	0.087
3	15	838	50	0.	35.0	150	300	0.035	0.366	0.218	0.172	0.280	0.208
3	25	845	57	0.	36.0	150	300	0.140	0.361	0.168	0.252	0.334	0.156
3	15	278	74	0.	39.0	175	350	0.338	0.394	0.049	0.351	0.375	0.044
3	35	612	28	0.	30.0	35	70	0.109	0.371	0.247	0.132	0.242	0.187
4	25	219	67	0.	38.0	190	380	0.493	0.509	0.032	0.467	0.454	0.011
4	25	454	71	0.	39.0	150	300	0.458	0.467	0.052	0.416	0.422	0.035
4	35	868	74	0.	39.0	175	350	0.397	0.422	0.039	0.432	0.452	0.063
4	25	134	66	0.	38.0	150	300	0.455	0.553	0.023	0.479	0.460	0.005
4	25	126	66	0.	38.0	150	300	0.468	0.561	0.001	0.482	0.461	0.005
4	25	176	67	0.	38.0	190	380	0.455	0.542	0.001	0.477	0.460	0.008
4	25	230	72	0.	39.0	170	340	0.413	0.507	0.014	0.477	0.463	0.012
4	25	340	71	0.	39.0	150	300	0.415	0.491	0.029	0.443	0.439	0.022
4	25	543	66	0.	38.0	150	300	0.337	0.448	0.039	0.383	0.398	0.049
4	25	597	69	0.	39.0	125	250	0.313	0.428	0.044	0.368	0.389	0.056
4	25	144	70	0.	39.0	140	280	0.479	0.502	0.033	0.492	0.471	0.006
4	25	240	69	0.	39.0	125	250	0.483	0.528	0.008	0.458	0.447	0.013
4	25	449	66	0.	38.0	150	300	0.374	0.478	0.032	0.403	0.410	0.037
4	25	446	66	0.	38.0	150	300	0.395	0.466	0.023	0.403	0.411	0.036
4	25	1155	48	0.	35.0	140	280	0.094	0.374	0.182	0.235	0.314	0.168
4	15	437	33	0.	30.0	50	100	0.137	0.372	0.163	0.158	0.228	0.126
4	15	227	107	0.	41.0	150	300	0.489	0.506	0.048	0.411	0.411	0.019
4	15	448	105	0.	41.0	150	300	0.375	0.419	0.065	0.355	0.377	0.050
4	15	839	102	0.	41.0	145	290	0.224	0.357	0.096	0.276	0.336	0.115
4	25	347	105	0.	41.0	150	300	0.441	0.520	0.001	0.473	0.465	0.020

(Continued)

Table 4 (Continued)

TIRE NO	TIRE DEFLECTION PERCENT	WHEEL LOAD LB	MEASURED CONE INDEX	SOIL PROPERTIES				TEST RESULTS			MODEL PREDICTIONS		
				COHESION C PSI	ANGLE OF FRICTION ϕ, DEG	SHEAR MODULUS G, PSI	BULK MODULUS K, PSI	DRAWBAR PULL P/W	TORQUE T/WR	SINKAGE Z/R	DRAWBAR PULL P/W	TORQUE T/WR	SINKAGE Z/R
4	25	194	94	0.	40.0	140	280	0.459	0.531	0.001	0.495	0.476	0.009
4	15	220	49	0.	35.0	150	300	0.364	0.406	0.057	0.330	0.340	0.027
4	15	442	53	0.	36.0	130	260	0.251	0.375	0.104	0.285	0.320	0.068
4	15	852	55	0.	36.0	140	280	0.081	0.358	0.180	0.216	0.293	0.150
4	15	814	53	0.	36.0	130	260	0.077	0.395	0.226	0.216	0.291	0.145
4	25	141	64	0.	38.0	150	300	0.582	0.543	0.003	0.478	0.459	0.006
4	25	168	65	0.	38.0	150	300	0.582	0.552	0.001	0.470	0.454	0.008
4	25	199	59	0.	36.0	150	300	0.452	0.543	0.038	0.430	0.420	0.012
4	25	800	62	0.	38.0	145	290	0.251	0.430	0.077	0.331	0.368	0.086
4	25	286	58	0.	36.0	150	300	0.427	0.494	0.029	0.409	0.408	0.021
4	25	166	62	0.	38.0	145	290	0.548	0.543	0.001	0.470	0.453	0.008
4	25	957	50	0.	35.0	150	300	0.151	0.335	0.119	0.271	0.331	0.129
4	25	618	21	0.	25.0	40	80	0.032	0.386	0.292	0.101	0.201	0.202
4	35	634	22	0.	25.0	40	80	0.180	0.365	0.193	0.151	0.241	0.164
6	35	206	29	0.	30.0	40	80	0.001	0.318	0.331	0.005	0.240	0.399
6	35	104	73	0.	39.0	175	350	0.250	0.319	0.069	0.388	0.495	0.091
6	35	91	33	0.	30.0	50	100	0.110	0.318	0.167	0.172	0.321	0.164
7	25	223	96	0.	40.0	140	280	0.448	0.461	0.015	0.389	0.423	0.081
7	15	334	59	0.	36.0	150	300	0.075	0.357	0.256	0.203	0.306	0.213
7	15	204	26	0.	25.0	50	100	-0.049	0.343	0.296	0.064	0.198	0.285
8	15	436	27	0.	25.0	75	150	-0.048	0.363	0.310	0.102	0.205	0.237
8	25	435	25	0.	25.0	40	80	0.039	0.357	0.285	0.122	0.211	0.212
9	15	228	95	0.	40.0	140	280	0.461	0.493	0.027	0.404	0.398	0.024
9	25	885	28	0.	30.0	35	70	-0.067	0.358	0.320	0.089	0.210	0.297
9	25	228	69	0.	39.0	125	250	0.544	0.541	0.016	0.475	0.444	0.014

(Continued)

Table 4 (Concluded)

TIRE NO	TIRE DEFLECTION PERCENT	WHEEL LOAD LB	MEASURED CONE INDEX	SOIL PROPERTIES				TEST RESULTS			MODEL PREDICTIONS		
				COHESION C PSI	ANGLE OF FRICTION ϕ, DEG	SHEAR MODULUS G, PSI	BULK MODULUS K, PSI	DRAWBAR PULL P/W	TORQUE T/WR	SINKAGE Z/R	DRAWBAR PULL P/W	TORQUE T/WR	SINKAGE Z/R
9	25	446	52	0.	36.0	130	260	0.379	0.440	0.035	0.381	0.381	0.050
9	35	458	30	0.	30.0	40	80	0.251	0.389	0.121	0.285	0.312	0.086
10	25	466	71	0.	39.0	140	280	0.496	0.521	0.001	0.456	0.444	0.019
10	35	899	73	0.	39.0	175	350	0.394	0.478	0.017	0.505	0.492	0.033
10	15	852	30	0.	30.0	40	80	0.094	0.351	0.179	0.116	0.212	0.186
10	35	1023	24	0.	25.0	40	80	0.209	0.399	0.17[illegible]	0.155	0.245	0.179
11	15	451	105	0.	41.0	150	300	0.523	0.550	0.019	0.414	0.408	0.017
11	25	863	19	0.	25.0	35	70	0.207	0.380	0.147	0.143	0.208	0.128
11	35	1331	19	0.	25.0	35	70	0.188	0.379	0.159	0.133	0.223	0.176
11	25	1205	59	0.	36.0	150	300	0.343	0.459	0.061	0.349	0.365	0.059
12A	0	94	56	0.	36.0	150	300	0.372	0.458	0.023	0.245	0.292	0.032
12A	0	170	56	0.	36.0	150	300	0.324	0.450	0.029	0.225	0.284	0.049
12A	0	268	56	0.	36.0	150	300	0.272	0.417	0.029	0.206	0.277	0.068
12A	0	375	56	0.	36.0	150	300	0.229	0.408	0.088	0.189	0.271	0.088
12A	0	572	56	0.	36.0	150	300	0.150	0.414	0.059	0.163	0.262	0.123
12A	0	100	56	0.	36.0	150	300	0.420	0.473	0.014	0.243	0.291	0.033
12A	0	208	56	0.	36.0	150	300	0.303	0.447	0.030	0.217	0.281	0.057
12A	0	295	56	0.	36.0	150	300	0.241	0.417	0.033	0.201	0.275	0.074
12B	0	108	56	0.	36.0	150	300	0.278	0.480	0.034	0.215	0.280	0.058
12B	0	182	56	0.	36.0	150	300	0.220	0.408	0.053	0.190	0.271	0.087
12B	0	292	56	0.	36.0	150	300	0.168	0.381	0.066	0.161	0.261	0.126
12B	0	385	56	0.	36.0	150	300	0.114	0.392	0.090	0.142	0.255	0.157
12B	0	188	56	0.	36.0	150	300	0.202	0.422	0.052	0.188	0.271	0.089
12C	0	93	56	0.	36.0	150	300	0.269	0.388	0.032	0.189	0.271	0.088
12C	0	188	56	0.	36.0	150	300	0.170	0.398	0.081	0.144	0.255	0.153

Table 5

Comparison of Test Data with Model Predictions for Clay; Nonzero Turn Angle

					SOIL PROPERTIES				TEST RESULTS			MODEL PREDICTIONS		
TURN ANGLE DEG	TIRE DEFLECTION PERCENT	SLIP PERCENT	WHEEL LOAD LB	MEASURED CONE INDEX	COHESION C PSI	ANGLE OF FRICTION ϕ, DEG	SHEAR MODULUS G, PSI	BULK MODULUS K, PSI	DRAWBAR PULL P/W	TORQUE T/WR	SIDE FORCE SF/W	DRAWBAR PULL P/W	TORQUE T/WR	SIDE FORCE SF/W
5.0	35	23.7	453.7	42.5	4.3	0.	100	200	0.480	0.580	0.190	0.473	0.536	0.155
5.0	15	9.1	444.2	42.1	4.3	0.	100	200	0.110	0.240	0.220	0.201	0.312	0.115
5.0	15	12.1	447.2	42.5	4.3	0.	100	200	0.140	0.260	0.220	0.240	0.350	0.116
5.0	15	22.2	439.1	42.9	4.3	0.	100	200	0.210	0.370	0.140	0.337	0.441	0.120
5.0	35	23.7	651.0	41.3	4.2	0.	100	200	0.290	0.420	0.120	0.309	0.403	0.120
10.0	35	5.0	453.9	39.6	4.1	0.	100	200	0.170	0.280	0.420	0.082	0.286	0.316
10.0	35	11.4	455.9	43.5	4.3	0.	100	200	0.270	0.380	0.370	0.242	0.420	0.328
10.0	35	17.8	455.9	41.5	4.2	0.	100	200	0.420	0.530	0.340	0.324	0.484	0.325
10.0	25	6.1	447.4	43.1	4.3	0.	100	200	0.080	0.140	0.410	0.122	0.299	0.284
10.0	25	9.6	451.2	41.2	4.2	0.	100	200	0.190	0.280	0.430	0.194	0.361	0.280
10.0	25	19.5	449.4	39.9	4.1	0.	100	200	0.290	0.410	0.320	0.311	0.462	0.281
10.0	25	22.4	901.1	42.3	4.3	0.	100	200	0.030	0.220	0.260	0.066	0.310	0.226
10.0	25	18.3	222.3	42.1	4.3	0.	100	200	0.610	0.740	0.580	0.489	0.713	0.481
15.0	15	3.4	443.1	39.9	4.1	0.	100	200	-0.070	0.030	0.450	-0.067	0.185	0.381
15.0	15	21.7	451.0	40.9	4.2	0.	100	200	0.150	0.300	0.440	0.193	0.426	0.400
15.0	15	13.8	448.7	43.6	4.3	0.	100	200	0.080	0.180	0.420	0.133	0.367	0.397
20.0	35	9.4	451.0	44.8	4.4	0.	100	200	0.100	0.120	0.580	0.043	0.396	0.757
20.0	35	20.2	450.8	44.2	4.4	0.	100	200	0.210	0.300	0.530	0.203	0.520	0.760
20.0	35	12.8	453.2	43.5	4.3	0.	100	200	0.170	0.200	0.570	0.105	0.440	0.743

Table 6

Comparison of Test Data with Model Predictions for Sand; Nonzero Turn Angle

					SOIL PROPERTIES				TEST RESULTS			MODEL PREDICTIONS		
TURN ANGLE DEG	TIRE DEFLECTION PERCENT	SLIP PERCENT	WHEEL LOAD LB	MEASURED CONE INDEX	COHESION C PSI	ANGLE OF FRICTION ϕ, DEG	SHEAR MODULUS G, PSI	BULK MODULUS K, PSI	DRAWBAR PULL P/W	TORQUE T/WR	SIDE FORCE SF/W	DRAWBAR PULL P/W	TORQUE T/WR	SIDE FORCE SF/W
5.0	35	5.4	456.8	44.2	0.	34.0	140	280	0.100	0.280	0.140	0.146	0.258	0.126
5.0	35	11.1	451.7	46.6	0.	35.0	125	250	0.200	0.370	0.130	0.234	0.344	0.129
5.0	35	18.4	448.5	44.4	0.	34.0	140	280	0.210	0.430	0.130	0.303	0.418	0.132
5.0	35	2.7	457.0	70.3	0.	39.0	150	300	0.090	0.210	0.210	0.073	0.178	0.122
5.0	35	9.7	459.8	68.5	0.	39.0	125	250	0.250	0.370	0.200	0.225	0.321	0.125
5.0	35	16.4	445.1	71.2	0.	39.0	160	320	0.310	0.440	0.180	0.338	0.424	0.126
10.0	35	3.7	445.1	40.9	0.	33.0	125	250	0.020	0.240	0.330	0.015	0.199	0.269
10.0	35	6.1	437.9	45.5	0.	34.0	150	300	0.060	0.270	0.330	0.120	0.289	0.268
10.0	35	7.5	441.8	45.1	0.	34.0	150	300	0.070	0.290	0.320	0.146	0.316	0.271
10.0	35	16.3	446.3	45.7	0.	34.0	150	300	0.210	0.410	0.270	0.236	0.418	0.283
10.0	35	17.9	447.8	46.0	0.	35.0	125	250	0.170	0.390	0.290	0.225	0.408	0.282
10.0	35	19.0	452.1	41.1	0.	34.0	100	200	0.170	0.430	0.270	0.176	0.377	0.282
10.0	15	2.0	442.4	49.5	0.	36.0	175	350	-0.100	0.240	0.250	-0.088	0.138	0.277
10.0	15	10.6	446.7	46.8	0.	35.0	125	250	-0.030	0.320	0.240	-0.019	0.268	0.301
10.0	15	24.0	444.7	43.3	0.	34.0	125	250	0.030	0.210	0.210	-0.063	0.268	0.306
10.0	25	21.2	449.6	44.0	0.	34.0	140	280	0.140	0.390	0.260	0.079	0.323	0.272
10.0	35	5.5	239.7	72.0	0.	39.0	160	320	0.120	0.290	0.360	0.261	0.356	0.235
10.0	35	9.9	234.3	72.0	0.	39.0	160	320	0.230	0.430	0.340	0.346	0.432	0.236
10.0	35	11.5	243.0	68.7	0.	39.0	125	250	0.240	0.420	0.330	0.322	0.419	0.242
10.0	35	19.3	240.6	72.5	0.	39.0	160	320	0.400	0.600	0.150	0.408	0.497	0.243
15.0	35	2.7	228.2	69.8	0.	39.0	150	300	-0.020	0.190	0.540	0.098	0.258	0.377
15.0	35	11.3	234.7	73.1	0.	39.0	175	350	0.150	0.390	0.460	0.328	0.456	0.372
15.0	35	14.3	239.9	66.5	0.	39.0	100	200	0.200	0.430	0.430	0.269	0.421	0.388
15.0	35	20.6	675.4	70.9	0.	39.0	150	300	0.120	0.350	0.400	0.110	0.401	0.472
15.0	15	21.0	463.8	74.2	0.	39.0	175	350	0.090	0.320	0.360	-0.046	0.331	0.487

(Continued)

Table 6 (Concluded)

					SOIL PROPERTIES				TEST RESULTS			MODEL PREDICTIONS		
TURN ANGLE DEG	TIRE DEFLECTION PERCENT	SLIP PERCENT	WHEEL LOAD LB	MEASURED CONE INDEX	COHESION C PSI	ANGLE OF FRICTION ϕ, DEG	SHEAR MODULUS G, PSI	BULK MODULUS K, PSI	DRAWBAR PULL P/W	TORQUE T/WR	SIDE FORCE SF/W	DRAWBAR PULL P/W	TORQUE T/WR	SIDE FORCE SF/W
15.0	25	8.8	449.6	74.2	0.	39.0	175	350	0.	0.170	0.500	0.119	0.353	0.443
15.0	25	16.2	459.8	72.0	0.	39.0	160	320	0.130	0.320	0.430	0.129	0.393	0.446
15.0	25	20.9	450.8	71.6	0.	39.0	160	320	0.210	0.380	0.420	0.106	0.380	0.432
15.0	35	23.3	232.0	48.6	0.	36.0	140	280	0.280	0.490	0.370	0.279	0.442	0.369
15.0	35	22.2	678.5	40.9	0.	34.0	140	280	0.050	0.370	0.380	0.003	0.356	0.475
15.0	25	22.2	455.3	46.0	0.	35.0	125	250	0.130	0.380	0.390	-0.003	0.321	0.437
15.0	35	6.1	460.2	78.9	0.	40.0	150	300	0.060	0.220	0.470	0.076	0.280	0.410
15.0	35	9.3	452.6	69.2	0.	39.0	125	250	0.050	0.220	0.510	0.103	0.317	0.420
15.0	35	11.6	459.8	68.7	0.	39.0	125	250	0.110	0.290	0.450	0.127	0.346	0.425
15.0	35	19.2	459.8	76.2	0.	40.0	125	250	0.260	0.410	0.360	0.191	0.412	0.433
20.0	35	17.7	448.7	44.9	0.	34.0	150	300	0.050	0.300	0.490	0.114	0.427	0.639
20.0	35	5.5	225.9	46.4	0.	34.0	140	280	0.	0.270	0.520	0.148	0.348	0.536
20.0	35	13.5	227.7	43.8	0.	34.0	130	260	0.080	0.360	0.480	0.246	0.450	0.552
20.0	35	20.9	227.1	47.3	0.	35.0	140	280	0.160	0.440	0.430	0.254	0.461	0.532
20.0	35	5.6	240.1	73.4	0.	39.0	125	250	0.	0.250	0.510	0.133	0.326	0.528
20.0	35	15.8	239.7	76.7	0.	40.0	125	250	0.130	0.360	0.490	0.273	0.456	0.533
20.0	35	22.3	233.4	81.3	0.	41.0	150	300	0.210	0.480	0.450	0.334	0.506	0.529
20.0	35	7.4	452.3	44.2	0.	34.0	140	280	-0.090	0.190	0.510	0.010	0.303	0.608

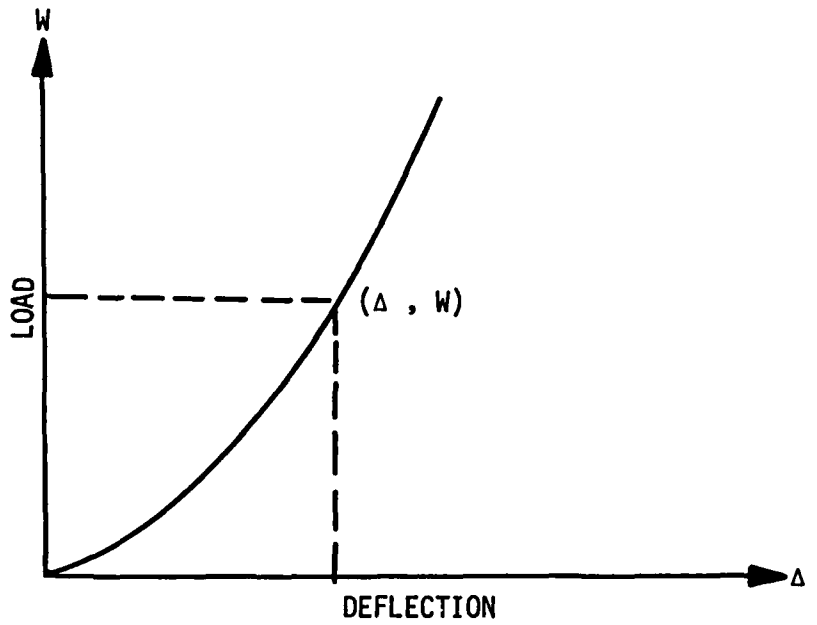

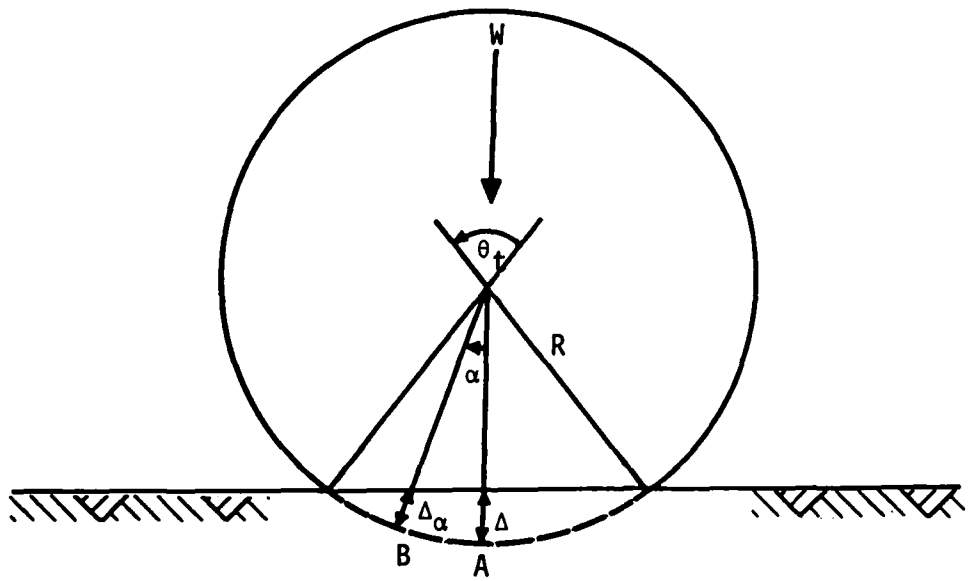

Figure 1. Load-deflection curve for a flexible tire on rigid surface

1. UNLOADED SECTION WIDTH (D)
2. UNLOADED RADIUS (R)
3. UNLOADED SECTION HEIGHT (h)
4. DEFLECTION AT GIVEN LOAD = $\frac{\Delta}{h}$

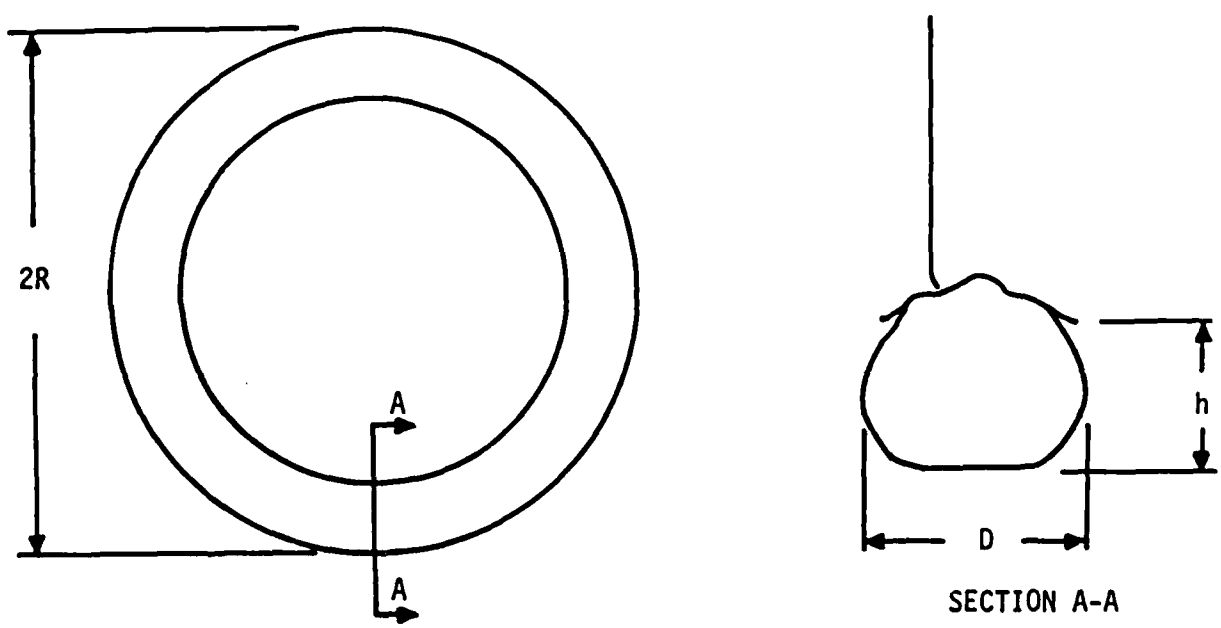

Figure 2. Tire geometry

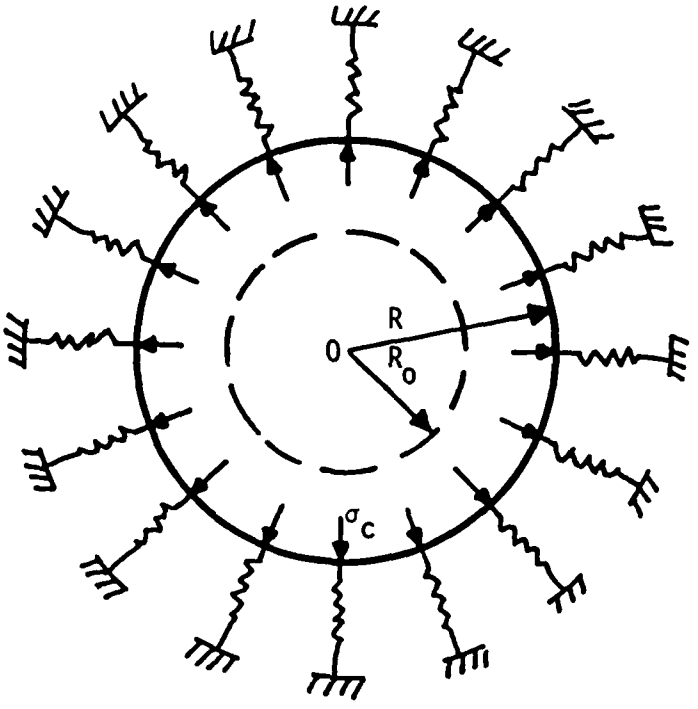

a. EXPANSION OF SPHERICAL CAVITY

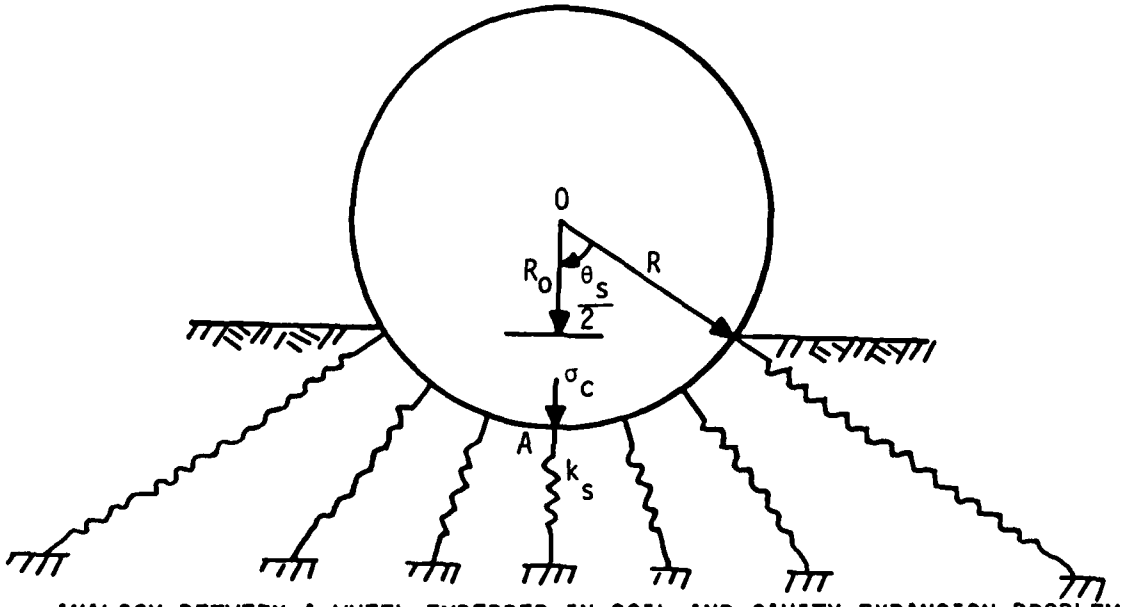

b. ANALOGY BETWEEN A WHEEL EMBEDDED IN SOIL AND CAVITY EXPANSION PROBLEM

Figure 3. Proposed model for computing the spring constant for soil

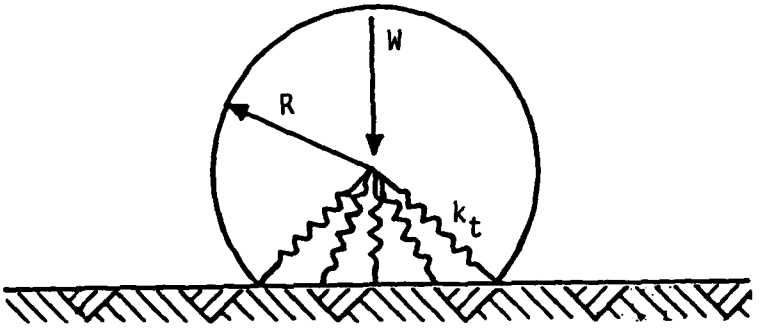

a. SPRING CONSTANT FOR FLEXIBLE TIRE (k_t)

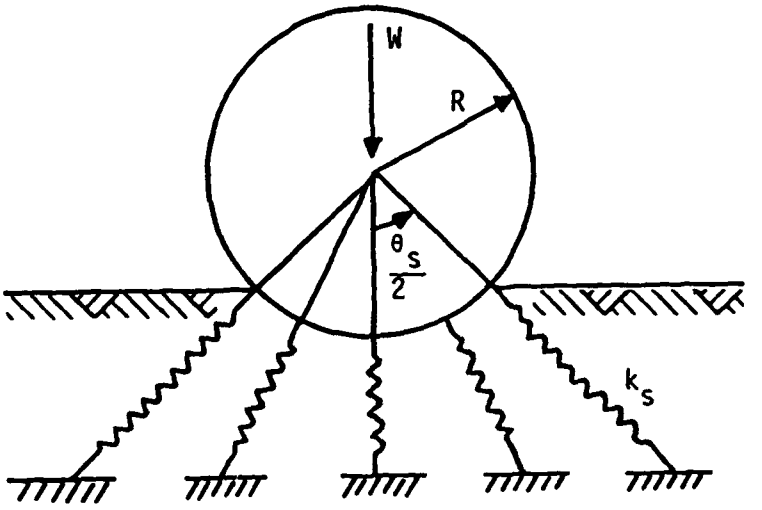

b. SPRING CONSTANT FOR SOIL (k_s)

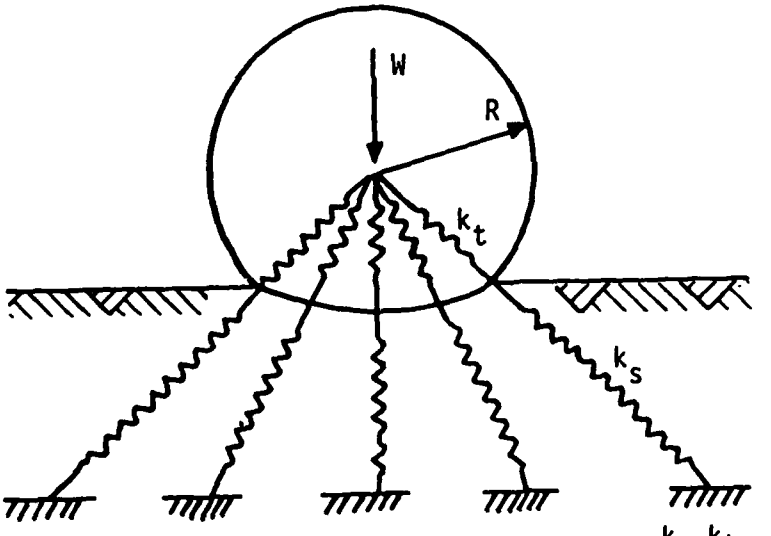

c. SPRING CONSTANT FOR SOIL-TIRE SYSTEM $\frac{k_s\ k_t}{k_s + k_t}$

Figure 4. Equivalent spring constant for soil-tire system

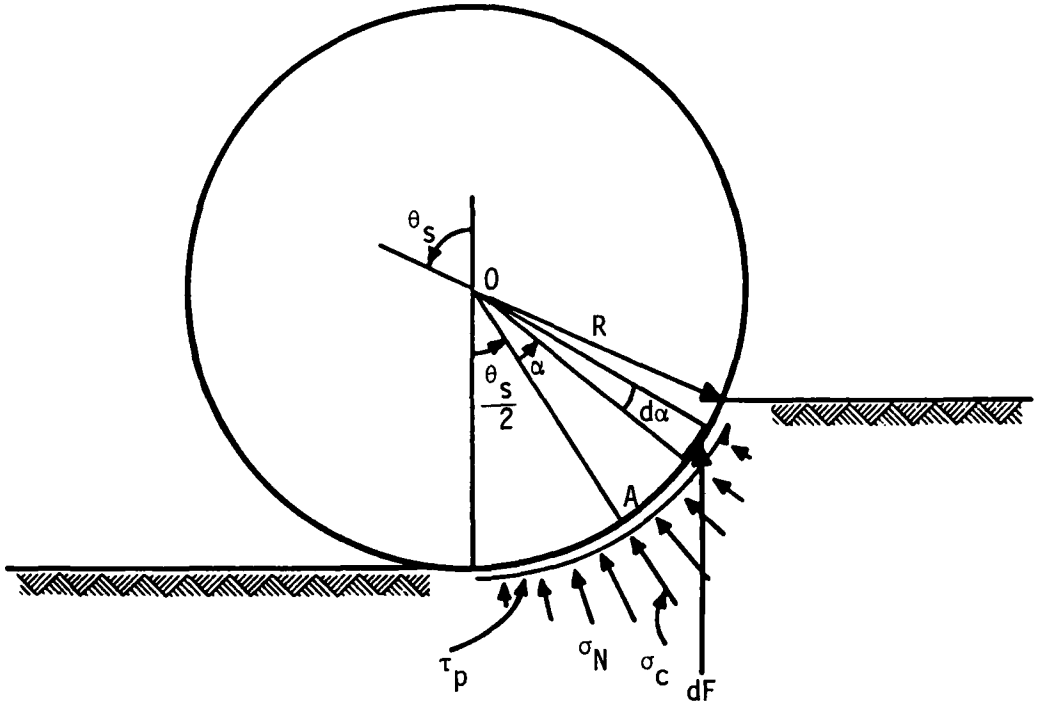

a. Normal stress distribution along the soil-tire interface

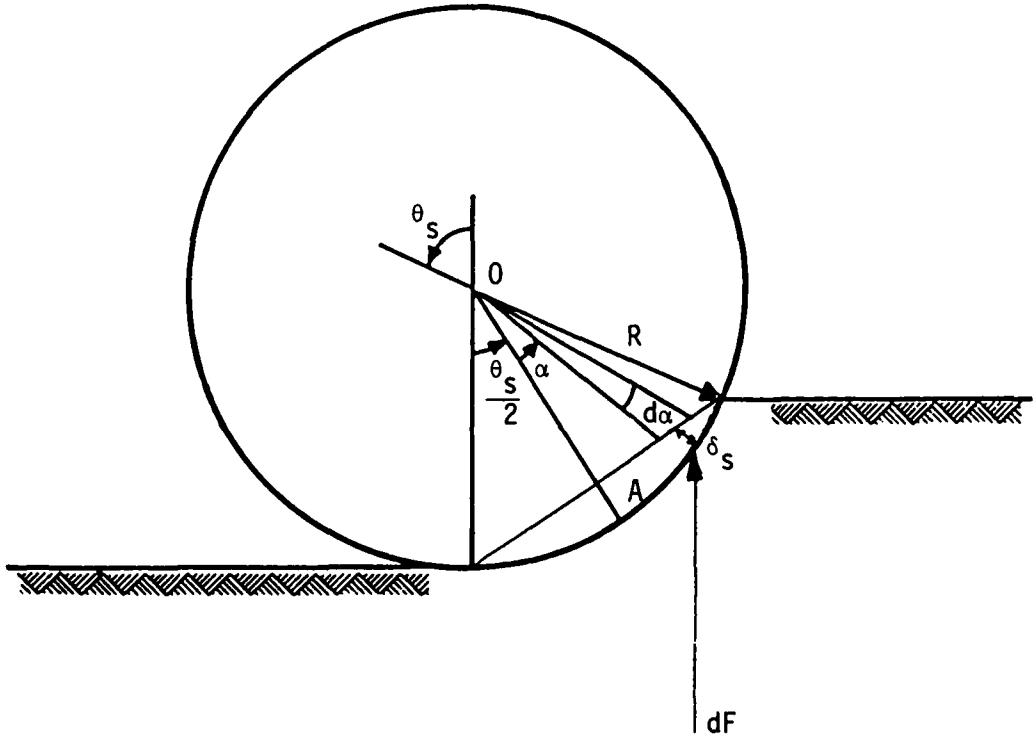

b. Soil deflection force relation

Figure 5. Soil-tire interface stress distribution

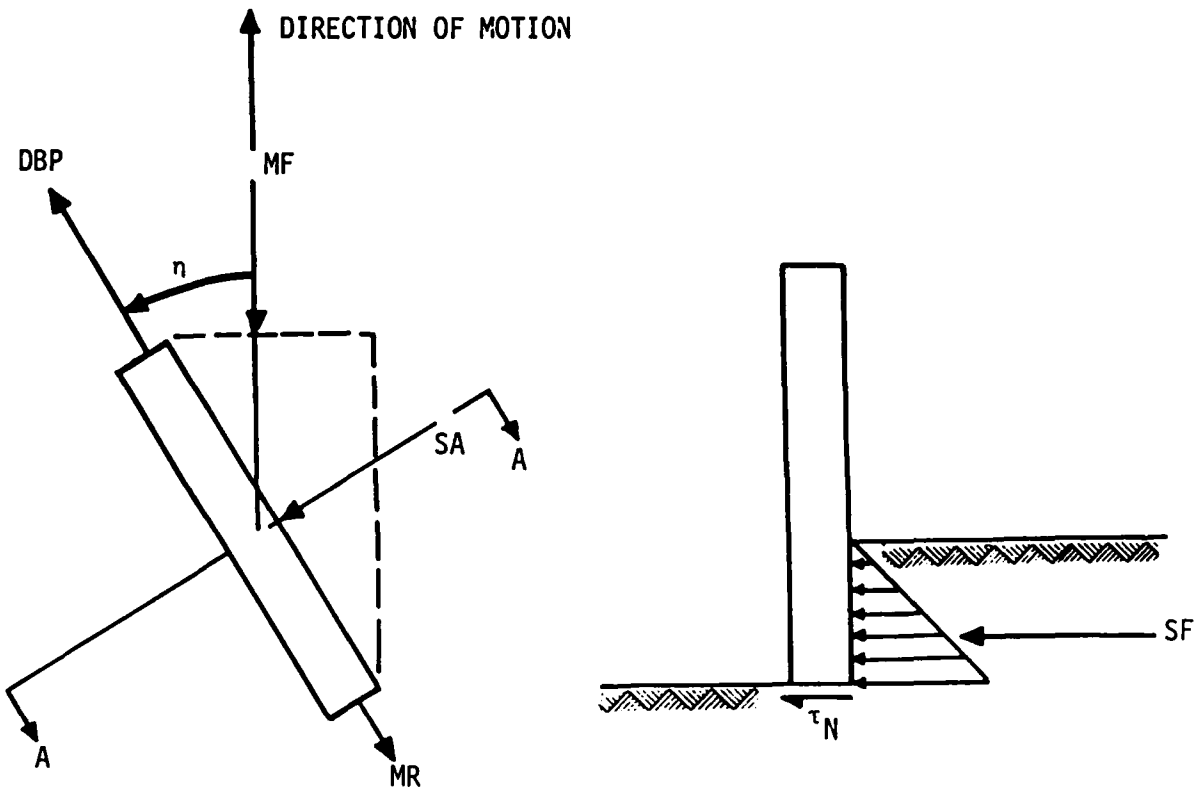

Figure 6. Geometry of the tire with turn angle η

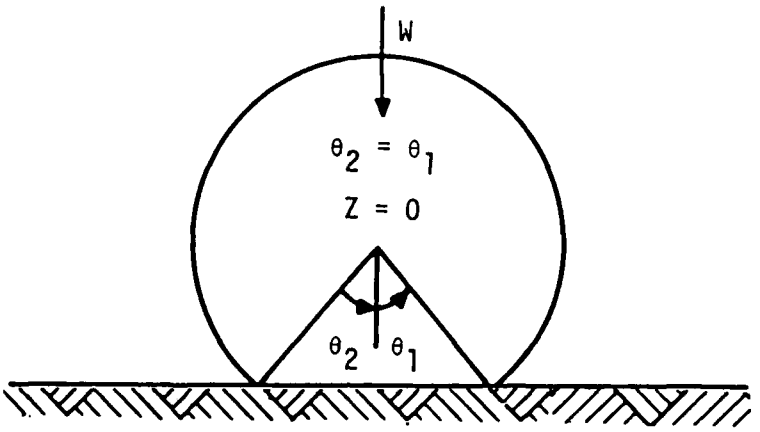

a. RIGID SURFACE-FLEXIBLE TIRE

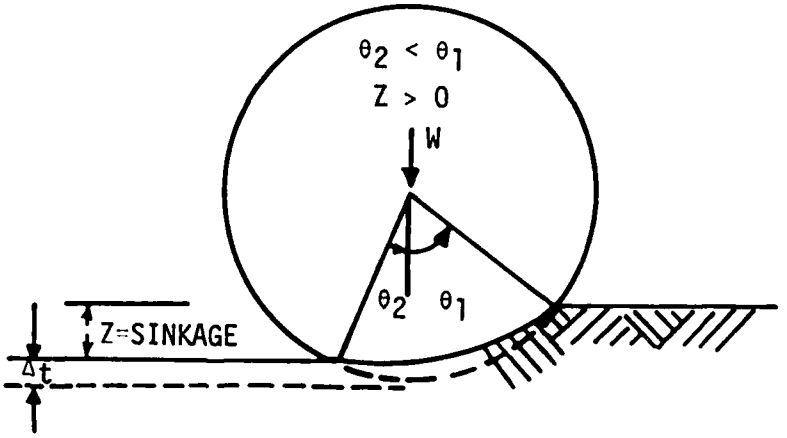

b. SOFT GROUND-FLEXIBLE TIRE

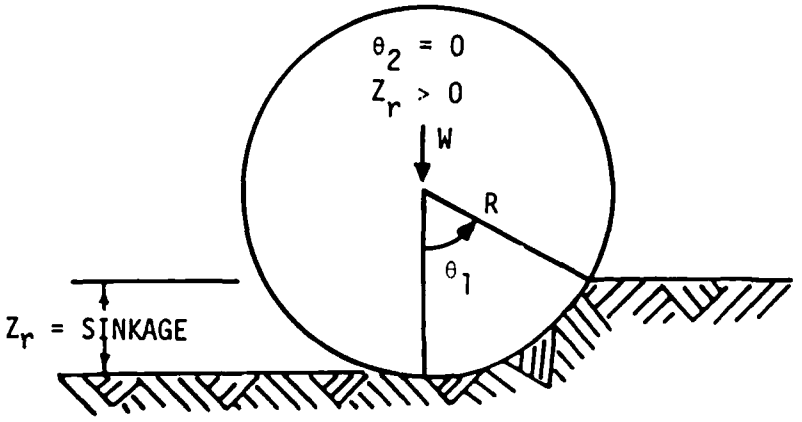

c. SOFT GROUND-RIGID TIRE

Figure 7. Variation of the central angles θ_1 and θ_2 and sinkage Z with relative rigidity of the tire and soil

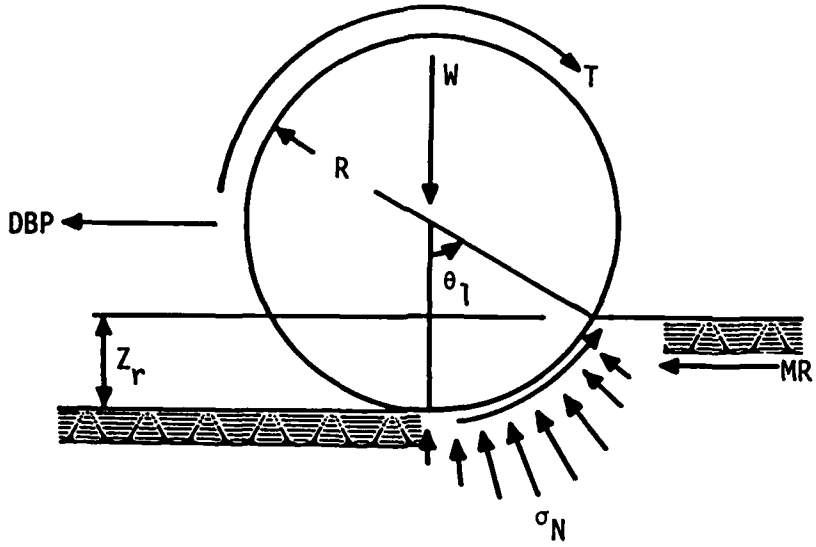

a. SINKAGE OF A RIGID WHEEL

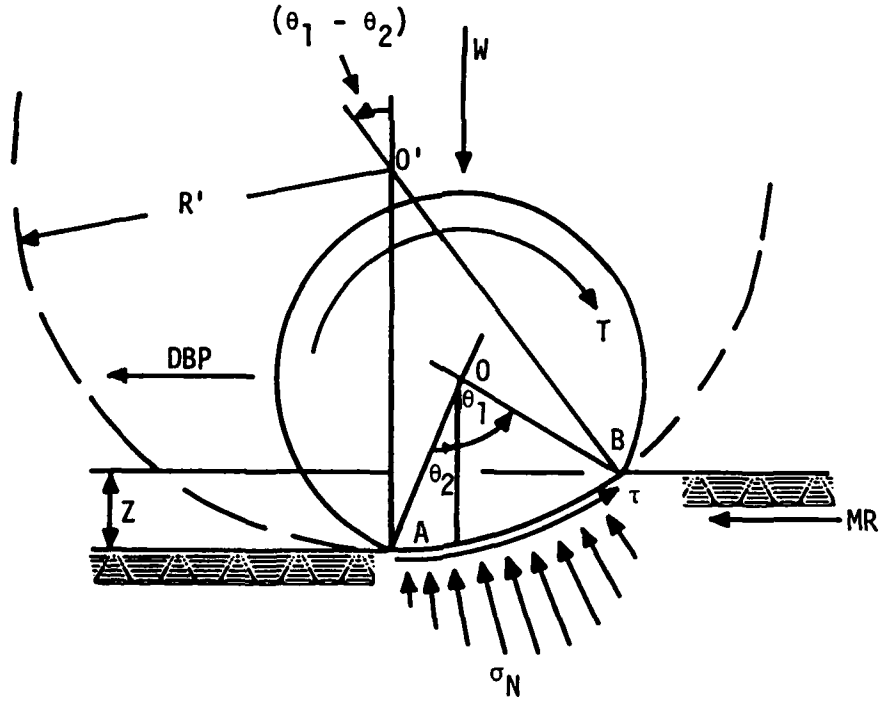

b. SINKAGE OF A FLEXIBLE WHEEL

Figure 8. Geometry of the problem

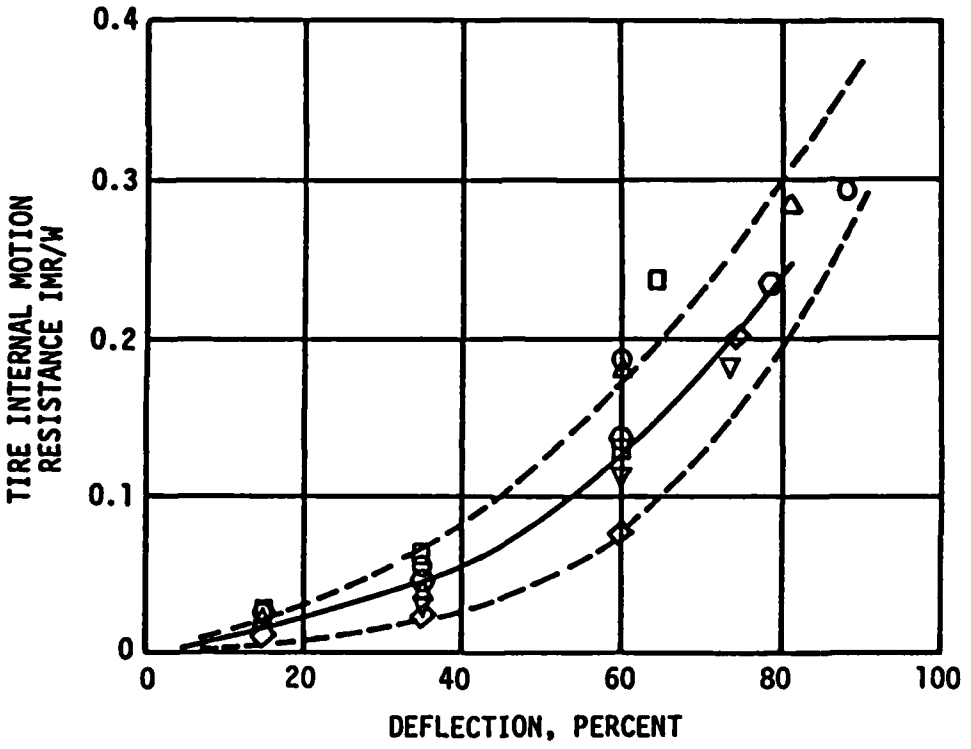

Figure 9. Tire internal motion resistance-deflection relation (Turnage 1976)

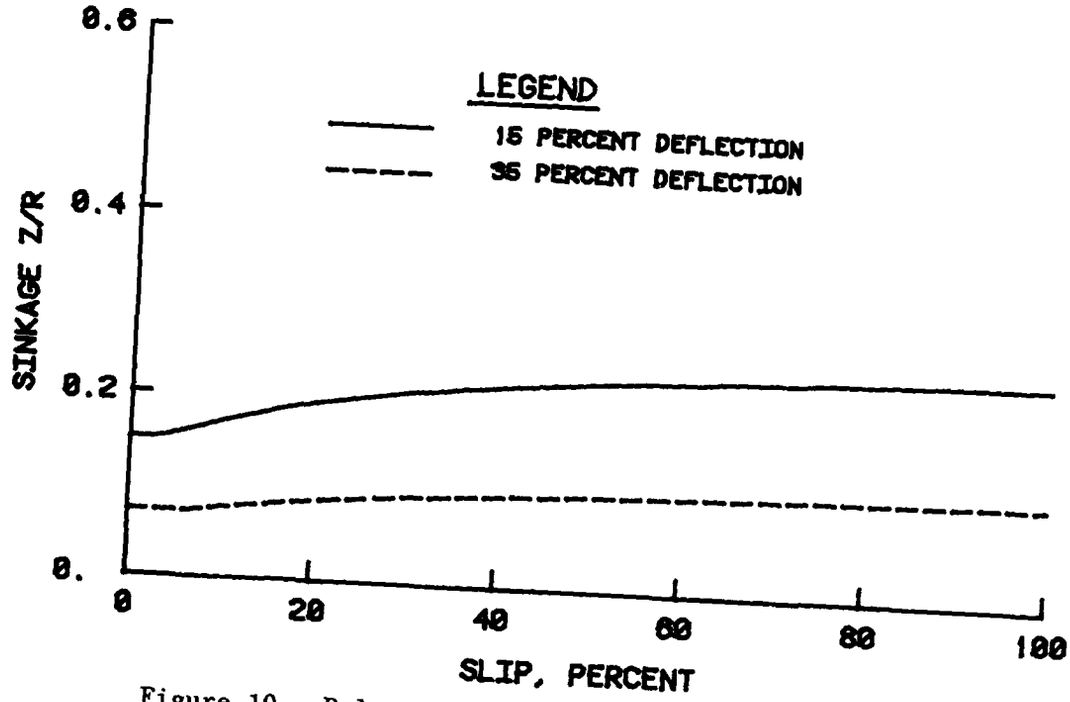

Figure 10. Relationship between sinkage and slip ratio for clay

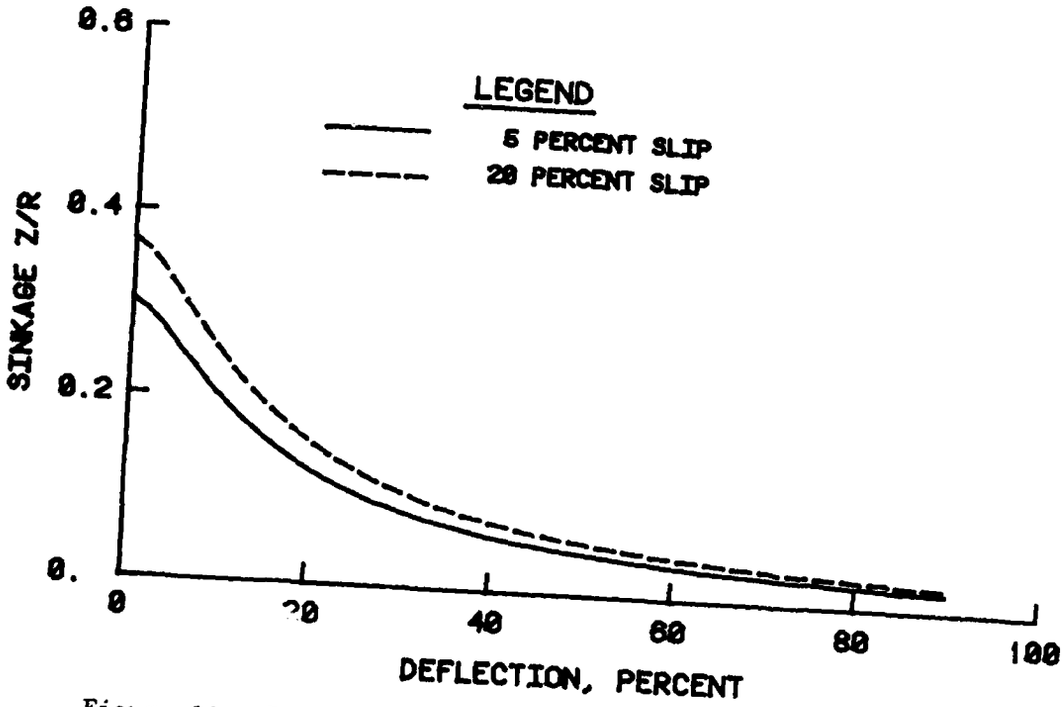

Figure 11. Relationship between sinkage and tire deflection for clay

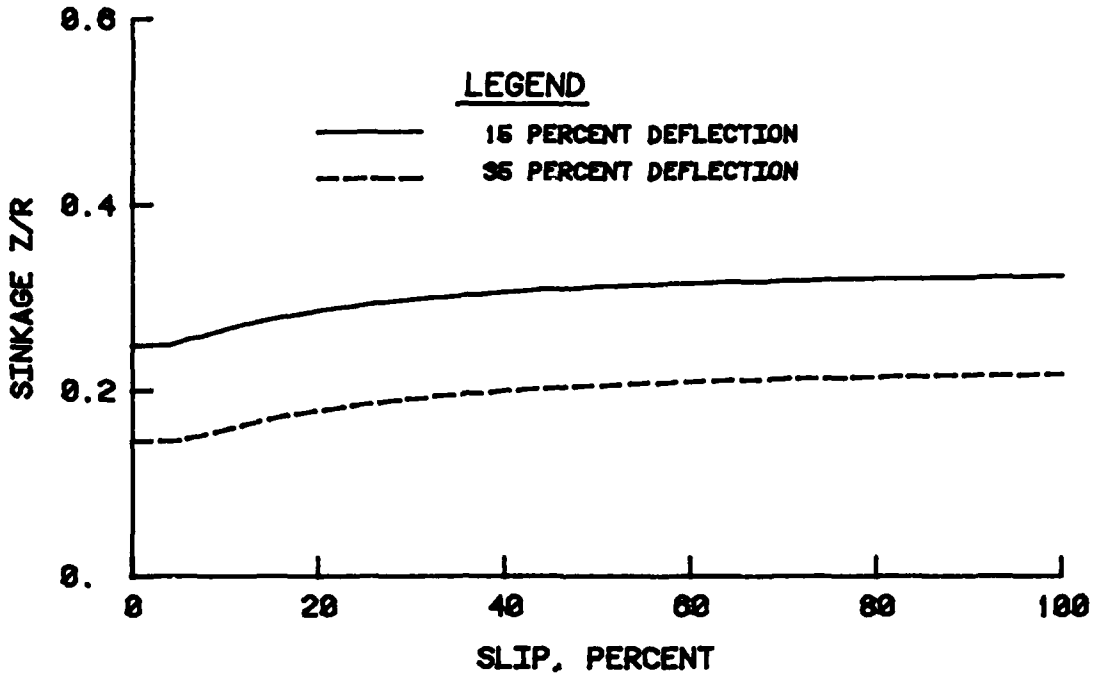

Figure 12. Relationship between sinkage and slip ratio for sand

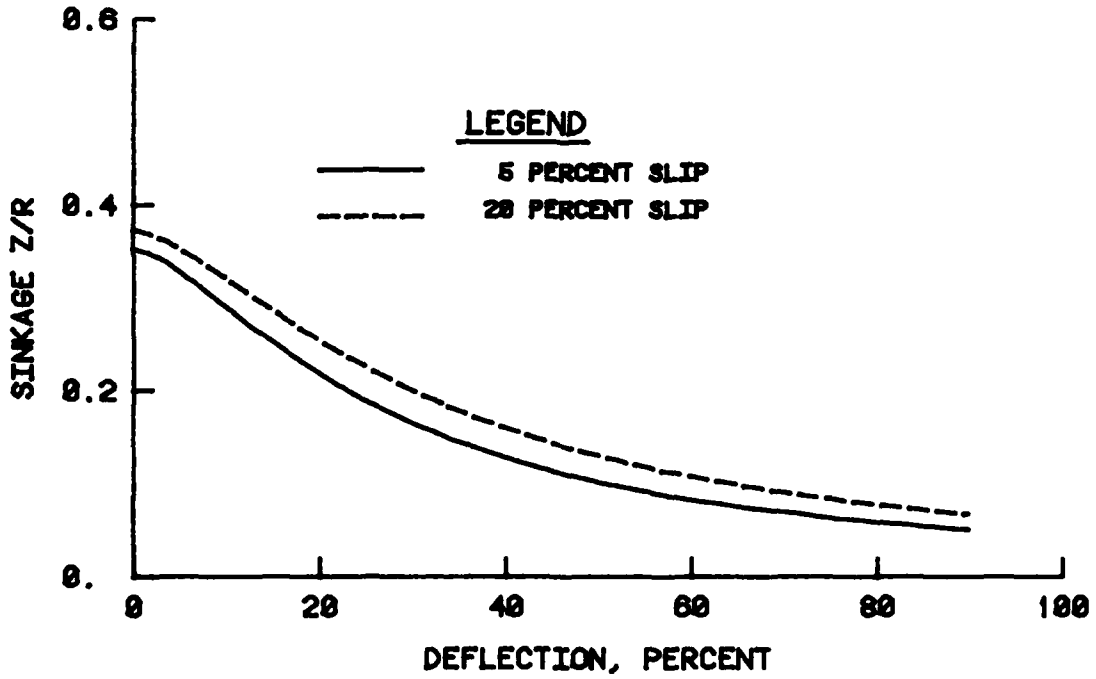

Figure 13. Relationship between sinkage and tire deflection for sand

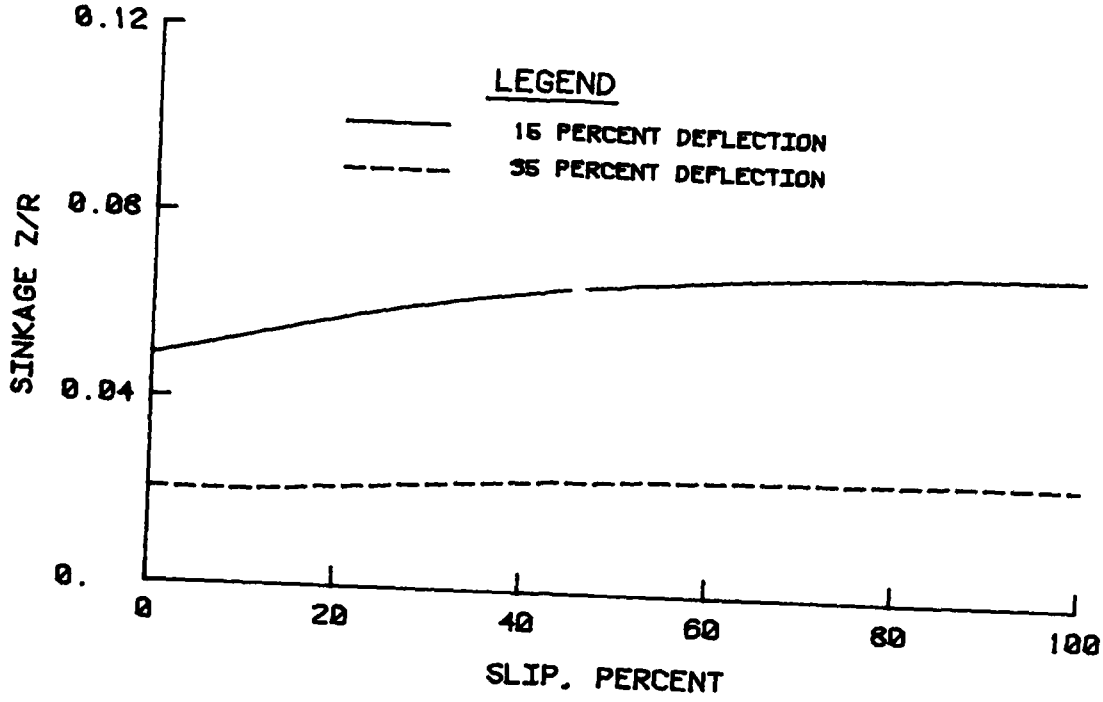

Figure 14. Relationship between sinkage and slip ratio for mixed soil

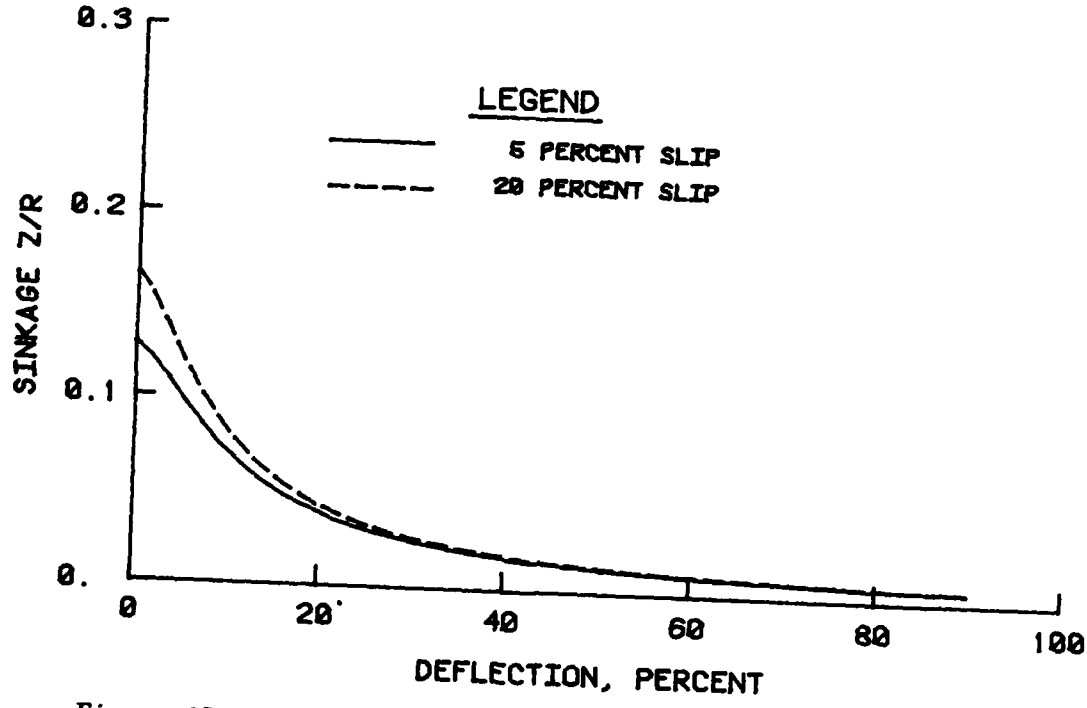

Figure 15. Relationship between sinkage and tire deflection for mixed soil

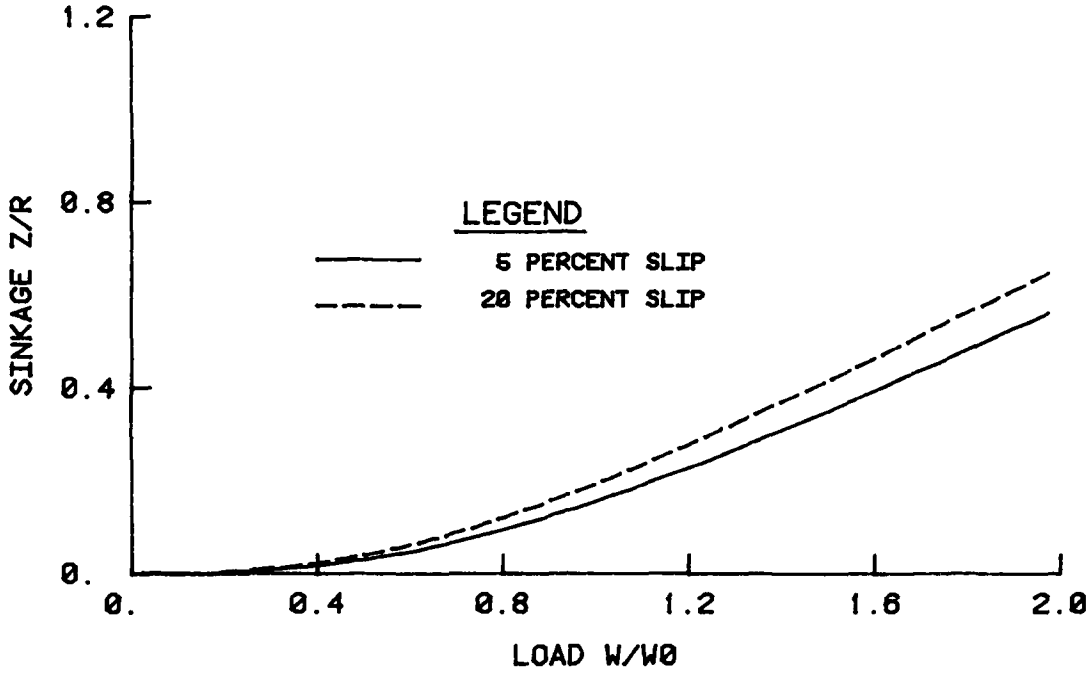

Figure 16. Relationship between sinkage and wheel load for clay; 15 percent tire deflection

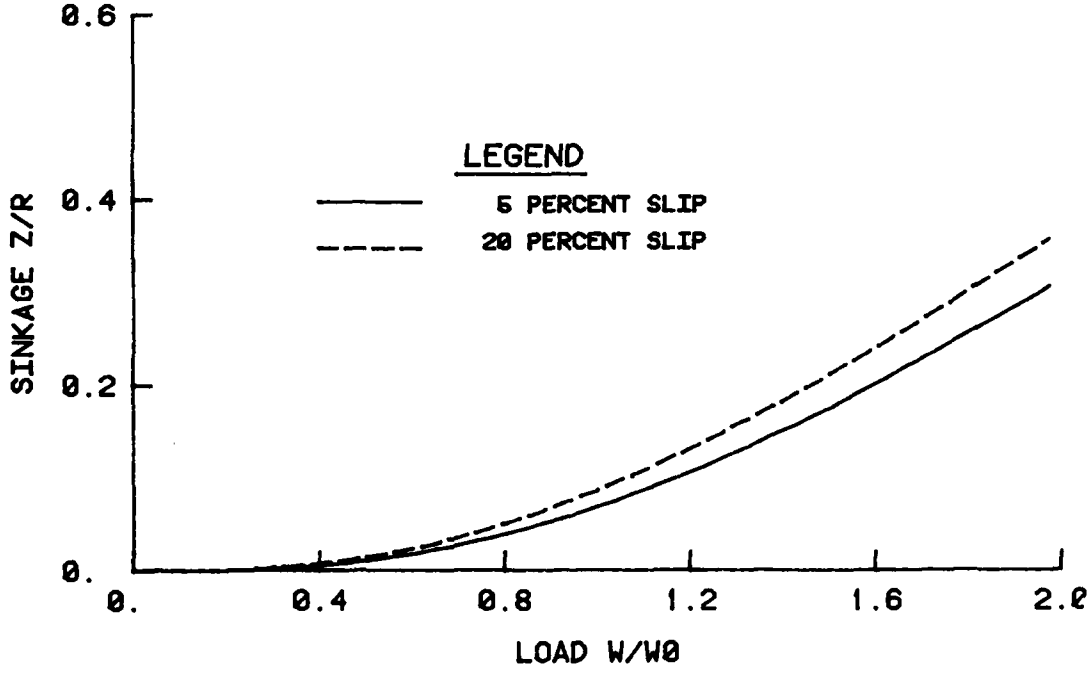

Figure 17. Relationship between sinkage and wheel load for clay; 35 percent tire deflection

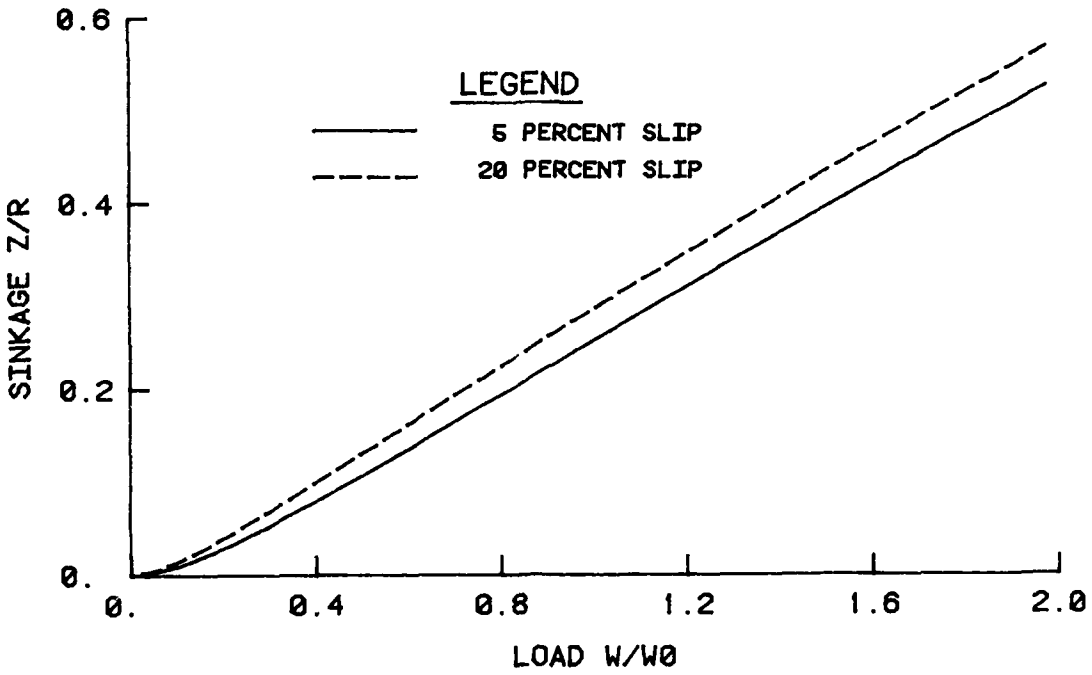

Figure 18. Relationship between sinkage and wheel load for sand: 15 percent tire deflection

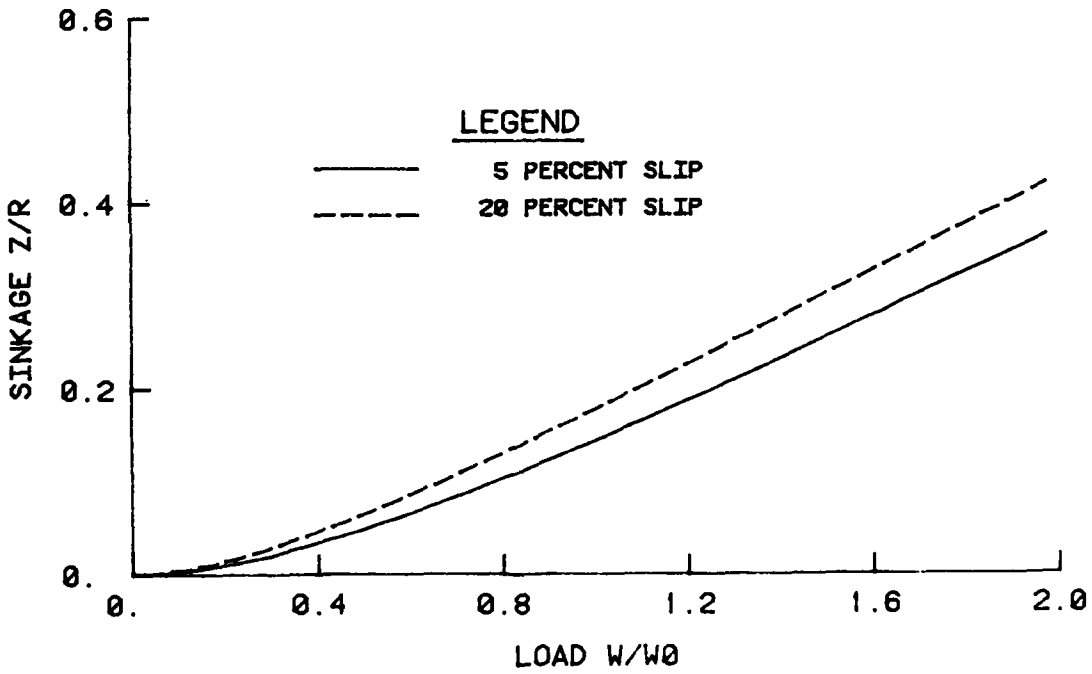

Figure 19. Relationship between sinkage and wheel load for sand; 35 percent tire deflection

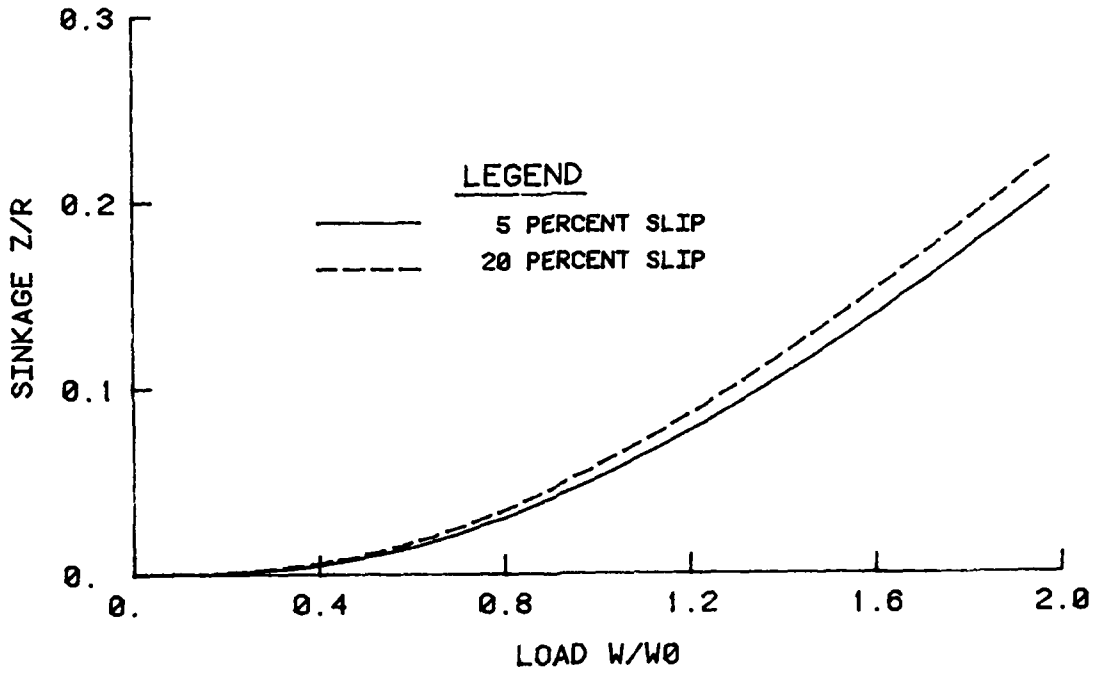

Figure 20. Relationship between sinkage and wheel load for mixed soil; 15 percent tire deflection

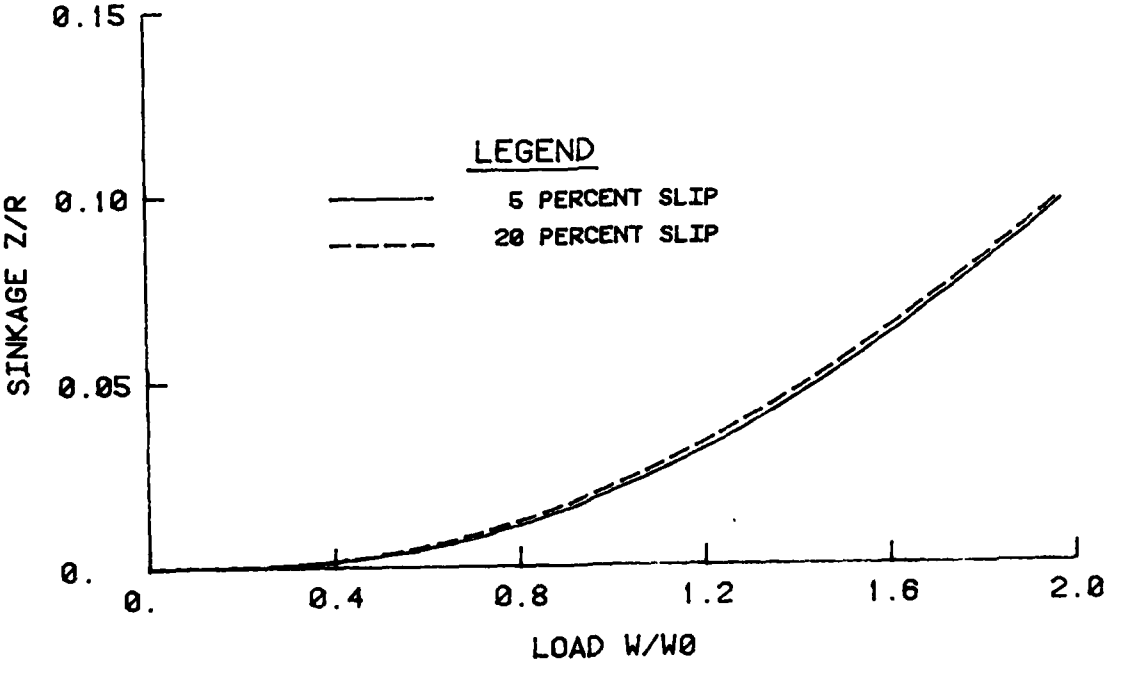

Figure 21. Relationship between sinkage and wheel load for mixed soil; 35 percent tire deflection

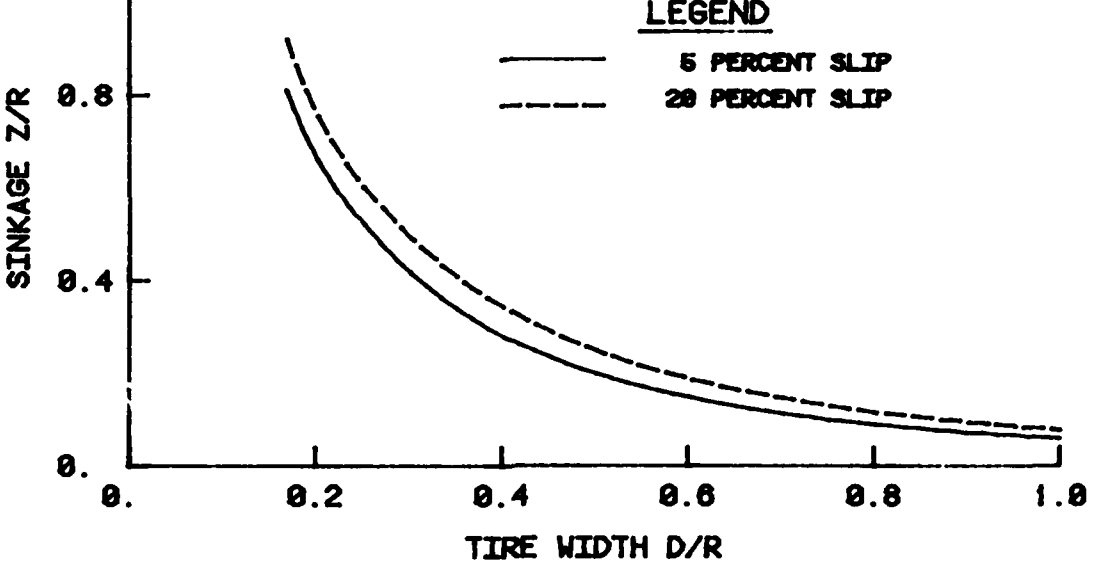

Figure 22. Relationship between sinkage and tire width for clay; 15 percent tire deflection

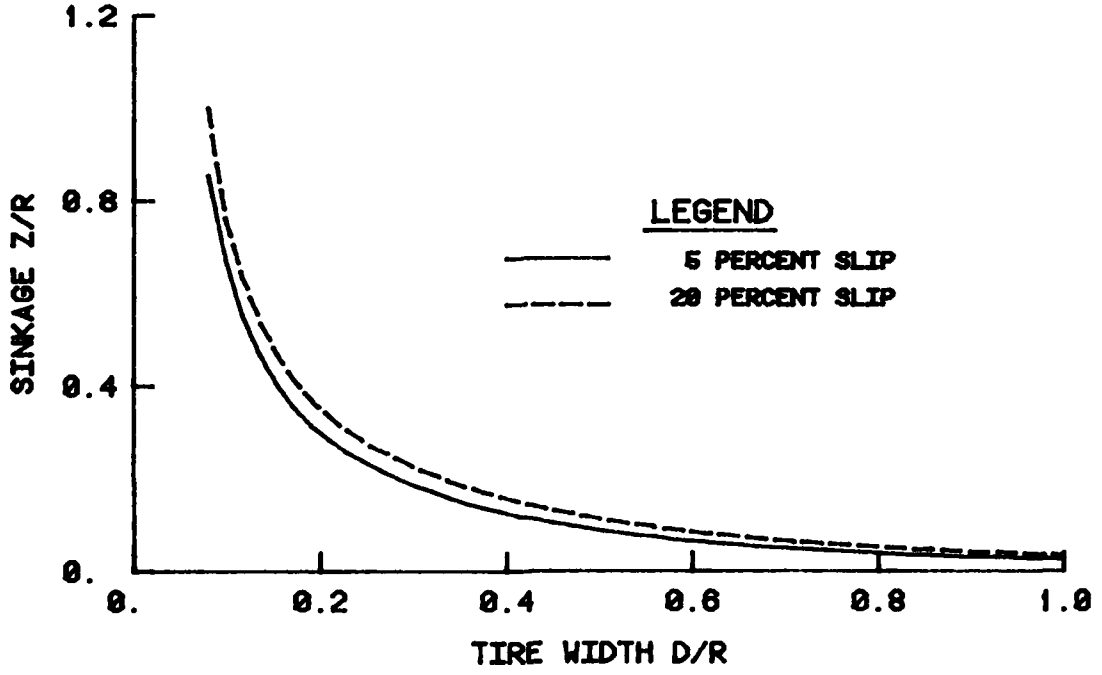

Figure 23. Relationship between sinkage and tire width for clay; 35 percent tire deflection

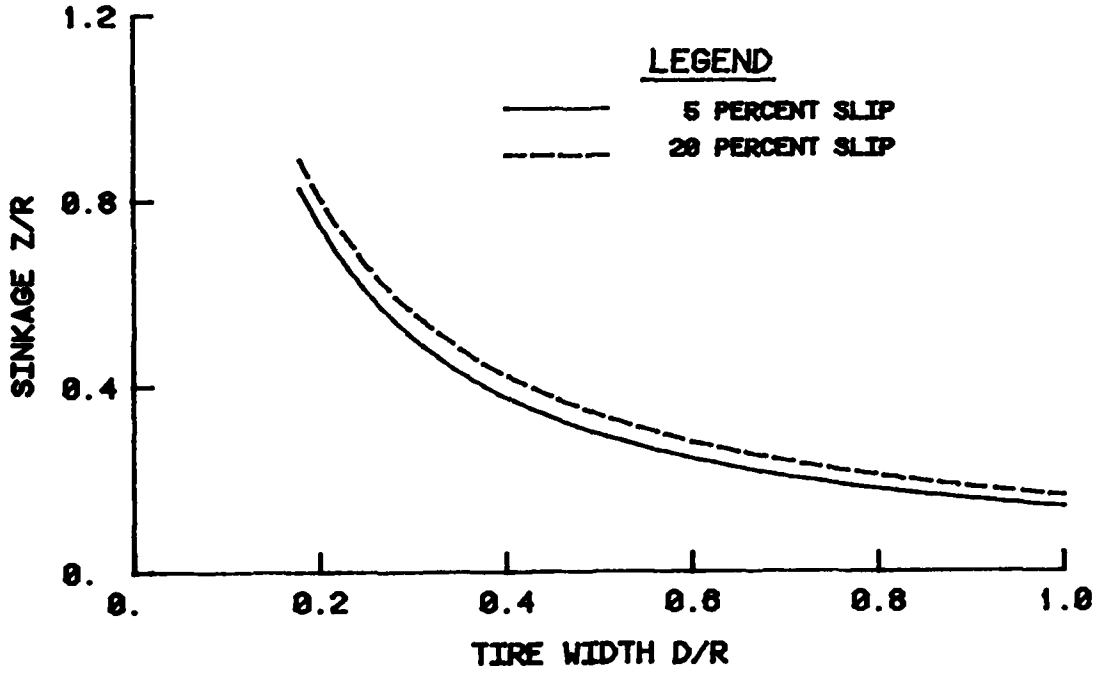

Figure 24. Relationship between sinkage and tire width for sand; 15 percent tire deflection

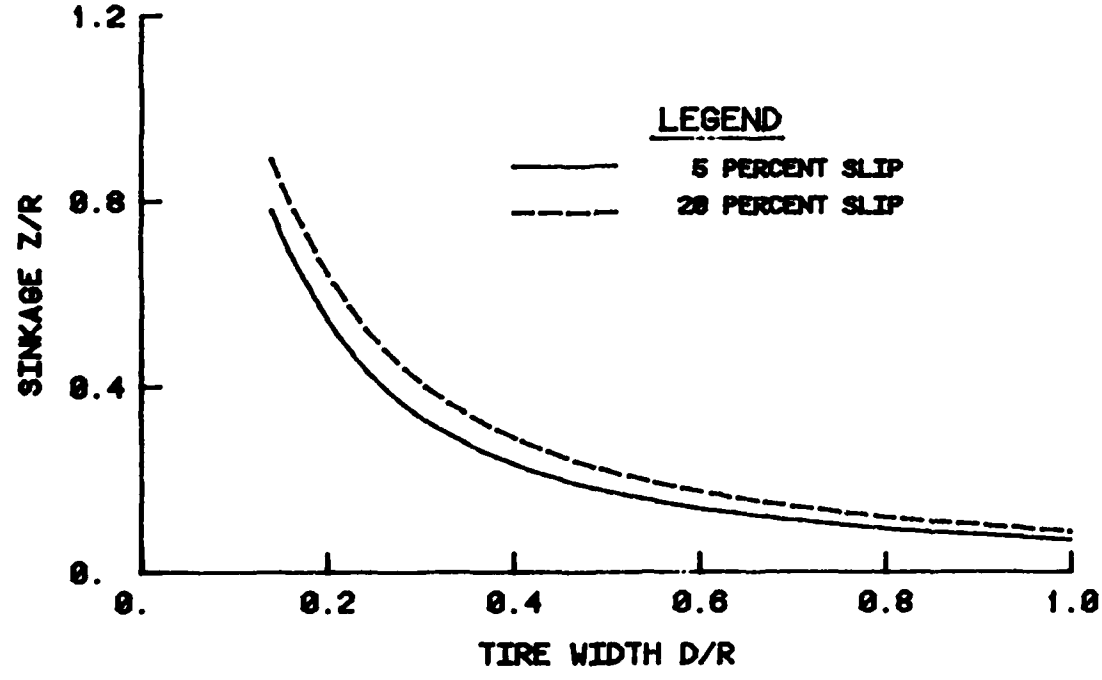

Figure 25. Relationship between sinkage and tire width for sand; 35 percent tire deflection

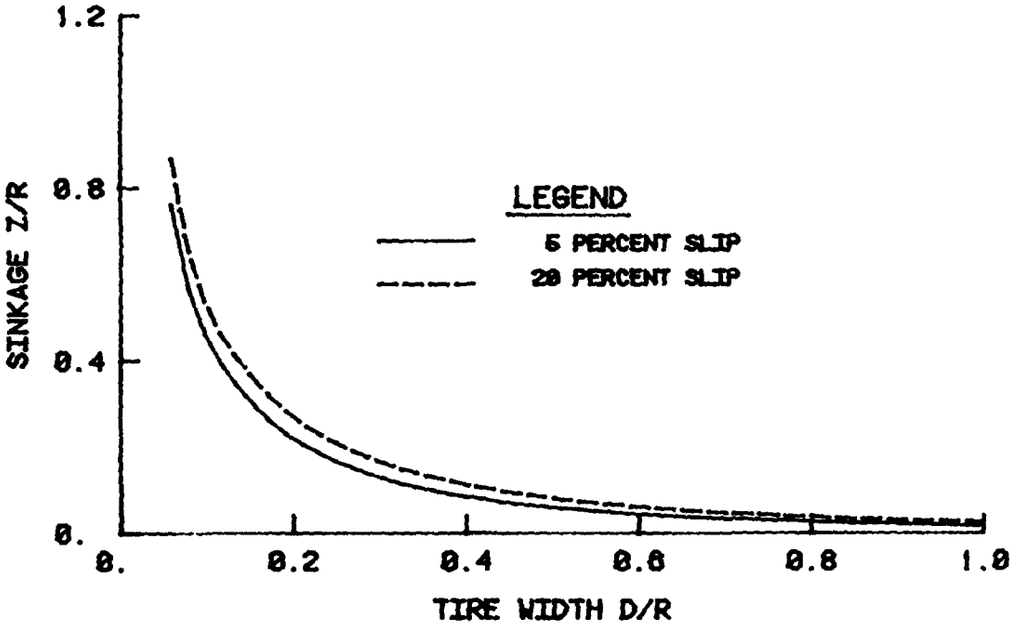

Figure 26. Relationship between sinkage and tire width for mixed soil; 15 percent tire deflection

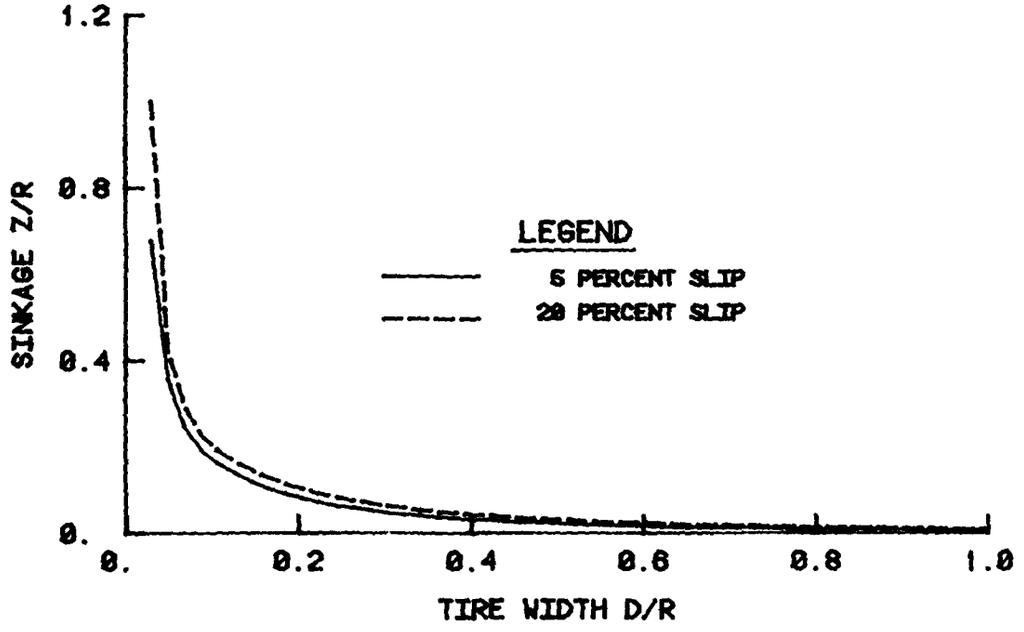

Figure 27. Relationship between sinkage and tire width for mixed soil; 35 percent tire deflection

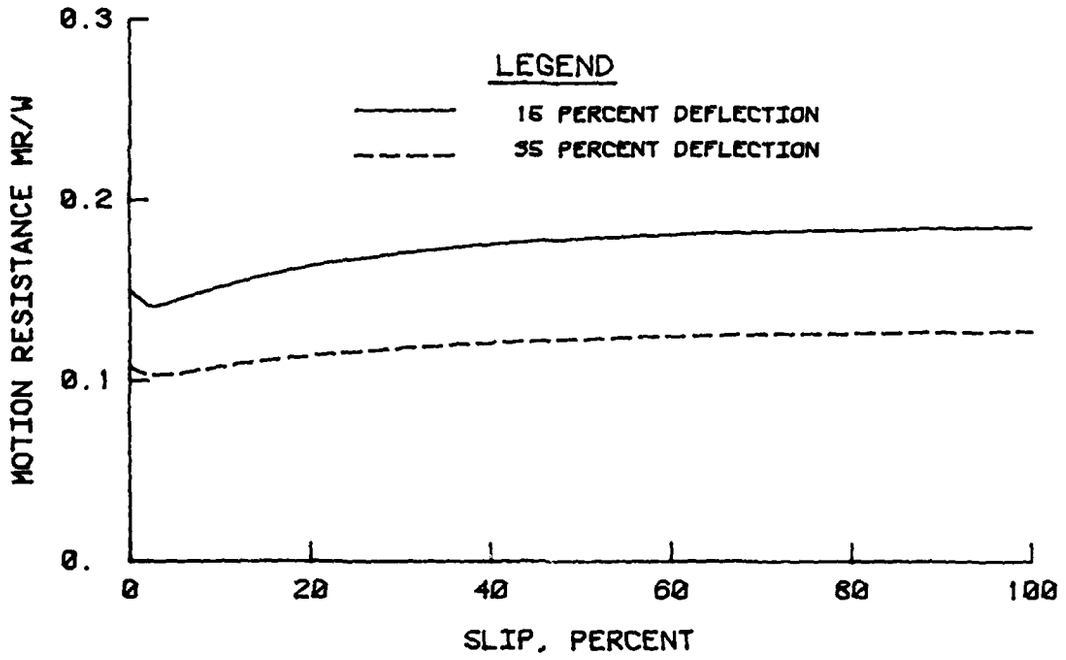

Figure 28. Relationship between motion resistance and slip ratio for clay

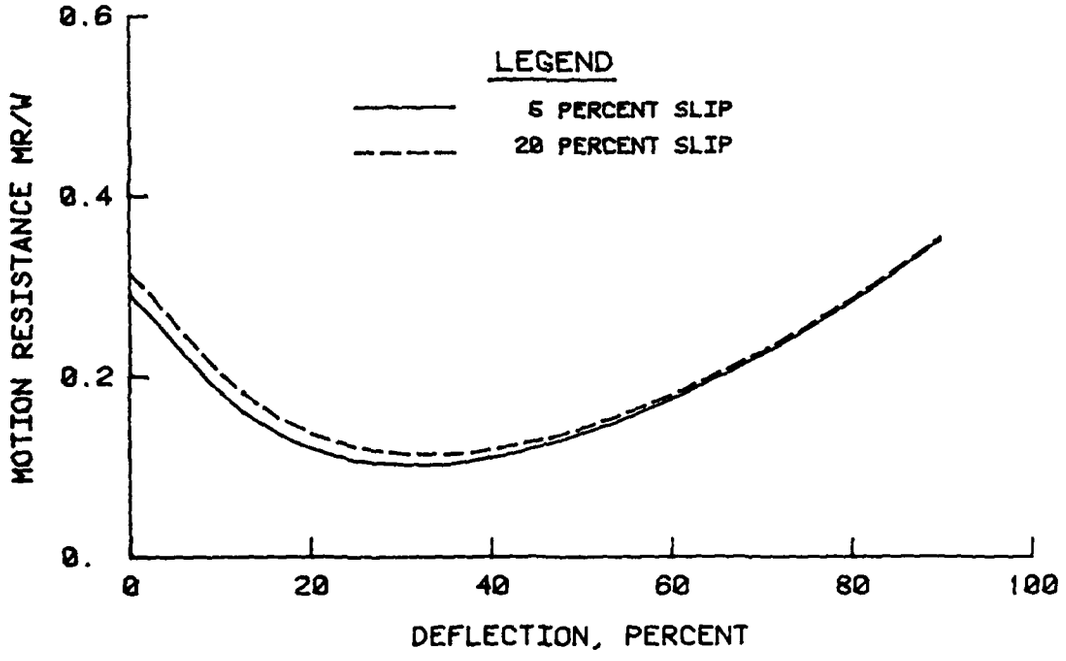

Figure 29. Relationship between motion resistance and tire deflection for clay

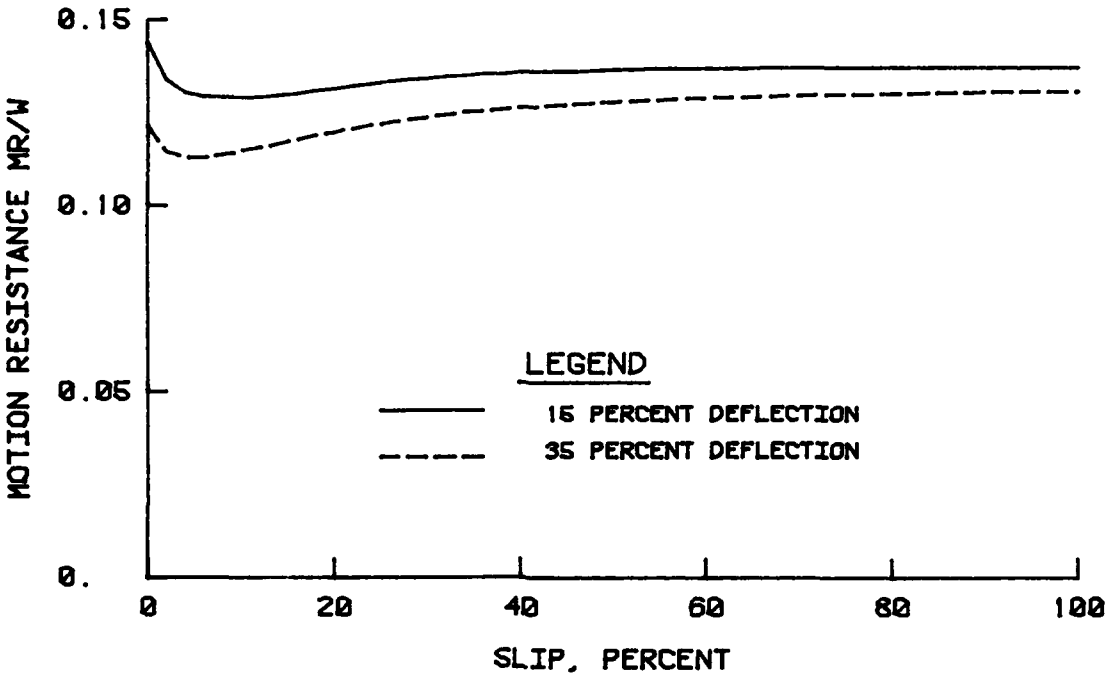

Figure 30. Relationship between motion resistance and slip ratio for sand

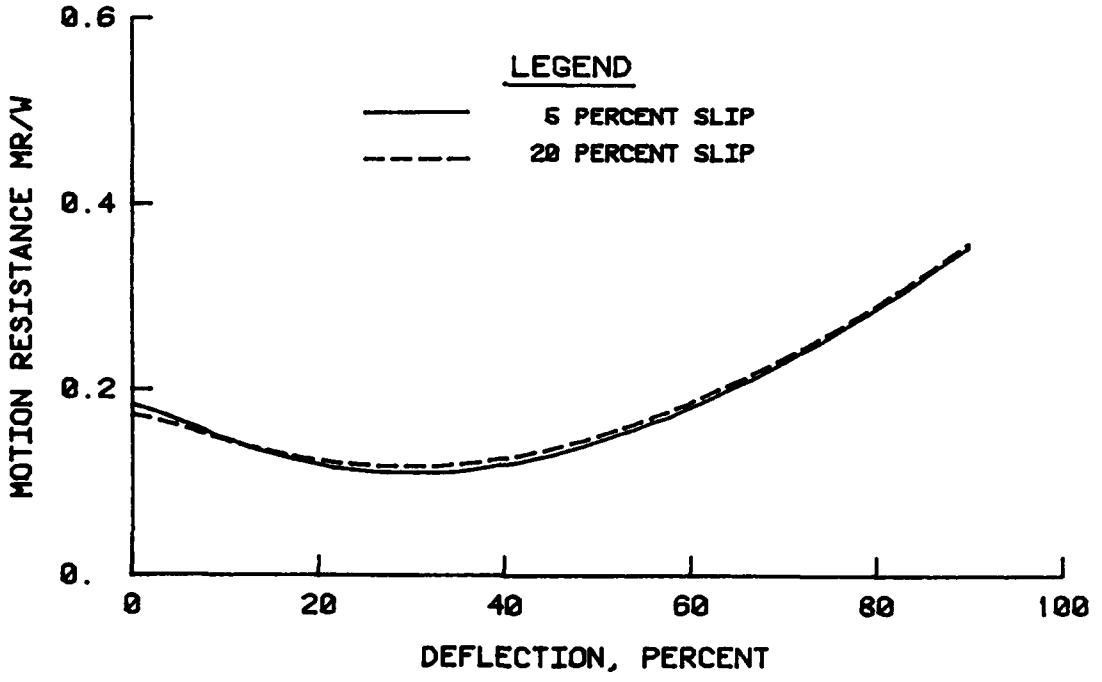

Figure 31. Relationship between motion resistance and tire deflection for sand

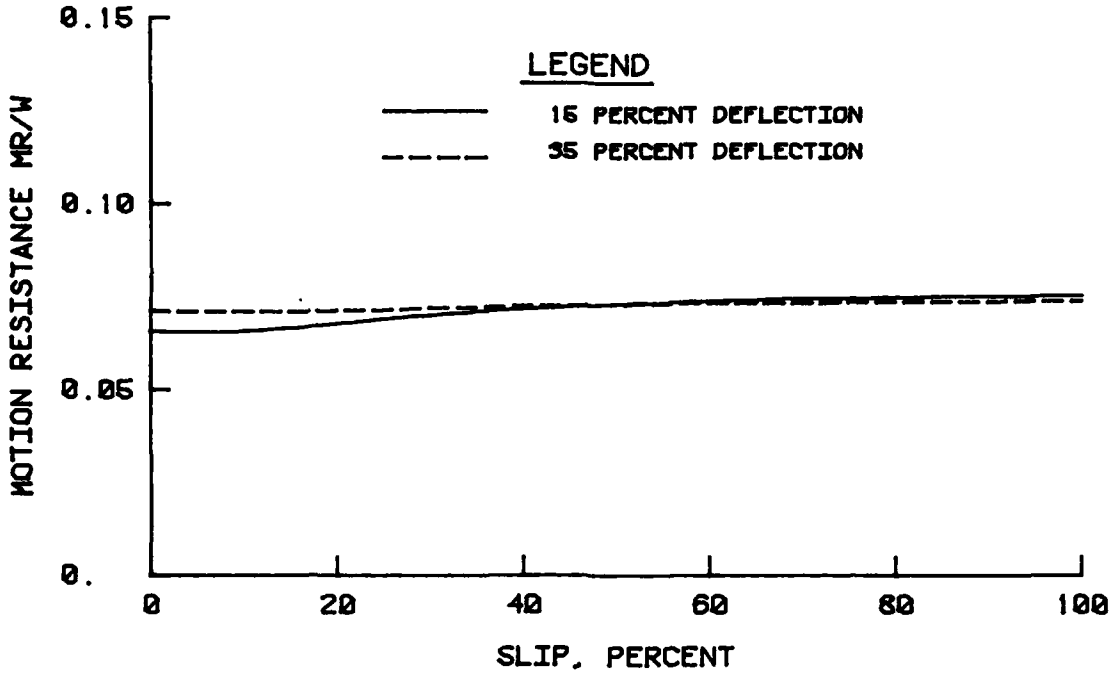

Figure 32. Relationship between motion resistance and slip ratio for mixed soil

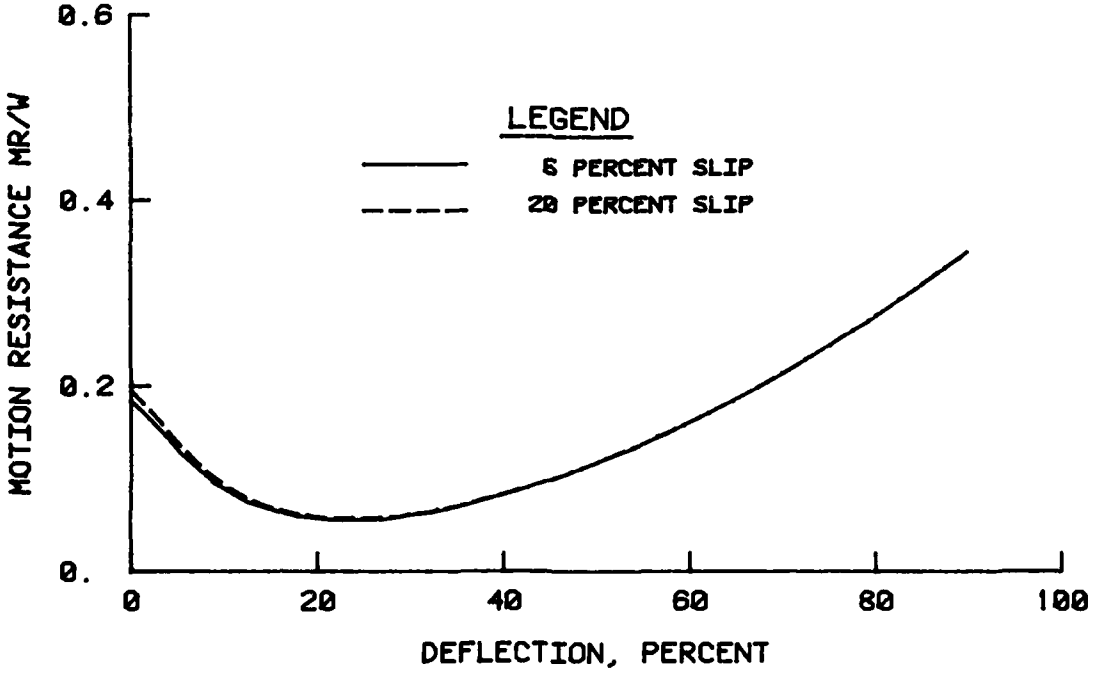

Figure 33. Relationship between motion resistance and tire deflection for mixed soil

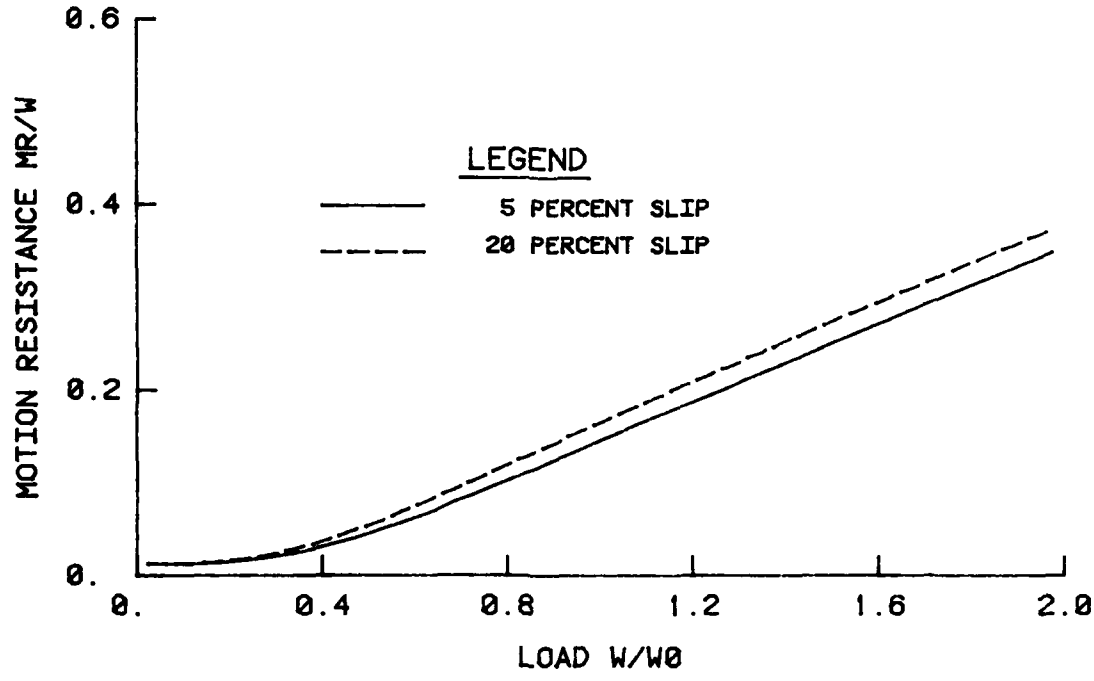

Figure 34. Relationship between motion resistance and wheel load for clay; 15 percent tire deflection

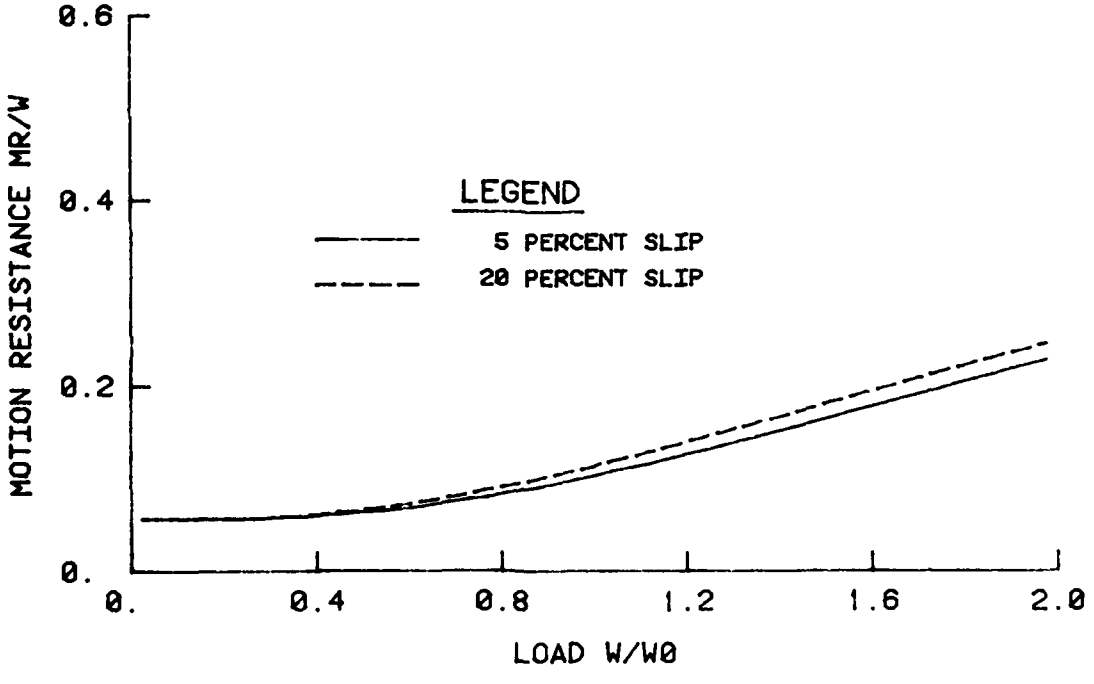

Figure 35. Relationship between motion resistance and wheel load for clay; 35 percent tire deflection

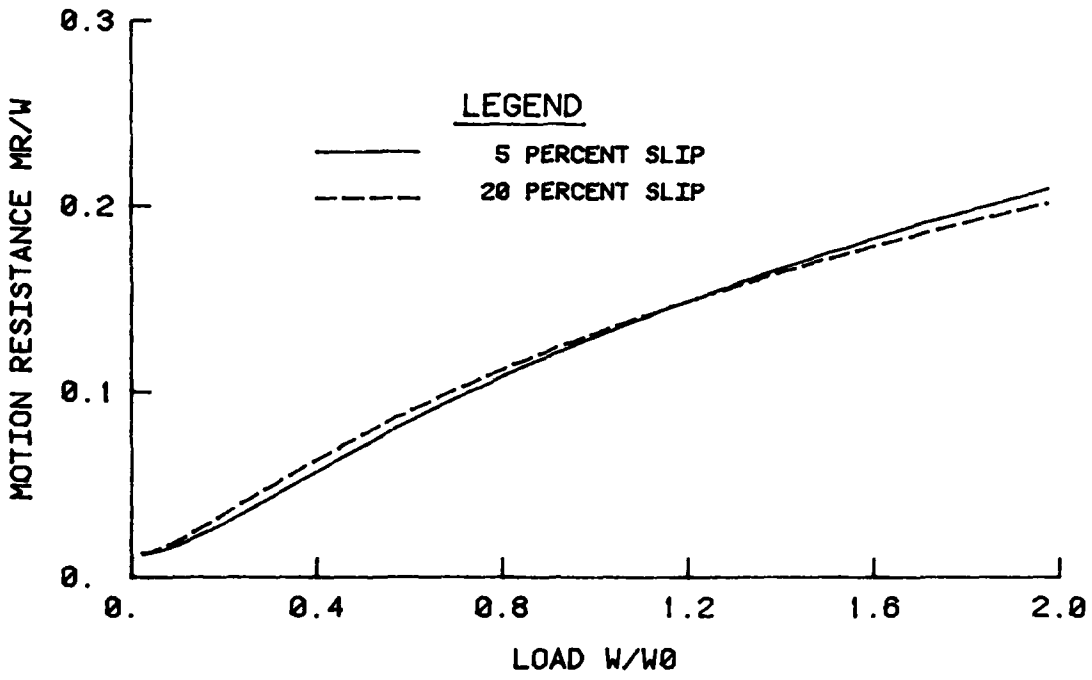

Figure 36. Relationship between motion resistance and wheel load for sand; 15 percent tire deflection

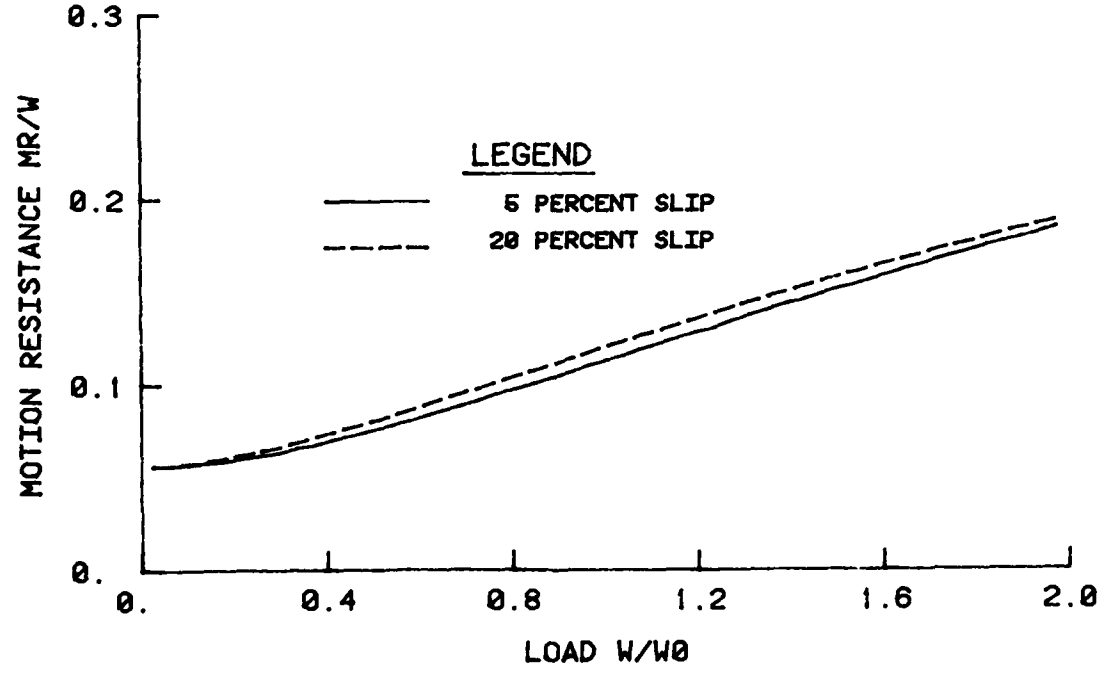

Figure 37. Relationship between motion resistance and wheel load for sand; 35 percent tire deflection

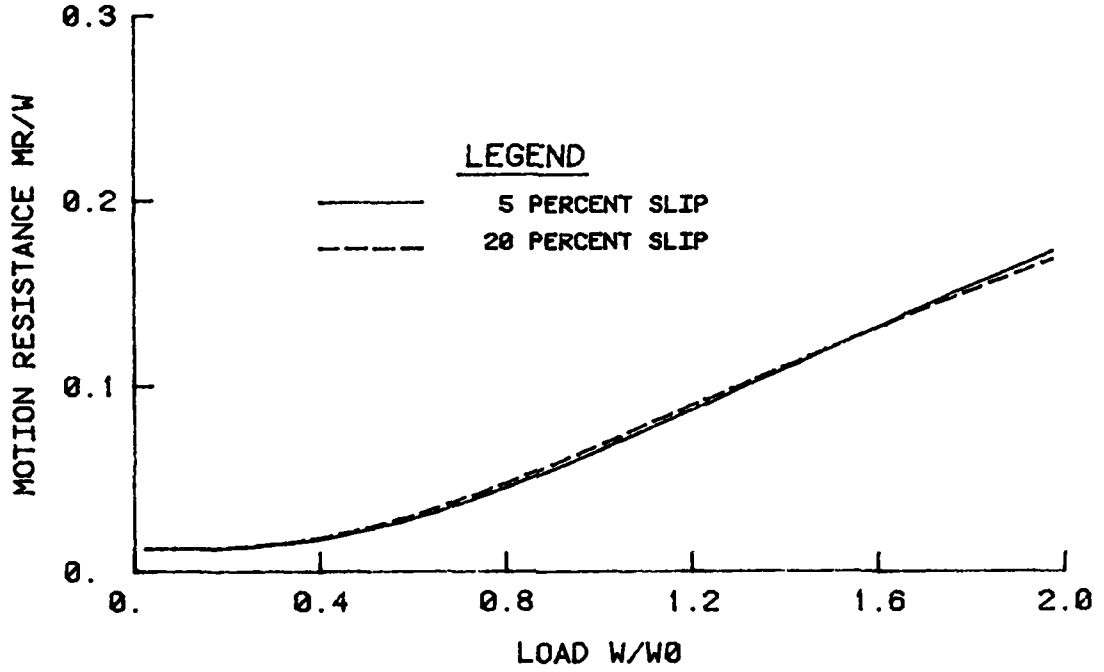

Figure 38. Relationship between motion resistance and wheel load for mixed soil; 15 percent tire deflection

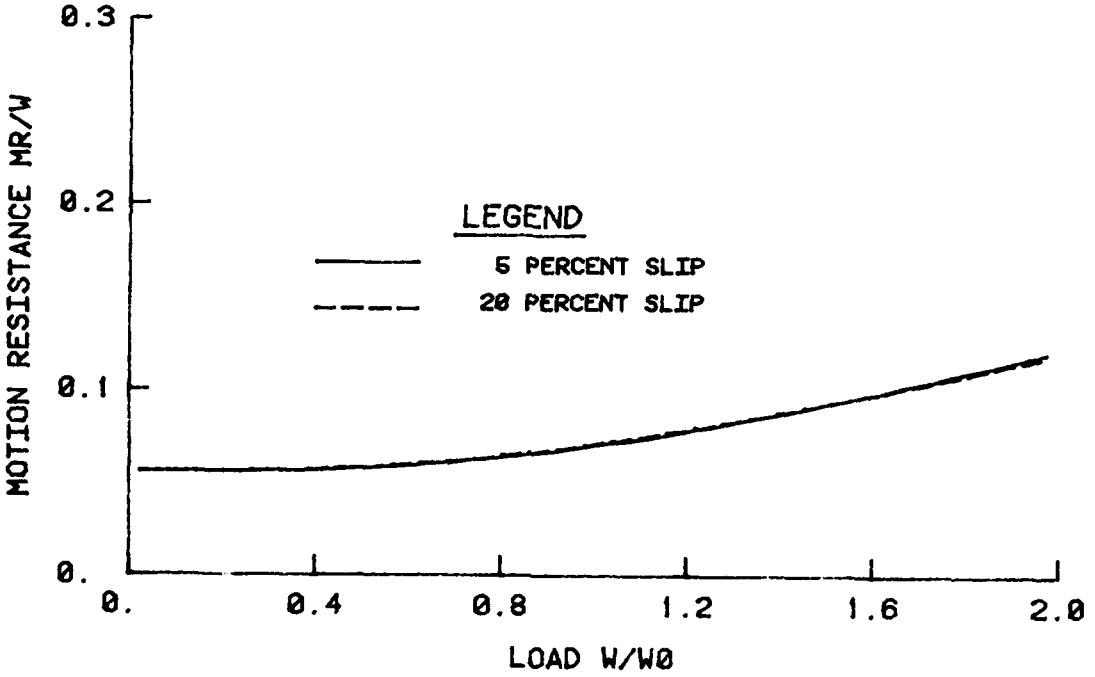

Figure 39. Relationship between motion resistance and wheel load for mixed soil; 35 percent tire deflection

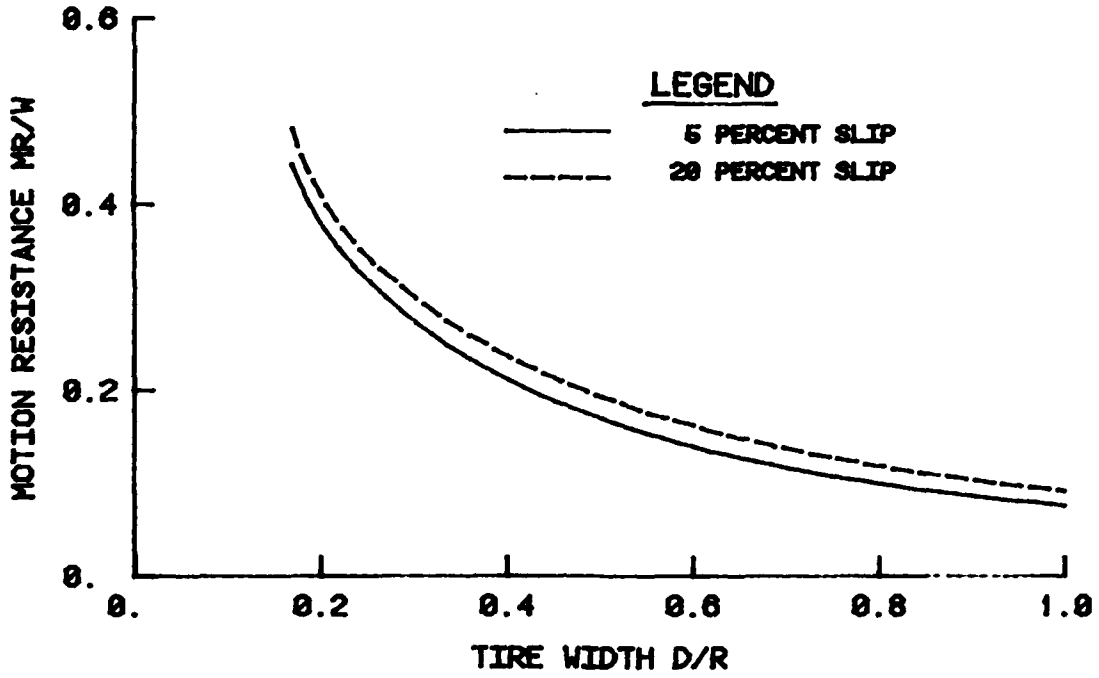

Figure 40. Relationship between motion resistance and tire width for clay; 15 percent tire deflection

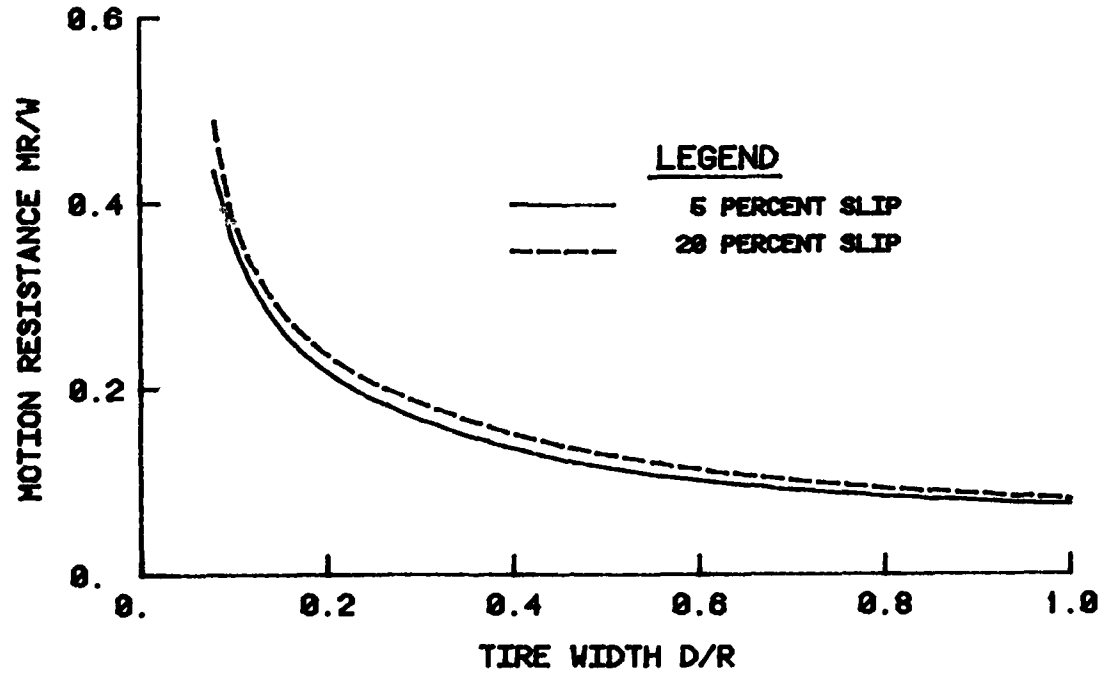

Figure 41. Relationship between motion resistance and tire width for clay; 35 percent tire deflection

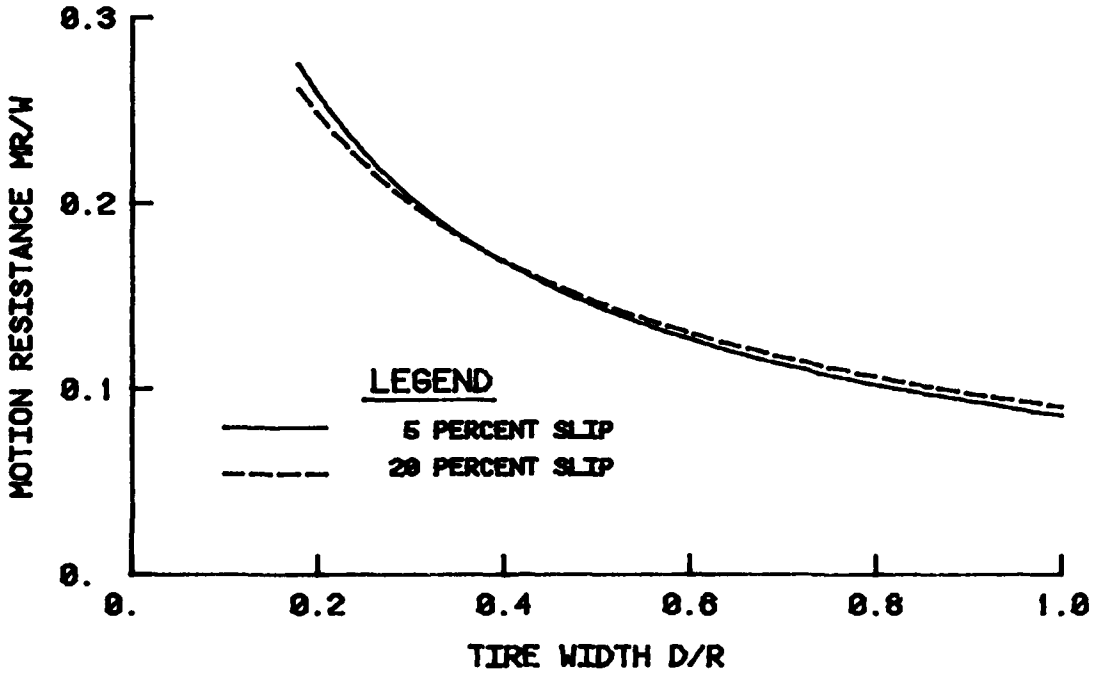

Figure 42. Relationship between motion resistance and tire width for sand; 15 percent tire deflection

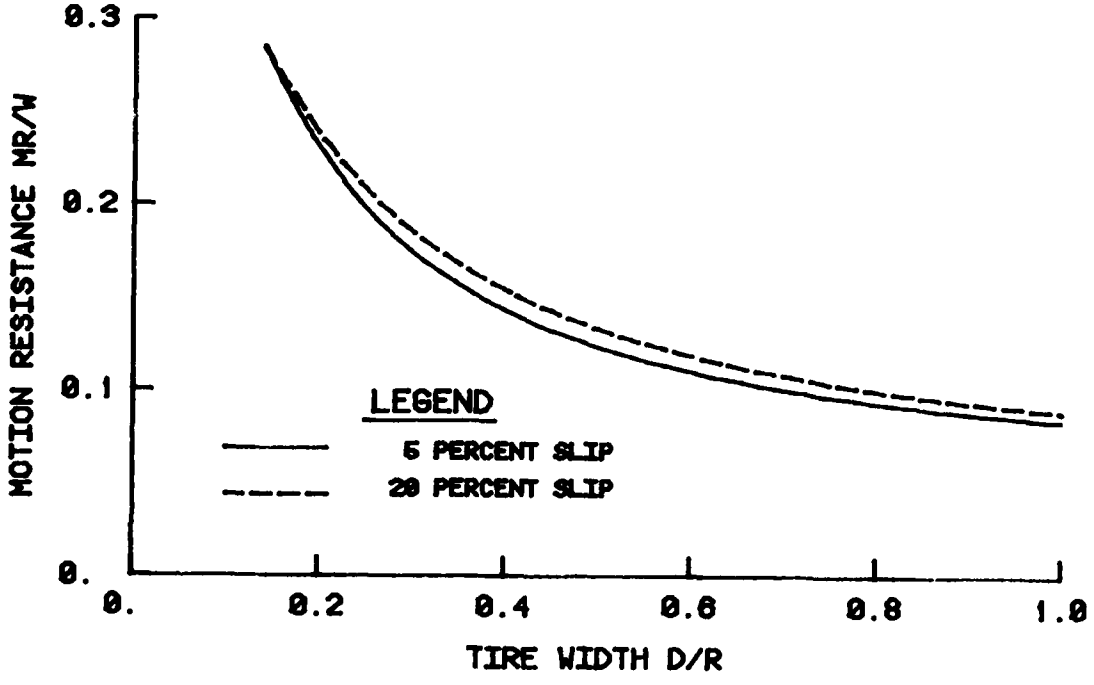

Figure 43. Relationship between motion resistance and tire width for sand; 35 percent tire deflection

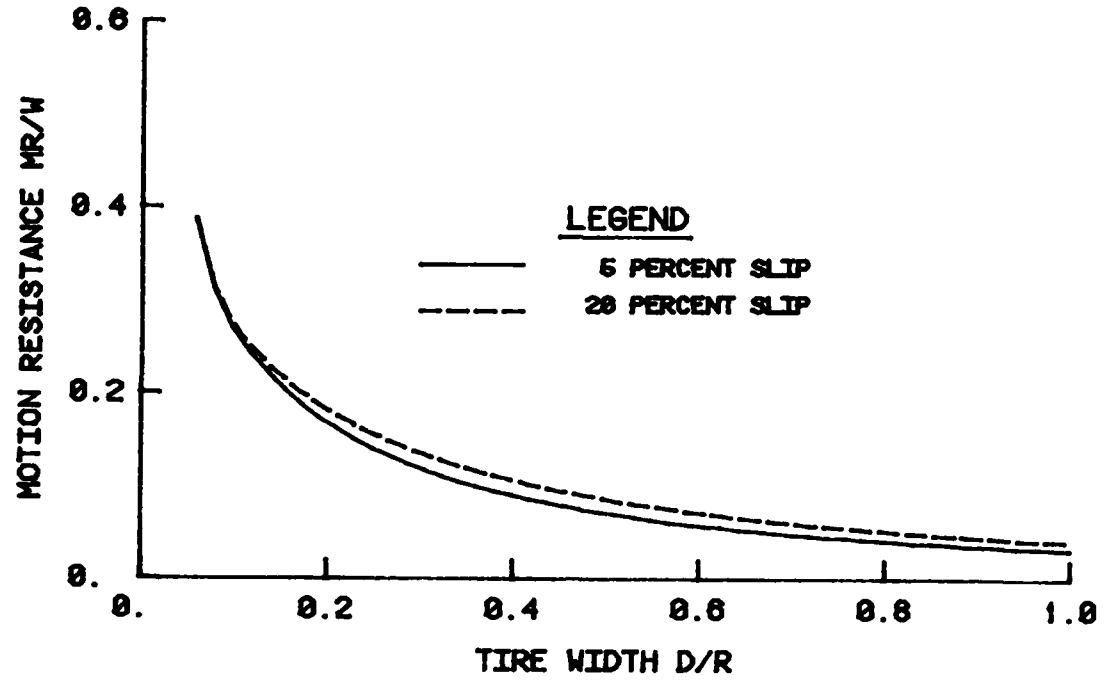

Figure 44. Relationship between motion resistance and tire width for mixed soil; 15 percent tire deflection

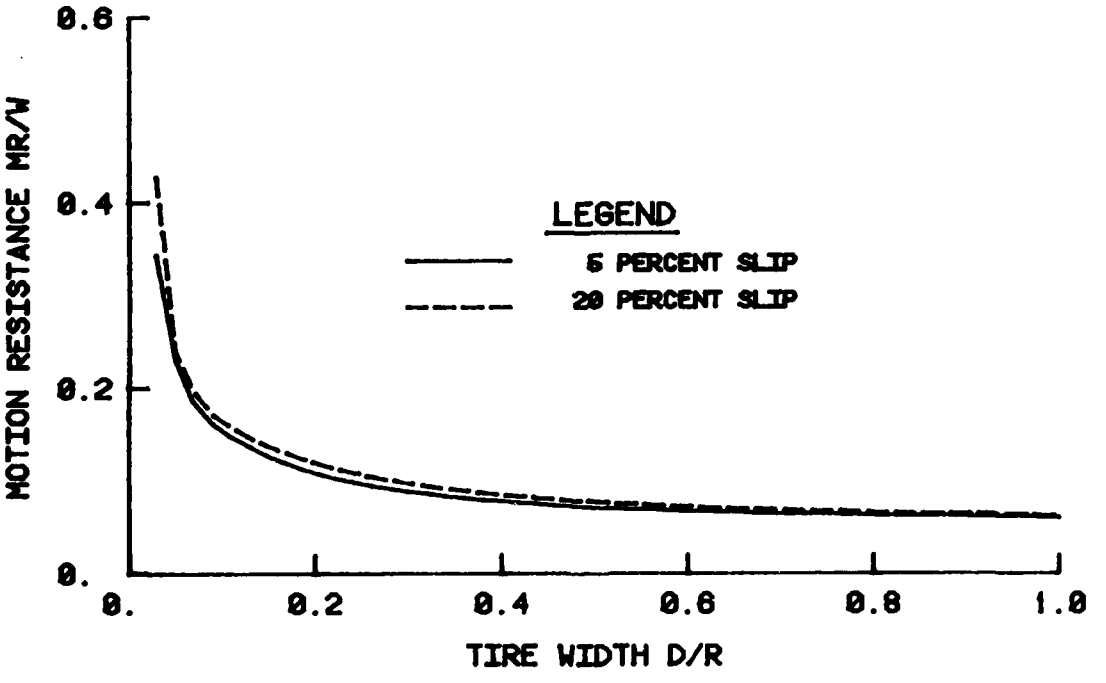

Figure 45. Relationship between motion resistance and tire width for mixed soil; 35 percent tire deflection

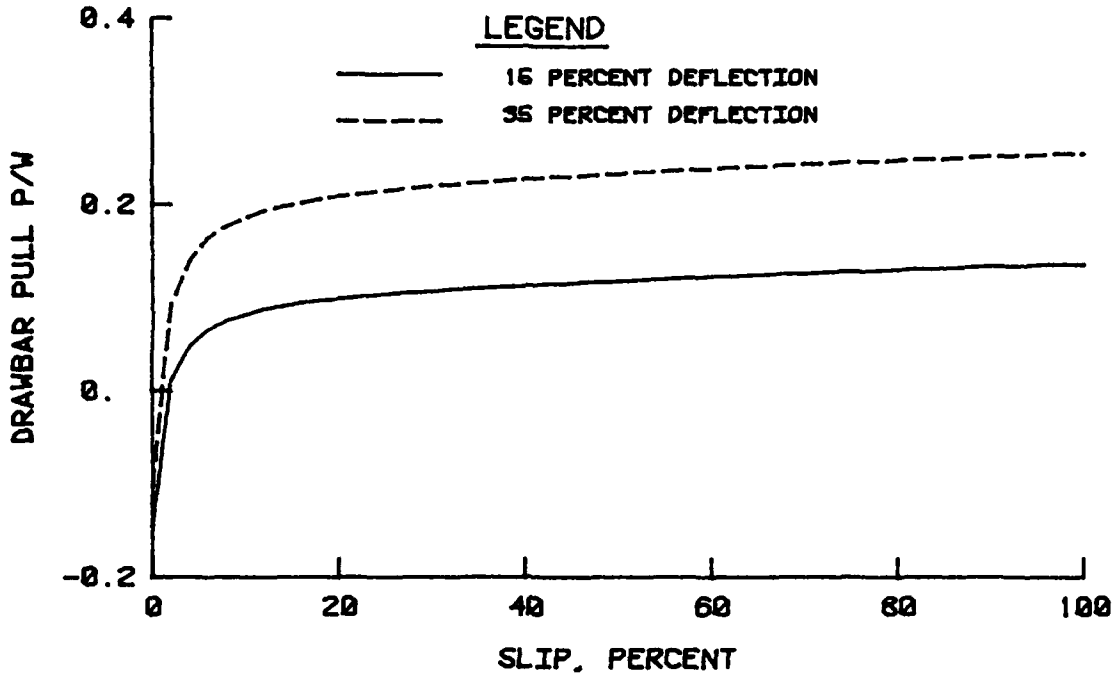

Figure 46. Relationship between drawbar pull and slip ratio for clay

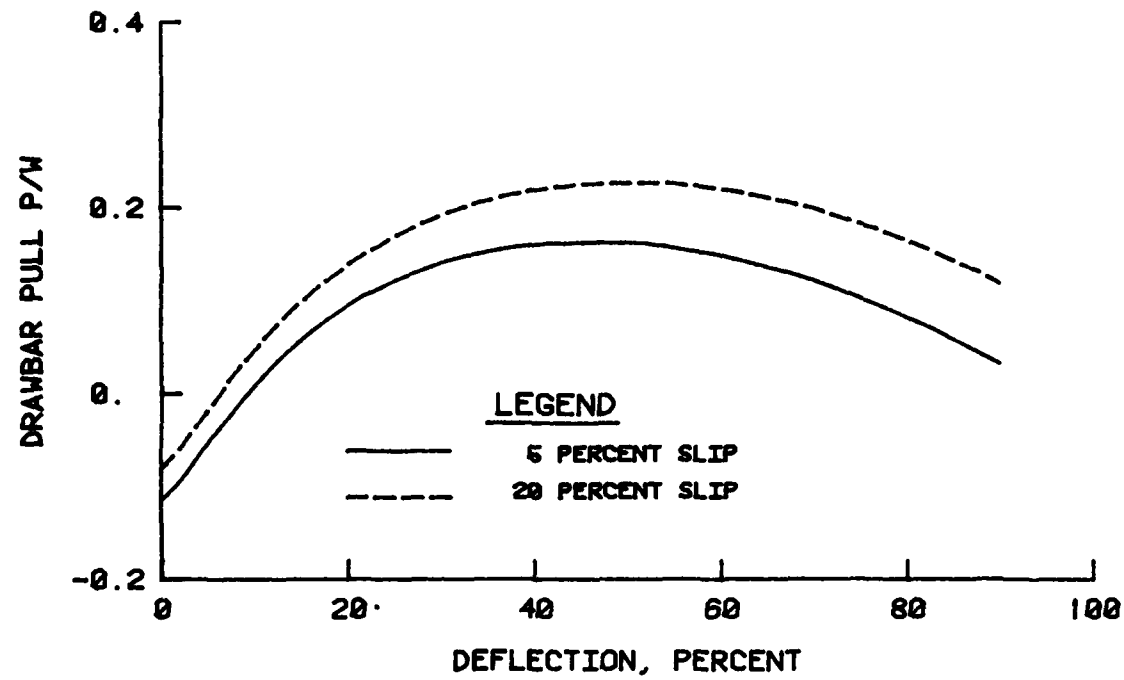

Figure 47. Relationship between drawbar pull and tire deflection for clay

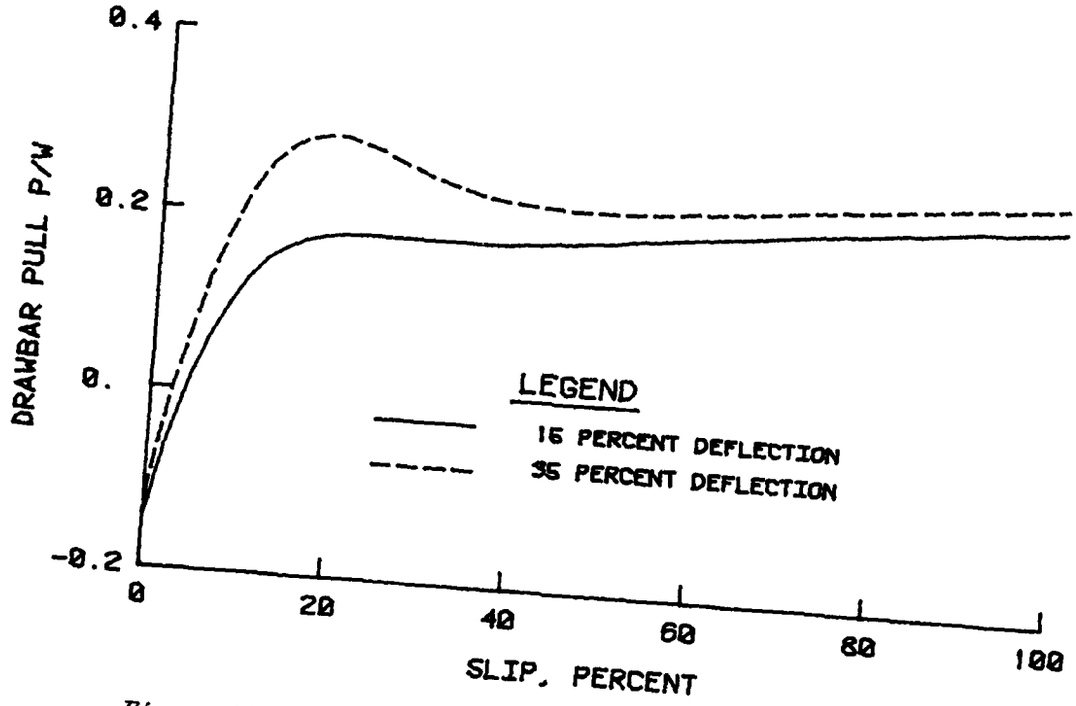

Figure 48. Relationship between drawbar pull and slip ratio for sand

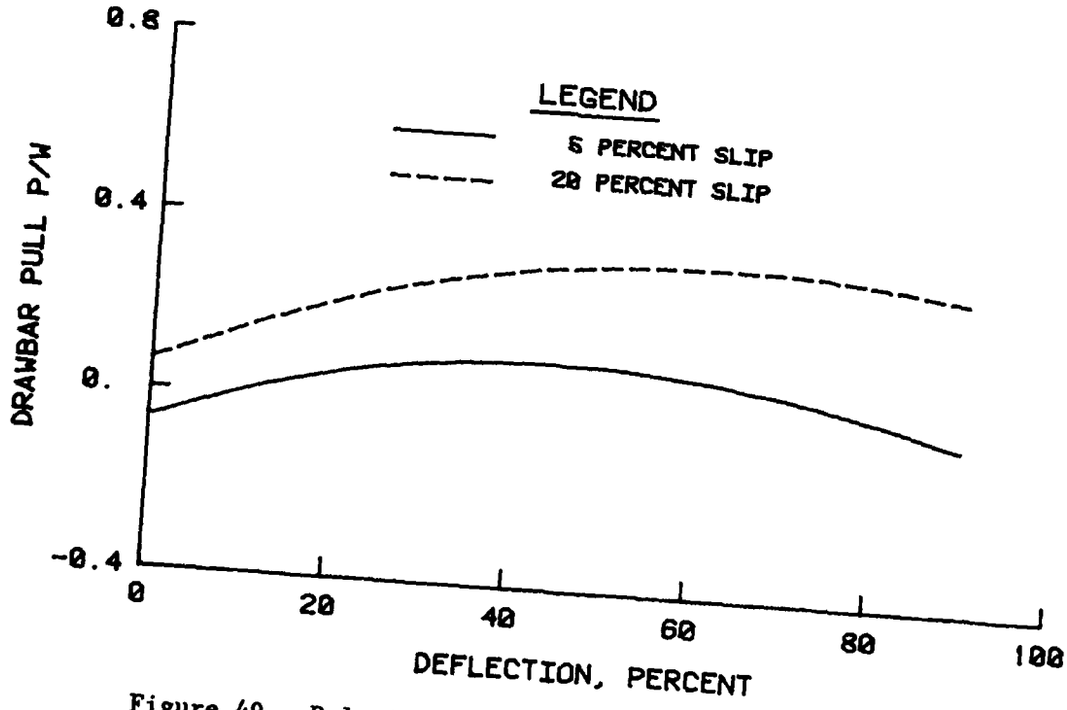

Figure 49. Relationship between drawbar pull and tire deflection for sand

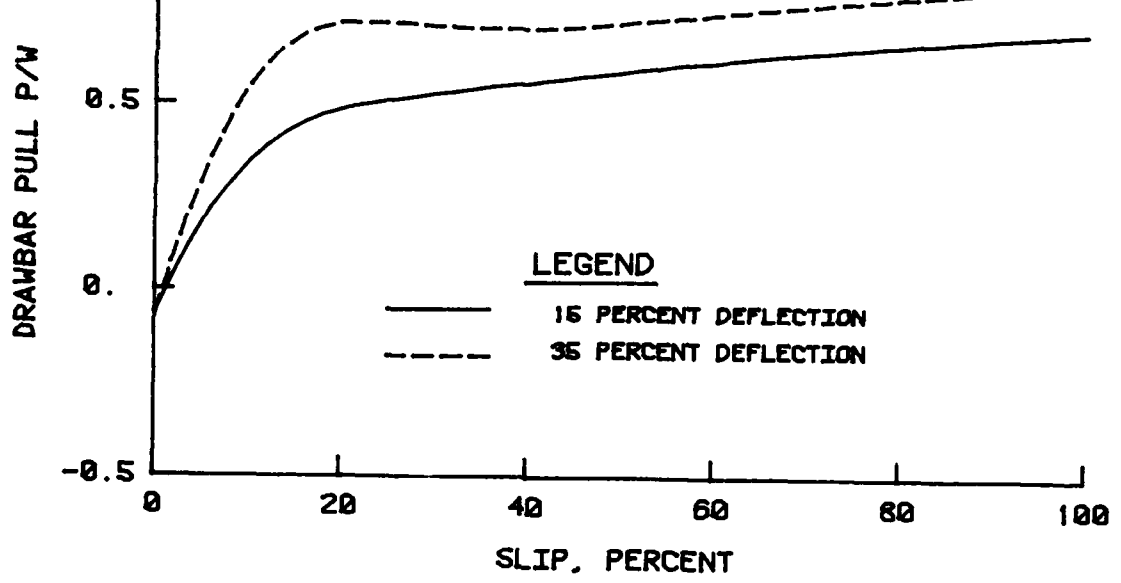

Figure 50. Relationship between drawbar pull and slip ratio for mixed soil

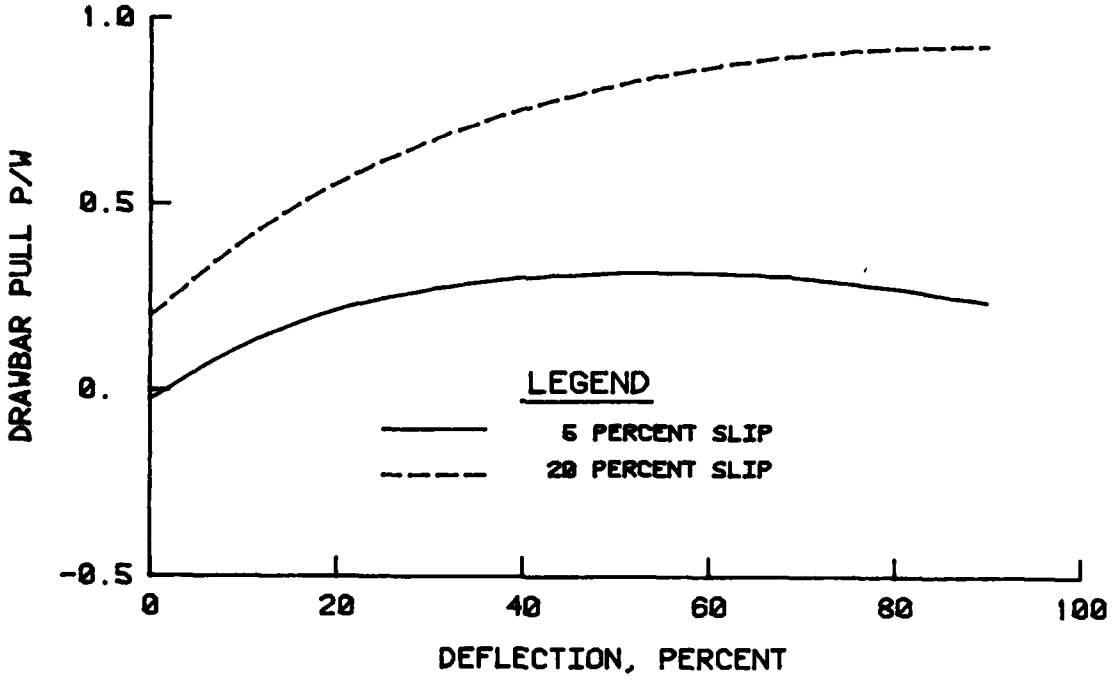

Figure 51. Relationship between drawbar pull and tire deflection for mixed soil

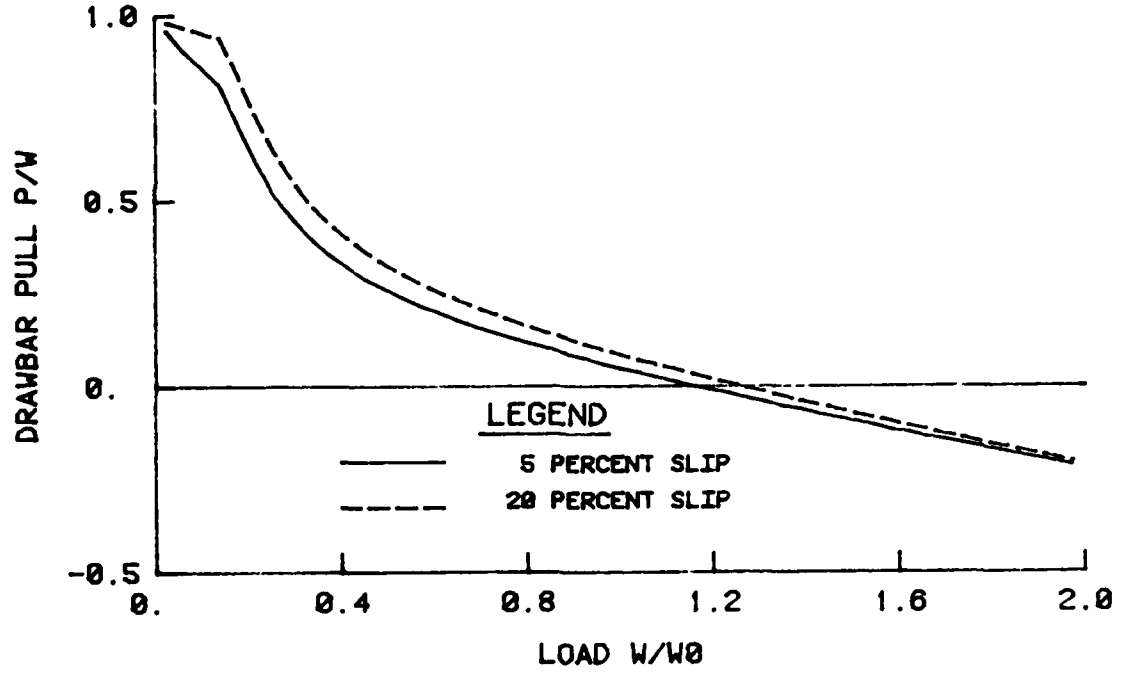

Figure 52. Relationship between drawbar pull and wheel load for clay; 15 percent tire deflection

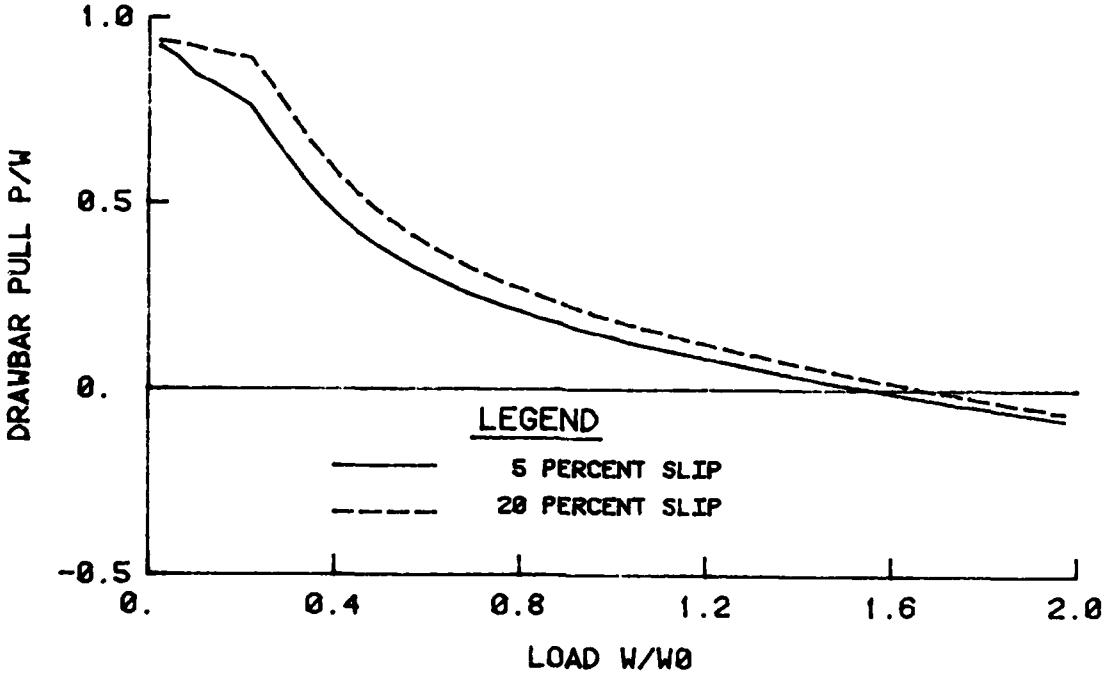

Figure 53. Relationship between drawbar pull and wheel load for clay; 35 percent tire deflection

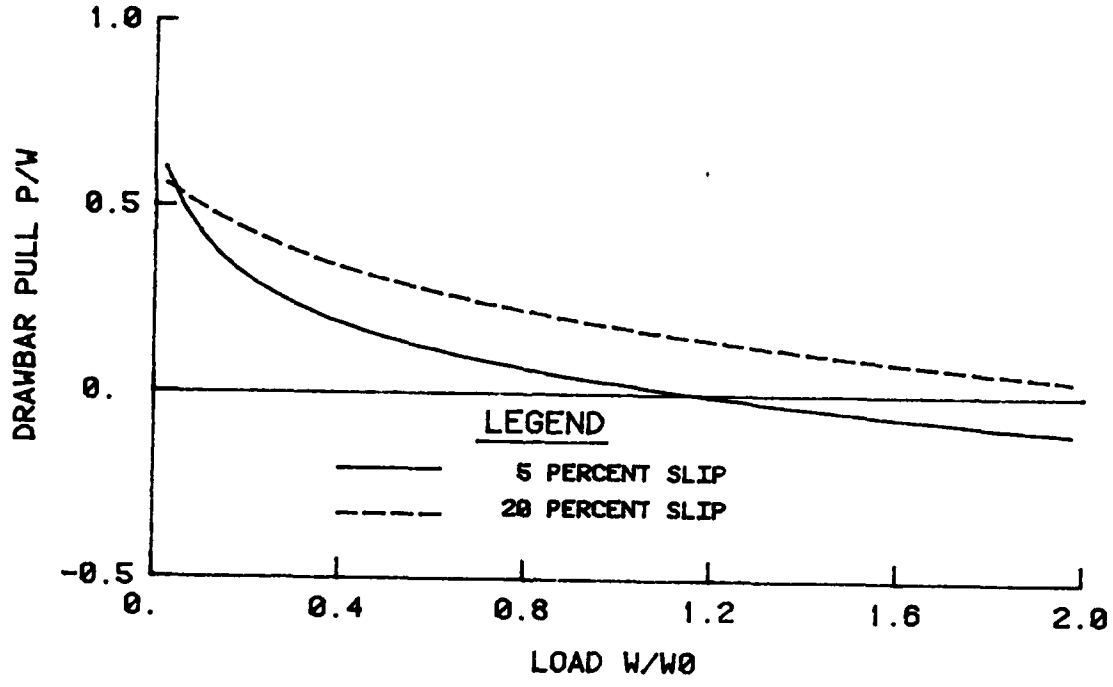

Figure 54. Relationship between drawbar pull and wheel load for sand; 15 percent tire deflection

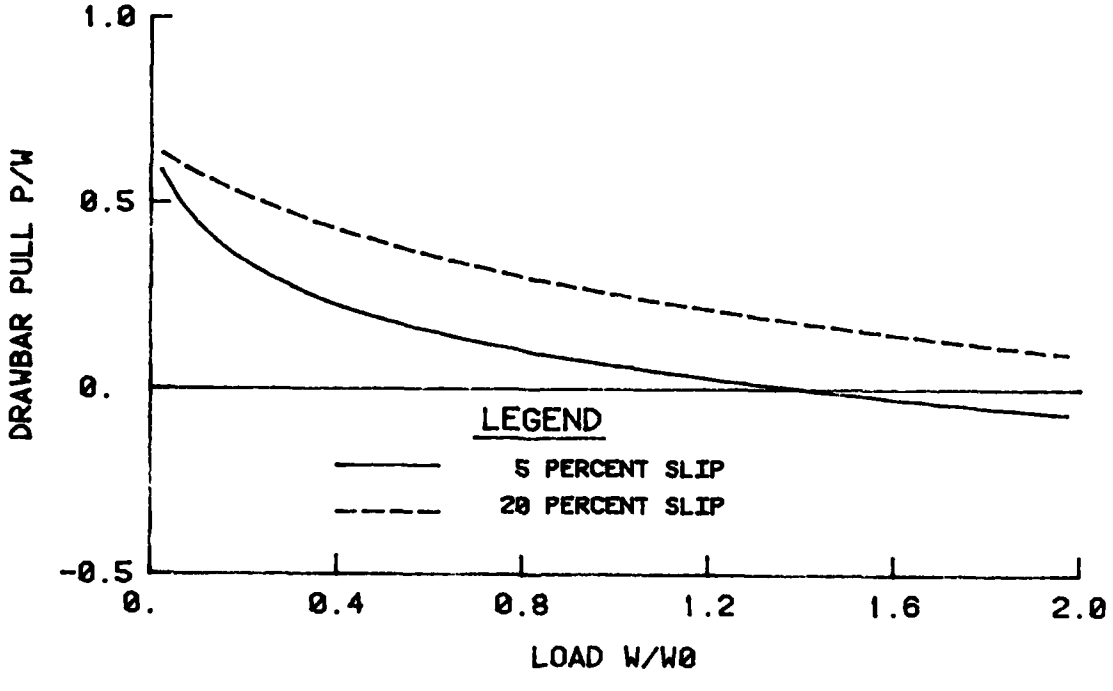

Figure 55. Relationship between drawbar pull and wheel load for sand; 35 percent tire deflection

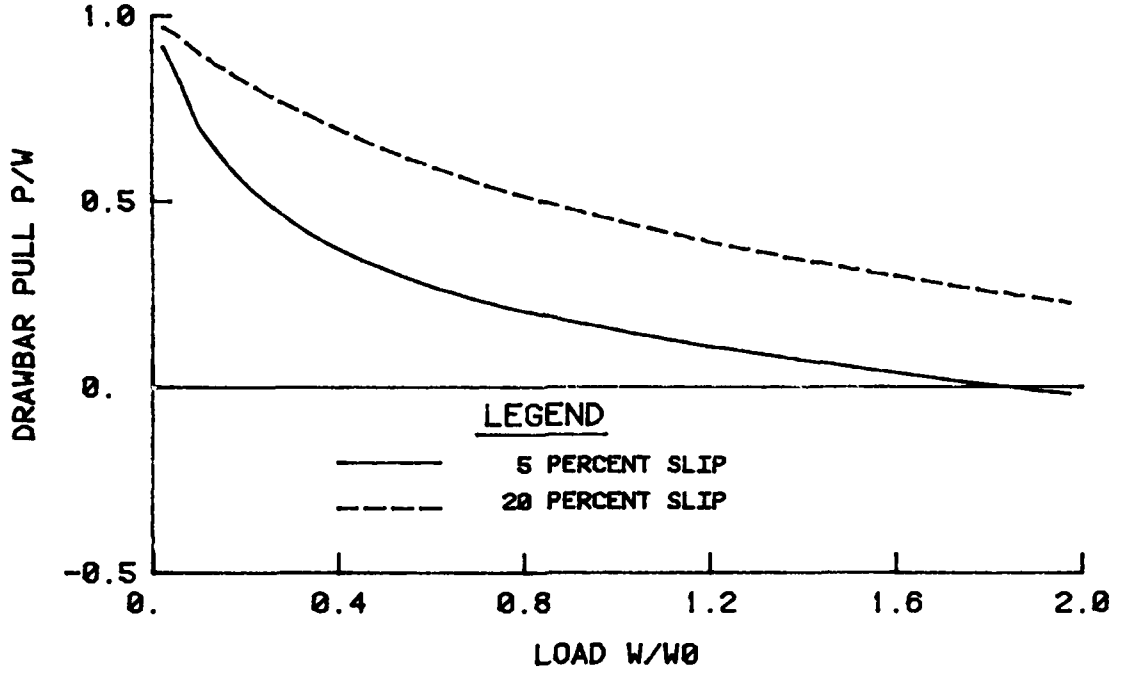

Figure 56. Relationship between drawbar pull and wheel load for mixed soil; 15 percent tire deflection

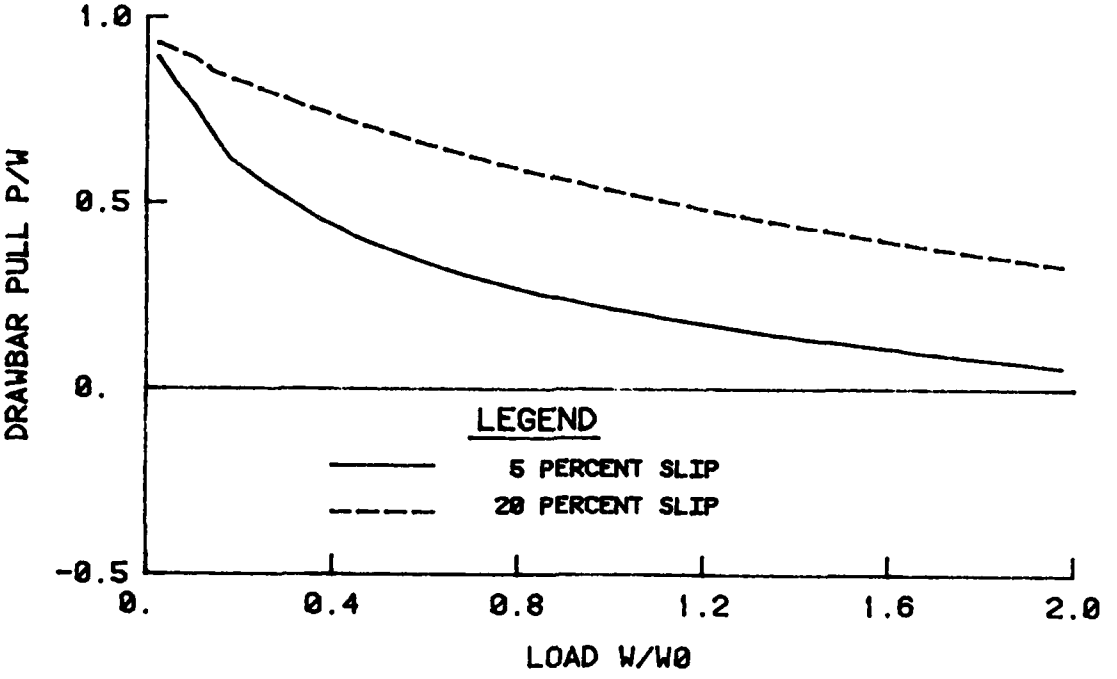

Figure 57. Relationship between drawbar pull and wheel load for mixed soil; 35 percent tire deflection

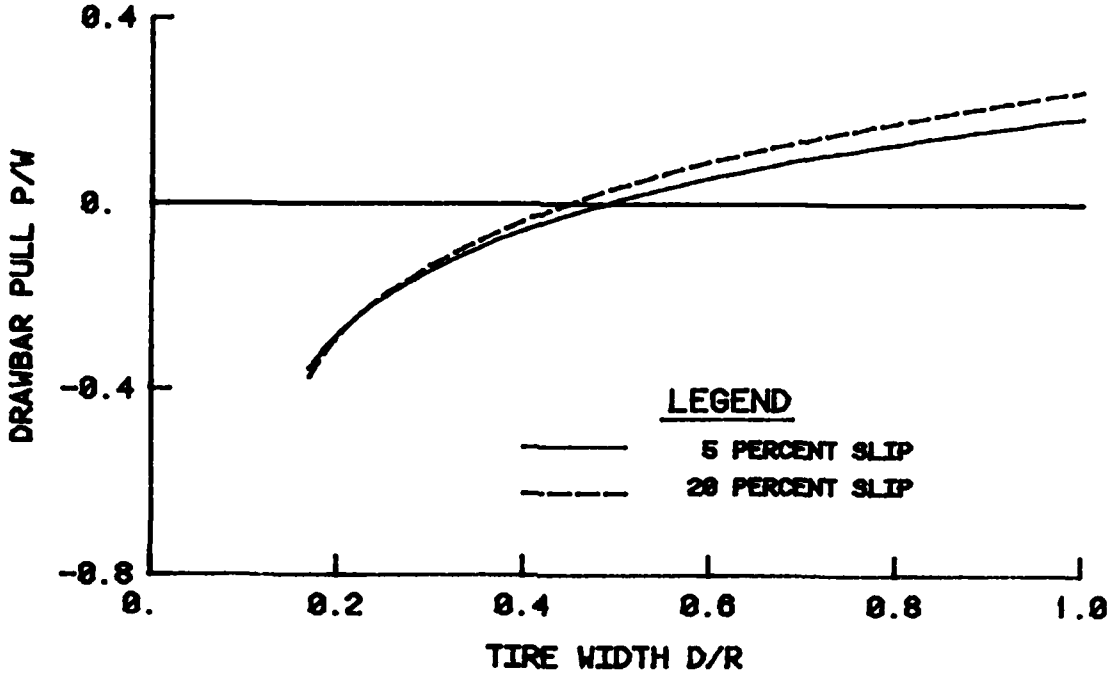

Figure 58. Relationship between drawbar pull and tire width for clay; 15 percent tire deflection

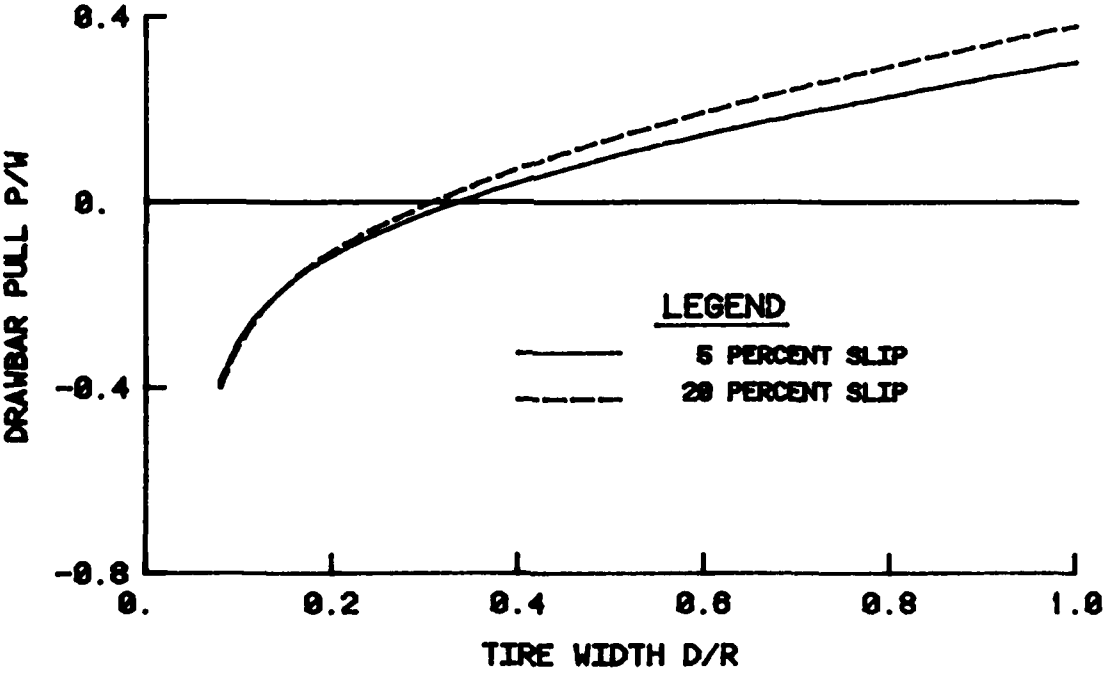

Figure 59. Relationship between drawbar pull and tire width for clay; 35 percent tire deflection

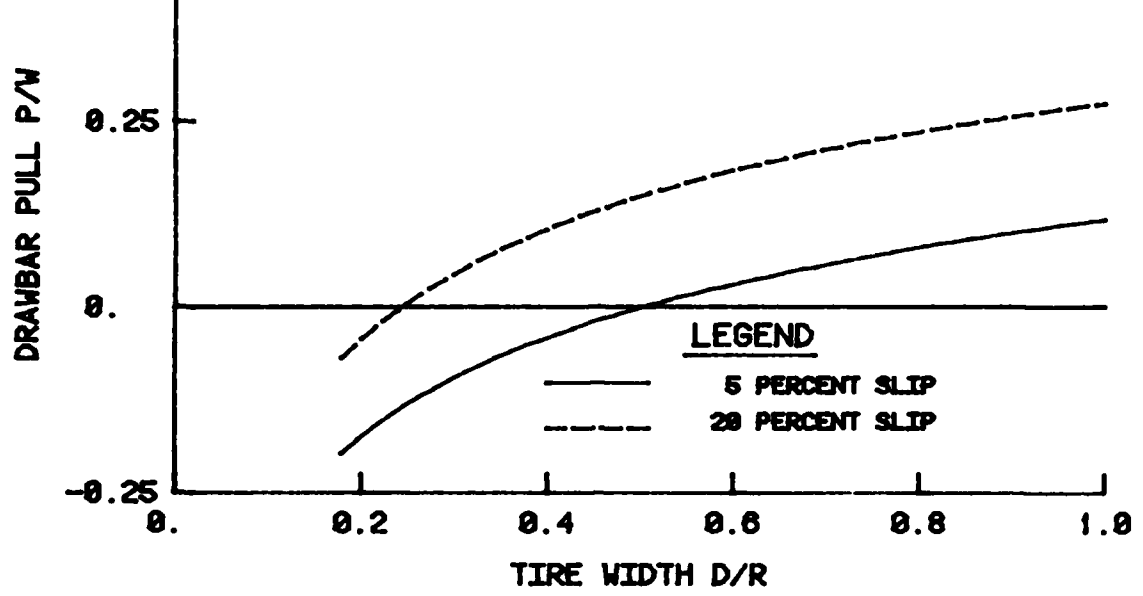

Figure 60. Relationship between drawbar pull and tire width for sand; 15 percent tire deflection

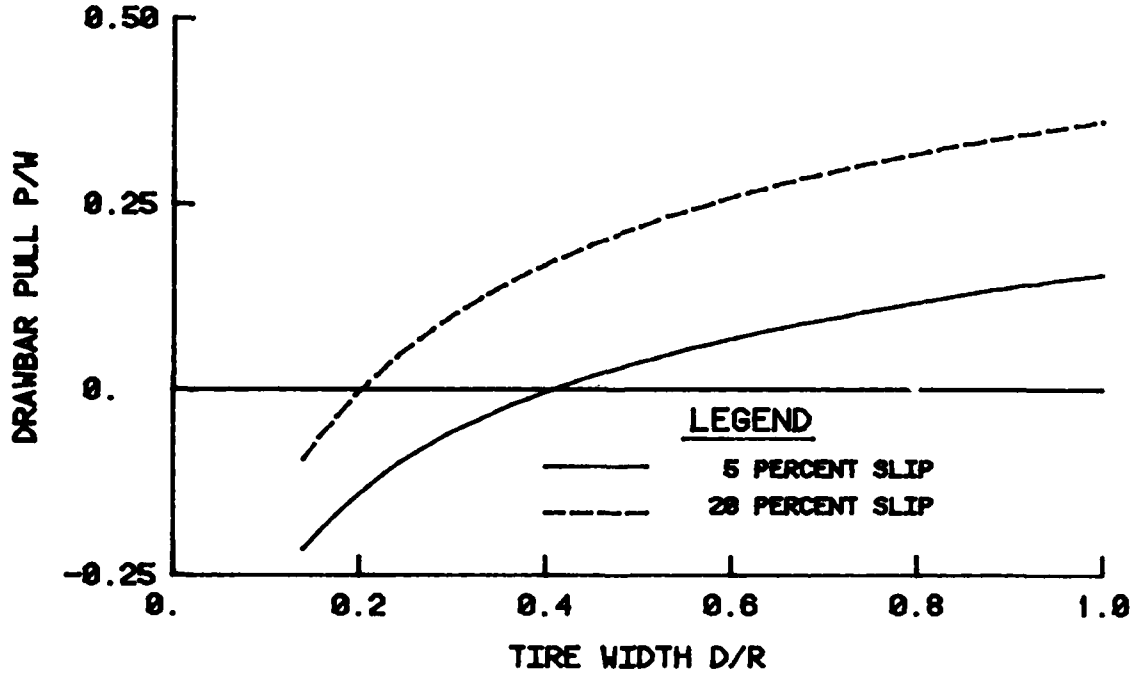

Figure 61. Relationship between drawbar pull and tire width for sand; 35 percent tire deflection

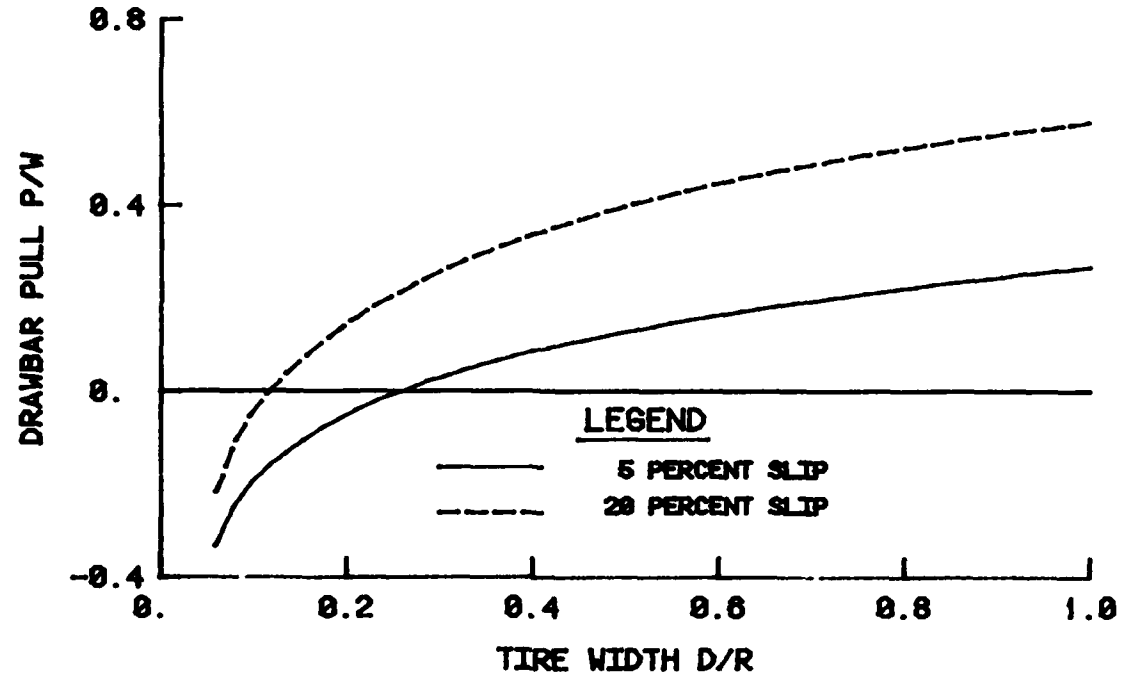

Figure 62. Relationship between drawbar pull and tire width for mixed soil; 15 percent tire deflection

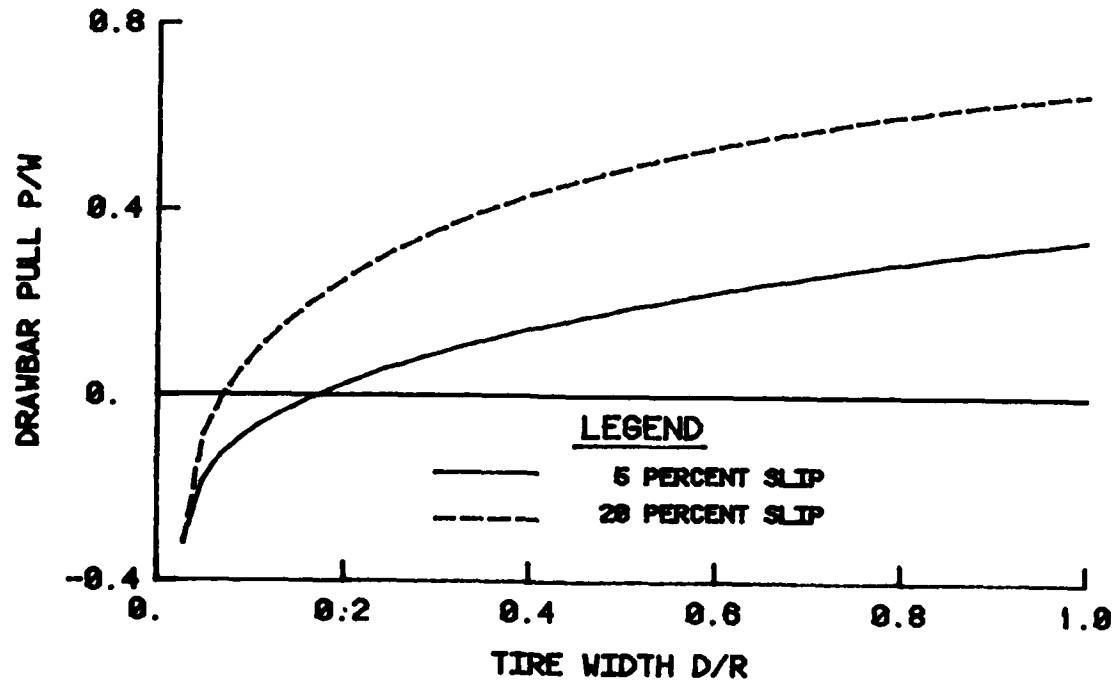

Figure 63. Relationship between drawbar pull and tire width for mixed soil; 35 percent tire deflection

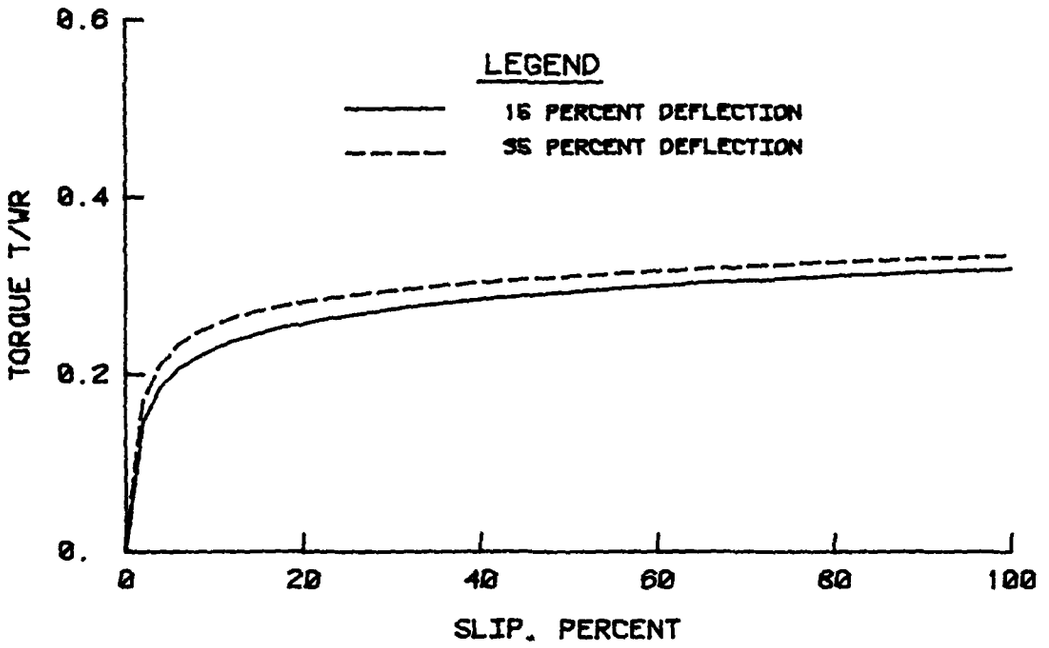

Figure 64. Relationship between torque and slip ratio for clay

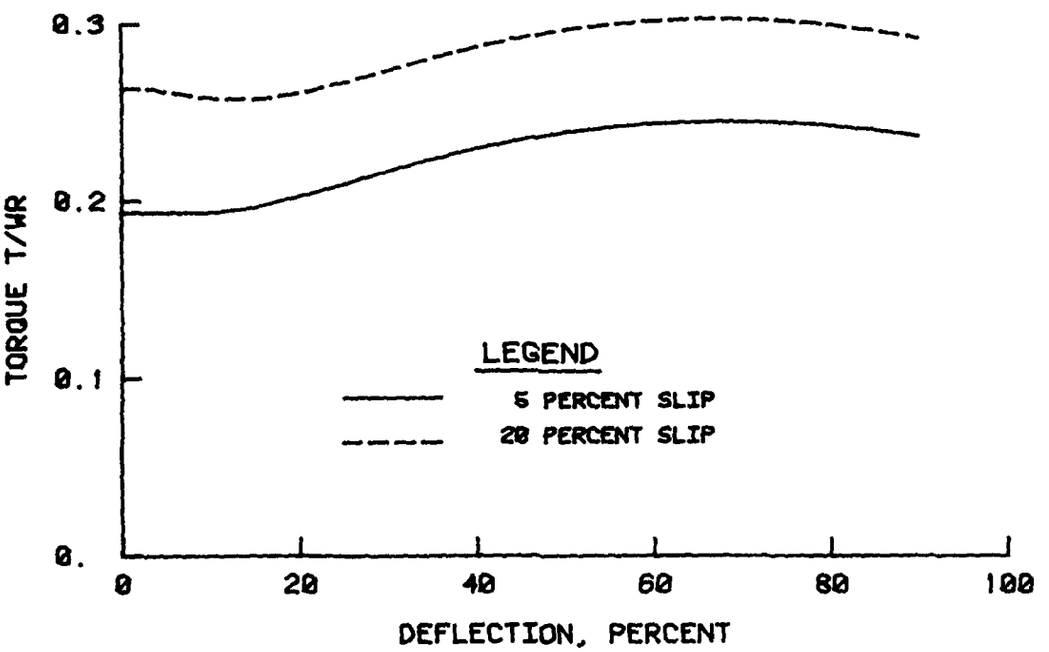

Figure 65. Relationship between torque and tire deflection for clay

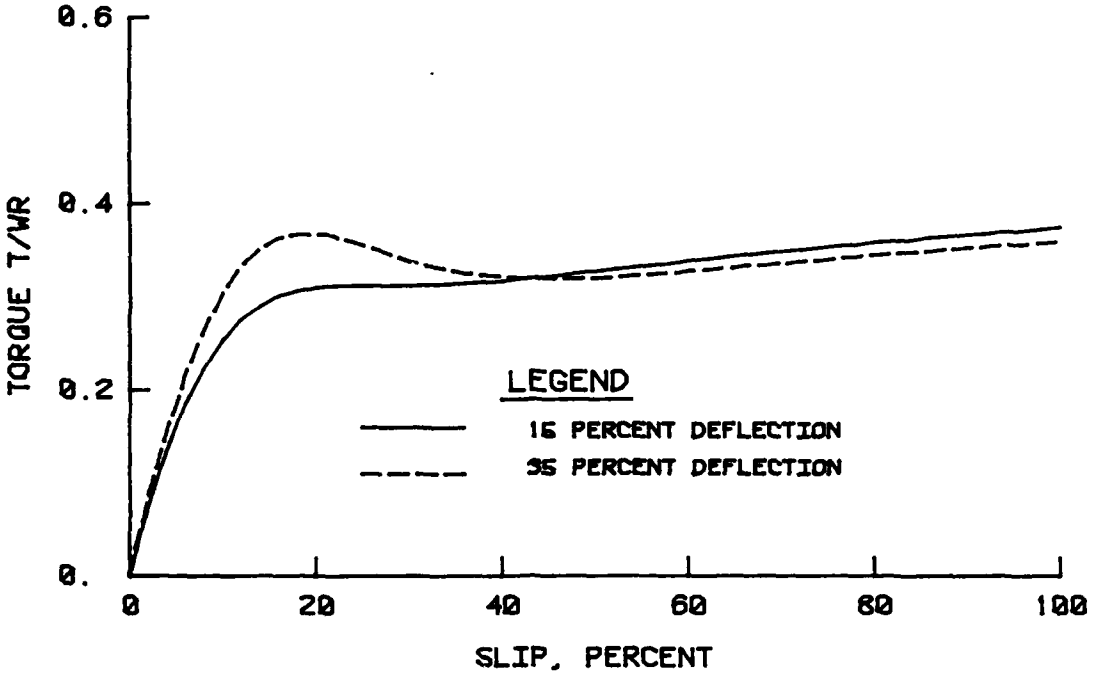

Figure 66. Relationship between torque and slip ratio for sand

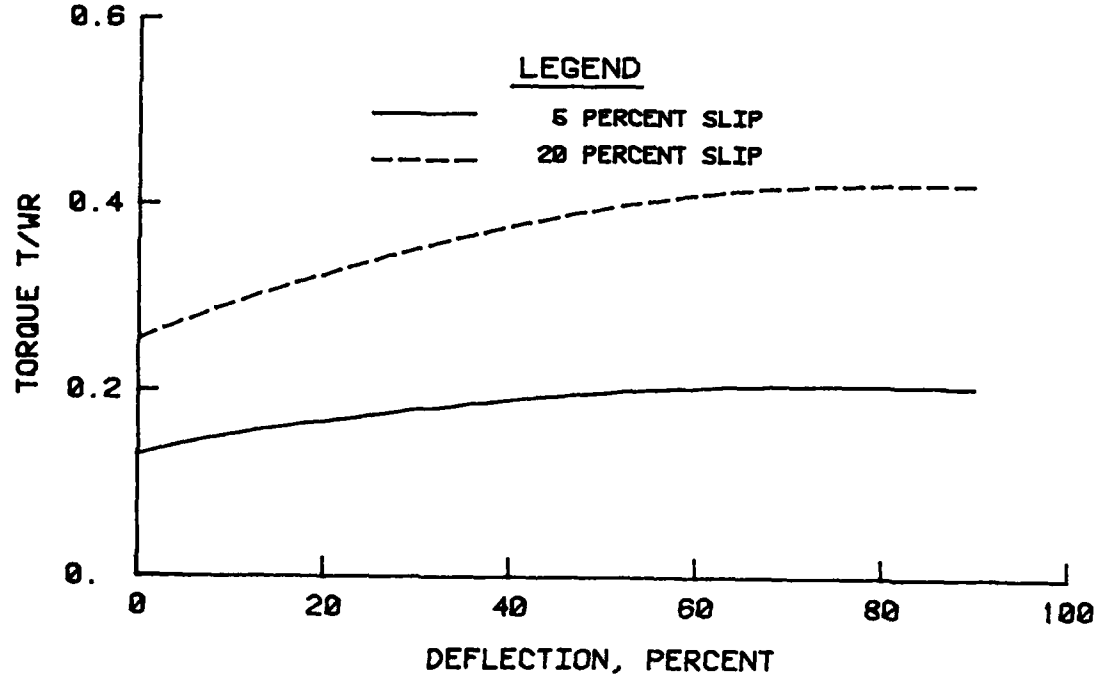

Figure 67. Relatipnship between torque and tire deflection for sand

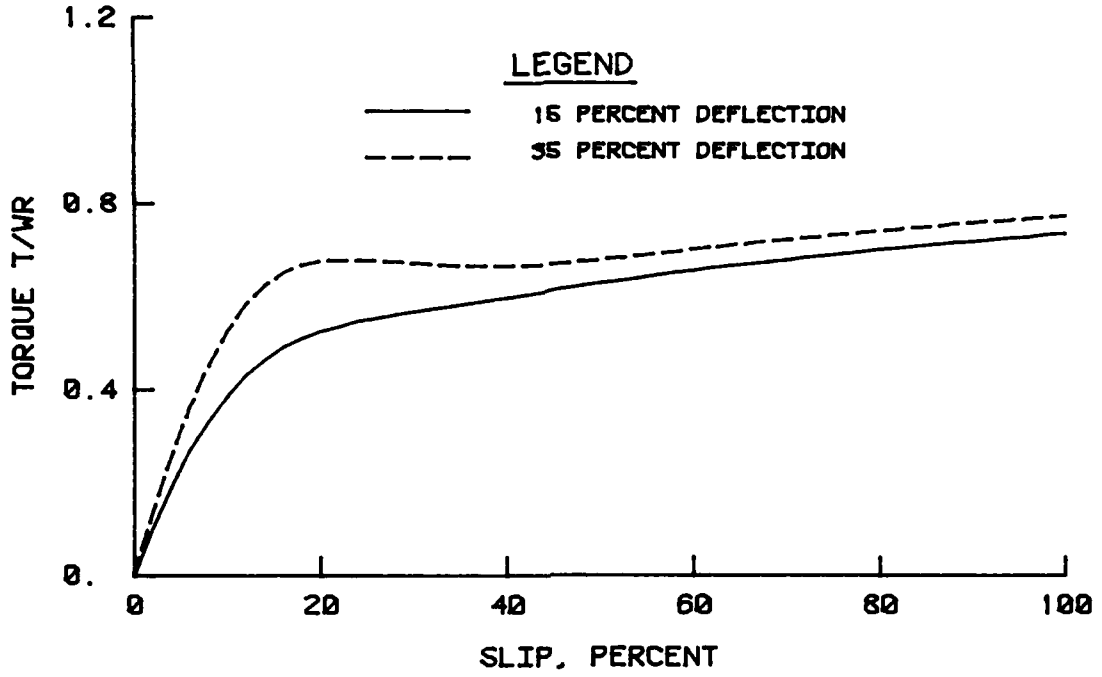

Figure 68. Relationship between torque and slip ratio for mixed soil

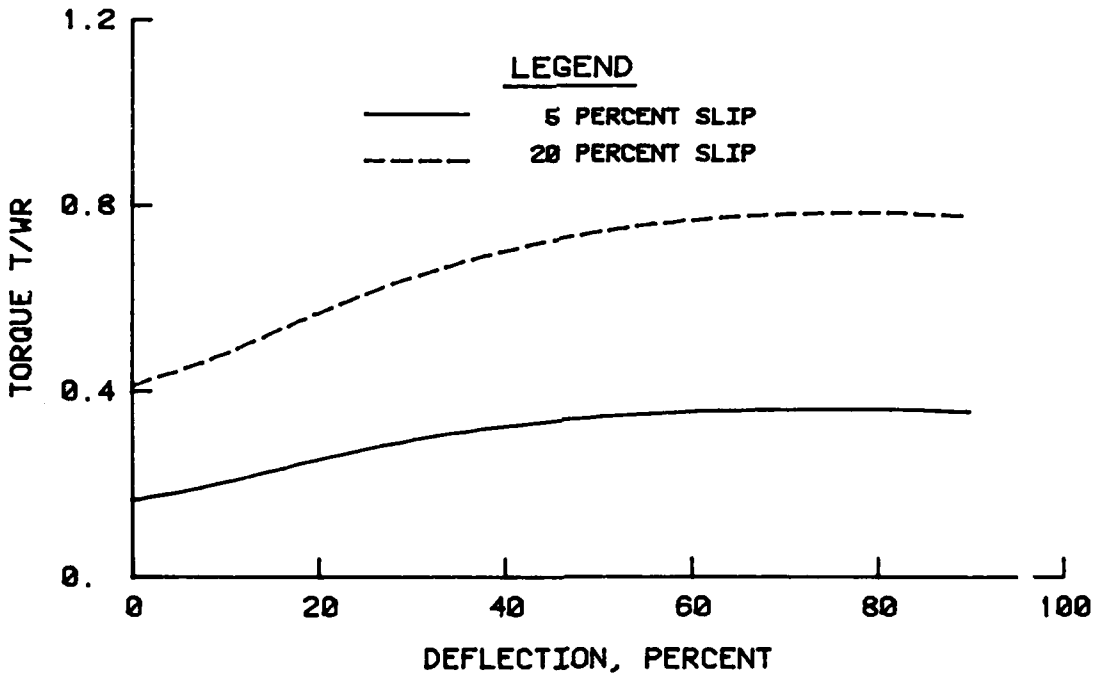

Figure 69. Relationship between torque and tire deflection for mixed soil

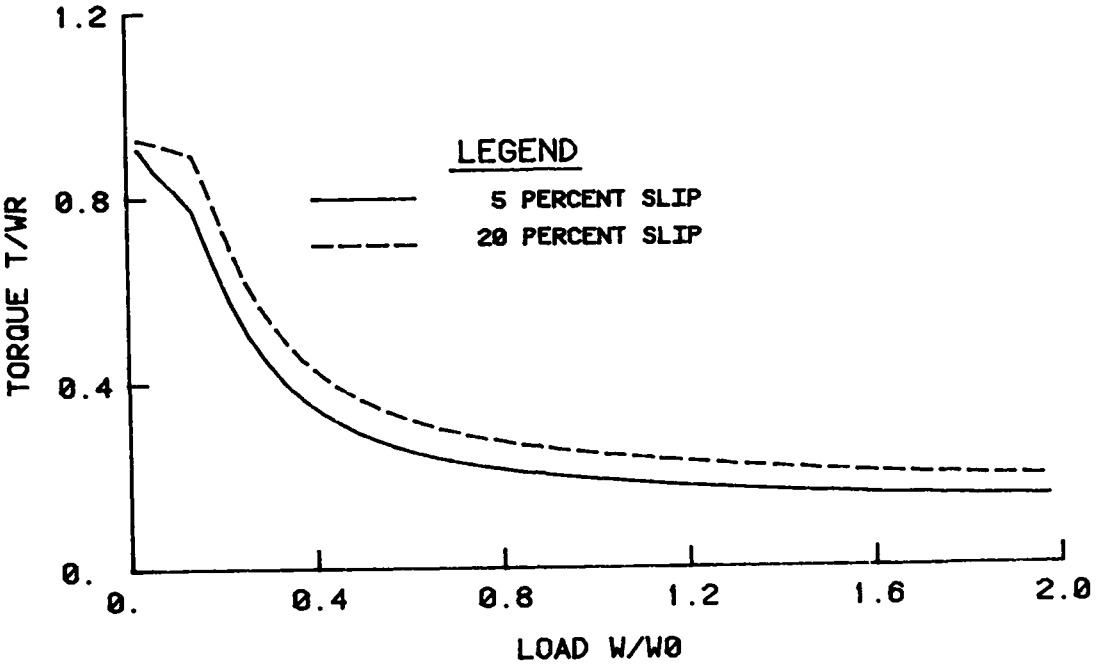

Figure 70. Relationship between torque and wheel load for clay; 15 percent tire deflection

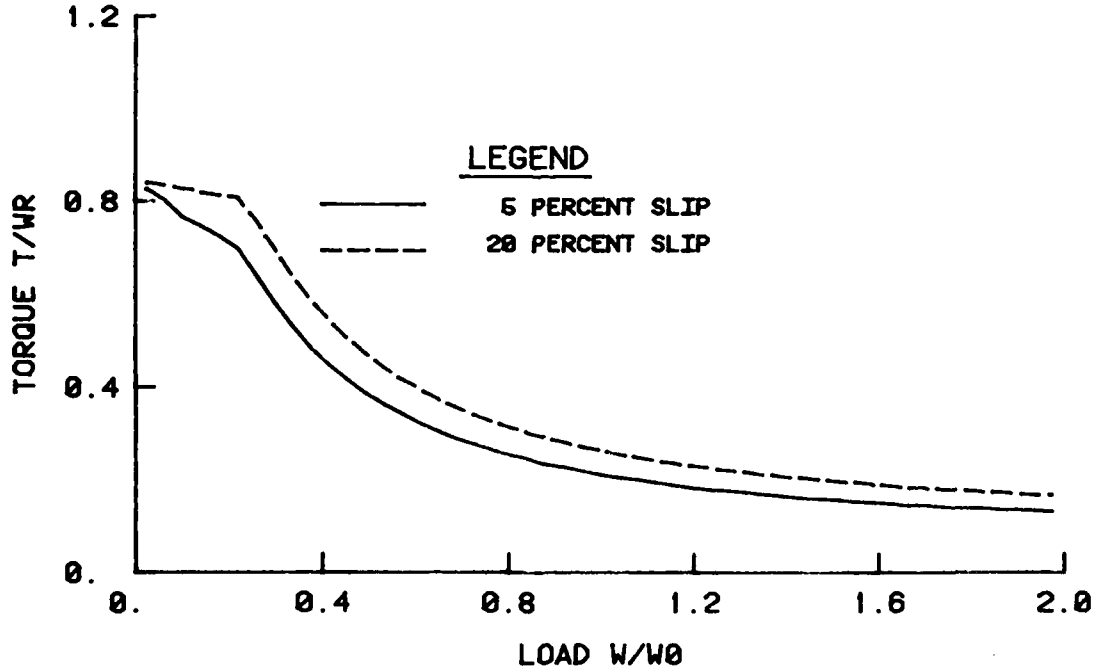

Figure 71. Relationship between torque and wheel load for clay; 35 percent tire deflection

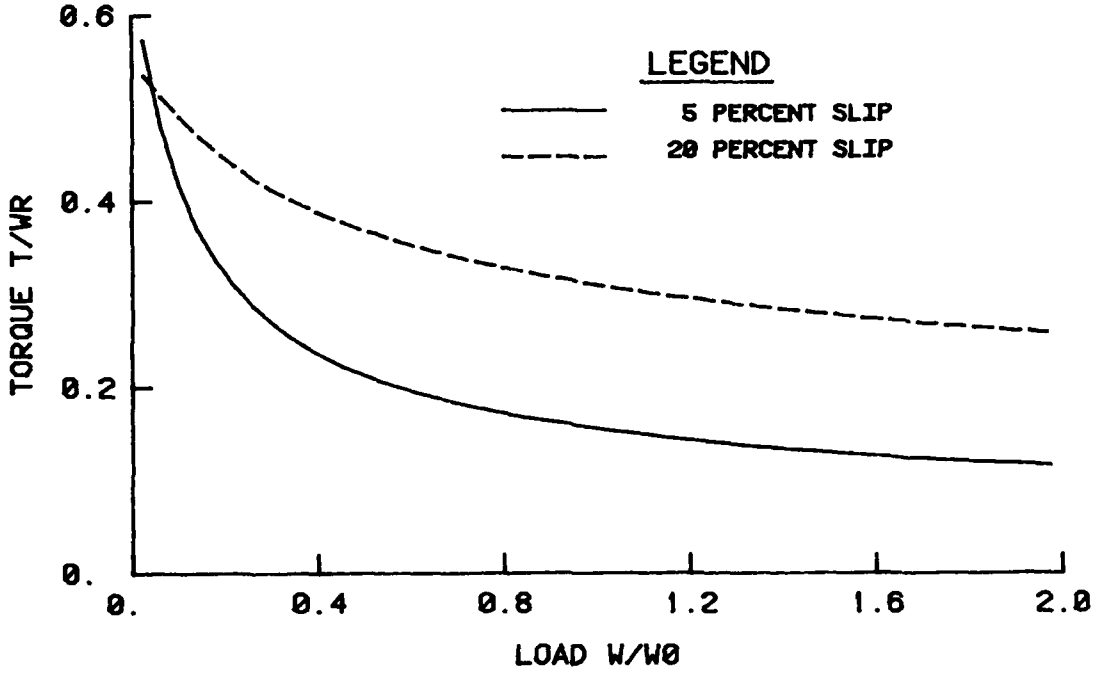

Figure 72. Relationship between torque and wheel load for sand; 15 percent tire deflection

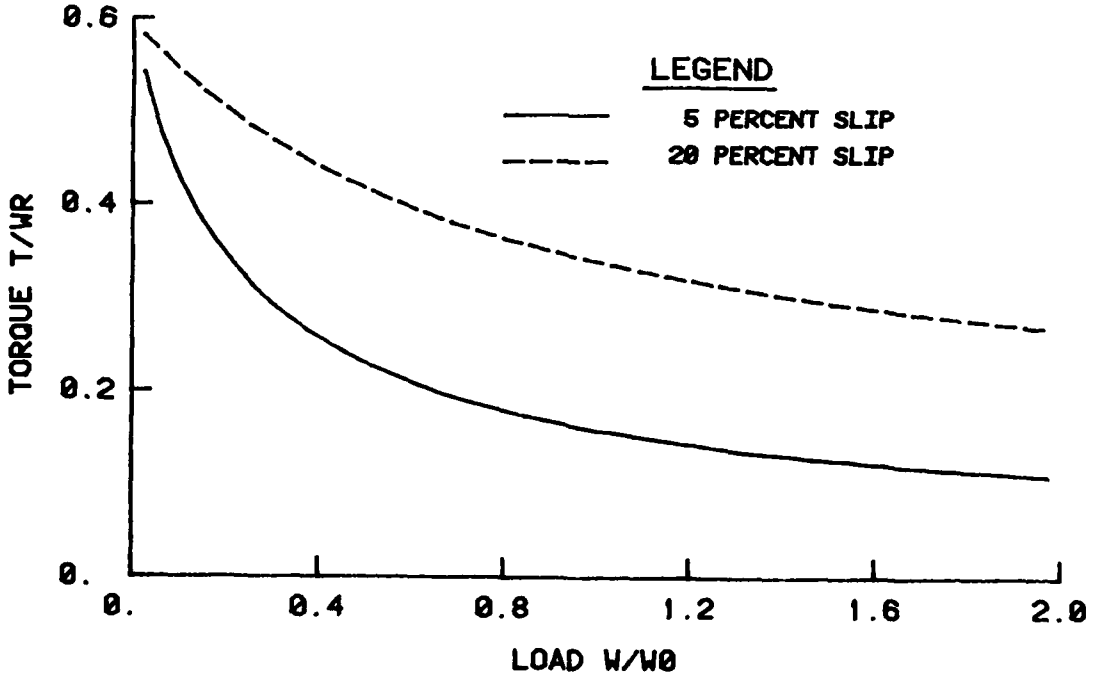

Figure 73. Relationship between torque and wheel load for sand; 35 percent tire deflection

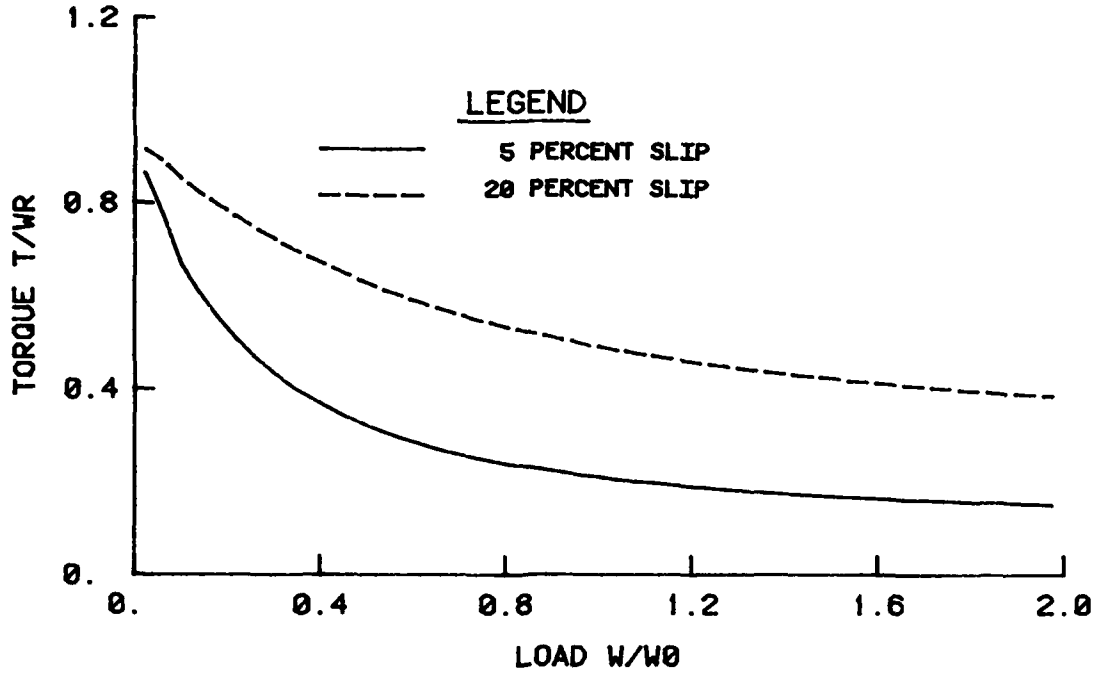

Figure 74. Relationship between torque and wheel load for mixed soil; 15 percent tire deflection

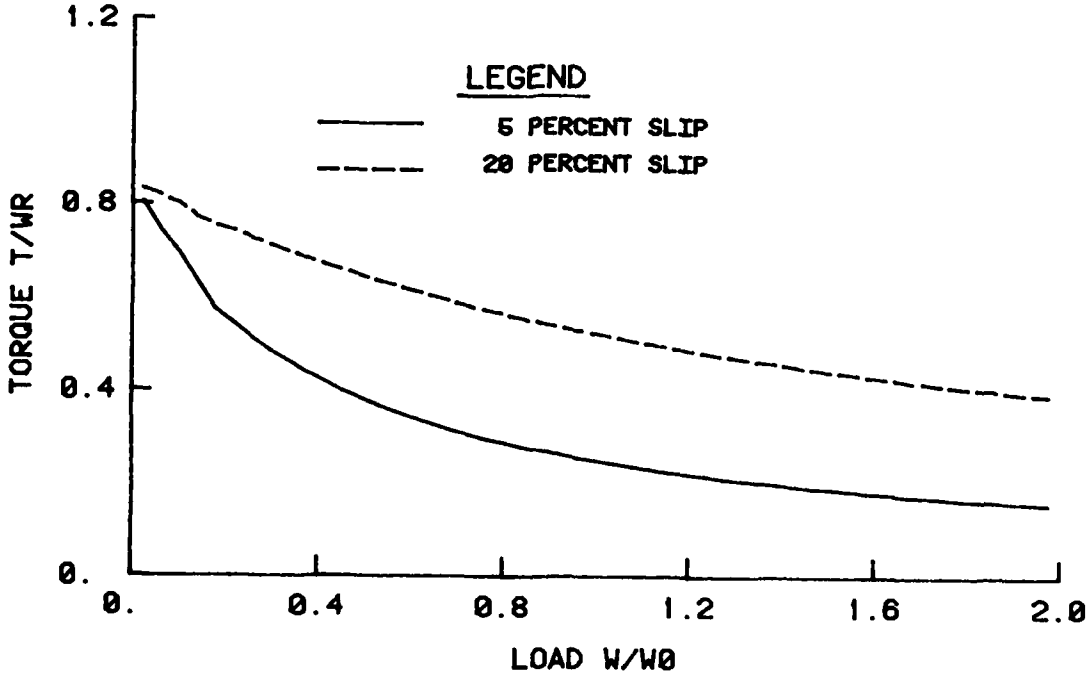

Figure 75. Relationship between torque and wheel load for mixed soil; 35 percent tire deflection

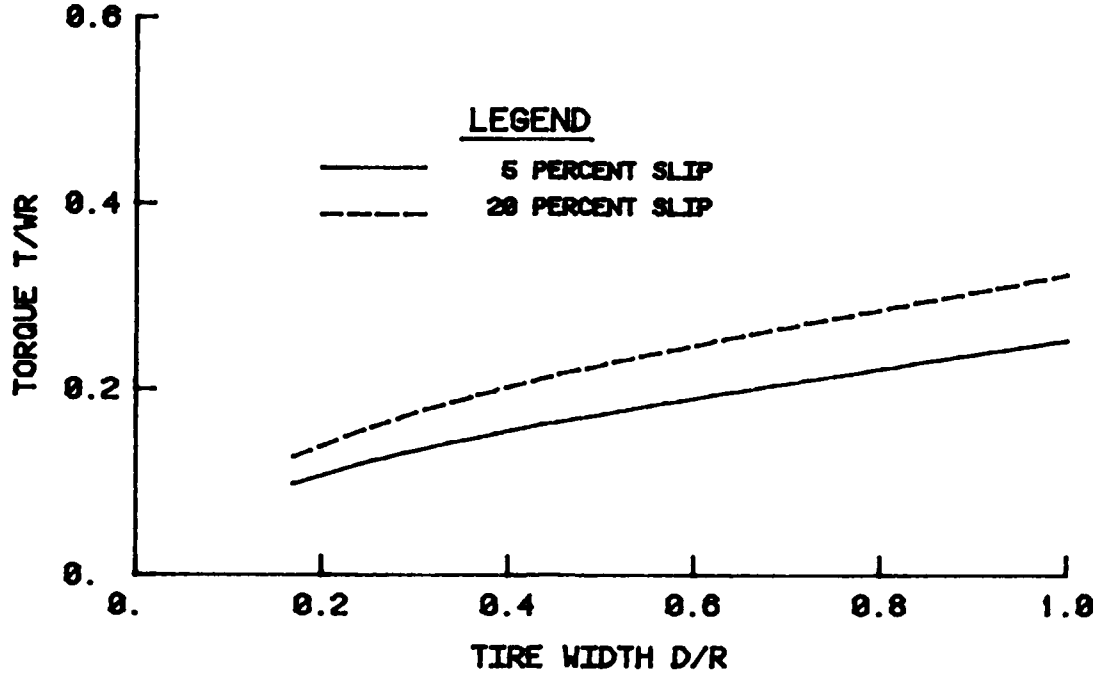

Figure 76. Relationship between torque and tire width for clay; 15 percent tire deflection

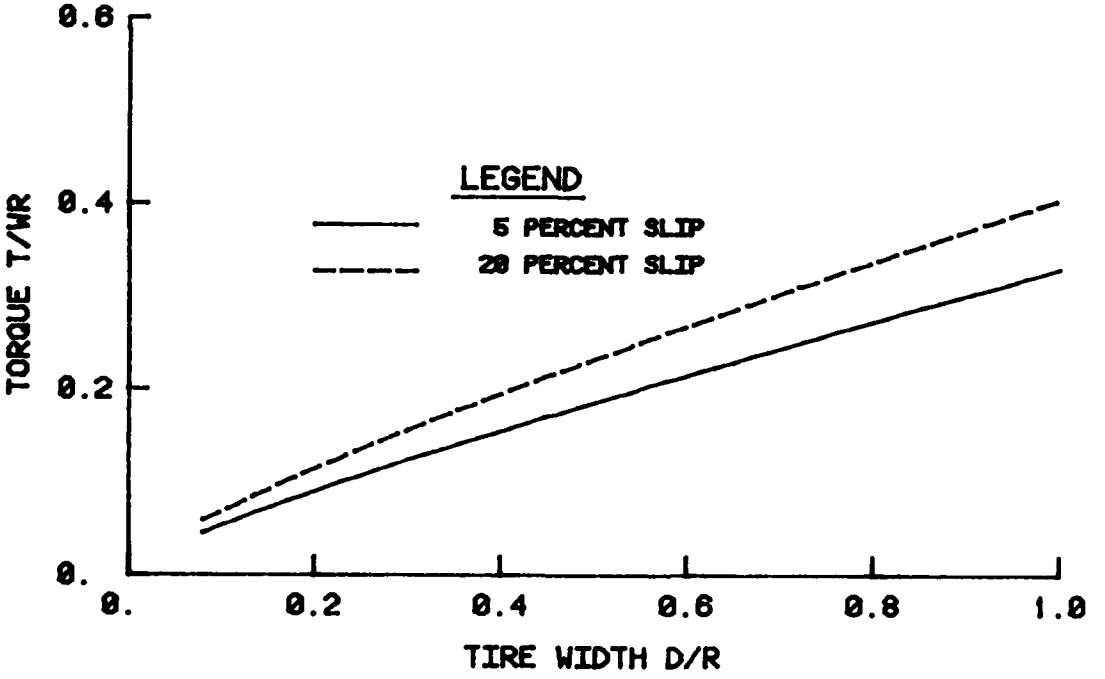

Figure 77. Relationship between torque and tire width for clay; 35 percent tire deflection

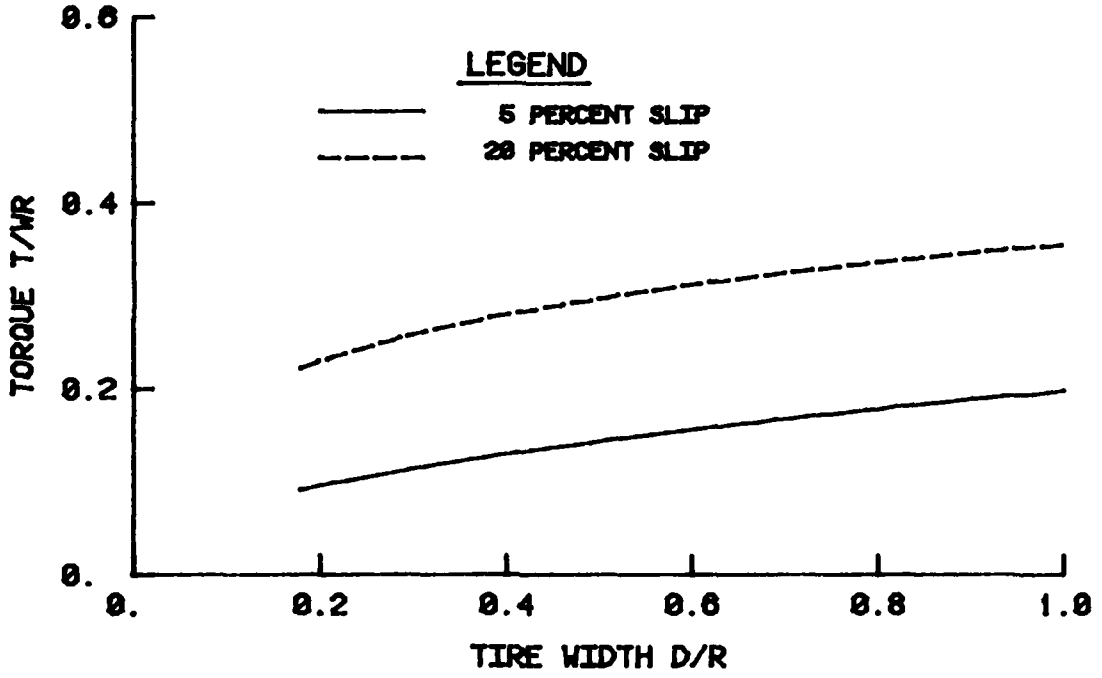

Figure 78. Relationship between torque and tire width for sand; 15 percent tire deflection

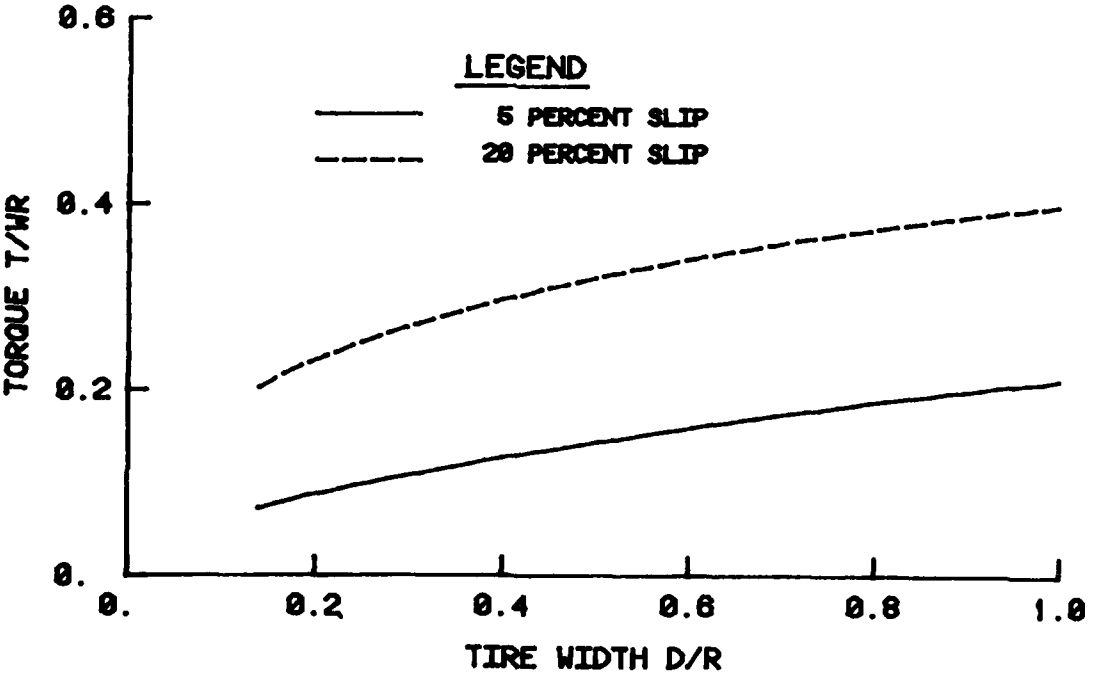

Figure 79. Relationship between torque and tire width for sand; 35 percent tire deflection

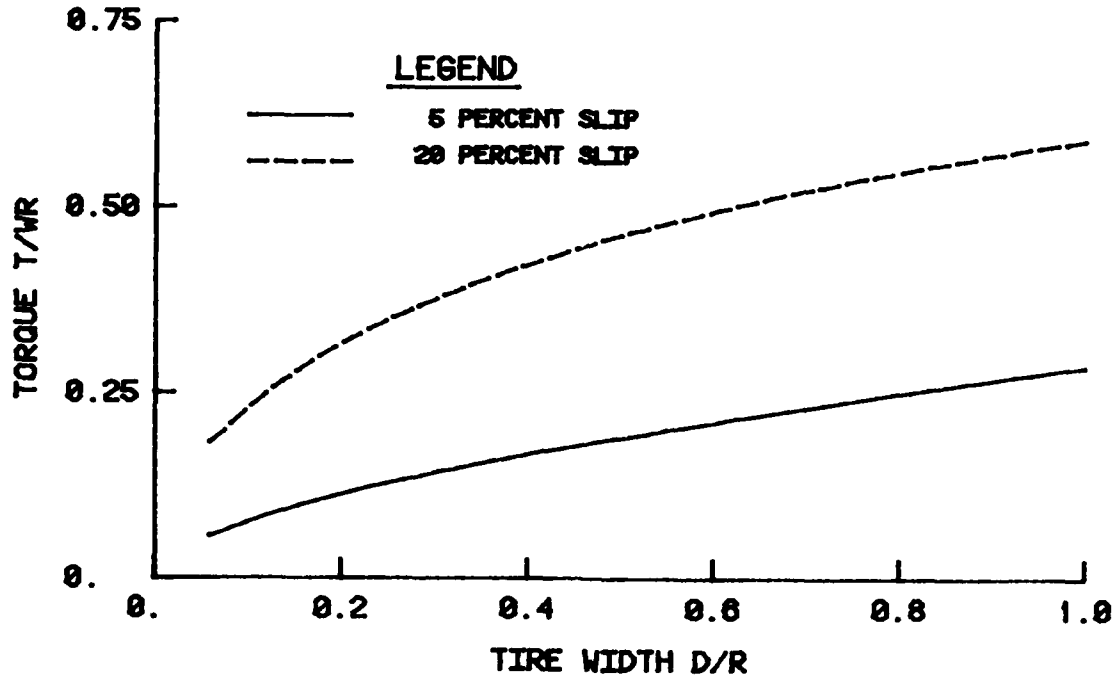

Figure 80. Relationship between torque and tire width for mixed soil; 15 percent tire deflection

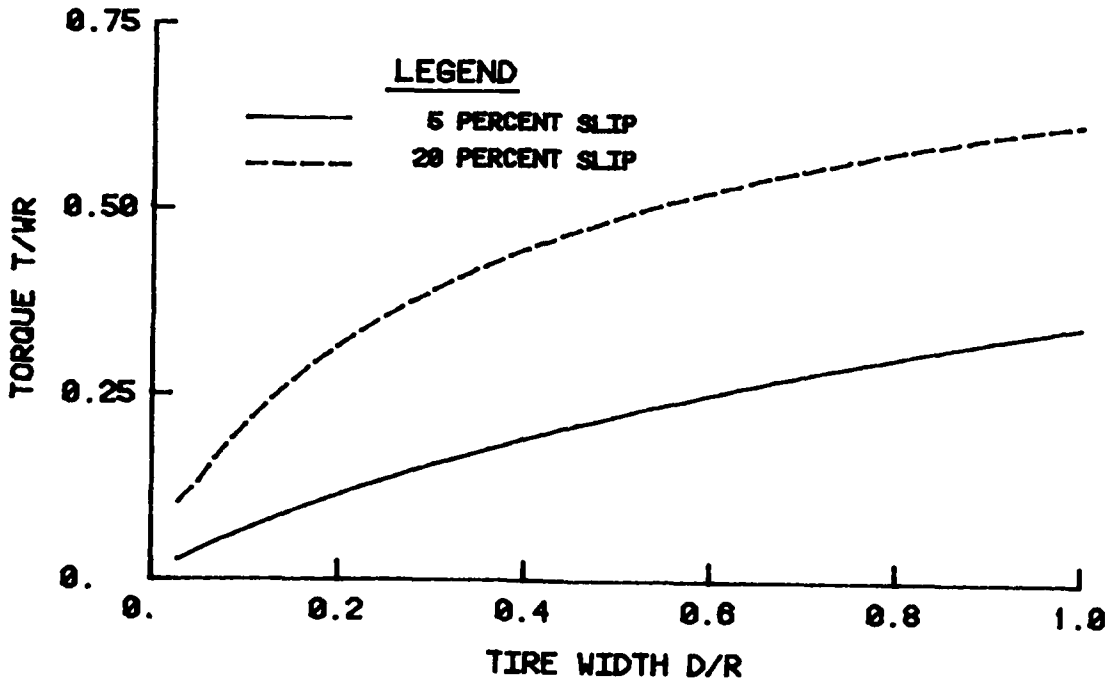

Figure 81. Relationship between torque and tire width for mixed soil; 35 percent tire deflection

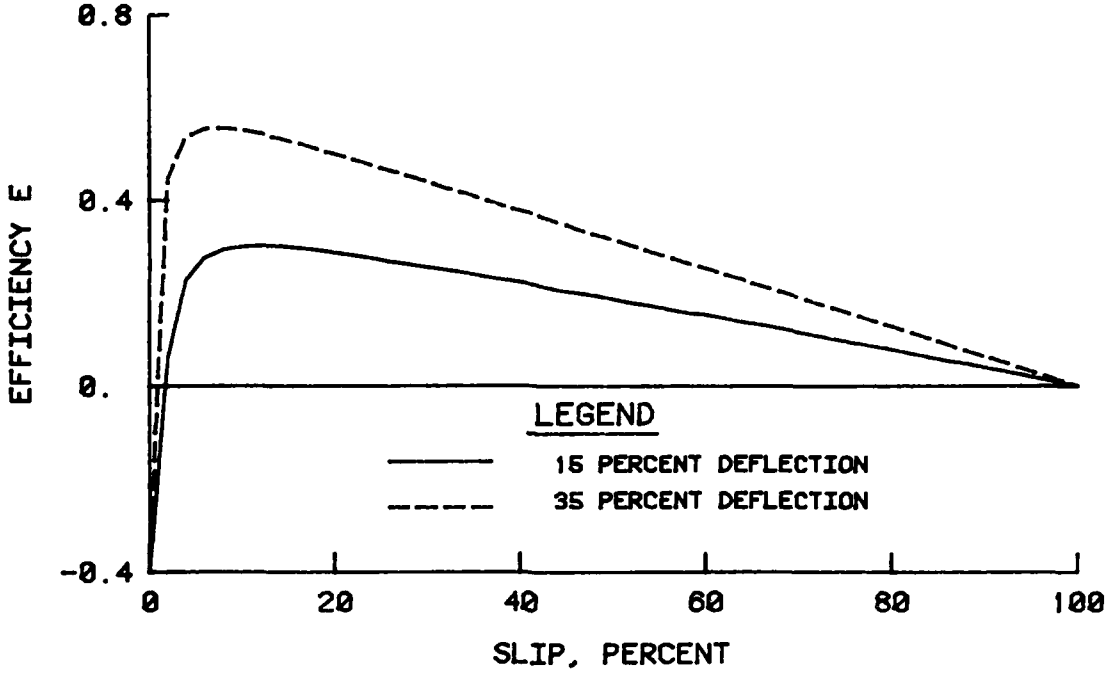

Figure 82. Relationship between efficiency and slip ratio for clay

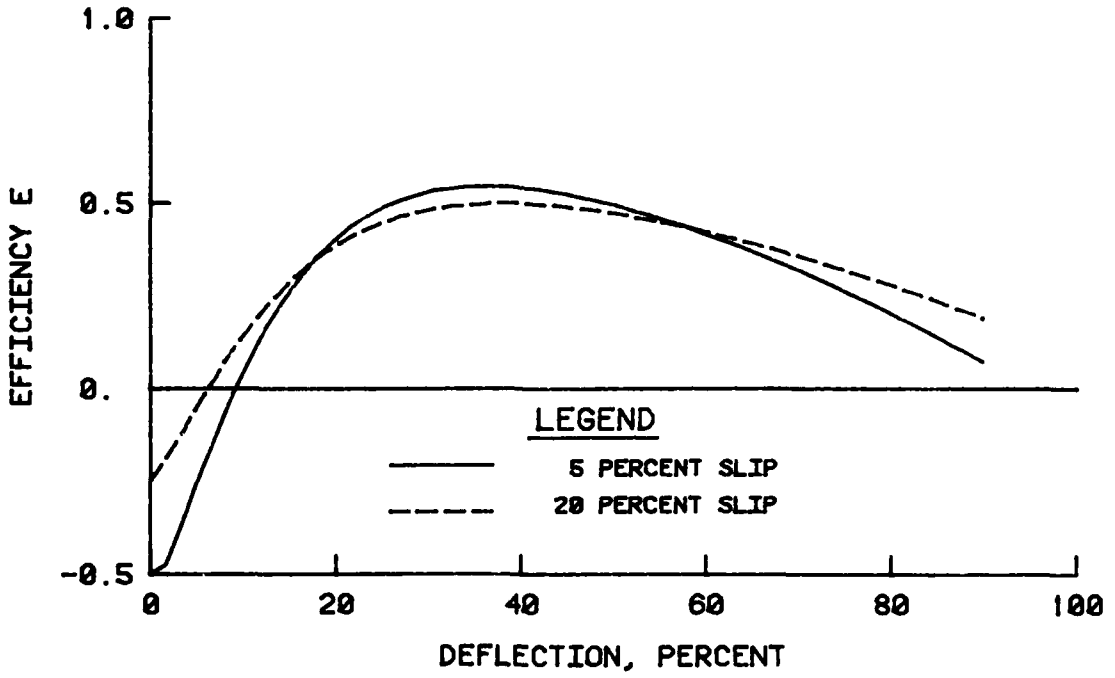

Figure 83. Relationship between efficiency and tire deflection for clay

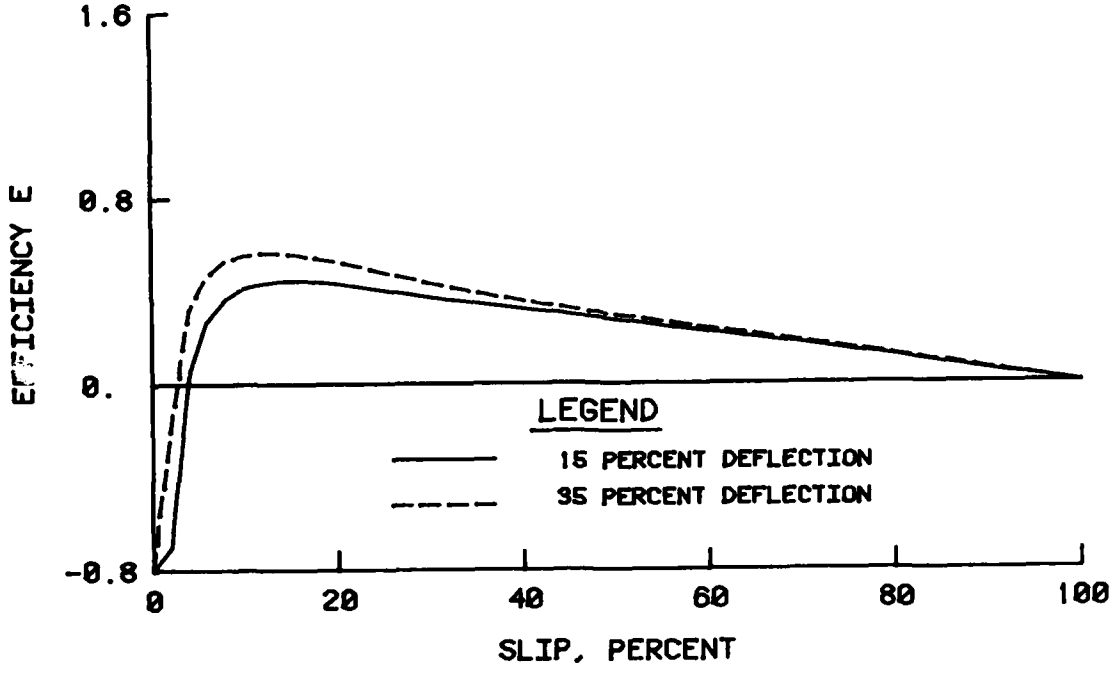

Figure 84. Relationship between efficiency and slip ratio for sand

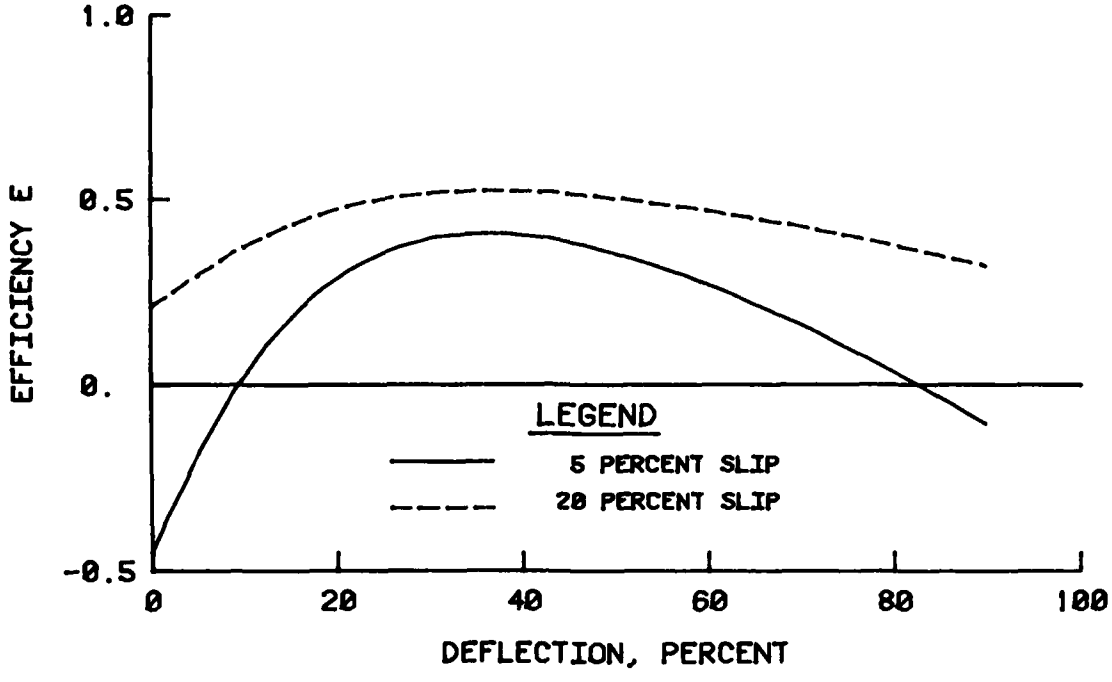

Figure 85. Relationship between efficiency and tire deflection for sand

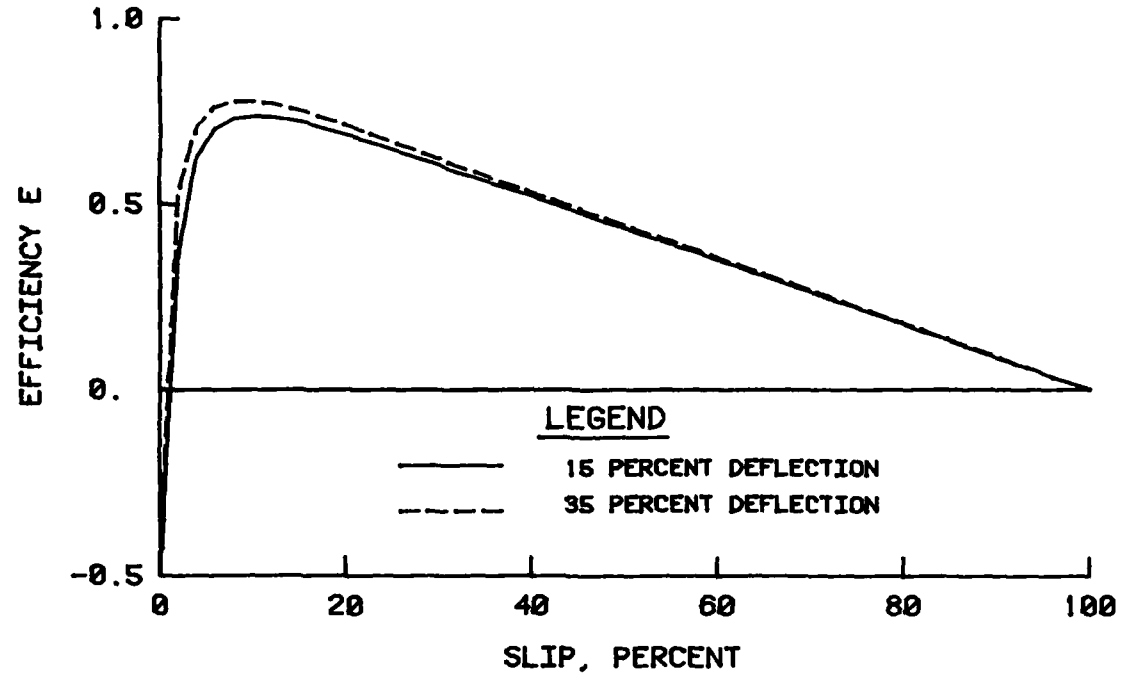

Figure 86. Relationship between efficiency and slip ratio for mixed soil

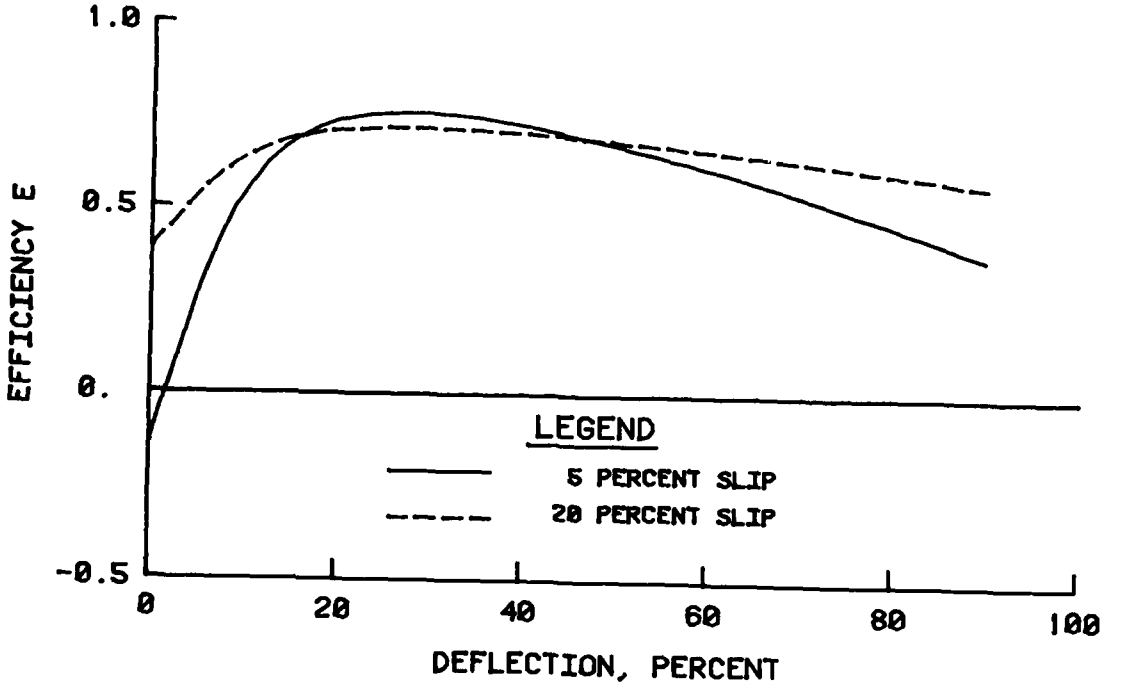

Figure 87. Relationship between efficiency and deflection for mixed soil

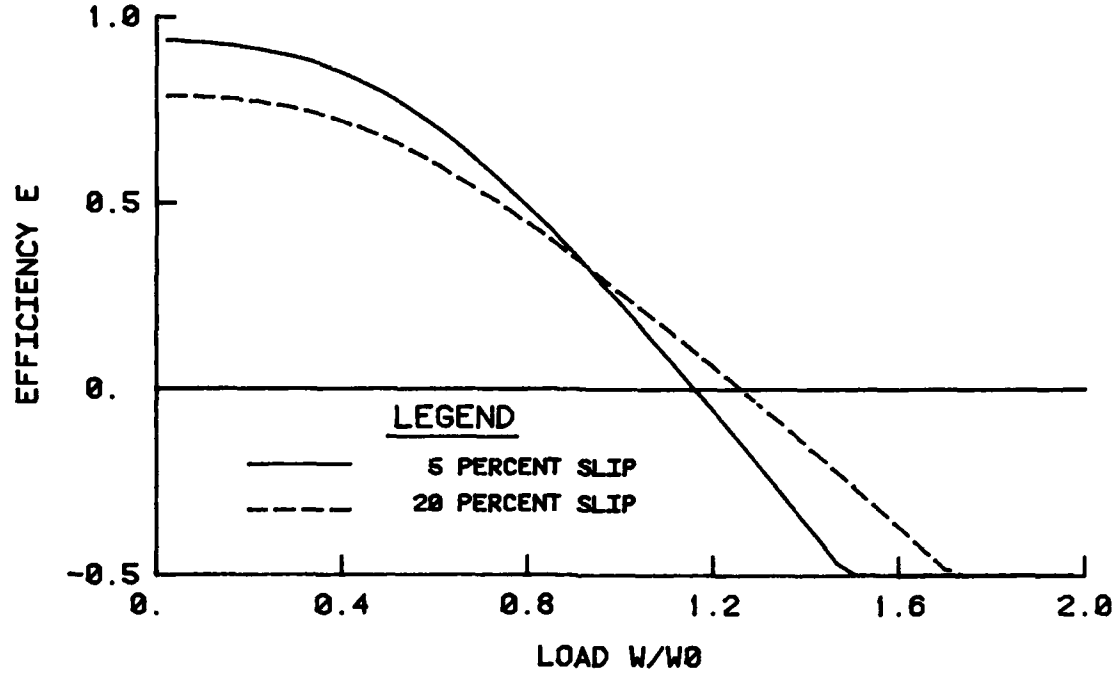

Figure 88. Relationship between efficiency and wheel load for clay; 15 percent tire deflection

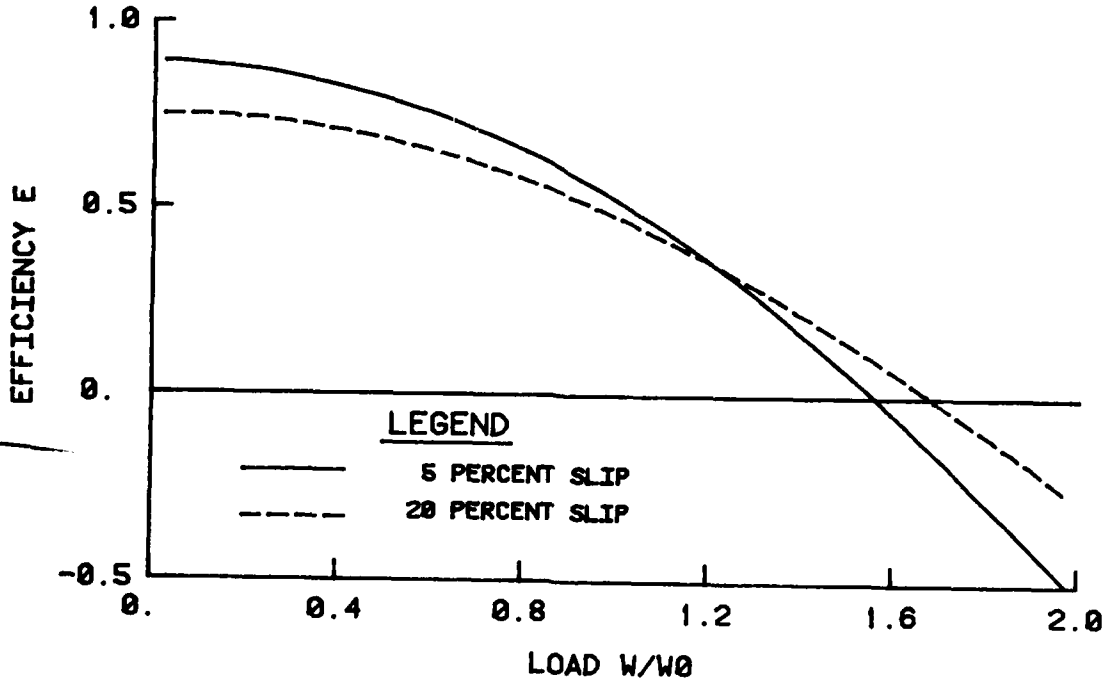

Figure 89. Relationship between efficiency and wheel load for clay; 35 percent tire deflection

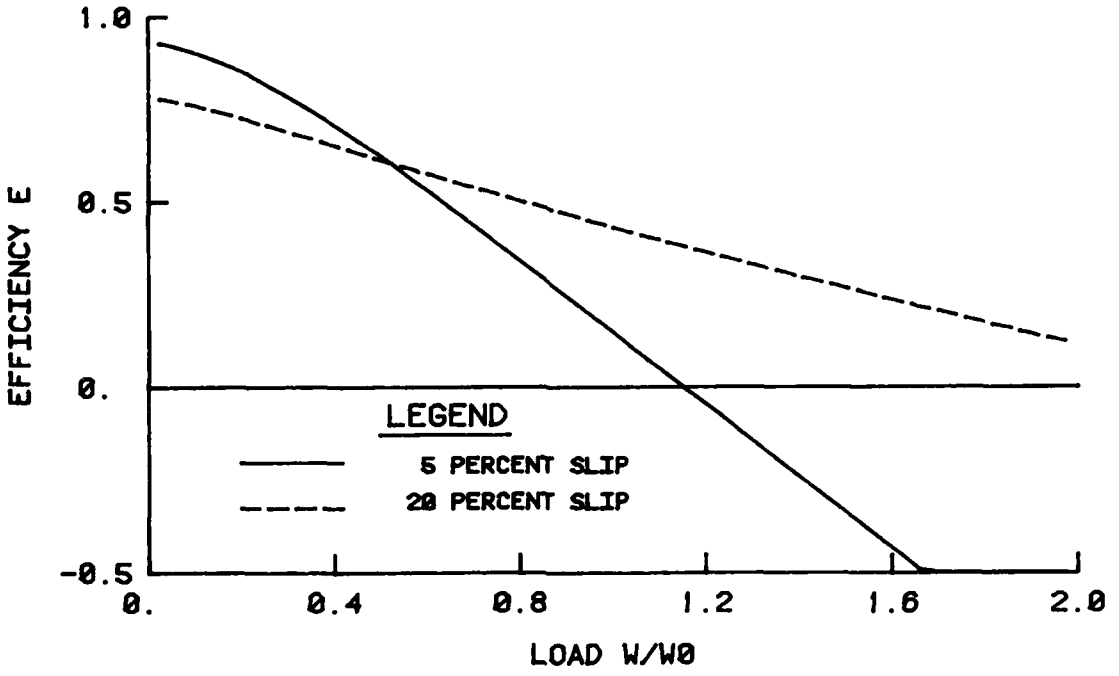

Figure 90. Relationship between efficiency and wheel load for sand; 15 percent tire deflection

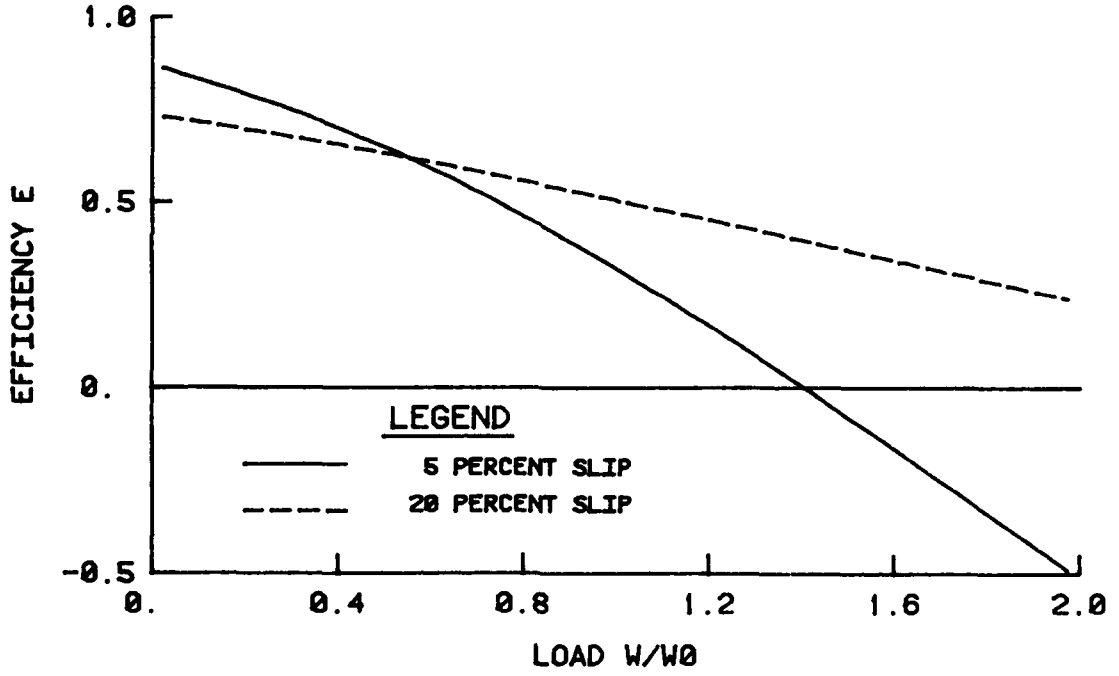

Figure 91. Relationship between efficiency and wheel load for sand; 35 percent tire deflection

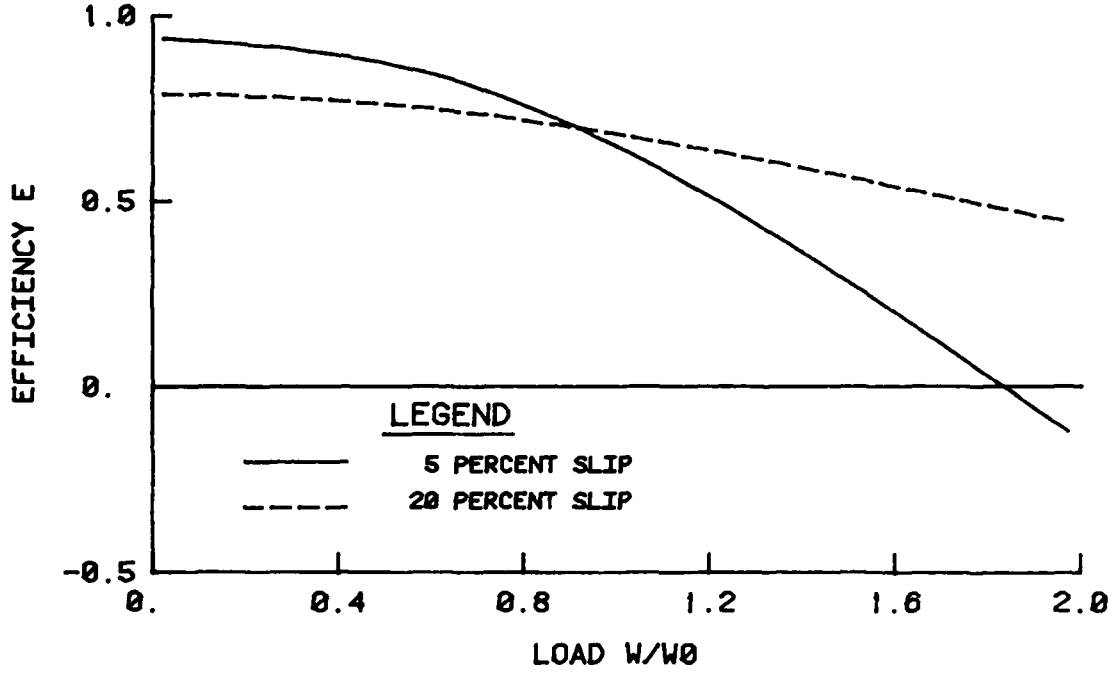

Figure 92. Relationship between efficiency and wheel load for mixed soil; 15 percent tire deflection

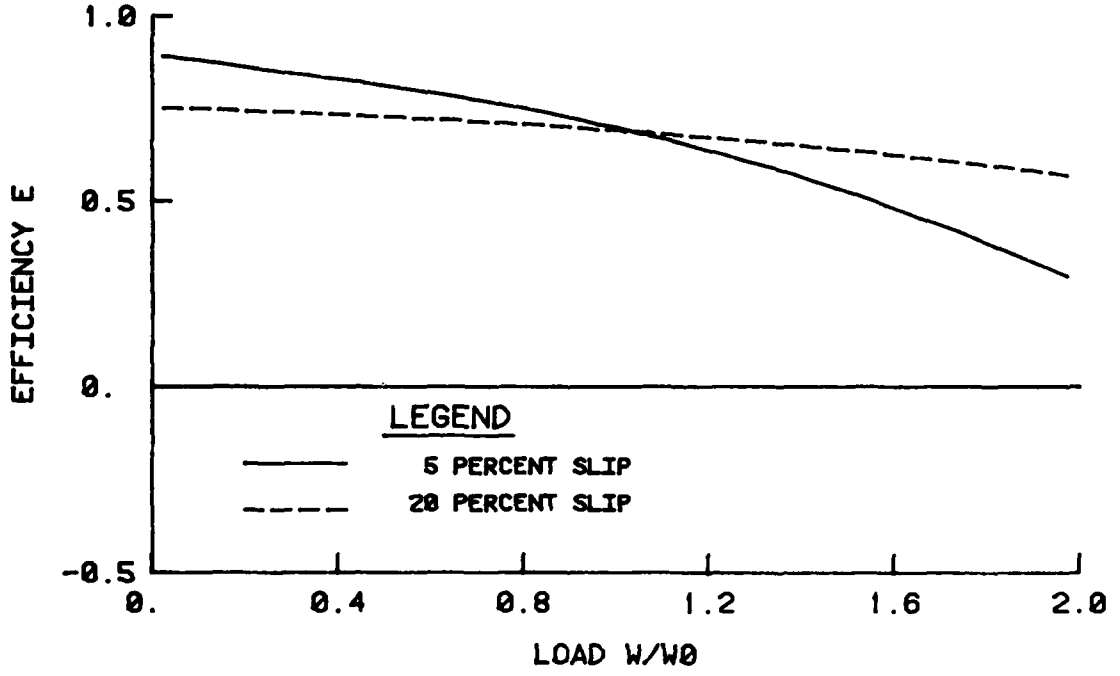

Figure 93. Relationship between efficiency and wheel load for mixed soil; 35 percent tire deflection

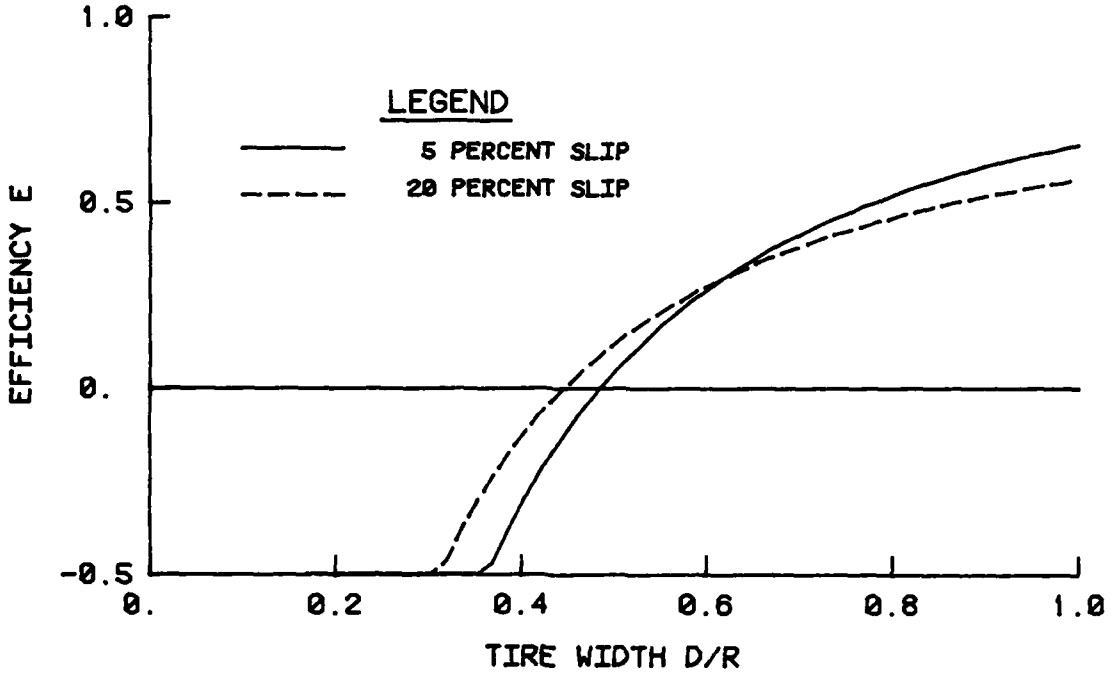

Figure 94. Relationship between efficiency and tire width for clay; 15 percent tire deflection

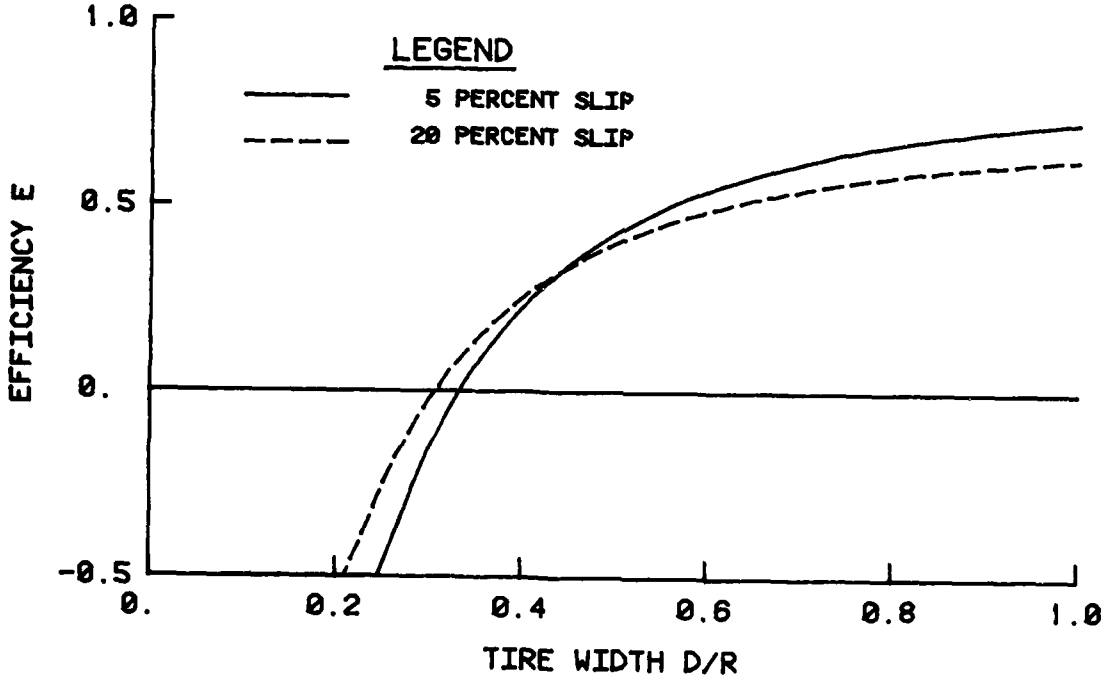

Figure 95. Relationship between efficiency and tire width for clay; 35 percent tire deflection

AD-A144 696 STEERABILITY ANALYSIS OF MULTIAXLE WHEELED EEHICLES 2/2
REPORT 1 DEVELOPMENT O.. (U) ARMY ENGINEER WATERWAYS
EXPERIMENT STATION VICKSBURG MS GEOTE..
UNCLASSIFIED G Y BALADI ET AL. JAN 84 WES/TR/GL-84-1 F/G 8/13 NL

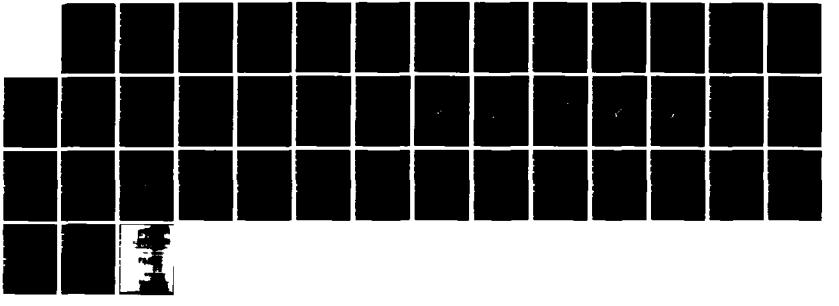

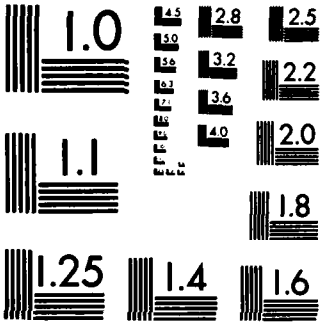

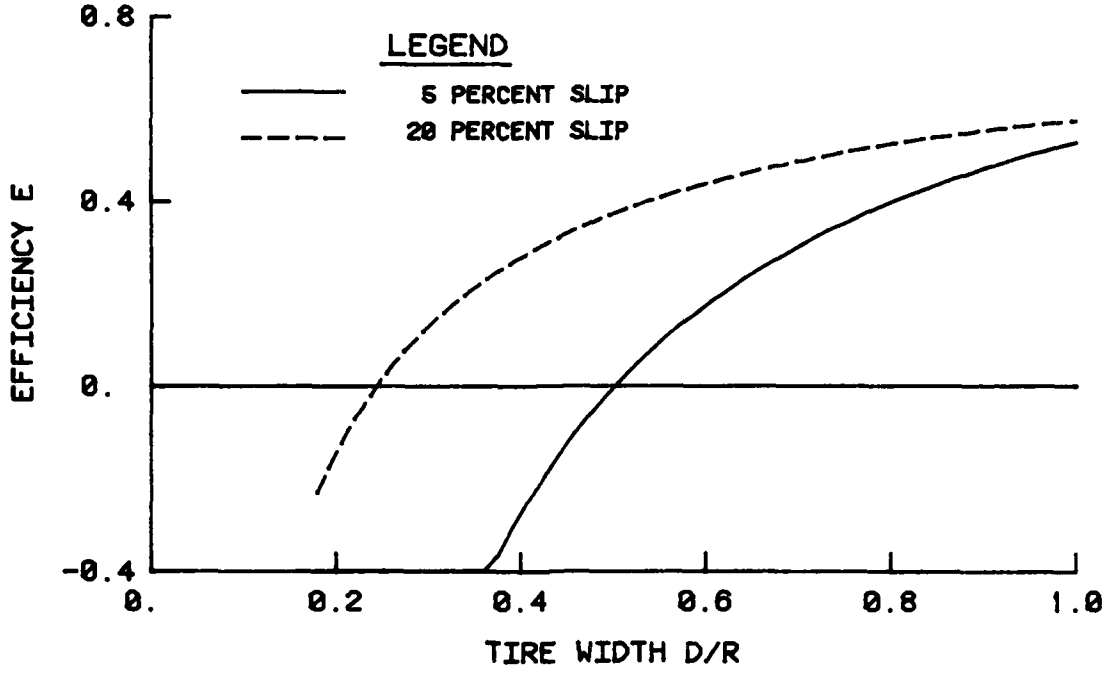

Figure 96. Relationship between efficiency and tire width for sand; 15 percent tire deflection

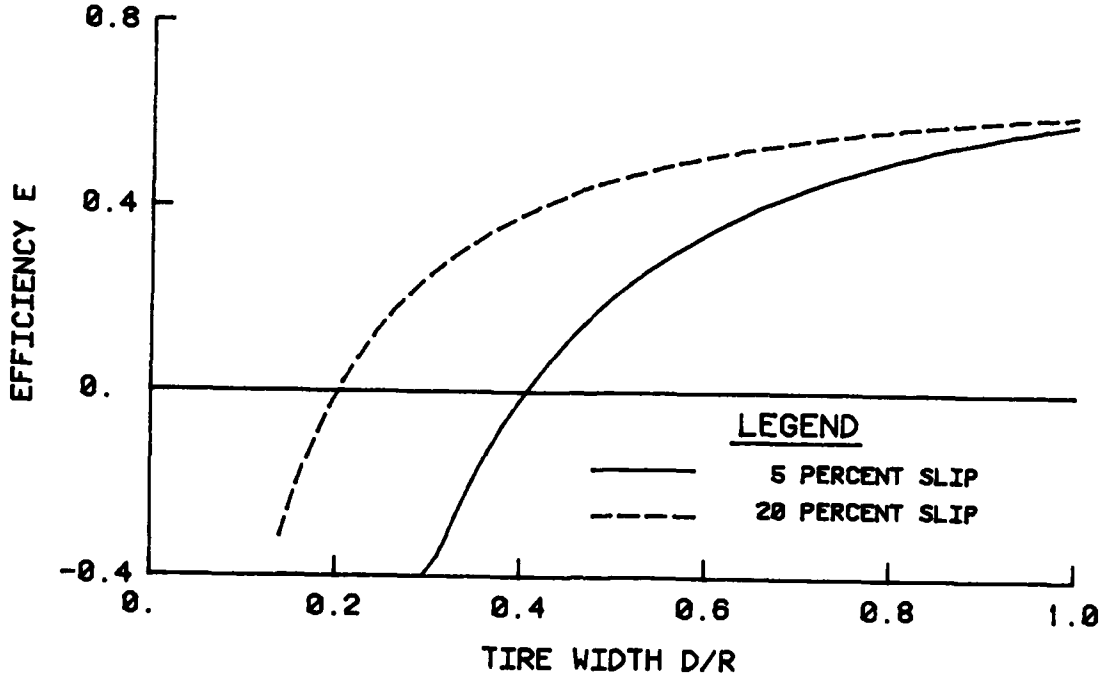

Figure 97. Relationship between efficiency and tire width for sand; 35 percent tire deflection

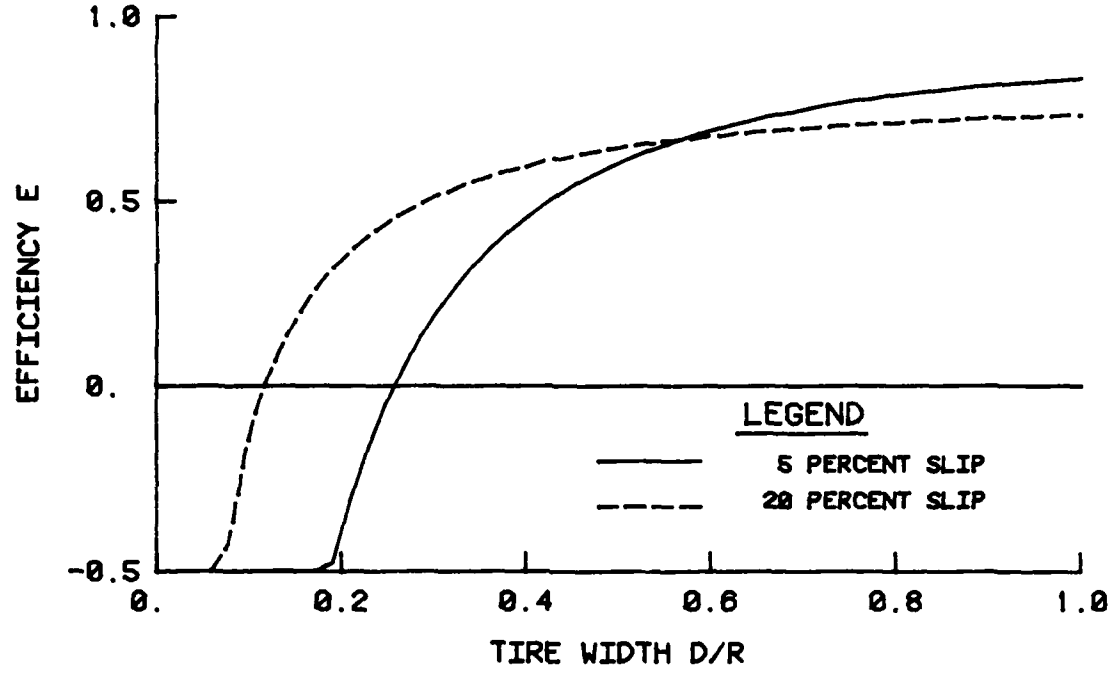

Figure 98. Relationship between efficiency and tire width for mixed soil; 15 percent tire deflection

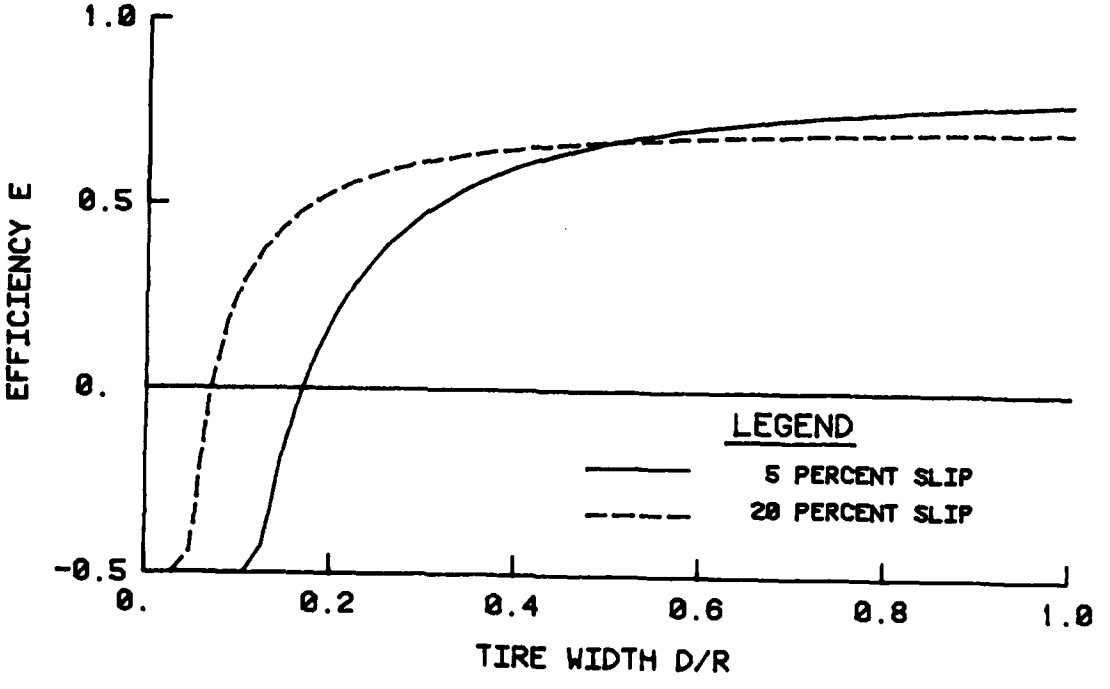

Figure 99. Relationship between efficiency and tire width for mixed soil; 35 percent tire deflection

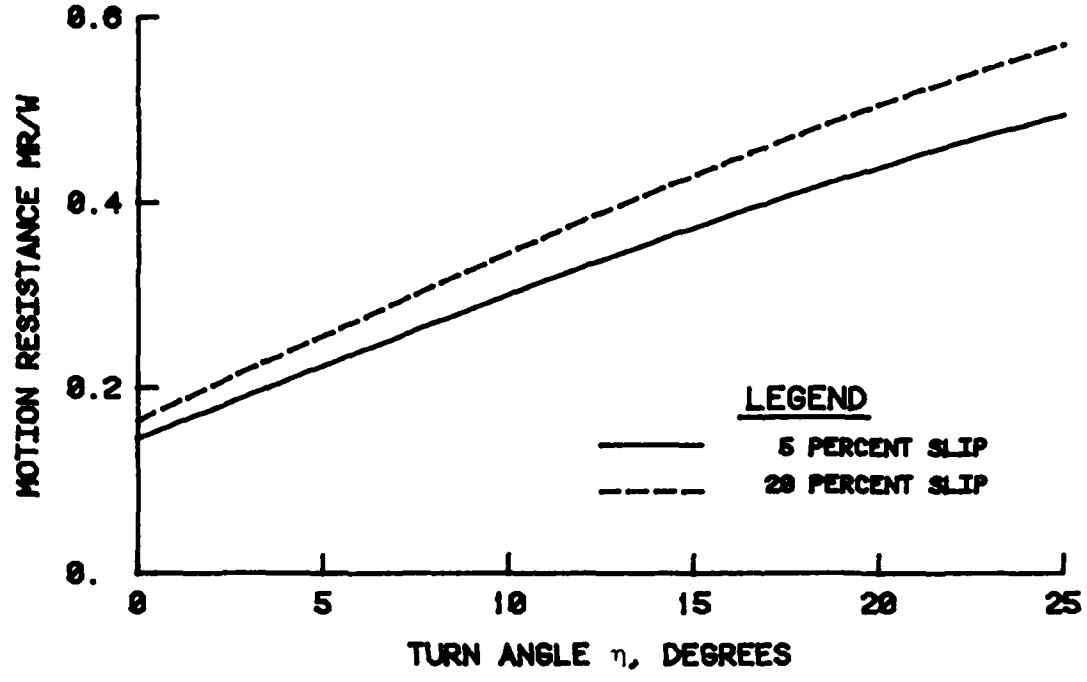

Figure 100. Relationship between motion resistance and turn angle for clay; 15 percent tire deflection

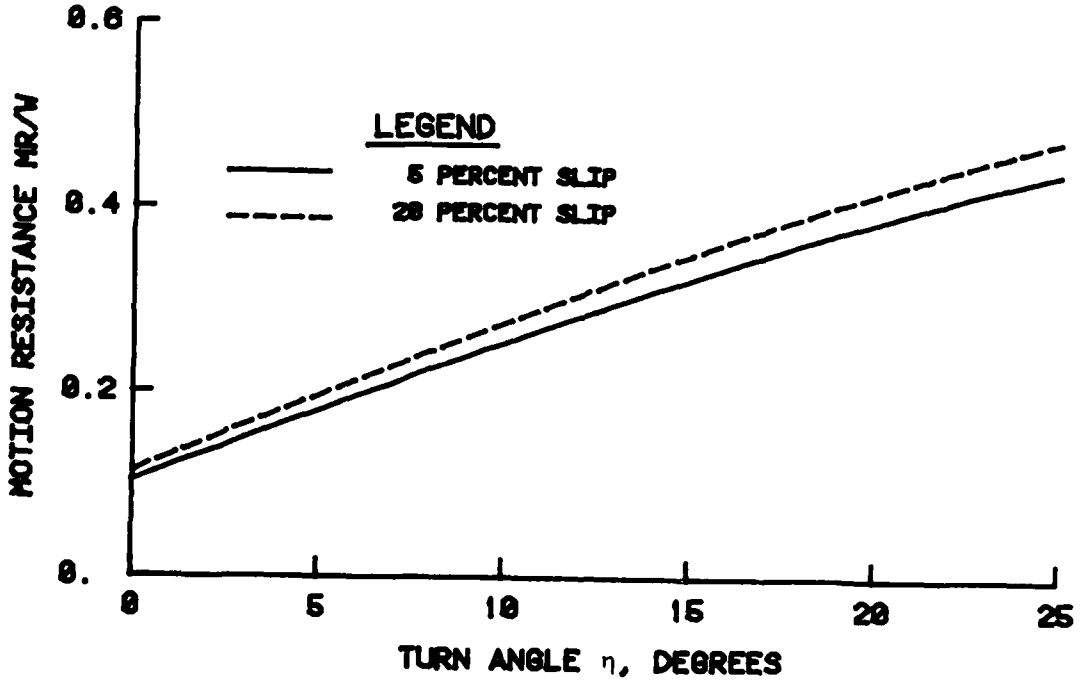

Figure 101. Relationship between motion resistance and turn angle for clay; 35 percent tire deflection

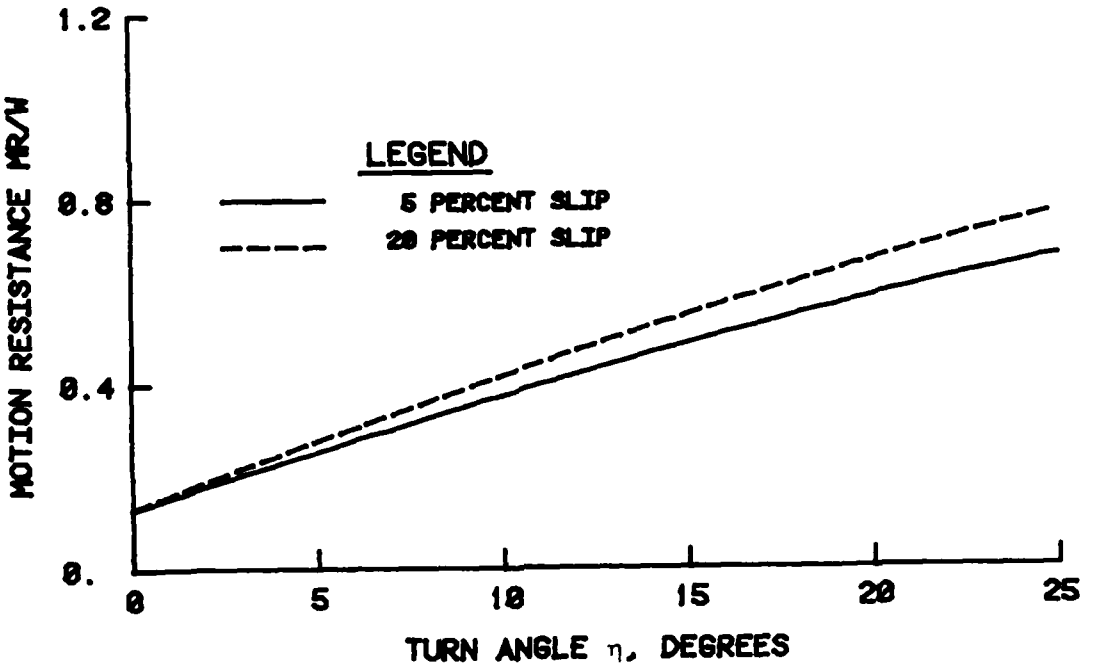

Figure 102. Relationship between motion resistance and turn angle for sand; 15 percent tire deflection

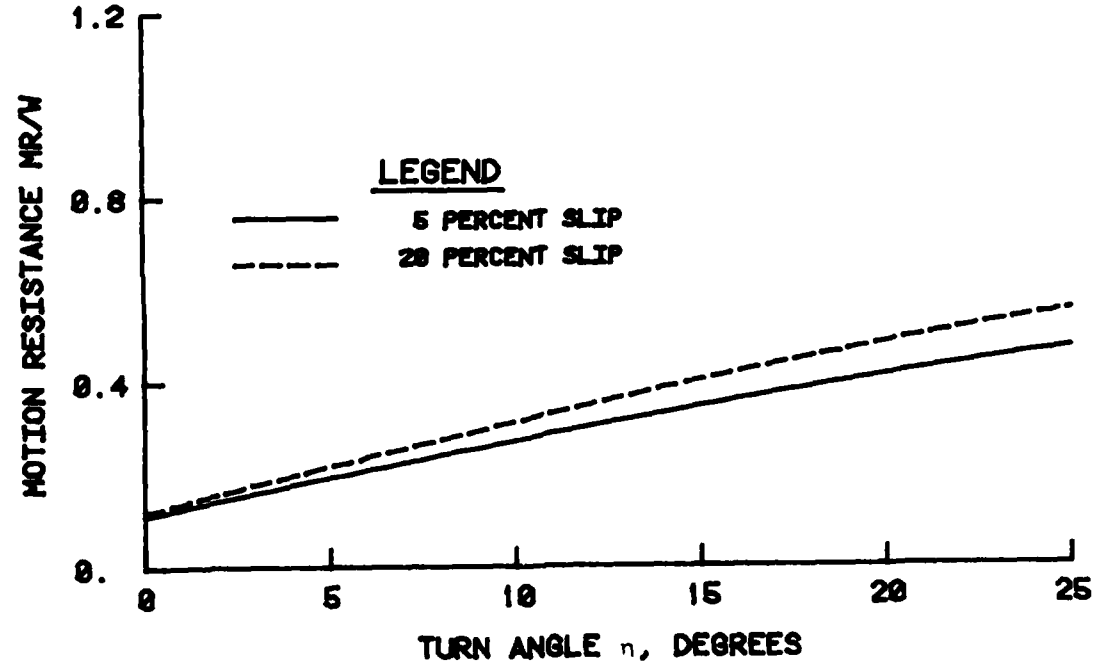

Figure 103. Relationship between motion resistance and turn angle for sand; 35 percent tire deflection

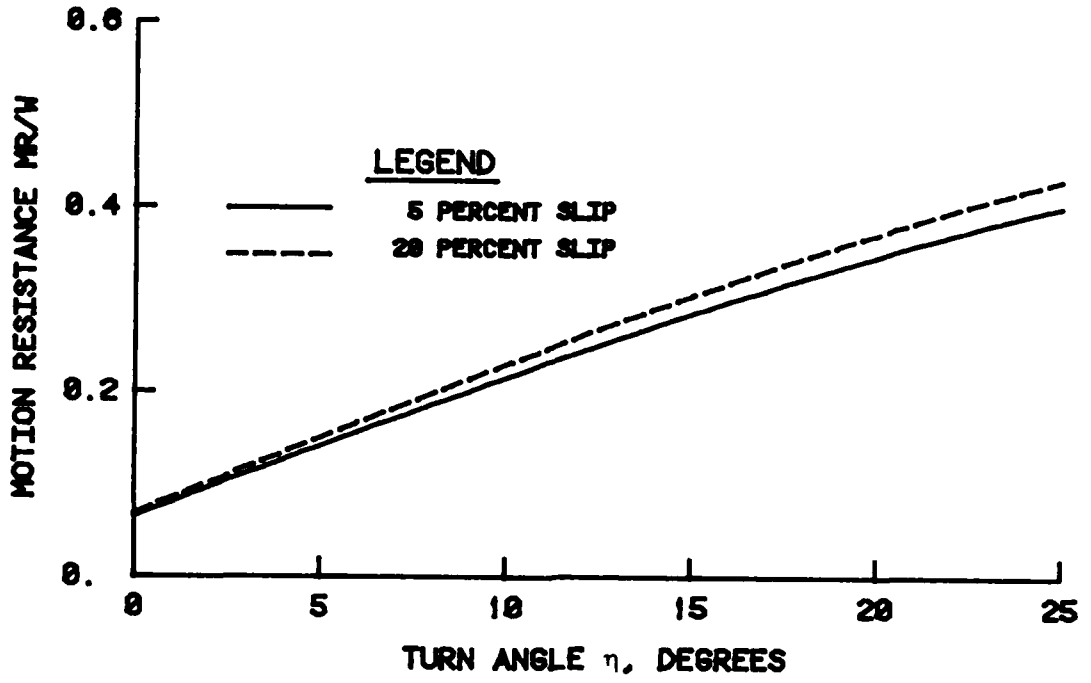

Figure 104. Relationship between motion resistance and turn angle for mixed soil; 15 percent tire deflection

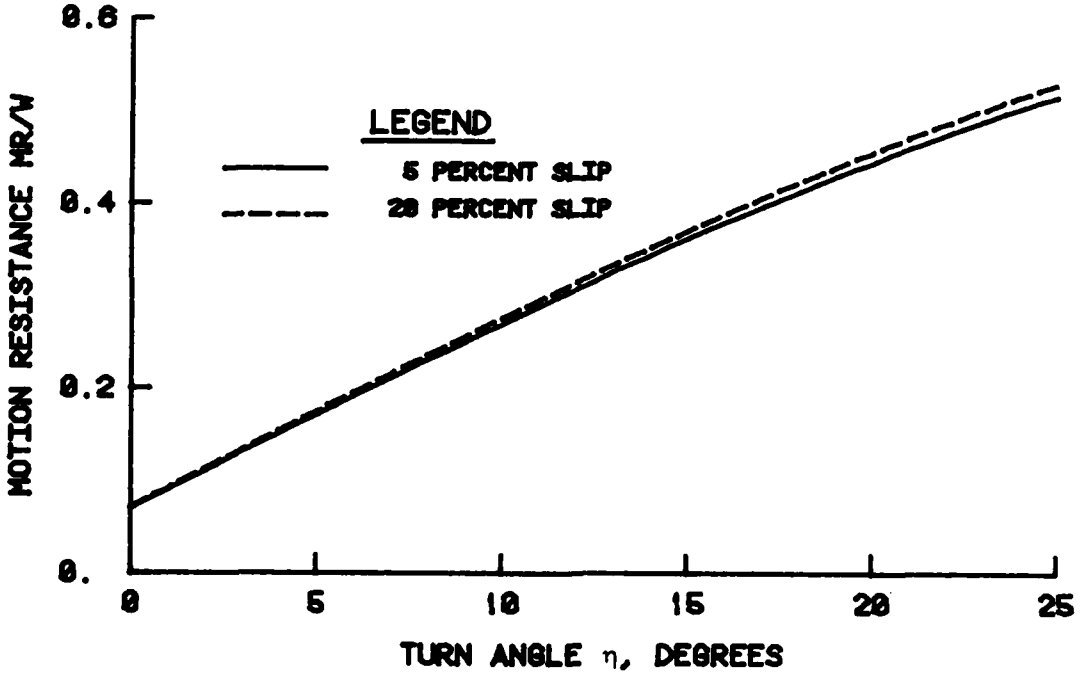

Figure 105. Relationship between motion resistance and turn angle for mixed soil; 35 percent tire deflection

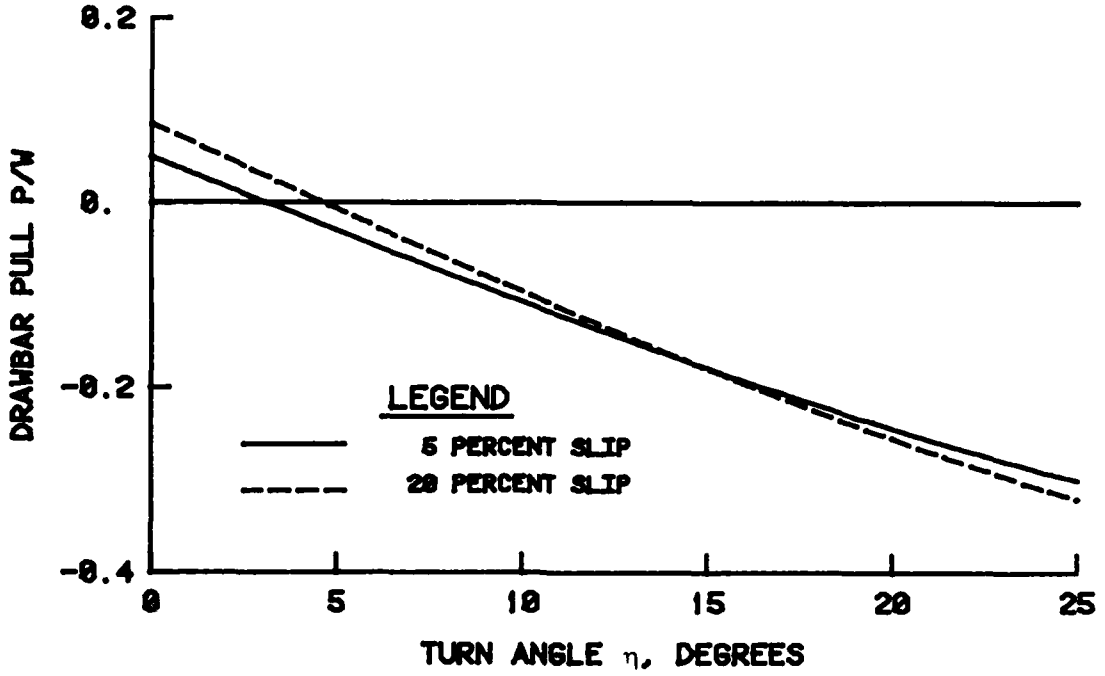

Figure 106. Relationship between drawbar pull and turn angle for clay; 15 percent tire deflection

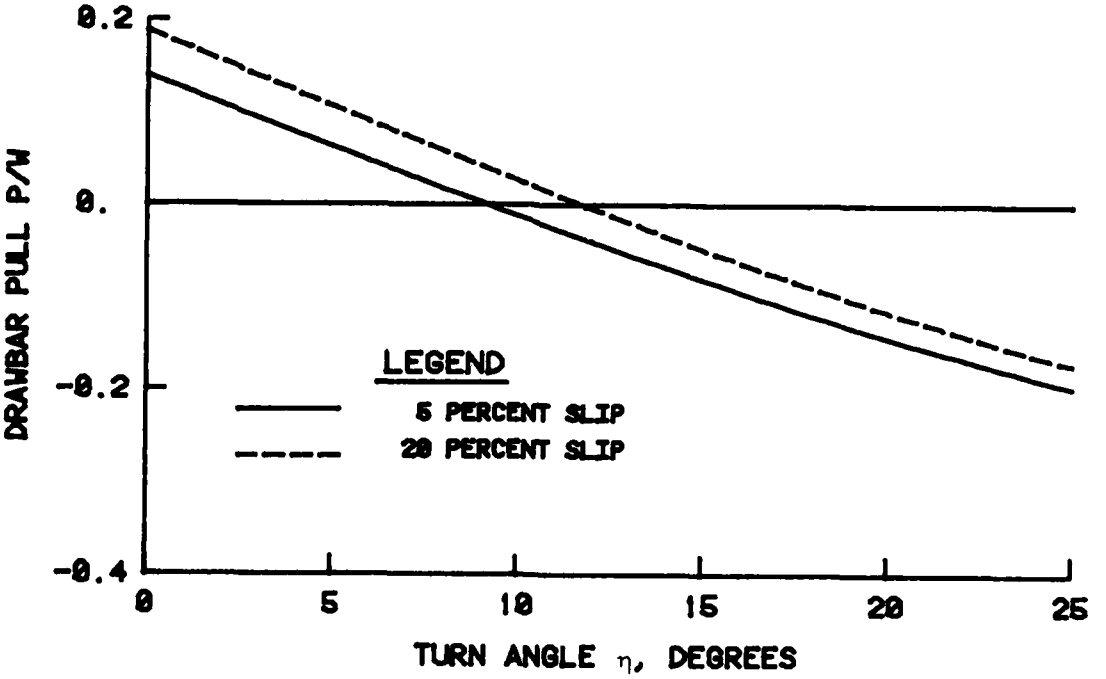

Figure 107. Relationship between drawbar pull and turn angle for clay; 35 percent tire deflection

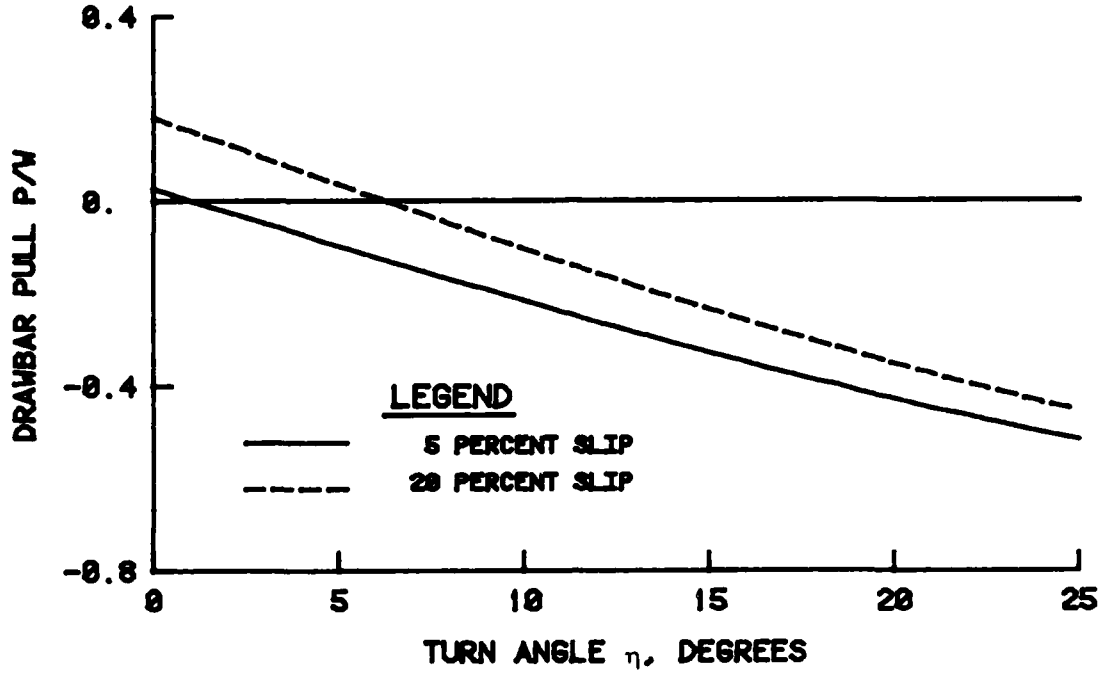

Figure 108. Relationship between drawbar pull and turn angle for sand; 15 percent tire deflection

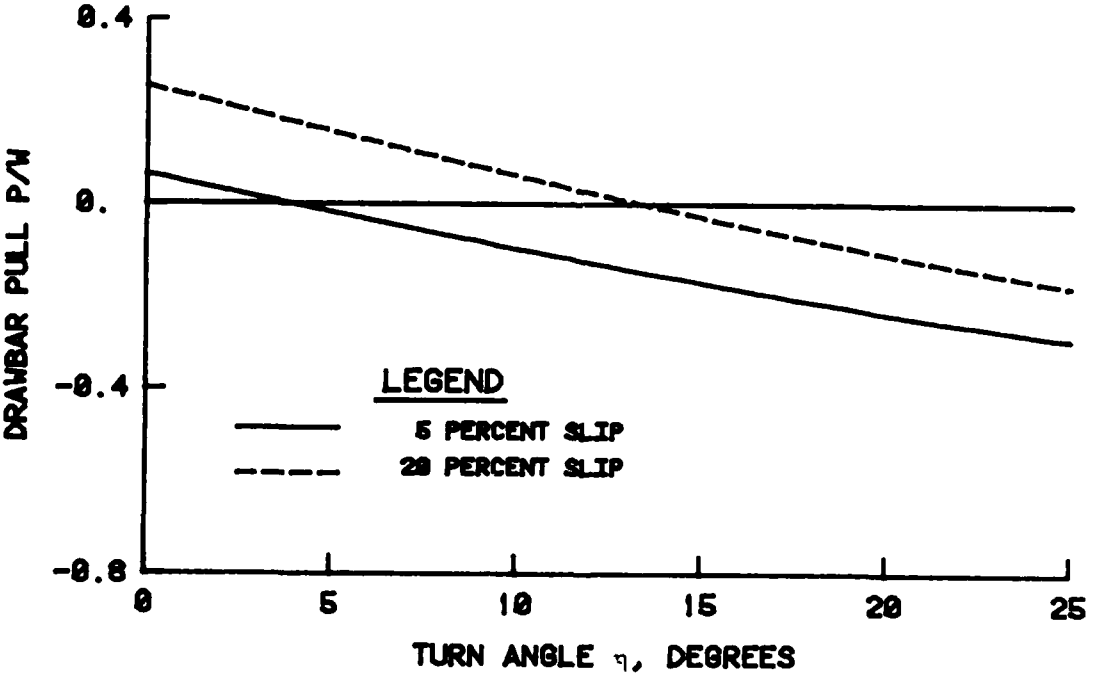

Figure 109. Relationship between drawbar pull and turn angle for sand; 35 percent tire deflection

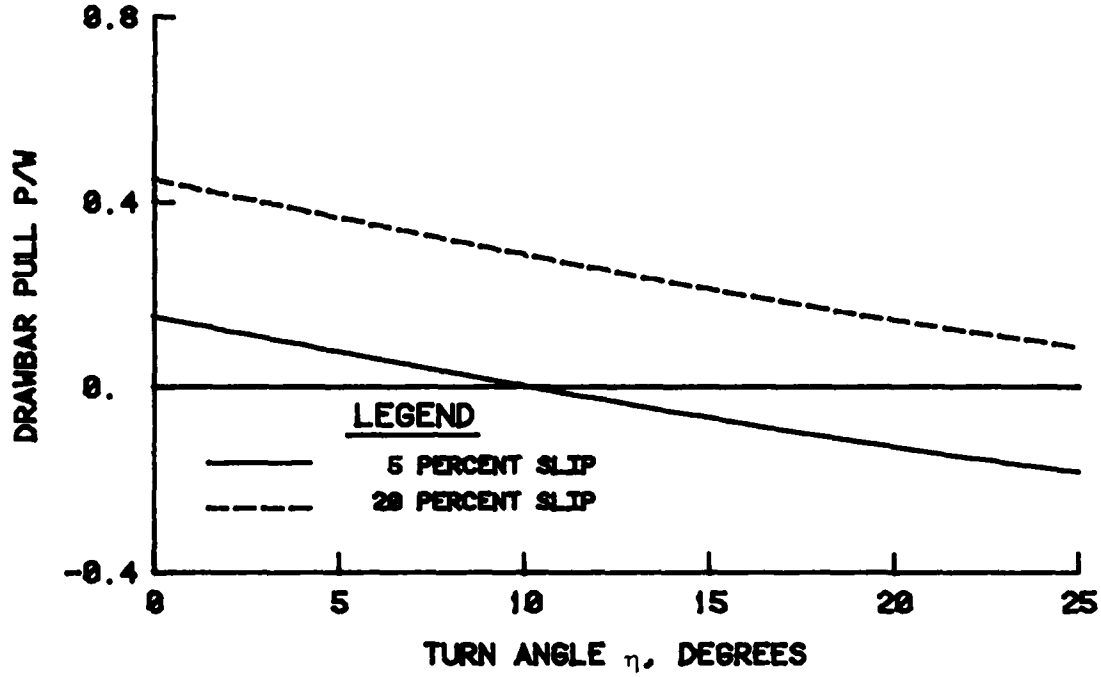

Figure 110. Relationship between drawbar pull and turn angle for mixed soil; 15 percent tire deflection

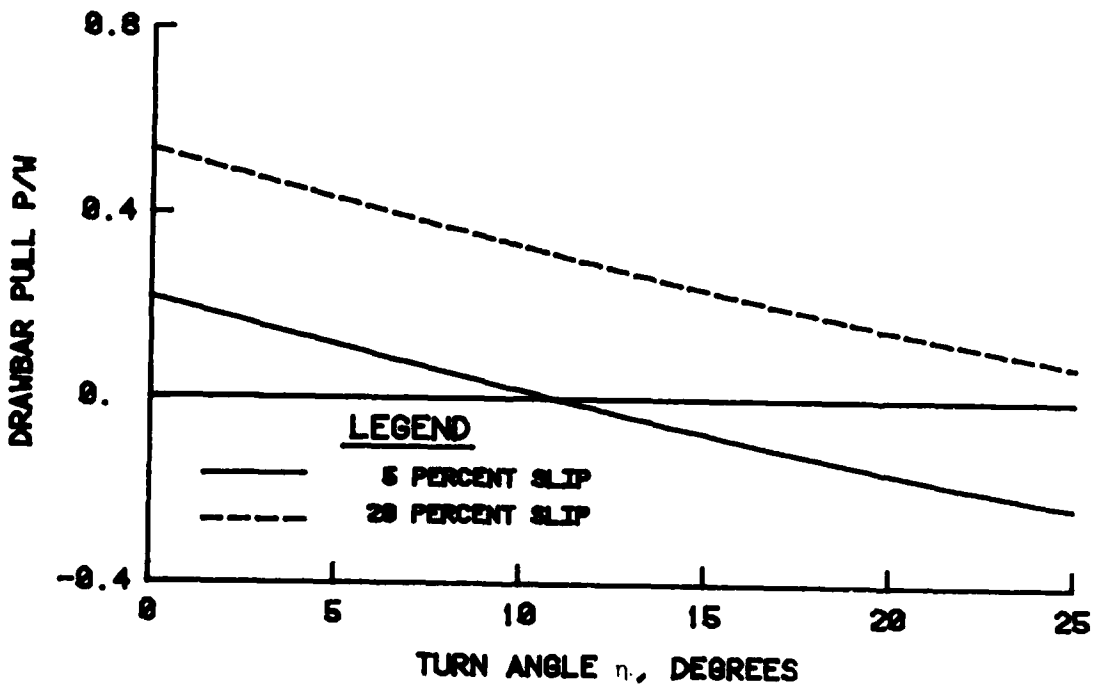

Figure 111. Relationship between drawbar pull and turn angle for mixed soil; 35 percent tire deflection

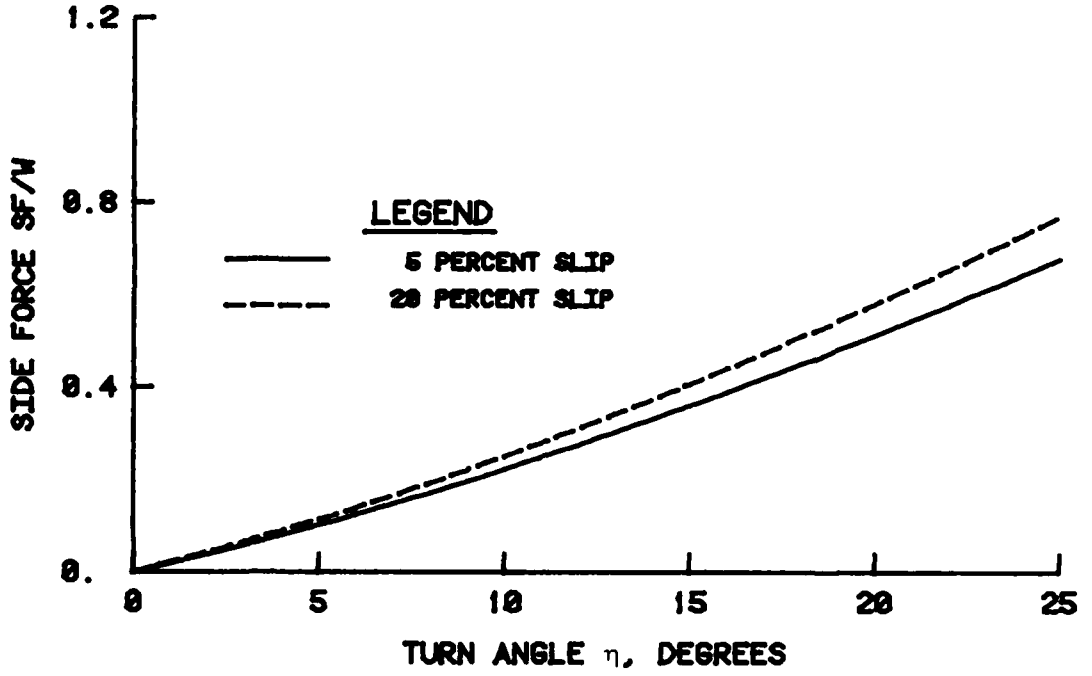

Figure 112. Relationship between side force and turn angle for clay; 15 percent tire deflection

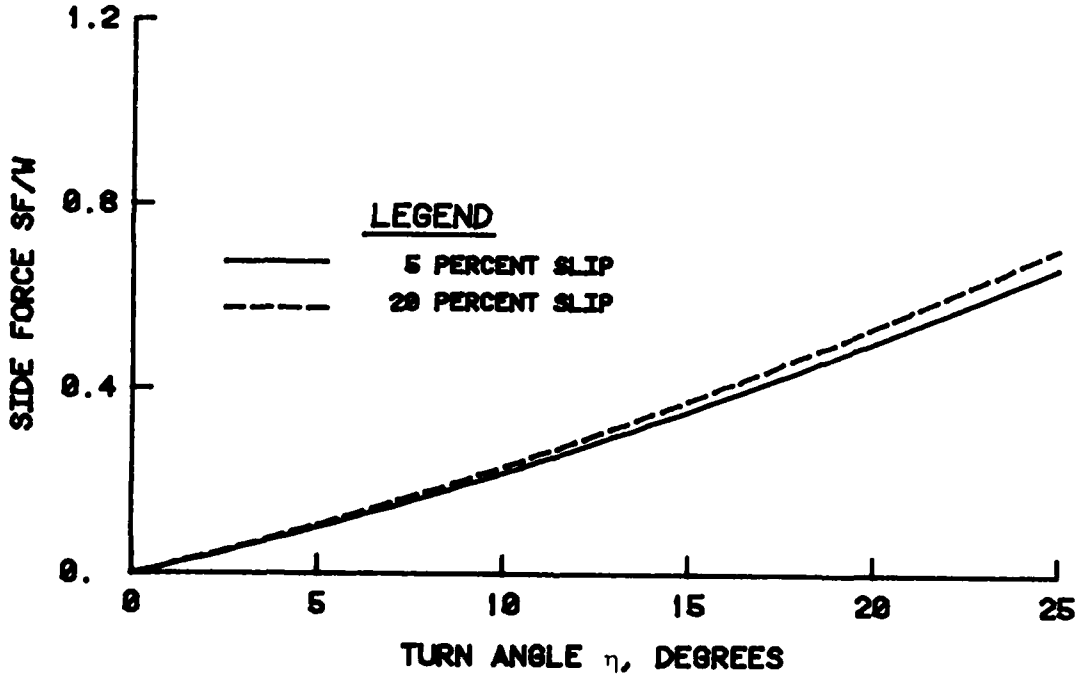

Figure 113. Relationship between side force and turn angle for clay; 35 percent tire deflection

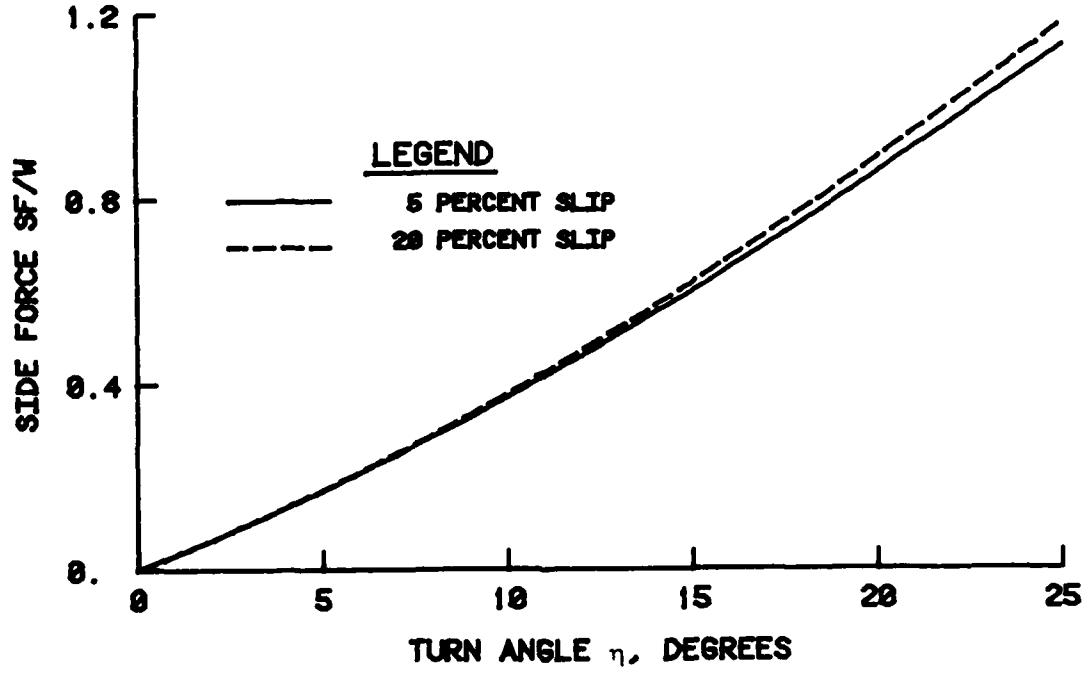

Figure 114. Relationship between side force and turn angle for sand; 15 percent tire deflection

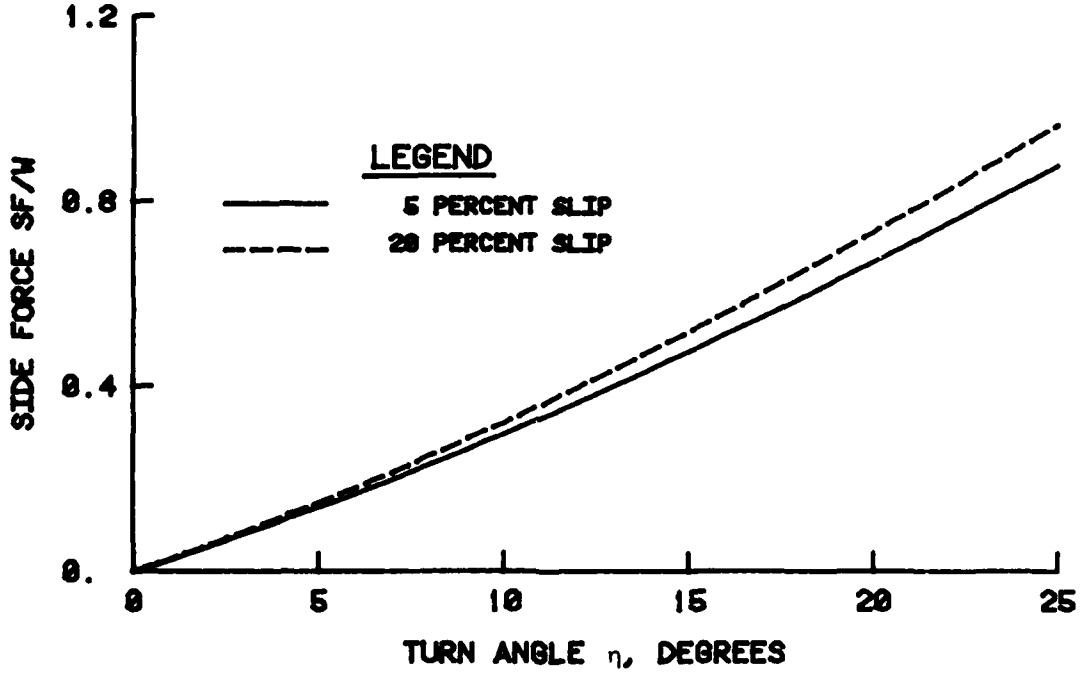

Figure 115. Relationship between side force and turn angle for sand; 35 percent tire deflection

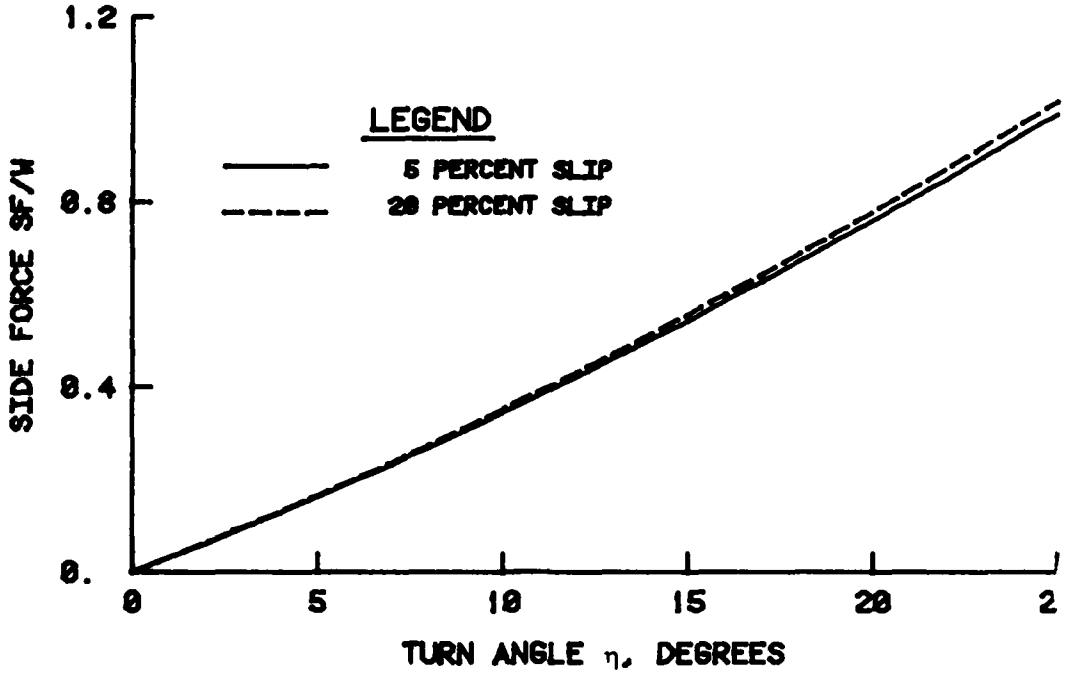

Figure 116. Relationship between side force and turn angle for mixed soil; 15 percent tire deflection

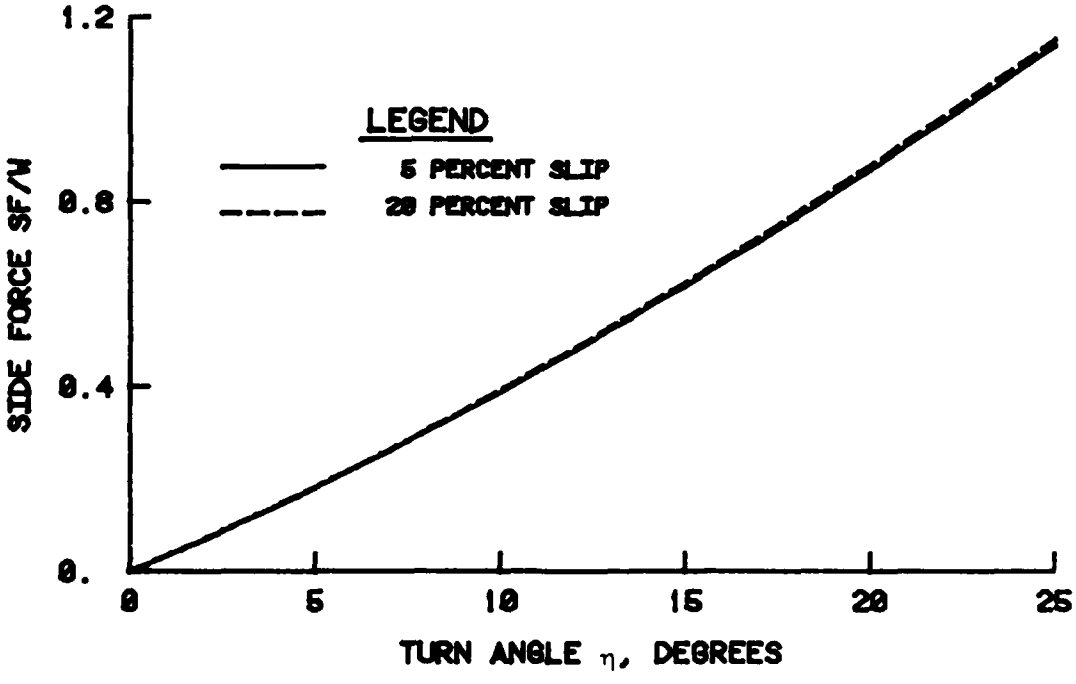

Figure 117. Relationship between side force and turn angle for mixed soil; 35 percent tire deflection

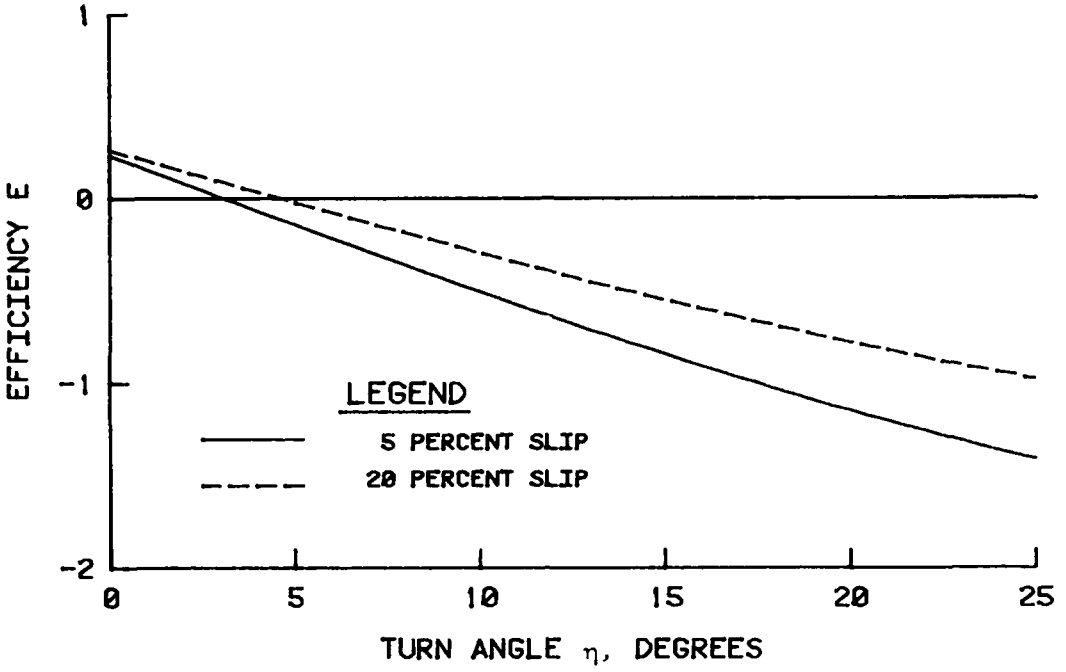

Figure 118. Relationship between efficiency and turn angle for clay; 15 percent tire deflection

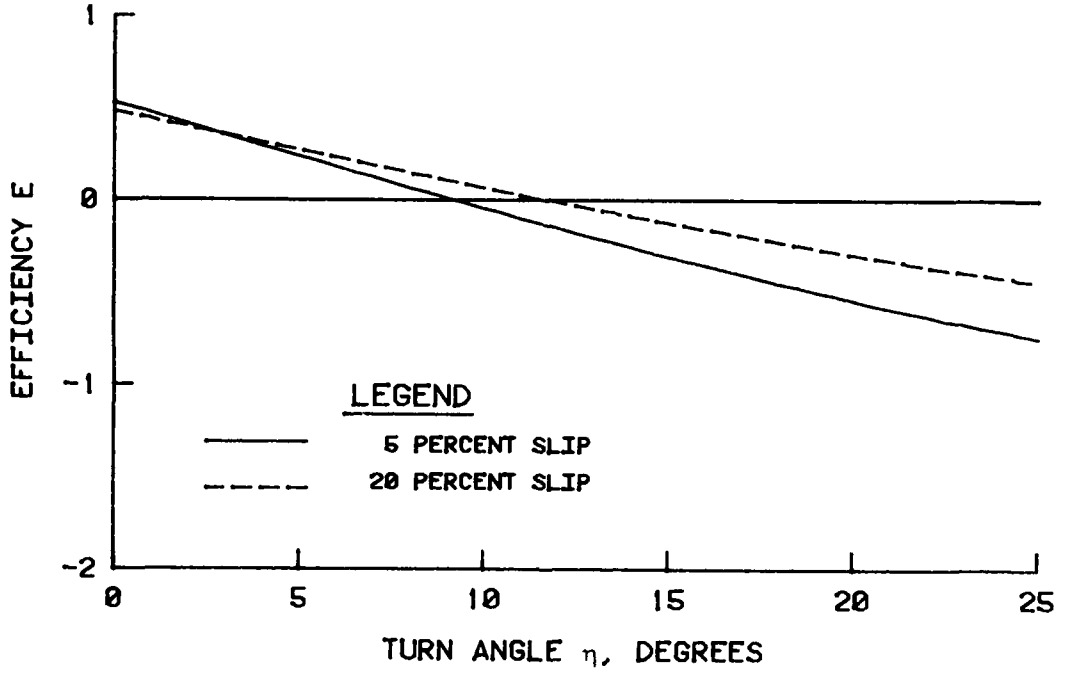

Figure 119. Relationship between efficiency and turn angle for clay; 35 percent tire deflection

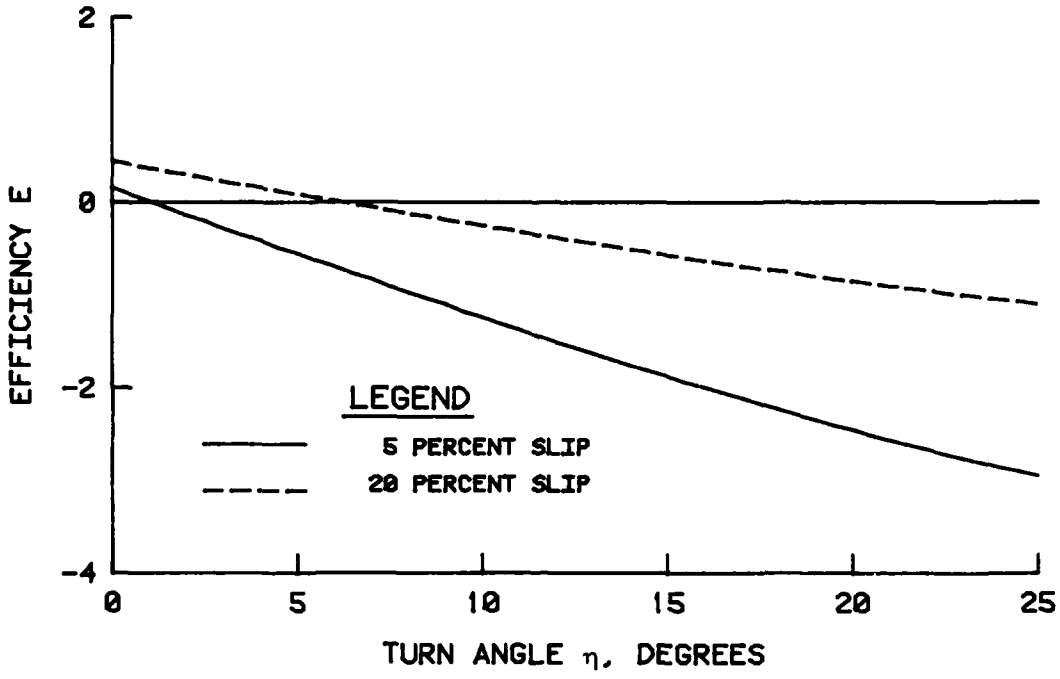

Figure 120. Relationship between efficiency and turn angle for sand; 15 percent tire deflection

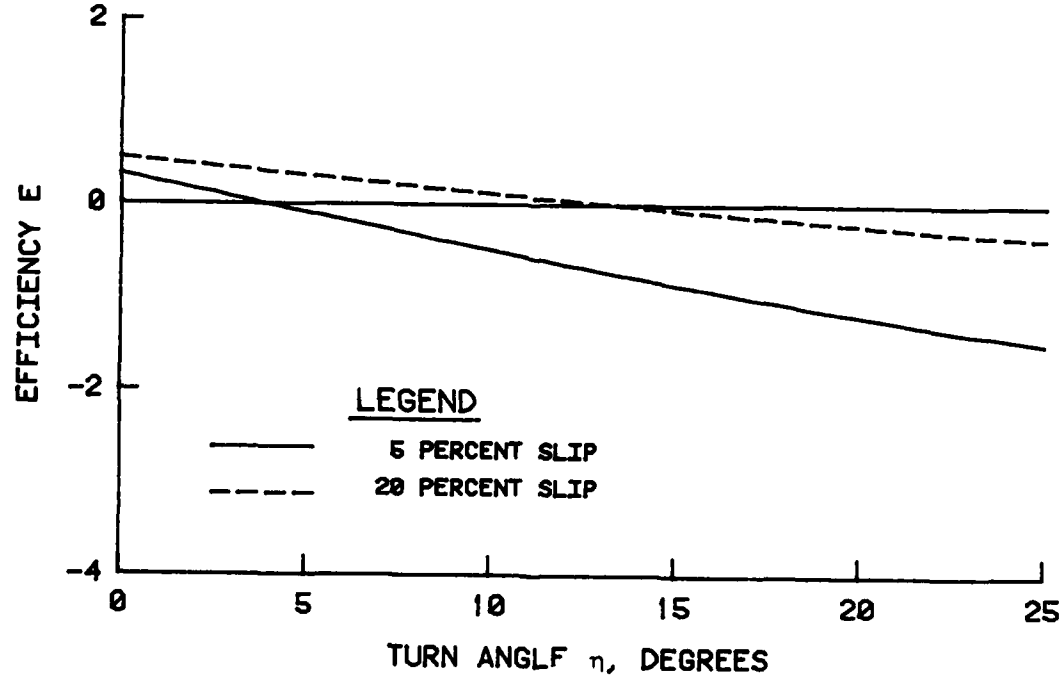

Figure 121. Relationship between efficiency and turn angle for sand; 35 percent tire deflection

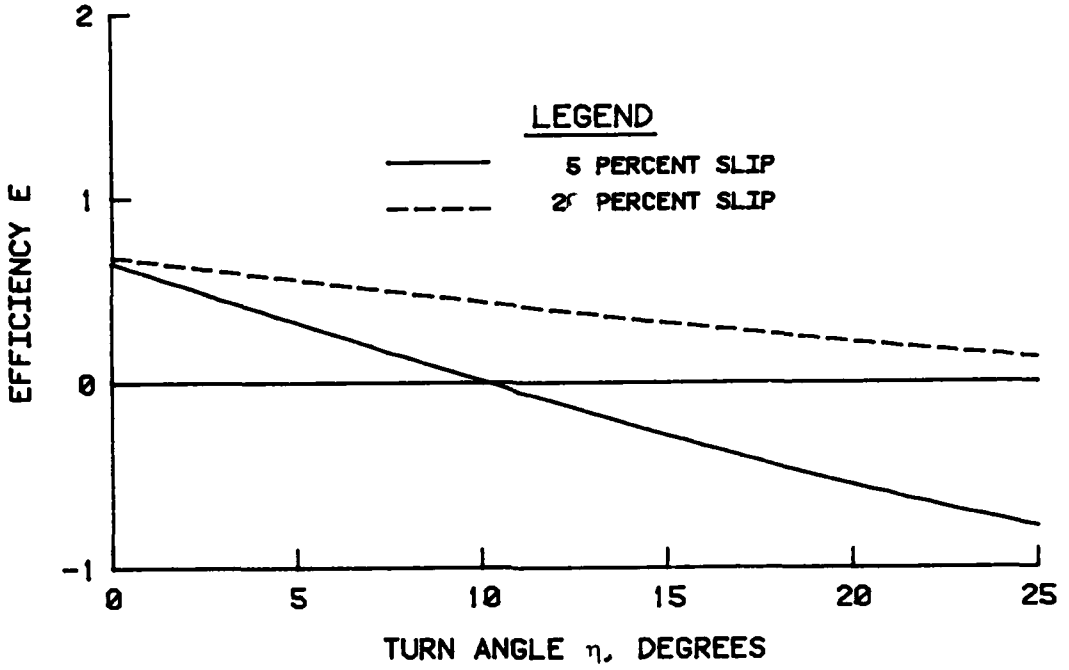

Figure 122. Relationship between efficiency and turn angle for mixed soil; 15 percent tire deflection

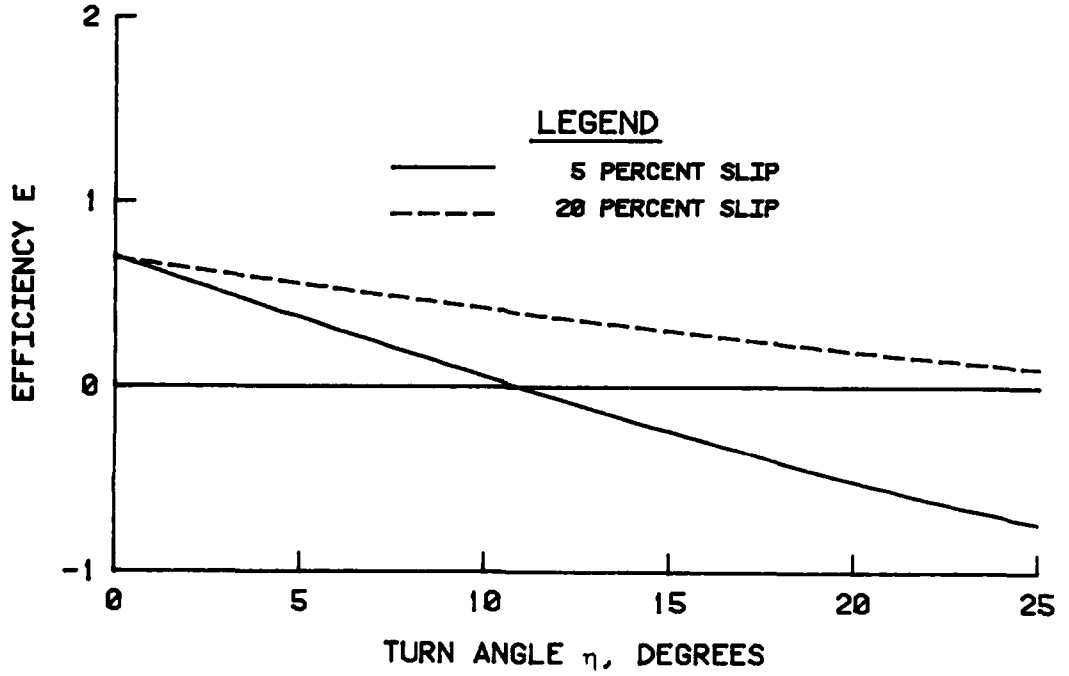

Figure 123. Relationship between efficiency and turn angle for mixed soil; 35 percent tire deflection

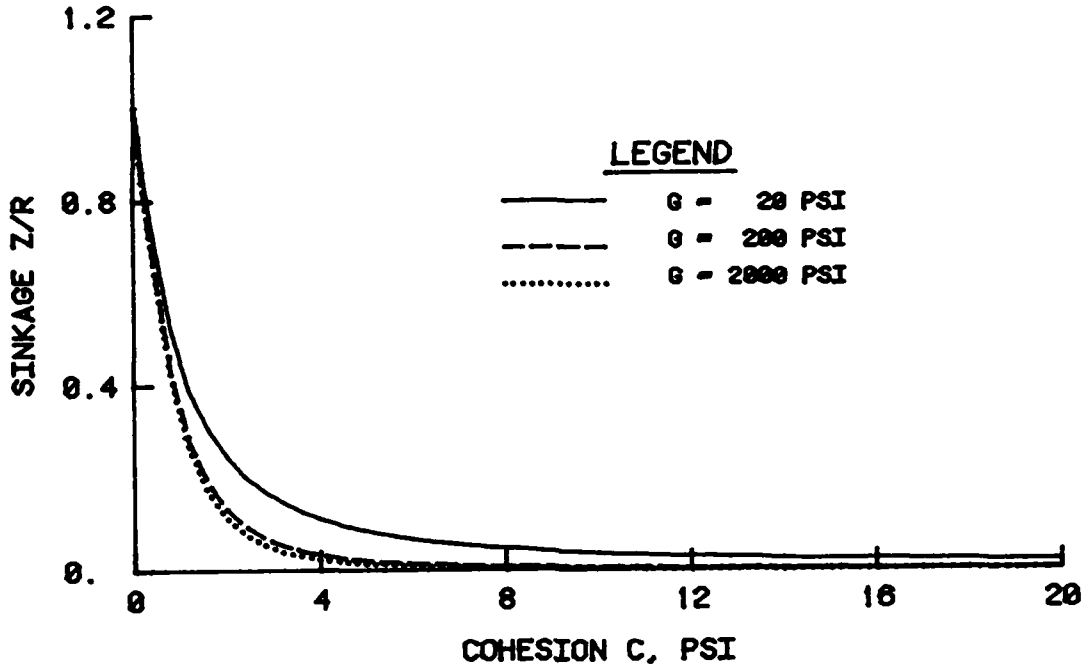

Figure 124. Relationship between sinkage and cohesion for clay

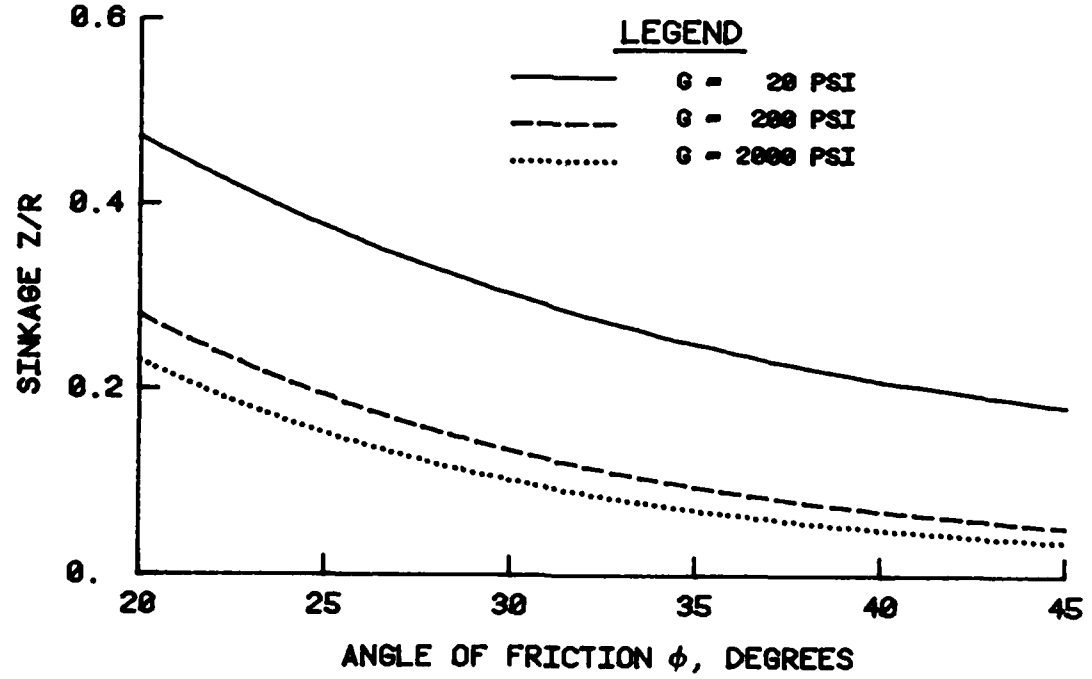

Figure 125. Relationship between sinkage and angle of friction for sand

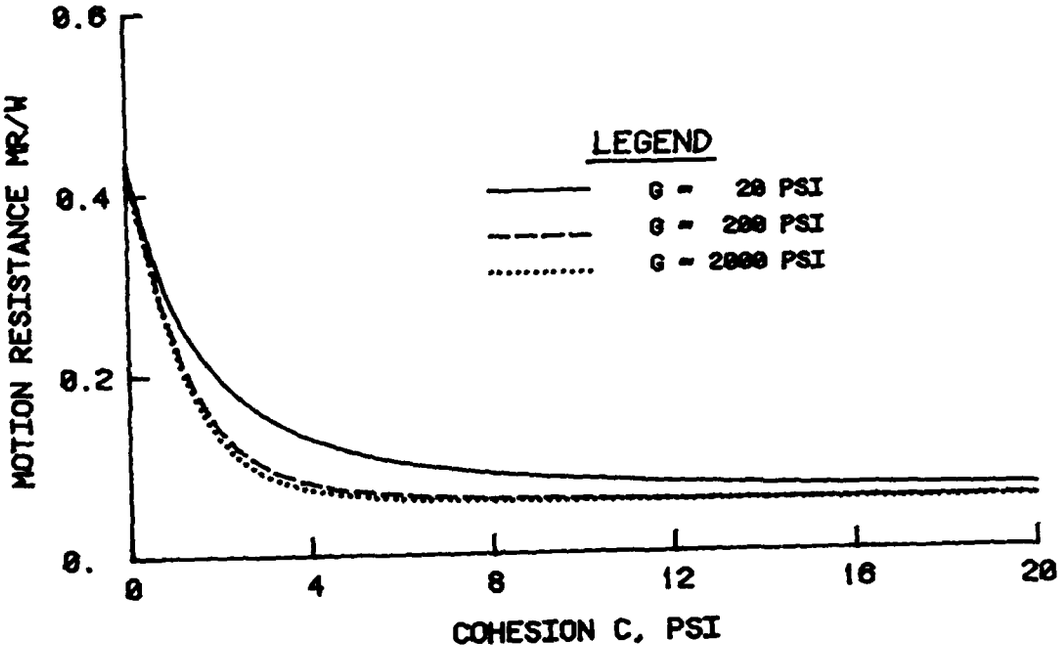

Figure 126. Relationship between motion resistance and cohesion for clay

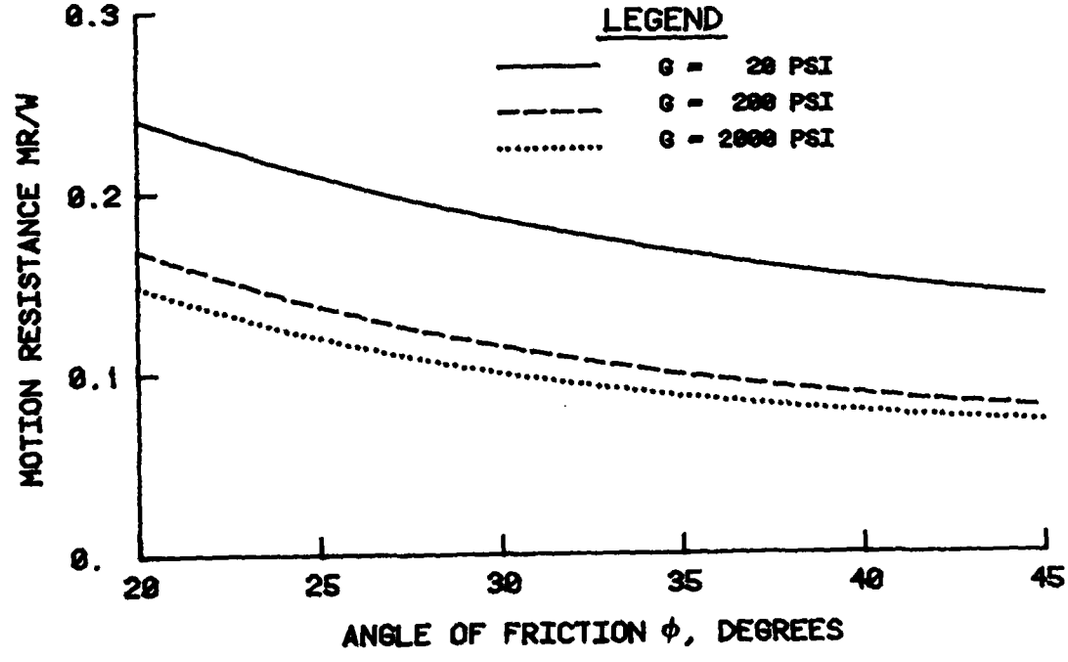

Figure 127. Relationship between motion resistance and angle of friction for sand

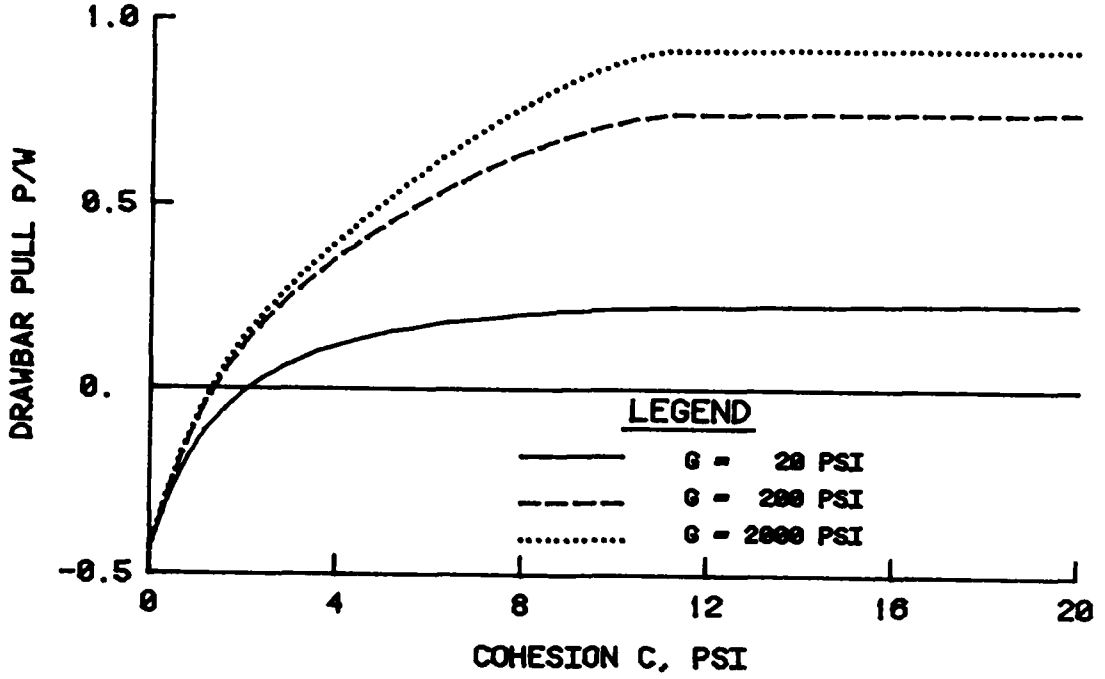

Figure 128. Relationship between drawbar pull and cohesion for clay

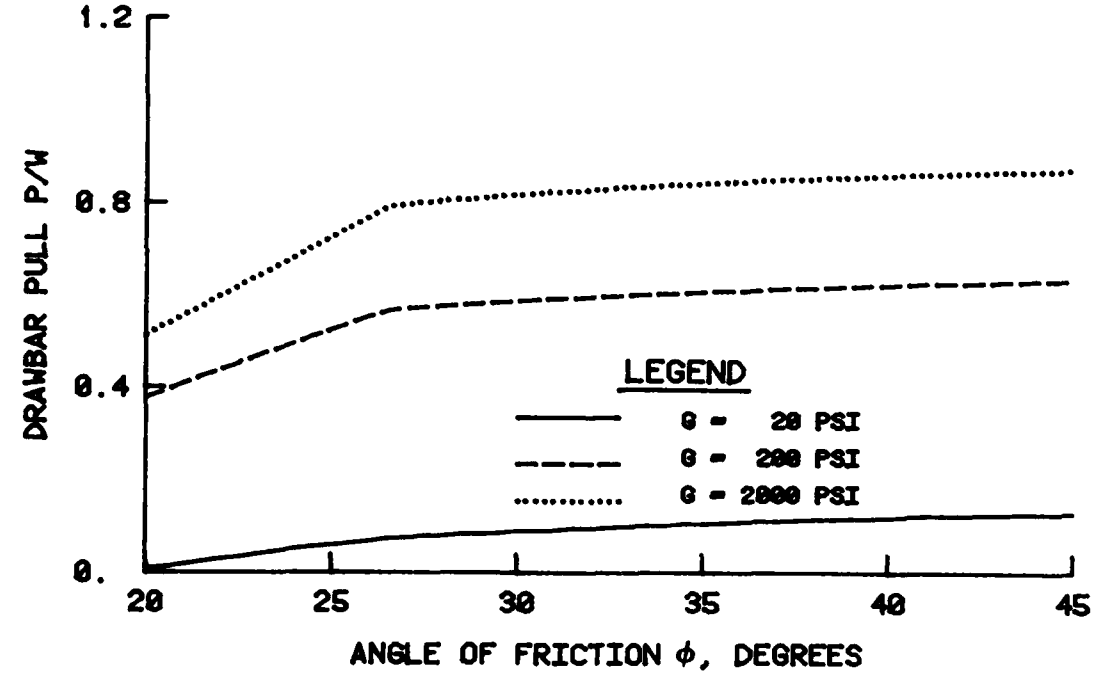

Figure 129. Relationship between drawbar pull and angle of friction for sand

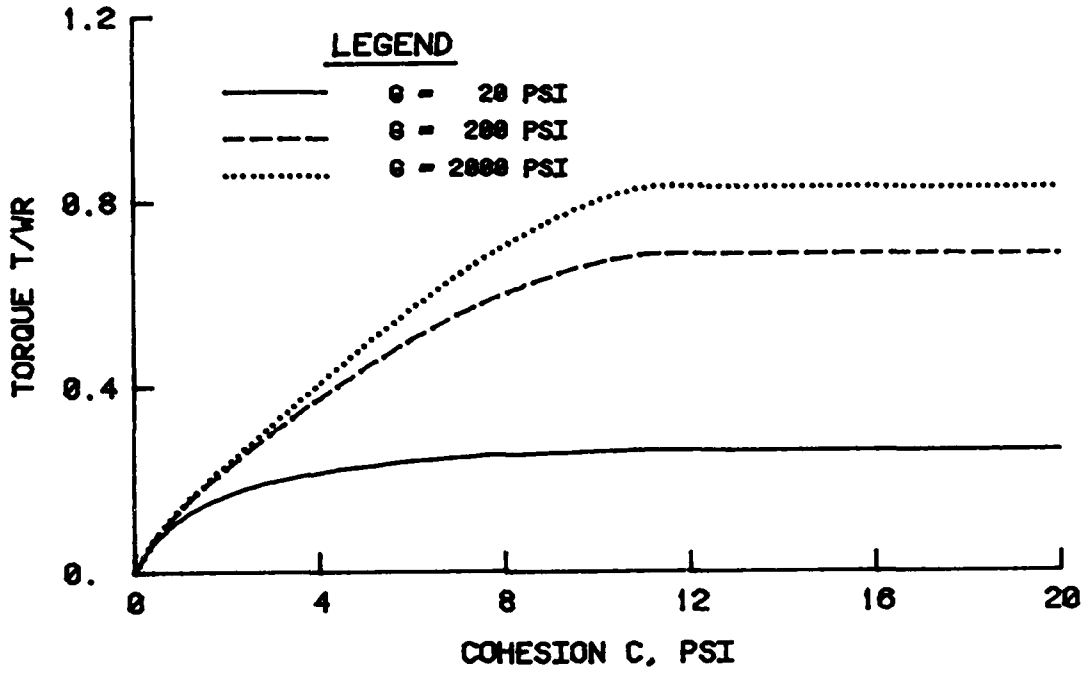

Figure 130. Relationship between torque and cohesion for clay

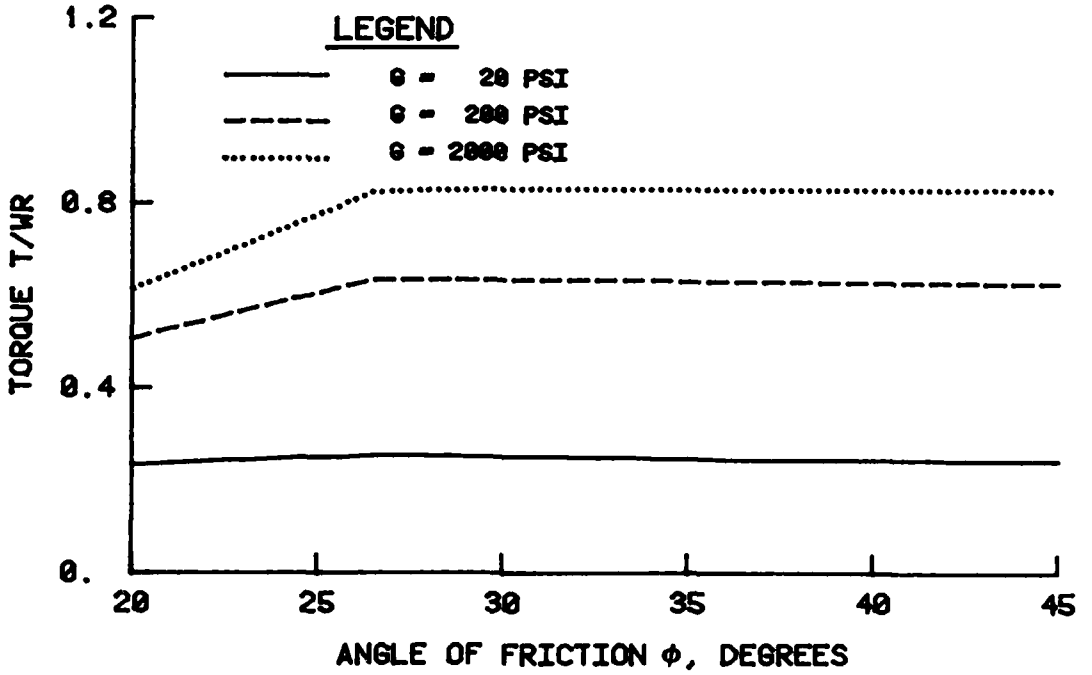

Figure 131. Relationship between torque and angle of friction for sand

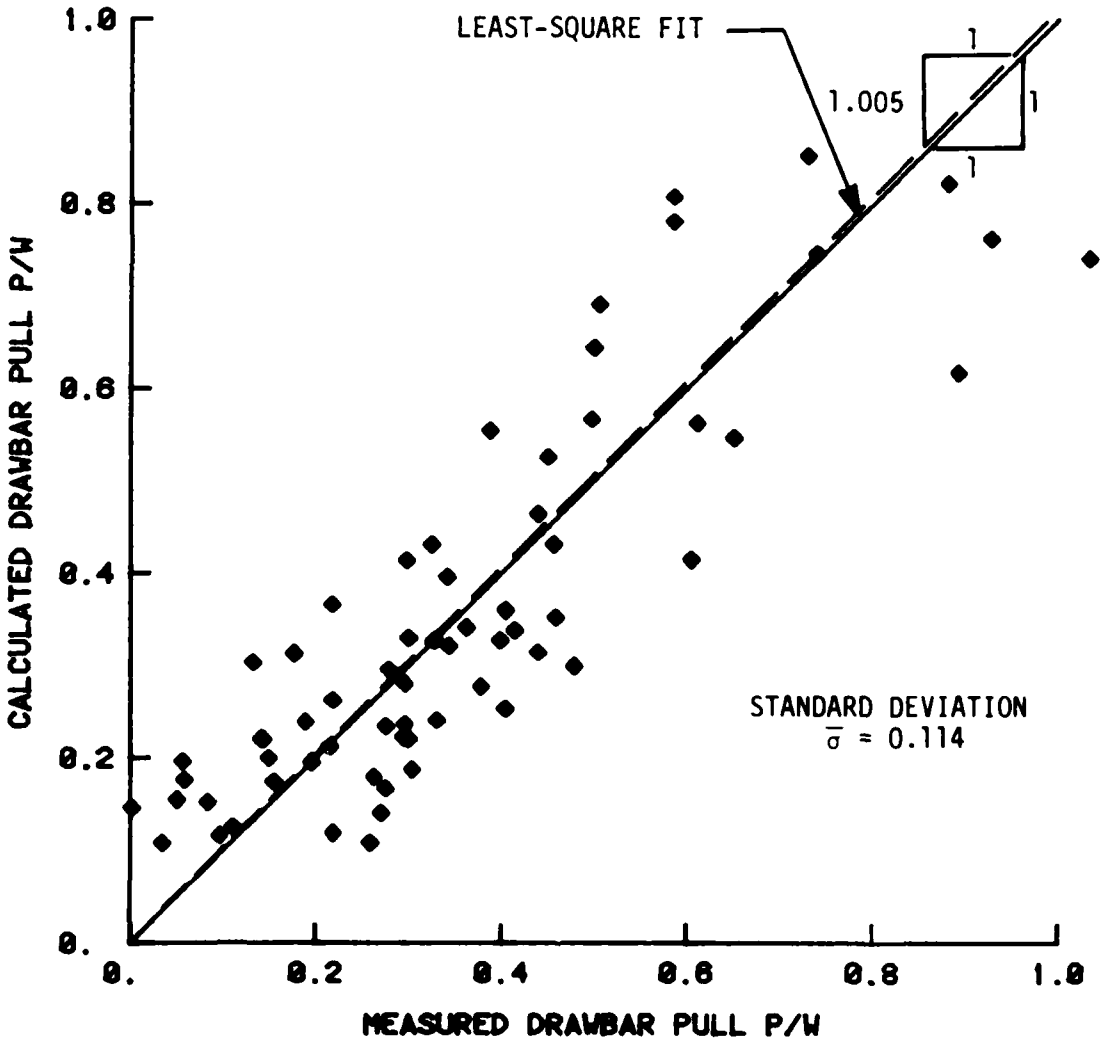

Figure 132. Comparison of predicted and measured drawbar pull for clay; 20 percent slip and zero turn angle

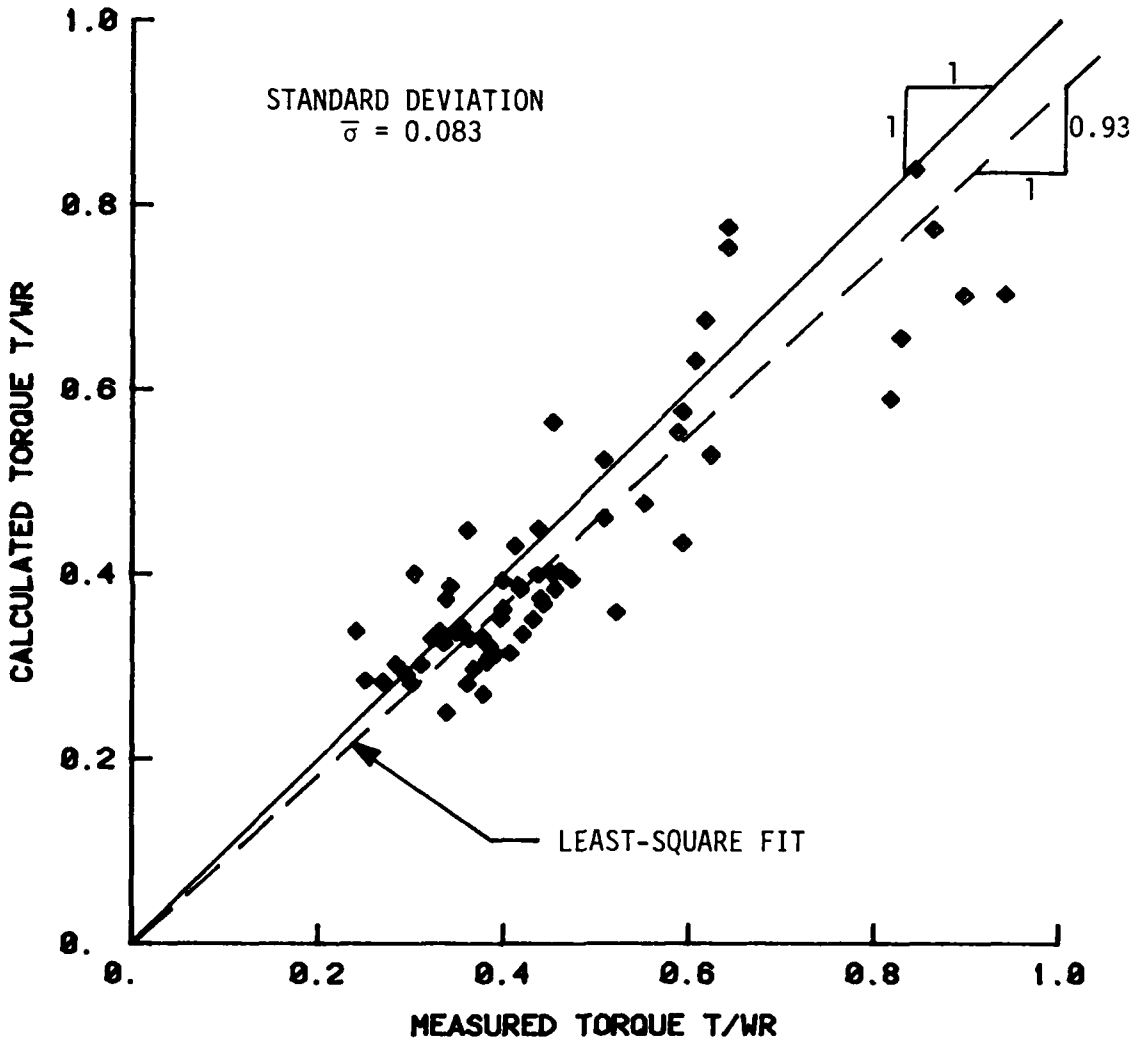

Figure 133. Comparison of predicted and measured torque for clay; 20 percent slip and zero turn angle

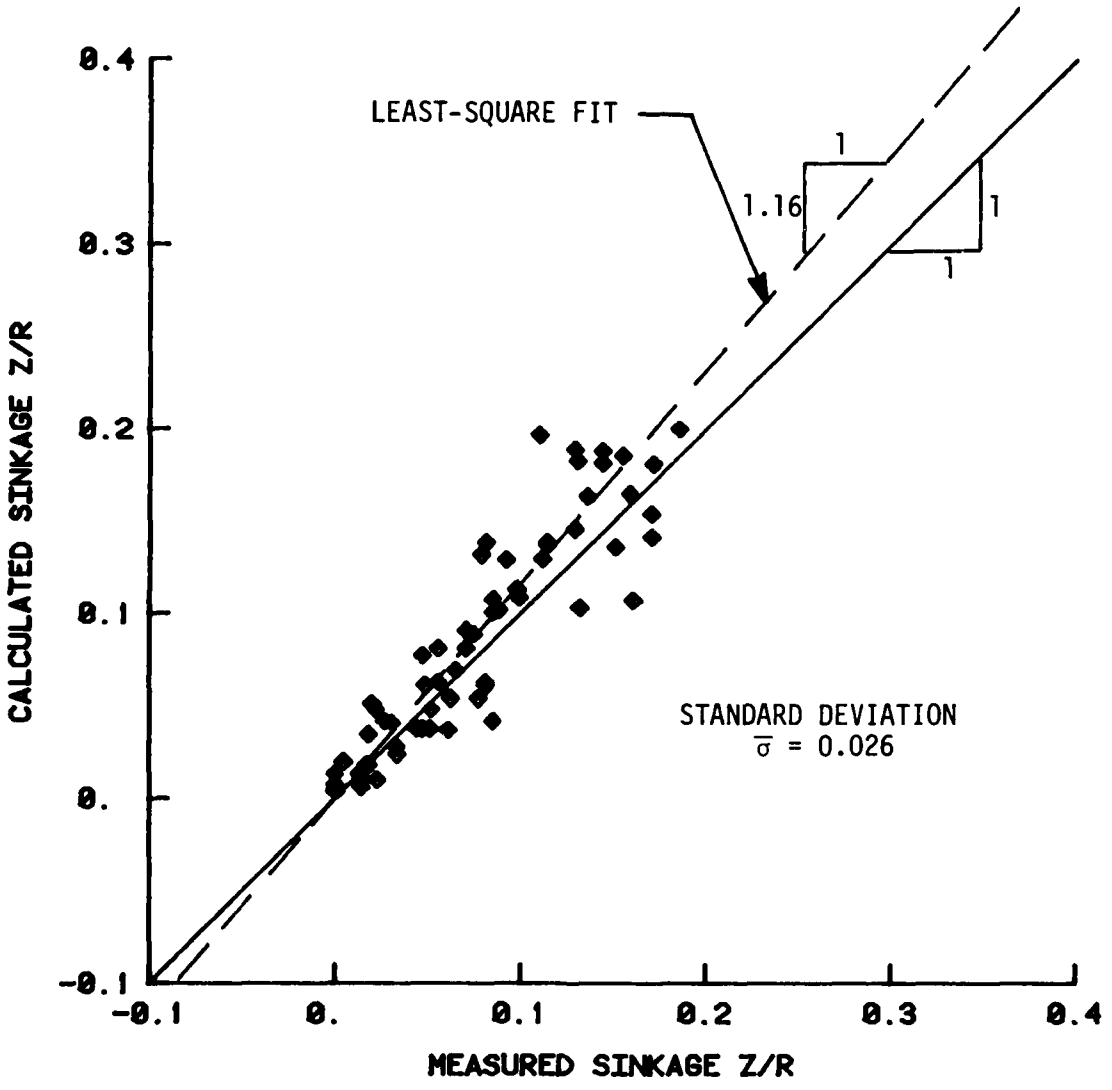

Figure 134. Comparison of predicted and measured sinkage for clay; 20 percent slip and zero turn angle

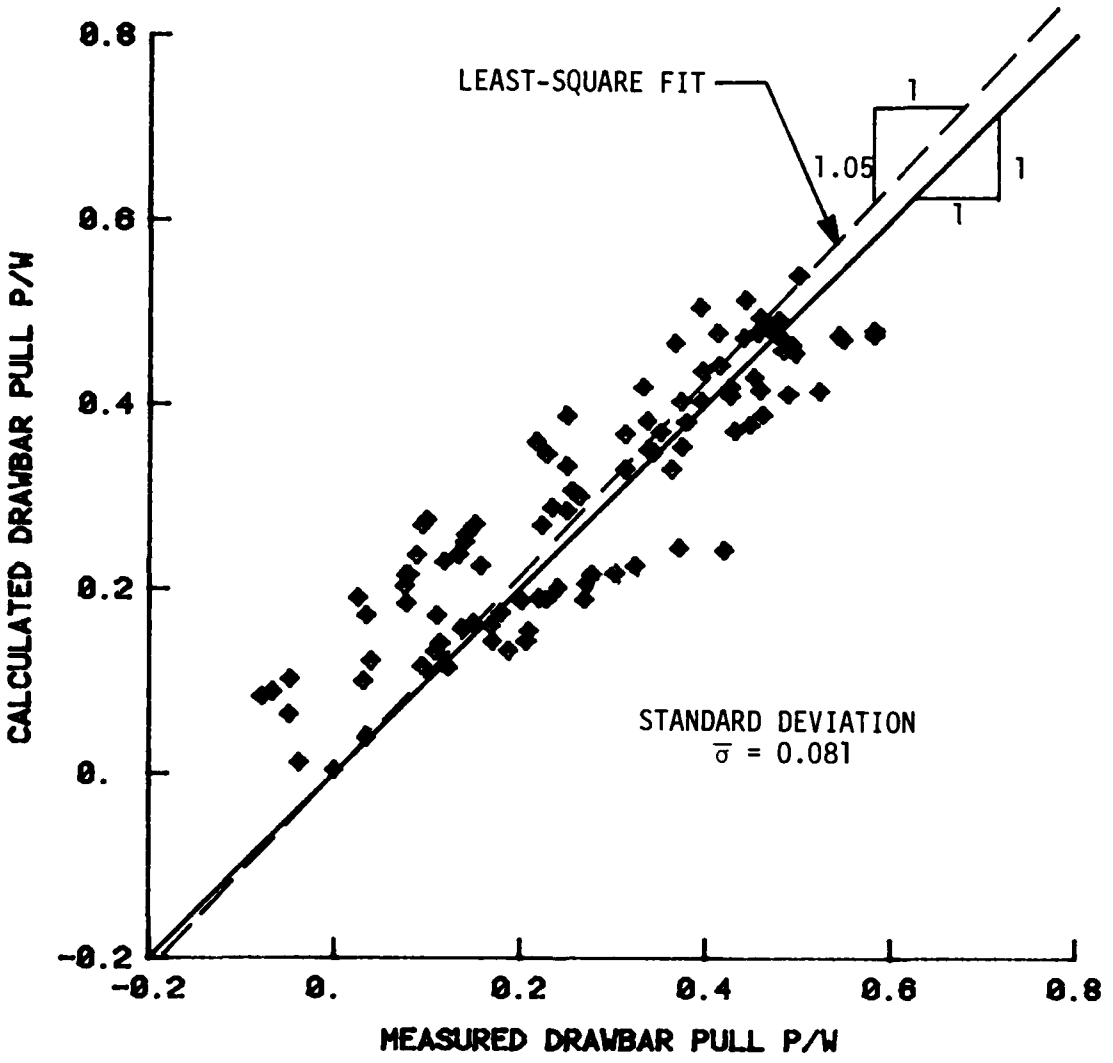

Figure 135. Comparison of predicted and measured drawbar pull for sand; 20 percent slip and zero turn angle

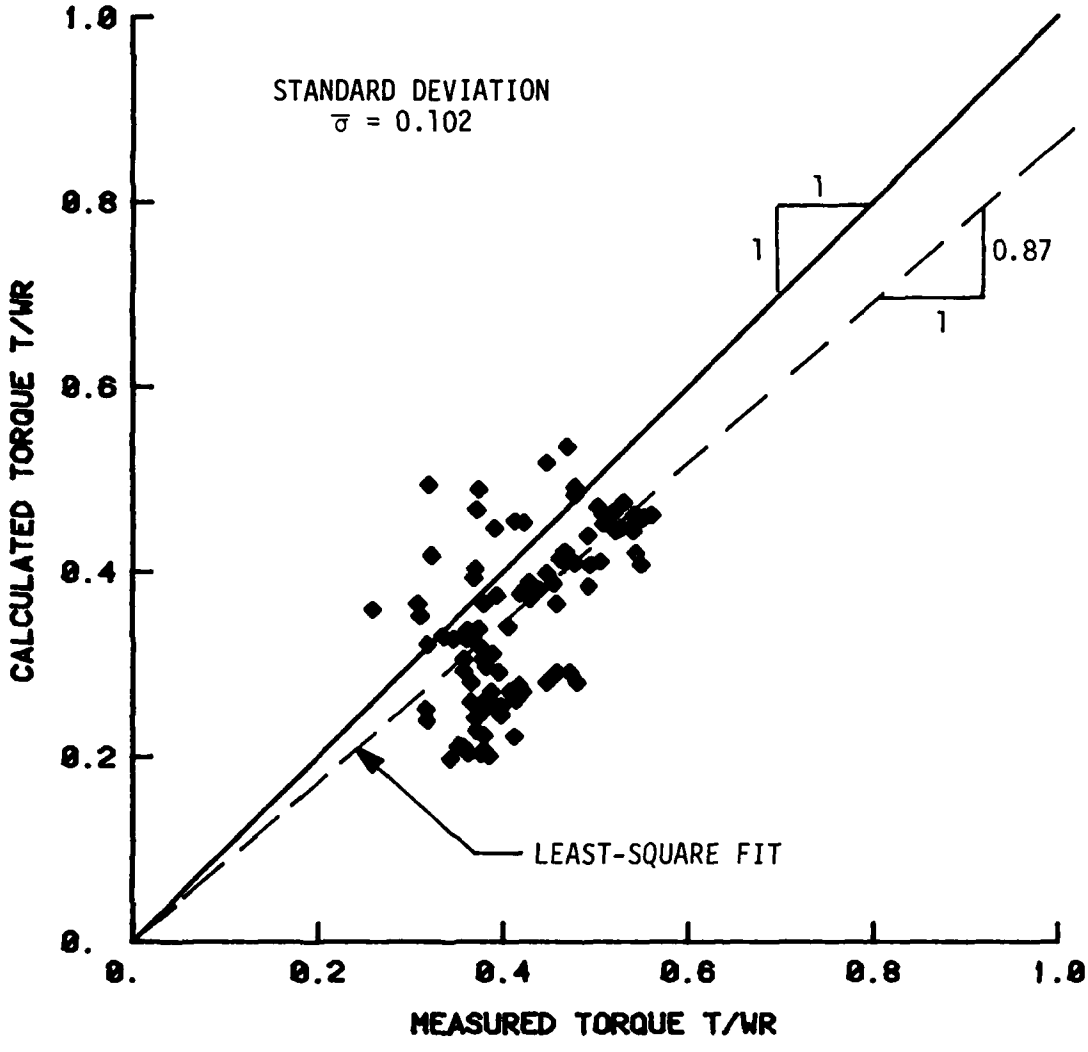

Figure 136. Comparison of predicted and measured torque for sand; 20 percent slip and zero turn angle

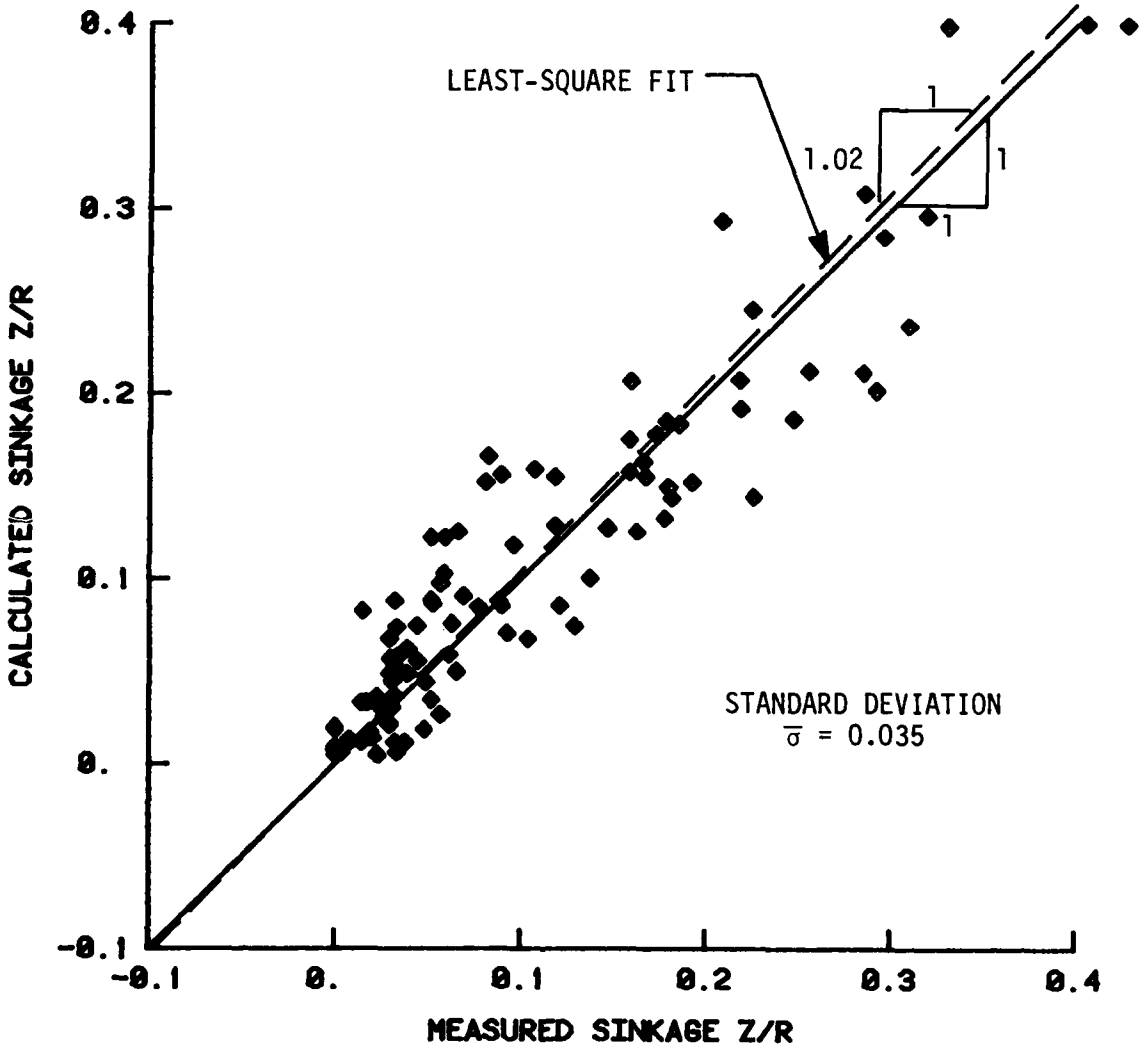

Figure 137. Comparison of predicted and measured sinkage for sand; 20 percent slip and zero turn angle

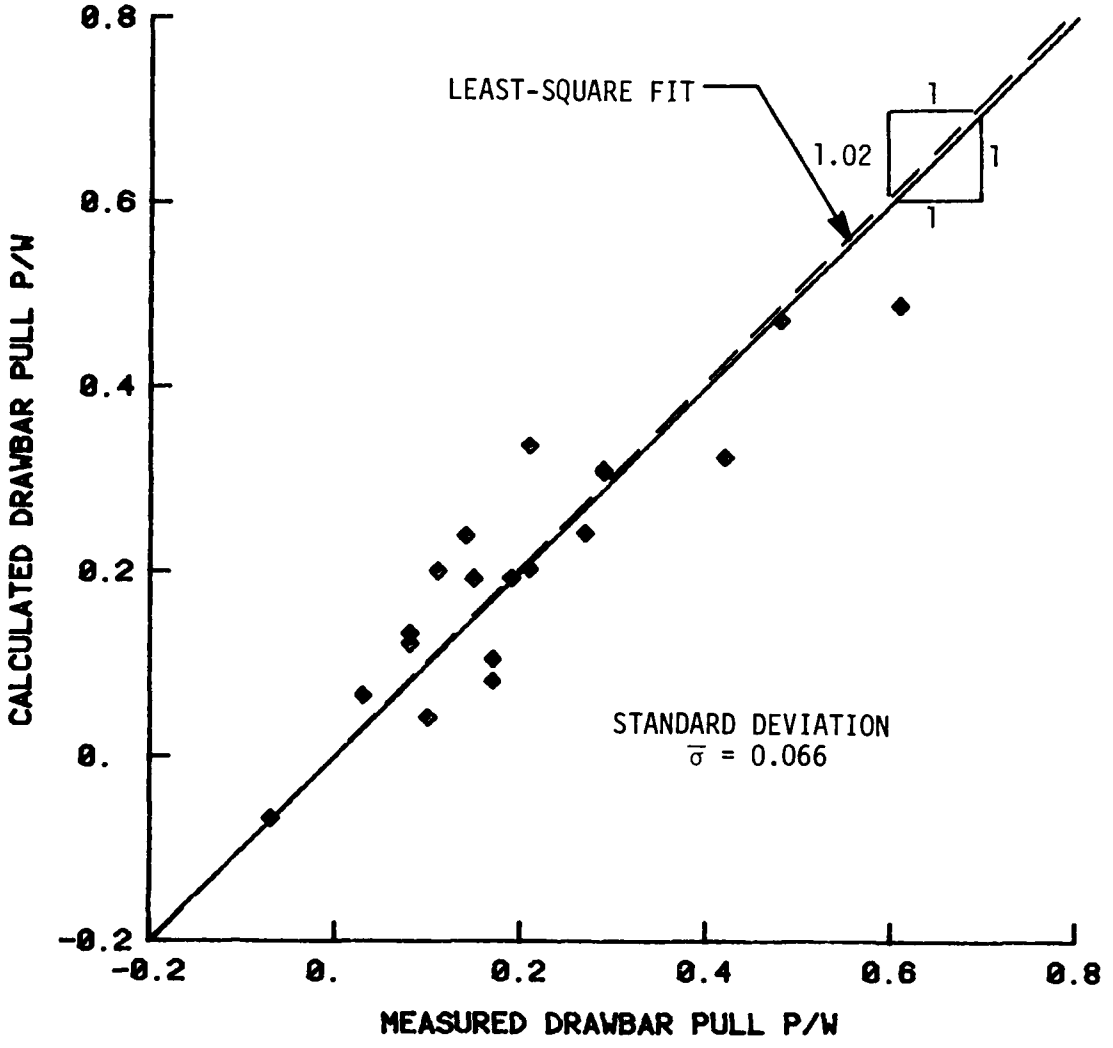

Figure 138. Comparison of predicted and measured drawbar pull for clay; nonzero turn angles

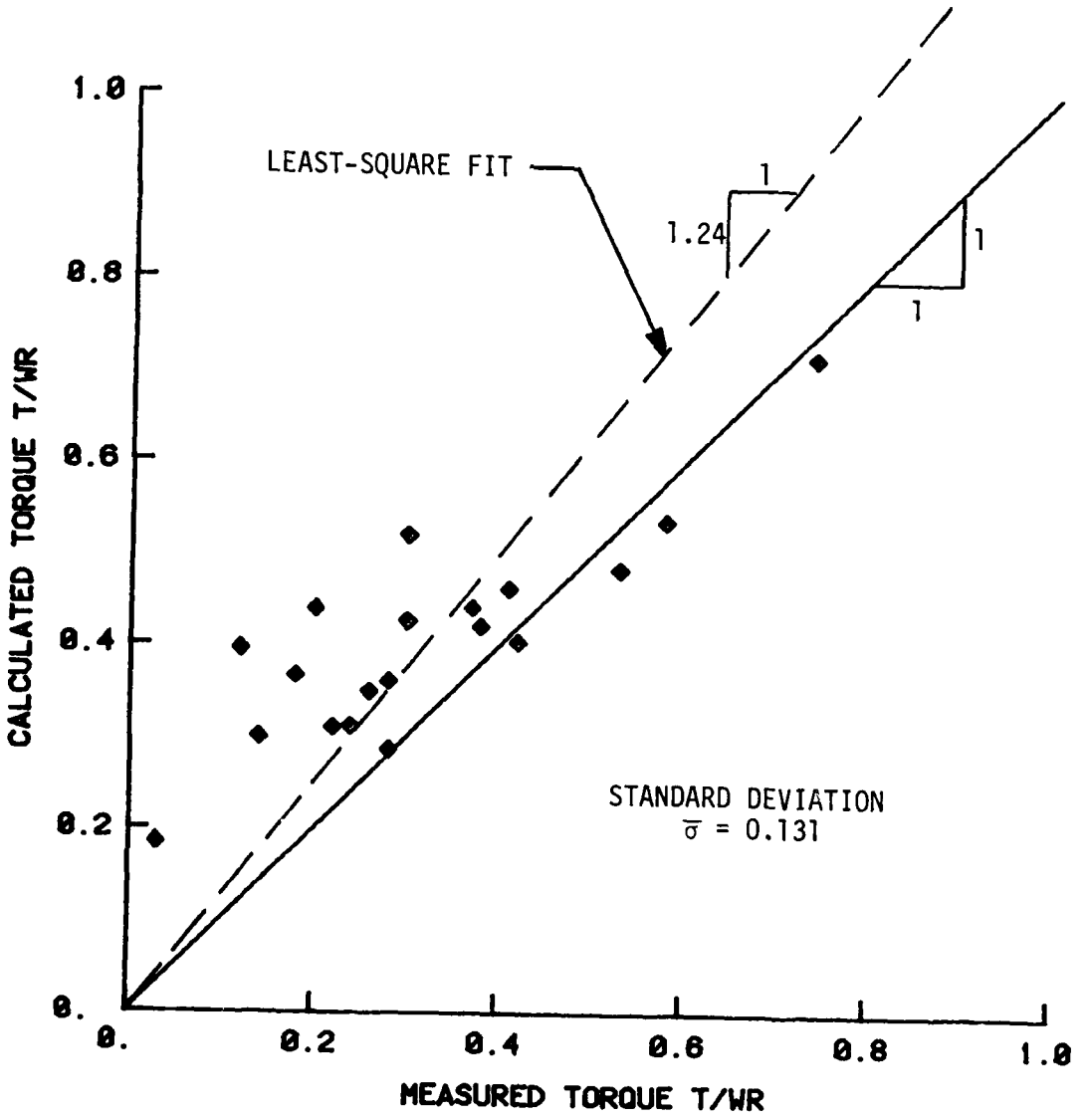

Figure 139. Comparison of predicted and measured torque for clay; nonzero turn angles

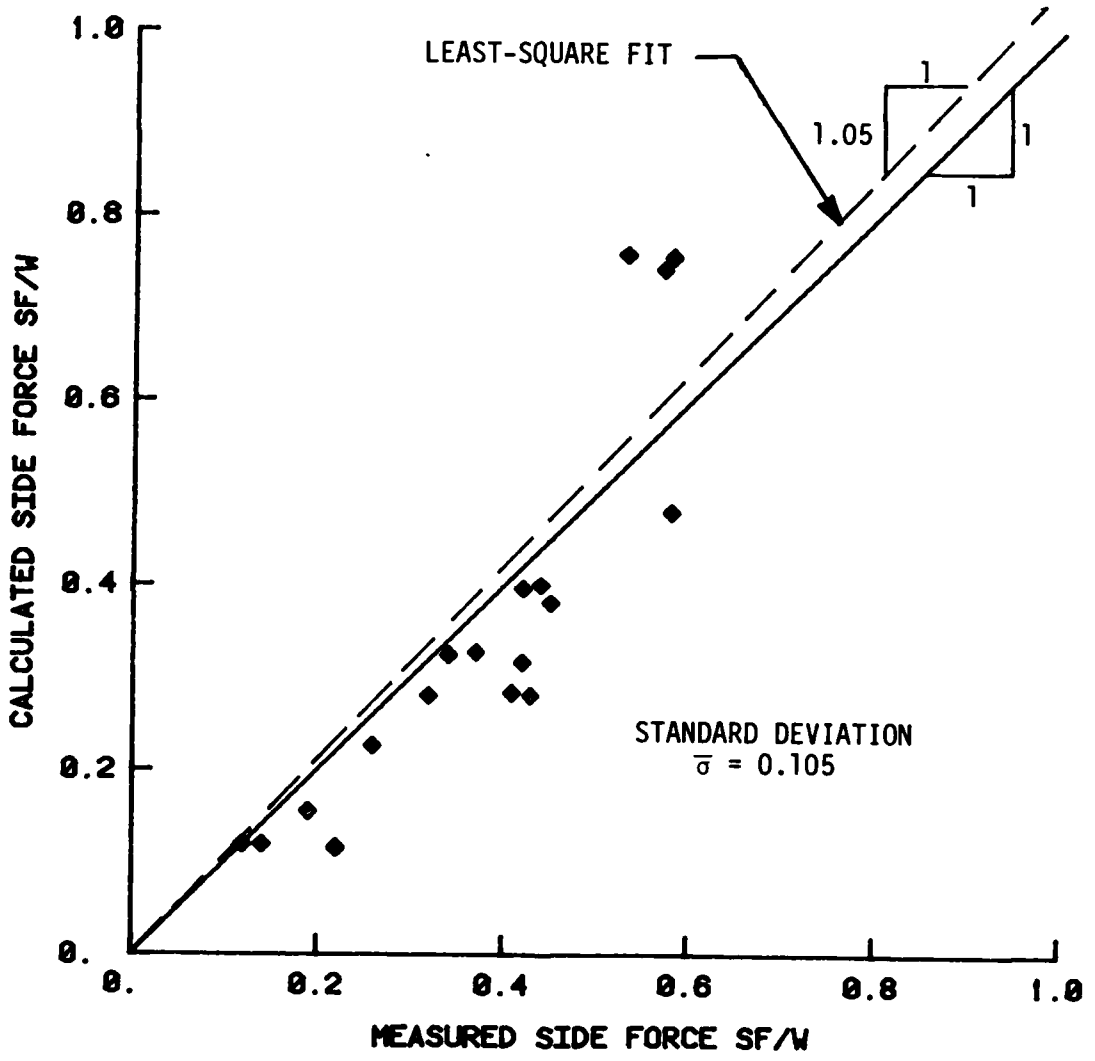

Figure 140. Comparison of predicted and measured side force for clay; nonzero turn angles

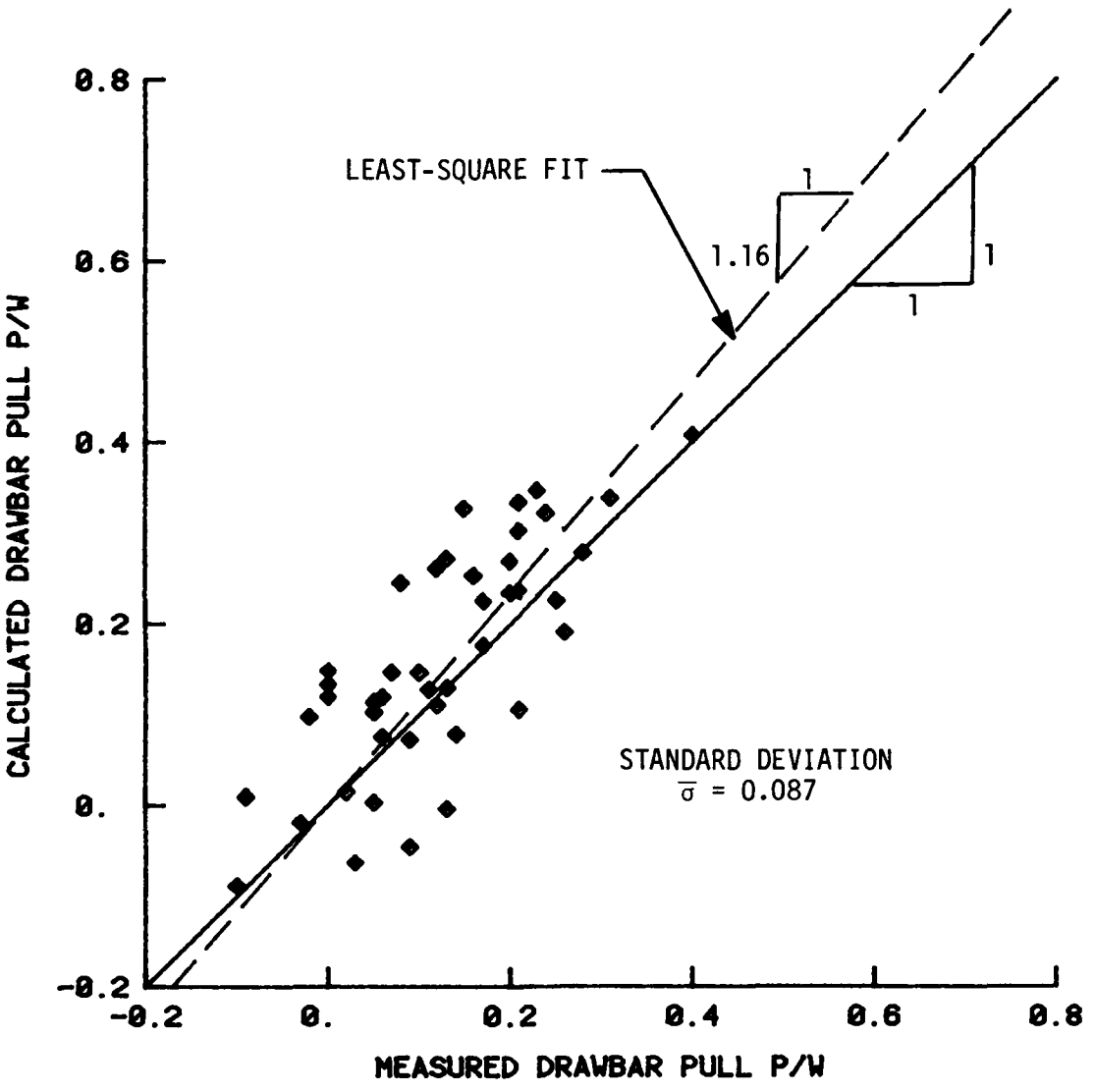

Figure 141. Comparison of predicted and measured drawbar pull for sand; nonzero turn angles

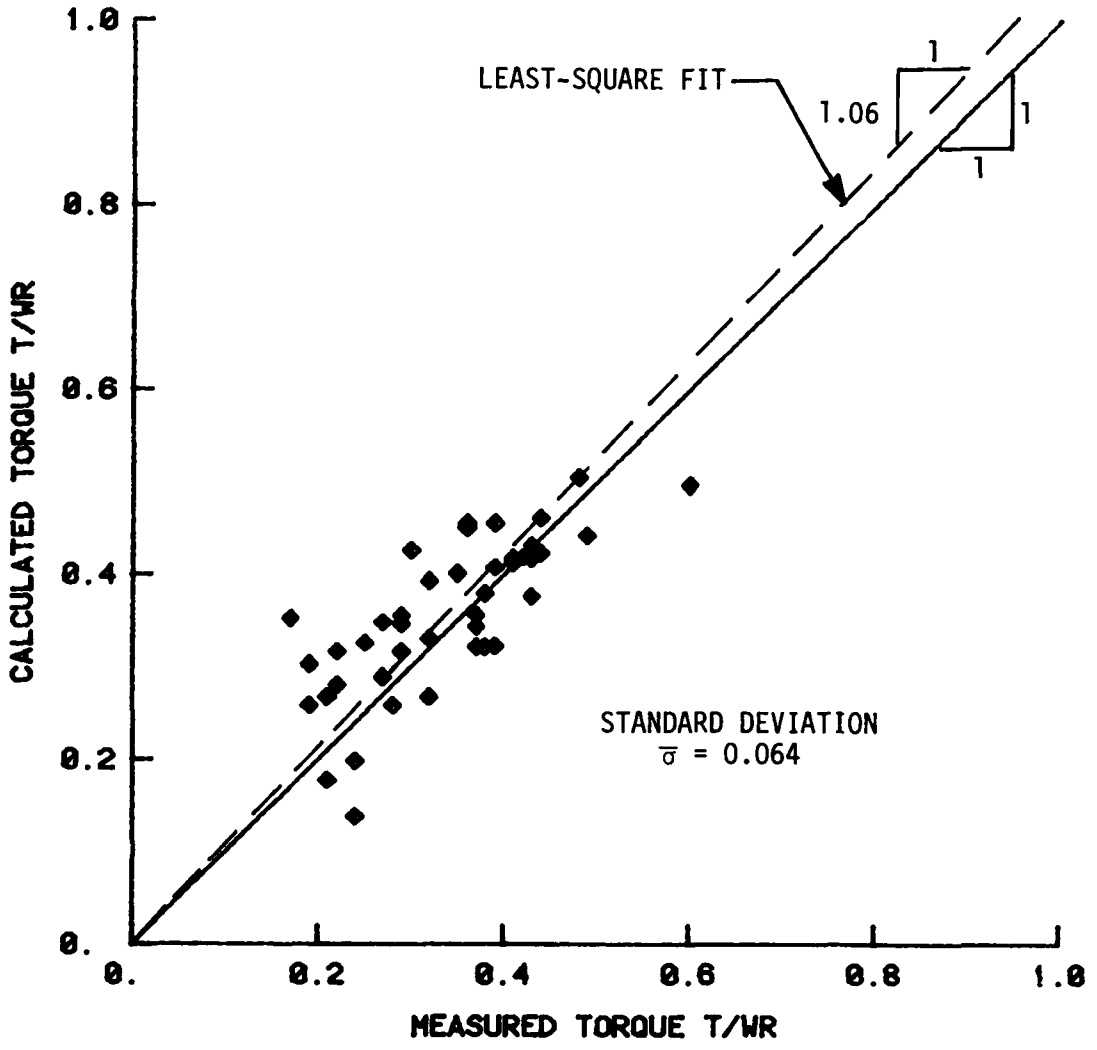

Figure 142. Comparison of predicted and measured torque for sand; nonzero turn angles

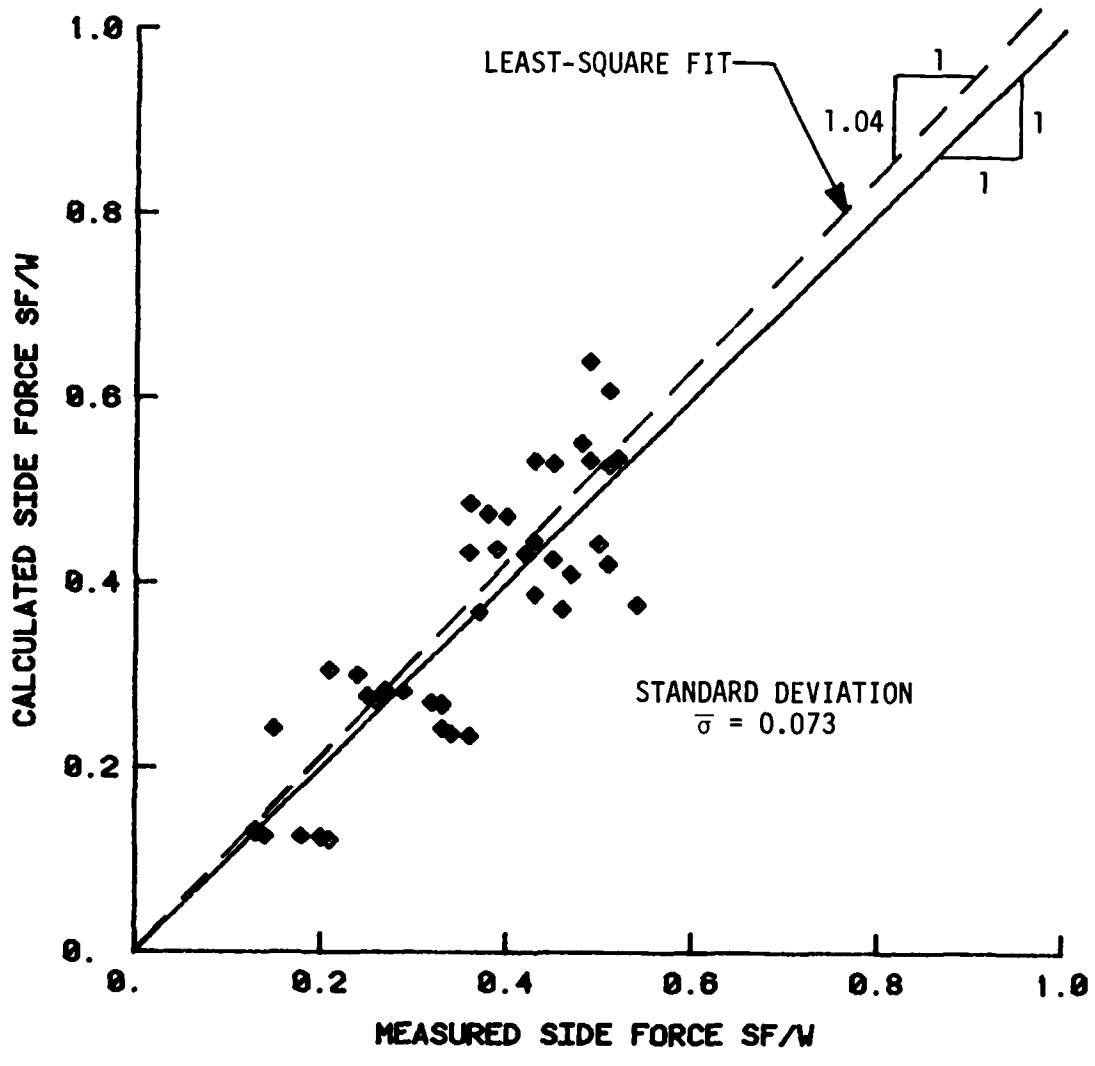

Figure 143. Comparison of predicted and measured side force for sand; nonzero turn angles

APPENDIX A: SOIL MODEL

Strength Components

1. One of the most important properties of soil affecting trafficability is in situ undrained shear strength. It has been found experimentally that the undrained shear strength of purely cohesive soils is relatively independent of the confining stress, but strongly affected by the time rate of shearing. On the other hand, the undrained shear strength of purely frictional soils is found to be relatively independent of the time rate of loading, but strongly dependent on confining pressure. The undrained shearing resistance of most soils, however, is due to both the frictional and cohesive components. The cohesive and frictional components of strength are usually summed to obtain the total shear strength of the material. For static loading (very slow rate of deformation), the shear failure envelope is defined by

$$\tau_M = C + \sigma \tan \phi \tag{A1}$$

where

τ_M = the maximum shear strength of the material in undrained loading condition.

C = the apparent cohesive strength of the material corresponding to static loading

σ = the normal stress

ϕ = the apparent angle of friction of the material

Equation A1 is shown graphically in Figure A1.

2. As noted previously, the shear strength of cohesive soils increases with the increasing rate of loading. For the range of loading rates associated with the motion of wheeled vehicles, the contribution to cohesive strength due to dynamic loading can be expressed as $C_d[1 - \exp(-\Lambda\dot{\varepsilon})]$, where C_d and Λ are material constants and $\dot{\varepsilon}$ is the time rate of shearing strain. In view of the above expression, the dynamic failure criterion takes the following form:

$$\tau_M = C + C_d[1 - \exp(-\Lambda\dot{\varepsilon})] + \sigma \tan \phi \tag{A2}$$

When Λ equals zero, the dynamic failure criterion (Equation A2) reduces to the static failure criterion (Equation A1). Both are shown graphically in Figure A1.

Shear Stress-Shear Strain Relation

3. Prior to failure, the shearing stress-strain characteristics of a variety of soils can be expressed by the following mathematical expression (Kondner 1963)*:

$$\tau = \frac{G\,\tau_M\,\varepsilon}{\tau_M + G|\varepsilon|} \tag{A3}$$

The behavior of Equation A3 is shown graphically in Figure A2, in which τ denotes shearing stress, ε is shearing strain, and G initial shear modulus. Substituting τ_M from Equation A2 into Equation A3, the shearing stress-strain relation for soil becomes

$$\tau = \frac{G\left[C + C_d - C_d \exp\left(-\Lambda\dot{\varepsilon}\right) + \sigma \tan\phi\right]\varepsilon}{G|\varepsilon| + C + C_d - C_d \exp\left(-\Lambda\dot{\varepsilon}\right) + \sigma \tan\phi} \tag{A4}$$

For purely cohesive soils, ϕ is 0 and τ is only a function of ε and $\dot{\varepsilon}$. For cohesionless or granular soils, C and C_d are zero, and τ is a function of ε and σ. For mixed soils exhibiting shearing resistance due to both frictional and cohesive components, τ is dependent on ε, $\dot{\varepsilon}$, and σ. The qualitative behavior of Equation A4 for these three conditions is shown in Figure A3. It should be pointed out that Equation A4 reduces to the rigid plastic soil model often used in mobility studies when an extremely large value is specified for G, and Λ is set to zero.

4. A method for determining the numerical values of the five material constants in Equation A4 has been outlined by Baladi and Rohani (1979).

---

* References cited in this appendix are listed in the References section at the end of the main text.

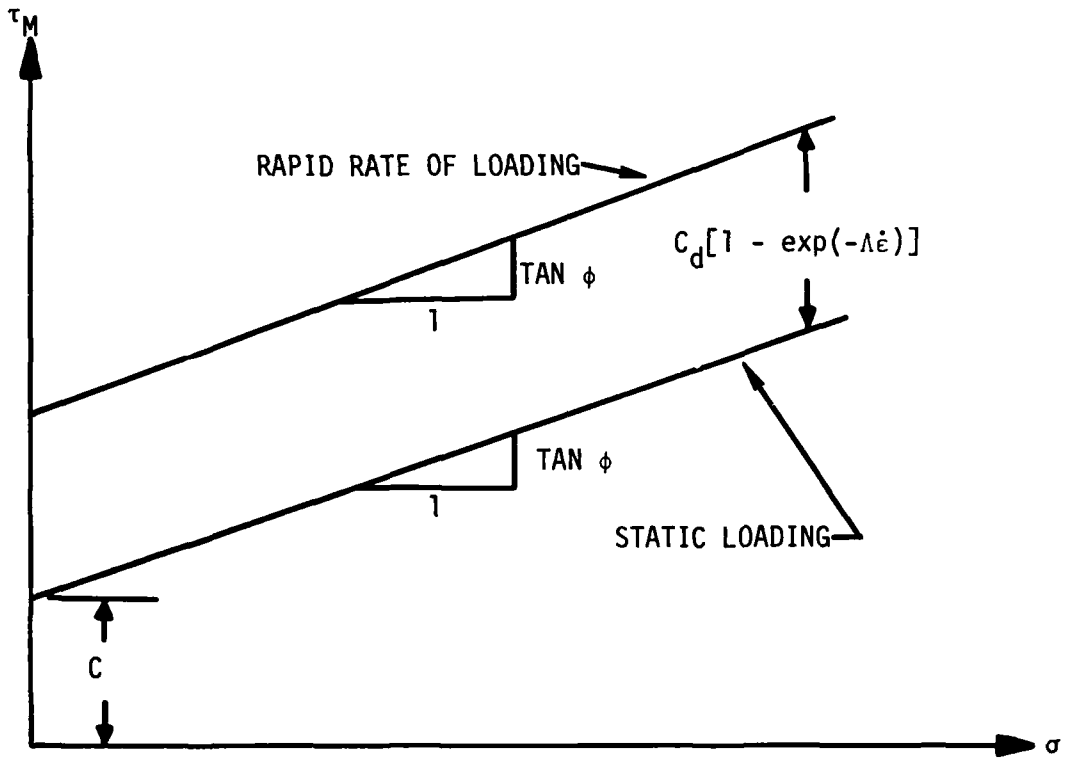

Figure A1. Proposed failure relation for soil

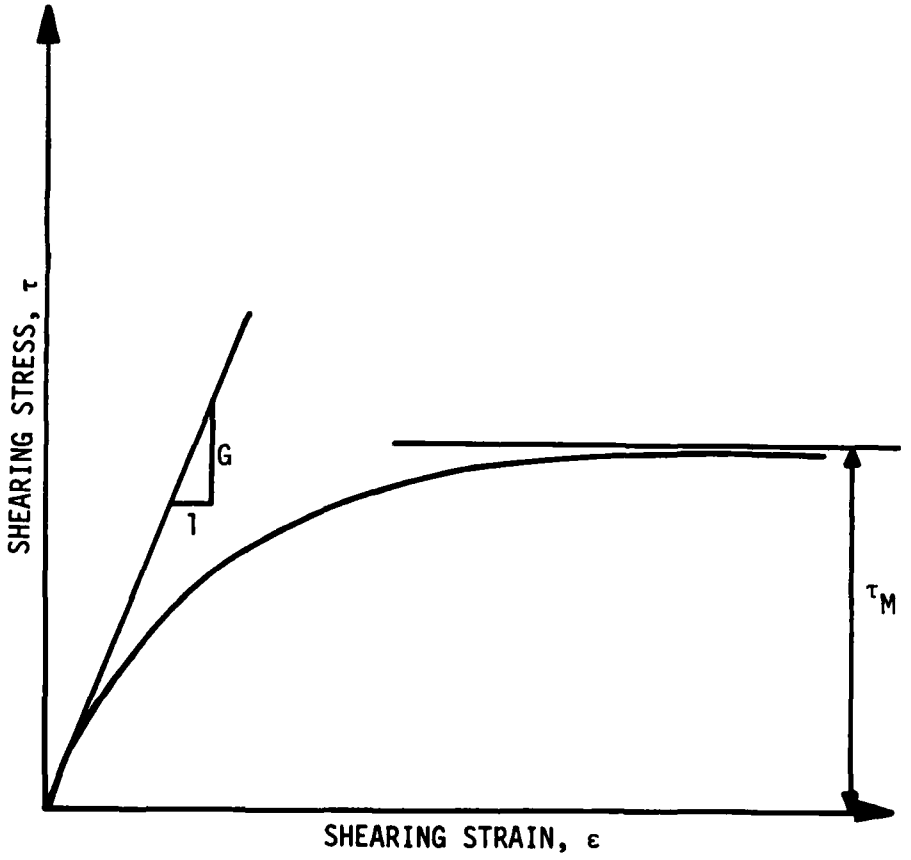

Figure A2. Proposed shear stress-shear strain relation during shearing process (Equation A3)

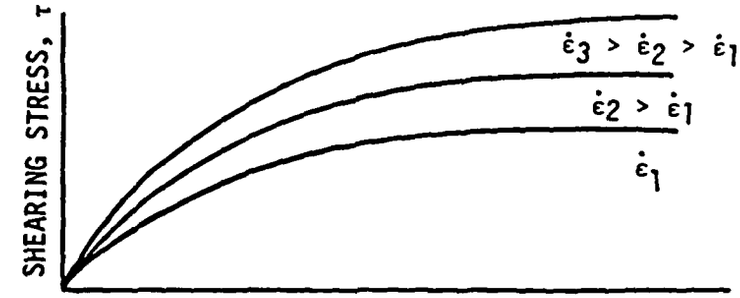

a. PURELY COHESIVE SOIL (τ INDEPENDENT OF σ)

b. GRANULAR SOIL (τ INDEPENDENT OF $\dot{\epsilon}$)

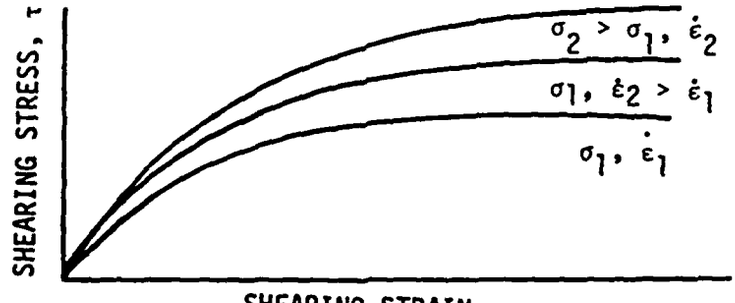

c. MIXED SOIL (τ DEPENDENT ON BOTH σ AND $\dot{\epsilon}$)

Figure A3. Qualitative behavior of the soil model (Equation A4) for various types of soil

APPENDIX B: SPHERICAL CAVITY EXPANSION AND SLIP-VOLUME CHANGE RELATION

The Theory of Spherical Cavity Expansion in an Elastic-Plastic Medium

1. The problem of expansion of a spherical cavity in an unbounded compressible elastic-plastic medium obeying the Mohr-Coulomb failure condition was first solved by Vesic (1972).* The objective of the problem is to determine the radial stress σ_c at the cavity surface necessary to maintain a slow expansion of the cavity. The Mohr-Coulomb failure condition for this problem can be written as

$$\sigma_r - \sigma_\theta = (\sigma_r + \sigma_\theta) \sin \phi + 2C \cos \phi \qquad \text{(B1)}$$

where

σ_r = radial stress
σ_θ = circumferential stress
ϕ = angle of internal friction
C = cohesion

It is assumed that prior to the application of the radial stress at the cavity surface the entire medium is in a state of ambient hydrostatic stress defined by q. The equation of equilibrium for the spherical geometry (Figure B1) reduces to

$$\frac{\partial \sigma_r}{\partial r} + 2 \frac{\sigma_r - \sigma_\theta}{r} = 0 \qquad \text{(B2)}$$

Vesic's solutions of Equations B1 and B2 result in the following generic expression for σ_r:

$$\sigma_r = (\sigma_c + C \cot \phi)\left(\frac{R_c}{r}\right)^{\alpha} - C \cot \phi \qquad \text{(B3)}$$

---

* References cited in this appendix are listed in the References section at the end of the main text.

For a cohesive soil, where $\tan \phi = 0$, the expression for σ_r takes the following form:

$$\sigma_r = \sigma_c - 4C \ln \frac{r}{R_c} \tag{B4}$$

At the cavity surface $r = R_c$ and Equations B3 and B4 indicate that $\sigma_r = \sigma_c$. The expression for σ_c is given as

$$\sigma_c = 3(q + C \cot \phi)\left(\frac{1 + \sin \phi}{3 - \sin \phi}\right) I_{rr}^{\alpha/3} - C \cot \phi \tag{B5}$$

For cohesive soils σ_c takes the following form

$$\sigma_c = \frac{4}{3} C(1 + \ln I_{rr}) + q \tag{B6}$$

2. In the above expressions

$q = \gamma z$ = in situ hydrostatic stress

$\alpha = 4 \sin \phi / 1 + \sin \phi$

$I_{rr} = \dfrac{I_r}{1 + I_r \bar{\Delta}}$ = reduced rigidity index

$I_r = \dfrac{G}{C + q \tan \phi}$ = rigidity index

γ = unit weight

z = depth from free surface

$\bar{\Delta}$ = plastic volumetric strain

G = elastic shear modulus

The rigidity index I_r represents the ratio of the elastic shear modulus of the material to its initial shear strength $C + q \tan \phi$. If the material is incompressible in the plastic range (i.e., $\bar{\Delta} = 0$), $I_{rr} = I_r$. Therefore, the role of the plastic compressibility is to reduce the effective rigidity of the material.

3. A procedure for determining plastic compressibility from the pressure-volumetric strain response of the material was developed by Bernard and Creighton (1976) by considering the average excess pressure* P_{ave} in the plastic zone. Assuming a linear pressure-volumetric strain response

---

* The hydrostatic stress due solely to the presence of the cavity.

characterized by the bulk modulus K, the plastic volumetric strain can be obtained from

$$\bar{\Delta} = \frac{P_{ave}}{K} \tag{B7}$$

The expression for P_{ave} is given as

$$P_{ave} = (q + C \cot \phi) \frac{3}{3 - \alpha} \frac{I_{rr} - I_{rr}^{\alpha/3}}{I_{rr} - 1} - 1 \tag{B8}$$

For cohesive soils P_{ave} takes the following form

$$P_{ave} = \frac{4}{3} C \left(1 - \frac{\ln I_{rr}}{I_{rr} - 1}\right) \tag{B9}$$

Since the reduced rigidity index I_{rr} is a function of $\bar{\Delta}$, an iterative procedure is required in order to use Equations B7 through B9.

4. In summary, the use of the cavity expansion pressure (Equations B5 and B6) requires five material constants: C, ϕ, γ, G, and K. The classical shear strength parameters (C, ϕ, and the shear modulus G) can be obtained from the results of either triaxial shear or direct shear tests. The bulk modulus K must be determined from the results of a hydrostatic test. For an incompressible material, the bulk modulus is infinite.

Volume Change Due to Slip

5. In order to apply the cavity expansion pressure to the analysis of the wheel-soil interaction problems, it is necessary to account for the additional volumetric strains in the plastic zone due to large shearing strains at the cavity surface caused by the motion of the wheel (i.e., slip). This effect can be accounted for by considering the total plastic volumetric strain as the sum of two components. The first component, which is due to hydrostatic pressure, is given by Equation B7. The second component, $\bar{\Delta}_s$, is referred to as volume change due to shearing strain (or slip). This volume change is postulated to take the following form:

$$\bar{\Delta}_s = \begin{cases} I_s[1 - \exp(-\bar{\eta}\varepsilon)], & \text{if } \bar{\Delta}_s > 0 \\ 0, & \text{if } \bar{\Delta}_s \leq 0 \end{cases} \tag{B10}$$

Figure B2 describes the qualitative behavior of Equation B10. As indicated in Figure B2, the parameter I_s denotes the maximum volumetric strain obtained at very large shearing strain. The parameter $\bar{\eta}$ defines the rate of change in volumetric strain due to an increase in ε. These two parameters are material constants that may be estimated from a plot of volumetric strain versus deviatoric strain obtained from the results of triaxial shear tests.* In view of Equations B7 and B10, the total plastic volumetric strain that must be used in the expression for σ_c is given as

$$\bar{\Delta}_{total} = \frac{P_{ave}}{K} + I_s[1 - \exp(-\bar{\eta}\varepsilon)] \qquad (B11)$$

---

* The performance of the wheel is not very sensitive to these parameters, and reasonable uncertainties in I_s and $\bar{\eta}$ do not greatly affect the behavior of the wheel.

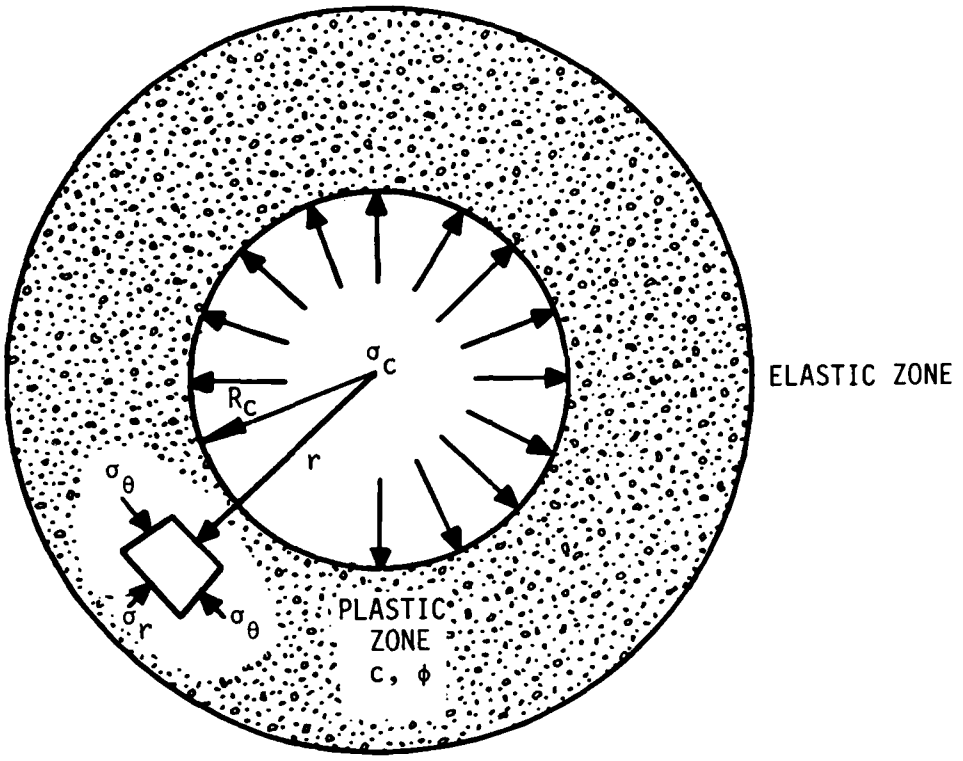

Figure B1. Slowly expanding spherical cavity in an unbounded elastic-plastic medium

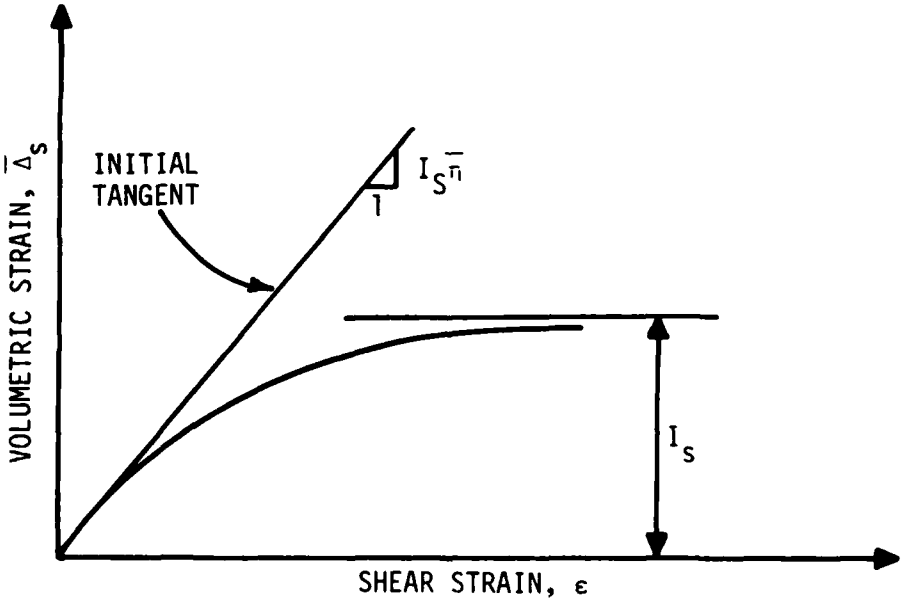

Figure B2. Proposed volumetric strain-shearing strain relation (Equation B10)

APPENDIX C: NOTATION

C	Cohesion
C_d	Rate effect parameters; material constants
CI	Cone index
D	Unloaded section width of the tire
dF	Vertical differential force
DBP	Drawbar pull applied on the tire
E	Efficiency of the tire
G	Shear modulus
h	Unloaded section height
I_s	Material constant related to volume change
IMR	Internal motion resistance of the tire
k_e	Equivalent spring constant for soil-tire system
k_s	Spring constant of the soil
k_t	Spring constant of the tire
MF	Motion resistance in the direction of motion
MR	Motion resistance in the plane of the tire
P	Drawbar pull
R	Radius of the tire
R'	Radius of a circle containing the deflected portion of the wheel
R_o	Initial radius of an expanded cavity
S	Slip of the wheel in the plane of the wheel
S_m	Slip of the wheel in the direction of motion
SF	Side force applied on the tire
T	Torque applied on the tire
W	Tire load
W_o	Tire load used for the parametric calculations = 1000 lb; wheel load
Z	Sinkage of a flexible wheel
Z_r	Sinkage of a rigid wheel
α	Generic angle
γ	Soil density
δ	Deflection
δ_s	Deflection of soil at a generic point
δ_t	Radial deflection of the tire at a generic point

Δ	Maximum deflection of the tire on a hard surface
Δ_t	Maximum deflection of the tire on a yielding soil
Δ_α	Deflection of the tire at the generic point
ε	Shearing strain
$\dot{\varepsilon}$	Time rate of shearing strain
η	Angle between the direction of motion and the plane of the wheel
$\bar{\eta}$	Material constant related to volume change
θ_s	$2 \cos^{-1}\left(\frac{R_o}{R}\right) = 2 \cos^{-1} \sqrt{1 - \frac{D}{\pi R}}$
θ_t	$2 \cos^{-1}\left(1 - \frac{\Delta}{R}\right)$
θ_1	$\cos^{-1}\left(1 - \frac{Z + \Delta_t}{R}\right)$
θ_2	$\cos^{-1}\left(1 - \frac{\Delta_t}{R}\right)$
Λ	Rate effect parameters; material constants
π	3.141
σ_c	Radial stress inside a cavity
σ_H	Horizontal stress distribution at the soil-tire interface
σ_N	Normal stress at the soil-tire interface
σ_r	Radial stress
σ_θ	Circumferential stress
σ_V	Vertical stress distribution at the soil-tire interface
$\bar{\sigma}$	Standard deviation
τ	Shear stress at the soil-tire interface
τ_M	Maximum shear strength of material in undrained loading condition
τ_N	Shear stress perpendicular to the plane of the wheel
τ_p	Shear stress in the plane of the wheel
ϕ	Angle of internal friction

END